Functional characterization of Dacapo (Dap) as a substrate of SCF-Rca1

DISSERTATION ZUR ERLANGUNG DES
DOKTORGRADES DER NATURWISSENSCHAFTEN (DR. RER. NAT.)
DER FAKULTÄT FÜR BIOLOGIE UND VORKLINISCHE MEDIZIN
DER UNIVERSITÄT REGENSBURG

Vorgelegt von
Manuel Saller

aus
Straubing

Im Jahr
2024

Das Promotionsgesuch wurde eingereicht am:
26.02.2024

Die Arbeit wurde angeleitet von:
Prof. Dr. Frank Sprenger

Unterschrift:

Für meine Eltern

Table of Contents

1. Abstract

Dacapo (Dap) – the *Drosophila* homolog of p21 and p27 – can inhibit CycE/Cdk2 and thereby block the transition from G1 phase to S phase of the cell cycle. Previous work showed that the E3 ubiquitin ligase CRL4-Cdt2 targets Dap for degradation. In addition, there were indications that the E3 ubiquitin ligase SCF-Rca1 could be involved in degradation of Dap. In this thesis data is shown, which substantiates that Dap is a substrate of SCF-Rca1. Furthermore, important insights into the exact mechanisms by which Dap is recognized by CRL4-Cdt2 and SCF-Rca1 were obtained.

Dap contains in the C-terminus a so-called PIP degron, a short 12 amino acid long motif that is required to mediate ubiquitination by CRL4-Cdt2. The PIP degron allows binding to the DNA clamp PCNA (proliferating cell nuclear antigen) and this association is required to be recognized by Cdt2, the substrate recognition module. Here, it was shown that the first amino acid (Q184) of the PIP degron in Dap is crucial for binding to PCNA and an alanine mutation of Q184 impedes degradation via CRL4-Cdt2. In addition, it was shown that a basic cluster at the C-terminal part of the PIP degron in Dap is essential for its degradation. The basic cluster might mediate interaction with DNA or Cdt2. Furthermore, it was demonstrated that regions in the N-terminal part of Dap mediate interaction with Cdt2.

Rca1 is an F-box containing protein that can assemble into SCF-complexes. The target of an SCF-Rca1 ubiquitin ligase could be Dap. Overexpression or knockdown of Rca1 can influence the stability of Dap. However, in part, these effects on Dap were indirect by induced cell cycle distribution changes and subsequent degradation by CRL4-Cdt2. To eliminate, or at least reduce these indirect effects, different approaches were taken, such as knockdown of Cdt2 or mutation of the PIP degron. After the activity of CRL4-Cdt2 was strongly reduced by different strategies, overexpression of Rca1 still decreased the stability of Dap and knockdown of Rca1 increased its stability. This substantiates our theory that Dap is a substrate of SCF-Rca1.

The PIP degron, responsible for the CRL4-Cdt2 mediated degradation was completely absent in an N-terminal fragment of Dap (Dap_1-125). This fragment was destabilized by Rca1 overexpression or stabilized by knockdown of Rca1, respectively. Dap_1-125 still contains binding sites for CycE and Cdk2 and is able to inhibit the CycE/Cdk2 complex. Using Dap_1-125 constructs we were able to show that binding of Dap to CycE and Cdk2 is required for its degradation via SCF-Rca1. In addition, we demonstrated that the N-terminal part of CycE in the CycE/Cdk2/Dap complex is needed to destabilize Dap_1-125. Based on this and further data obtained in this thesis, we propose the following model for the degradation of Dap via SCF-Rca1: Dap (an IDP (intrinsically disordered protein)) binds CycE/Cdk2 in G1 phase to fulfill its role as inhibitor of CycE/Cdk2. To induce the G1/S transition at the end of G1 phase an unknown kinase phosphorylates Cdk2. This phosphorylation could allow restricted Cdk2 kinase activity that results in

phosphorylation of the associated CycE in the N-terminal region. Subsequently, a kinase gets recruited to the phosphorylated site and could phosphorylate CycE in the C-terminal region and also Dap. Thereafter, phosphorylated Dap is recognized by SCF-Rca1. By this mechanism it could be ensured that only Dap, which already fulfilled its function in the cell cycle is targeted for degradation. This is in line with the regulation of other CKIs (inhibitors of Cyc/Cdk complexes), which are also only targeted for degradation after they have actively regulated the cell cycle.

2. Introduction

2.1 The eukaryotic cell cycle

In eukaryotes, cell reproduction occurs by a series of events called the cell cycle. During this process chromosomes are duplicated and subsequently distributed into two daughter cells (**Figure 1**). The events are usually divided into four phases. The gap phases (G1, G2) are separating the synthetic (S) and the mitotic phase (M) from each other.

In G1 phase the cell decides whether it starts a new round of division or exits from the cell cycle. The letter occurs, if growth conditions are unfavorable or the cell encounters inhibitory signals from other cells. This condition is also referred to as G0 phase. If the cell is committed to a new cell cycle, the genetic material is doubled by DNA replication in S phase. As a result, chromosomes consist of two identical sister chromatids. In G2 phase the cell prepares for the following M phase. Damage of DNA that may have occurred can be repaired or rather the cell undergoes apoptosis. The M phase is subdivided into mitosis and cytokinesis.

Mitosis comprises five stages: prophase, prometaphase, metaphase, anaphase and telophase. In prophase DNA of the sister chromatids is condensed more tightly. Furthermore, the in S phase duplicated centrosomes are separated and the mitotic spindle develops. In prometaphase the nuclear envelope is broken down. This allows the microtubules, which emanate from the centrosomes, to bind to chromosomes via their kinetochores. In metaphase chromosomes become bioriented meaning that kinetochores only interact with microtubules from the opposite centrosome. In anaphase the sister chromatids are separated and are transported to opposite poles. In telophase the single chromatids become condensed and are enclosed in the regenerated nucleus. In addition, the mitotic spindle is dissolved. Finally, the cell cycle is completed after cytokinesis, in which both daughter cells are separated (Morgan 2007).

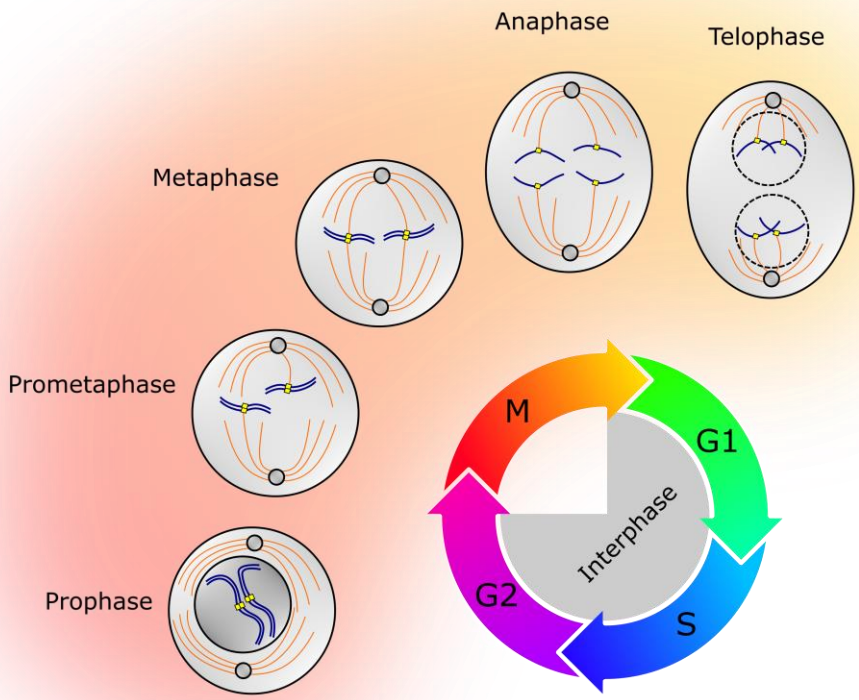

Figure 1 | The eukaryotic cell cycle
The eukaryotic cell cycle is subdivided into interphase (G1-, S-, G2- phase) and M phase. In the gap phases (G1, G2) the cell prepares for the following phase. DNA is replicated in S phase, which results in chromosomes with two identical sister chromatids. M phase is divided into mitosis and cytokinesis. The four phases of mitosis, in which the nuclear envelope is broken down and the sister chromatids are pulled to opposite poles of the cell, are depicted. In addition, telophase is shown in which the single sister chromatids are enclosed in the newly formed nuclear envelope. The cell cycle ends with cytokinesis, in which the cell is divided into mother and daughter cell. Figure assembled from data in (Morgan 2007).

2.2 Cyclin dependent kinases – the key players of the cell cycle control system

The cell cycle contains numerous events that must be carried out in a specific sequence. To achieve this, an army of proteins work together in the so-called cell-cycle control system. Cyclin dependent kinases (Cdks) play a key role here. Cdks phosphorylate proteins resulting in altered activity or interaction with other proteins. In higher eukaryotes there are several Cdks (Cdk1, Cdk2, Cdk 4, Cdk6) that are directly involved in cell-cycle control. In addition, there are numerous Cdks that are involved in transcription and

other processes, which, however, are not described in detail here. The activity of Cdks is regulated by phosphorylation as well as binding of regulatory proteins (**Figure 2**).

Cdks are partially activated by binding of regulatory subunits called cyclins. There are divers cyclin types, which are essential in different cell cycle phases. While the concentration of Cdks is relatively constant, the concentration of cyclins oscillates during the cell cycle. This contributes to an oscillation of Cdk activity. For full activation, Cdks must be phosphorylated adjacent to the kinase active site by Cdk-activating kinases (CAKs). Furthermore, inhibitory phosphorylation of Cdks by kinases of the Wee1 family must be reversed by the phosphatases of the Cdc25 family.

Cdks can be kept in an inactive state by binding of Cdk inhibitor proteins (CKIs). In animals, these CKIs are subdivided into two families, Cip/Kip and INK4 family, each with a distinct mechanism of Cdk inhibition. The Cip/Kip members bind to both cyclin and Cdk, whereas INK inhibitors bind to the monomeric form of Cdk and therefore prevent the binding of cyclins. In *Drosophila* there are two CKIs, Dacapo (Dap), which is a member of the Cip/Kip family, and Roughex (Rux) that belongs neither to the Cip/Kip nor to the INK4 family (Morgan 2007).

For the recognition of substrates, the Cdk itself, its cyclin partner and in some cases cyclin dependent kinase subunits (Cks) are involved. Cdks recognize substrates with some preference for the S/T-P-X-K/R sequence with S/T being phosphorylated (Malumbres 2014). Short motifs on substrates mediate recognition by cyclins. Different motifs are used for this depending on the cyclin type. For instance, cyclin A and E interact with an RxL motif (also called cy (cyclin binding) motif). Cks promotes effective phosphorylation of substrates that contain clusters of multiple phosphorylation sites. Cks binds to Cdk and provides an accessory binding site that recognizes phosphorylated residues. Therefore, after one residue of a substrate has been phosphorylated, Cks increases the affinity of Cdk for the substrate and facilitates the phosphorylation of neighboring residues (Morgan 2007). In *Drosophila*, there are two types of Cks proteins (Cks85A and Cks30a) (Ghorbani et al. 2011).

A) Activation of Cdks:

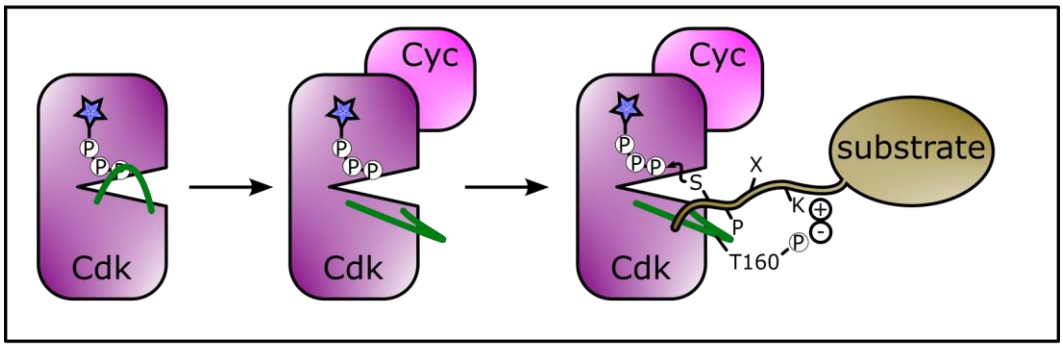

B) Negative regulation of Cdks by phosphorylation of Y15:

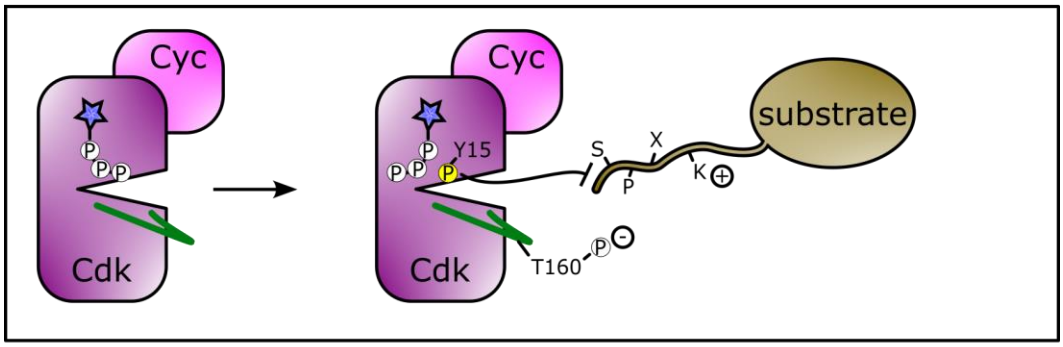

C) Negative regulation of Cdks by CKIs:

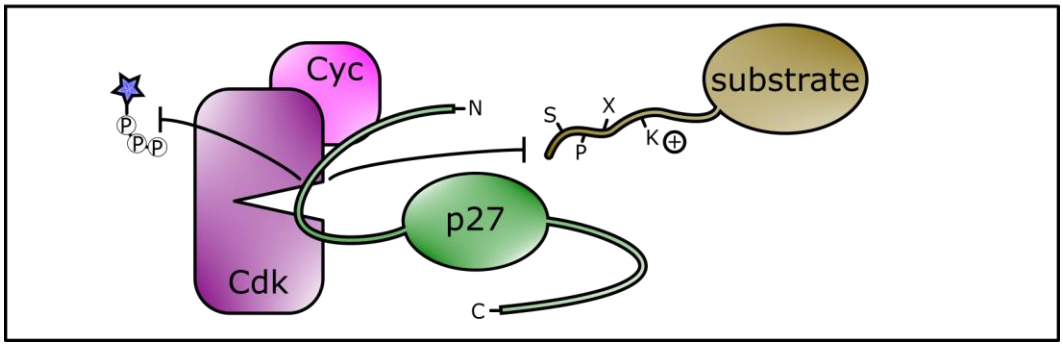

Figure 2 | Regulation of Cdk activity

A) On the left side, the Cdk kinase with ATP (blue asterisk) in its active site is shown. The T-loop (depicted in green) blocks the active-site cleft. After binding of the cyclin (Cyc) (scheme in the middle), the T-loop is shifted out of the active-site entrance. In addition, threonine 160 (T160) is phosphorylated by a Cdk-activating kinase (CAK) (scheme on the right). This phosphorylation allows the binding of a substrate that contains the SPXK consensus sequence: The proline (P) of this SPXK sequence interacts with the backbone of the T-loop. The positively charged lysine (K) interacts with the negatively charged phosphate on T160. Thereafter, the hydroxyl oxygen of the serine (S) is in the right position for nucleophilic attack on the γ-phosphate of ATP. The depicted model is based on crystallographic studies of human Cdk2 and its partner cyclin A. It serves as a good representative for all Cdks, although details of Cdk activation seem to be different in some Cdk complexes. **B)** Cdk activity can be abolished by inhibitory phosphorylation (yellow filled phosphorylation site) of tyrosin (e.g. Y15) catalyzed by kinases of the Wee1 family. **C)** In addition, binding of Cdk inhibitor proteins (CKIs) can impede the activity of Cyc/Cdk complexes. Some CKIs such as p27 inhibit the Cyc/Cdk complex and abolish binding of ATP (shown in scheme), whereas others prevent binding of cyclins to Cdk (not shown). Figure assembled from data in (Morgan 2007).

According to the classical view of cell cycle regulation, different cyclin/Cdk complexes are required to initiate certain cell cycle events. For instance, cyclin E-Cdk2 is needed to initiate S phase, whereas cyclin A, together with Cdk1 or Cdk2, contributes to the continuation of S phase and to entry into mitosis. Finally, cyclin B-Cdk1 facilitates entry into mitosis (Hochegger et al. 2008). However, on closer inspection it turns out that in most cases the responsibilities are shared among different cyclin-Cdk complexes (Bloom and Cross 2007). Frequently the later cyclin-Cdk can compensate for the absence of earlier cyclin-Cdks. For instance, a single mitotic cyclin-Cdk is sufficient to drive the complete cell cycle in fission yeast (Coudreuse and Nurse 2010). However, to fine tune different thresholds at which certain cell cycle events are triggered the cell sequentially activates different Cdks and cyclins. A combination of cyclin-specific docking motifs and Cks1-dependent phosphorylation ensures that substrates are phosphorylated by certain cyclin-Cdks to varying degrees. This creates unlimited combinations of Cdk input-output functions. Using cyclin-Cdks with changing but also a common baseline specificity offers many advantages. First, if there were an exclusively specific kinase pathway evolved for each cell cycle stage, it would be difficult to maintain phosphorylation of proteins (e.g. those preventing rereplication) that must remain phosphorylated during a long period of the cell cycle. In addition, the system becomes very robust, since anomalies in cyclin accumulation waves can be overcome by using mitotic cyclin-Cdks as a key to every threshold (Örd and Loog 2019).

2.3 The ubiquitin proteasome system

To assure the strict unidirectionality of the cell cycle, the main components of the cell cycle system must be degraded in a precise spatial and temporal manner. This is achieved by the so-called ubiquitin proteasome system (UPS), in which proteins are ubiquitinated in such a way so that they are recognized by the 26S proteasome. A three-step enzymatic cascade facilitates ubiquitination of substrates (**Figure 3**). First, the small protein ubiquitin (76 aa) is bound and activated by an E1 ubiquitin activating enzyme in an ATP dependent manner. Thereafter, it is transferred to an E2 ubiquitin conjugating enzyme. Finally, an E3 ubiquitin ligase specifically binds the target protein to mediate the transfer of ubiquitin to a lysine residue in the substrate. Substrate specificity is mainly conferred by E3s rather than E2s and E1s. Thus, there are much more E3s (in *Drosophila* approx. putative 200) than E2s (in *Drosophila* approx. 30) and E1s (in *Drosophila* only Uba1) ((Lee et al. 2008; Michelle et al. 2009; Du et al. 2011). Proteins can be ubiquitinated in different ways what is expressed with the term ubiquitin code. If only one single ubiquitin is attached to a protein substrate, this is called monoubiquitination. If numerous ubiquitin molecules are attached,

they can either be bound to different lysines in the substrate (multi-monoubiquitination) or to ubiquitin that is already attached to the substrate (polyubiquitination).

In case of polyubiquitination, the C-terminus of ubiquitin can be linked to one of seven internal lysine residues (K6, K11, K27, K29, K33, K48, K63) or the N-terminus (M1) of another ubiquitin molecule (Bassermann et al. 2014). This results in ubiquitin-chains with different linkage-types. Ubiquitin chains that contain only a single linkage type are called homotypic (Akutsu et al. 2016). In contrast, heterotypic chains comprise mixed linkages and can also be branched meaning that one ubiquitin is ubiquitinated at two or more sites (Meyer and Rape 2014). In addition, ubiquitin can be modified by post-translational modifications such as acetylation and phosphorylation (Kliza and Husnjak 2020). Deubiquitylating enzymes (DUBs) can hydrolyze linkages between ubiquitin molecules or ubiquitin and substrates, which makes ubiquitination a reversible modification (Clague et al. 2013).

Depending on the ubiquitin code, the substrates have different fates, for instance with respect to DNA repair, trafficking, immunity and proteostasis. Although biological significance of some ubiquitin modifications (e.g. K48- and K63) is well studied, the functional significance of other ubiquitin modifications is still far from being fully understood. Degradation of ubiquitinated substrates by the 26S proteasome is often mediated by K48-linked chains, whereby other linkages are used as well (Maupin-Furlow 2011; Bard et al. 2018).

The 26S proteasome has a complex architecture: The proteolytic active sites reside within the chamber of the barrel-shaped 20S core particle. These sites are accessible only through narrow pores that exclude folded polypetides. Access to the pores is controlled by the 19S regulatory particle (RP), which caps one or both ends of the 20S core particle. The RP is subdivided into the base and lid. The base provides multiple binding sites for ubiquitin and ubiquitin-like proteins (UBLs). In addition, it applies mechanical pulling force to unfold polypeptides, and then translocates the substrates into the 20S core. The lid removes substrate-attached ubiquitin chains before substrates are released into the base (Bard et al. 2018).

Besides the appropriate ubiquitination code, substrates must contain an unstructured region, either at the terminus (at least 20-30 aa) or as an internal flexible loop to be degraded by the 26S proteasome. If substrates do not contain such a flexible initiation region, AAA+ unfoldases (VCP in higher eukaryotes), may completely or at least partially unfold them to create these unstructured regions (Ye et al. 2017).

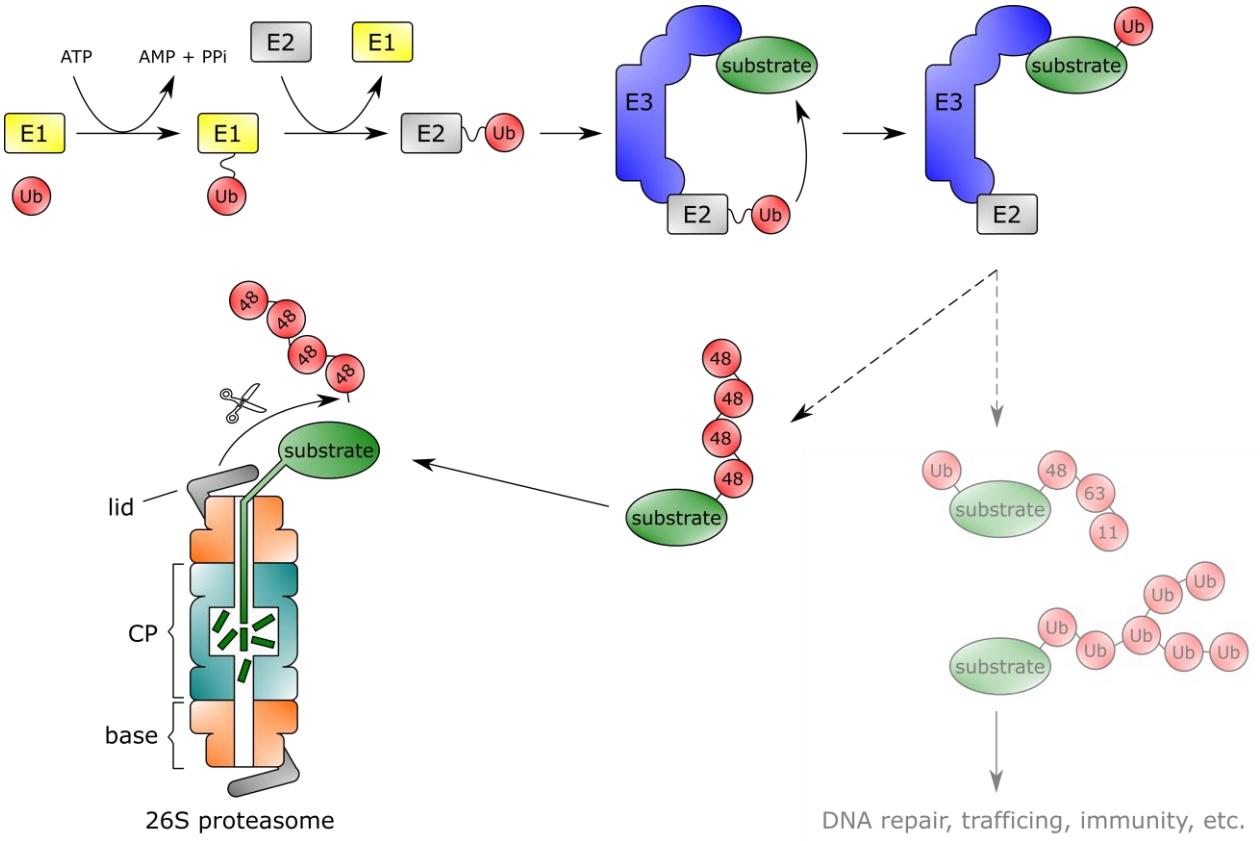

Figure 3 | The ubiquitin proteasome system
The ubiquitin proteasome system (UPS) comprises ubiquitination of substrate proteins and their subsequent degradation in the 26S proteasome. First, the C-terminus of ubiquitin is bound to a cysteine residue of an E1 (ubiquitin-activating enzyme) via a high energy thioester bond using ATP. Thereafter, the activated ubiquitin is transferred to an E2 (ubiquitin-conjugating enzyme) that gives rise to a second thioester intermediate. An E3 (ubiquitin ligase) catalyzes the transfer of ubiquitin from E2 to a lysine residue of the substrate resulting in an isopeptide bond. The steps described above can be repeated, with ubiquitin molecules being bound either to the substrate (multi-monoubiquitination) or to an already attached ubiquitin (polyubiquitination). In case of polyubiquitination, ubiquitin can bind to different lysines or the N-terminus of the already attached ubiquitin resulting in numerous chain types. Only some of these chains (e.g. K48-linked ubiquitin chains) mark the substrate for degradation in the 26S proteasome. Other linkages of ubiquitin are involved for instance in DNA repair or trafficking. The lid of the proteasome contains deubiquitinases (DUBs) that remove substrate-attached ubiquitin chains. The base controls the access of substrates to the 20 S core particle (CP), in which they are proteolytically degraded. Figure assembled from data in (Maupin-Furlow 2011) and (Komander and Rape 2012).

2.4 E3 ubiquitin ligases

All E3s contain an E2-ubiquitin binding domain and are classified based on the structure of this domain as well as their ubiquitin transfer mechanism. There are three classes of E3s identified to date: RING (really interesting new gene), HECT (homologous to E6AP C-terminus) and RBR (RING-between-RING). Whereas RING E3s catalyze the direct transfer of ubiquitin from E2-ubiquitin to the substrate, HECT and RBR E3s first receive ubiquitin themselves by a catalytic cysteine before they transfer it to the substrate (Buetow and Huang 2016).

E3s target substrates by different mechanisms. Some E3s harbor protein-protein interaction domains to which a substrate can bind directly or indirectly via an interacting partner. Furthermore, there are E3s that contain domains that interact with non-protein molecules to facilitate substrate binding and ubiquitination. For instance, the E3 cullin-RING ligase (CRL) can associate with the sugar-binding receptor FBS1 (CRL-FBS1) to ubiquitinate N-linked glycoproteins (Mizushima et al. 2007). In addition, some E3s do not specifically recognize substrates but contain domains that recruit them to certain locations within the cell where they then ubiquitinate any accessible protein. For instance, the E3 CRL-DDB binds to pyrimidine dimer photolesions and ubiquitinates DNA-bound XPC and DDB2 to initiate the nucleotide excision repair pathway (Scrima et al. 2008; El-Mahdy et al. 2006).

RING E3s are the largest class of E3s. According to bioinformatic forecast there are approximately 600 RING E3s in humans. The commonality of these E3s is the presence of a RING domain with which E2-ubiquitin is recruited and which contributes to ubiquitin transfer (Deshaies and Joazeiro 2009). For proper folding of the RING domain two zinc ions are needed, which are coordinated by cysteine and histidine residues. Some RING domains do not function as monomers but are only active if they act as oligomers. For instance, cIAP2 is only active when homodimerized via its RING domain (Mace et al. 2008). Another example is MDM2, which is only active if it heterodimerizes with MDMX (Badciong and Haas 2002). In addition, some RING E3s such as Cullin-RING E3 ubiquitin ligases (CRLs) and the anaphase promoting complex/cyclosome (APC/C) contain numerous subunits. U-box proteins also belong to the RING E3s and resemble the classical RING E3s in structure and mechanism. However, U-box proteins do not contain zinc ions (Buetow and Huang 2016).

CRLs are the largest family of E3s with over 400 members known in mammals (Nguyen et al. 2017) (**Figure 4**). They contain the following subunits: Rbx1 (or Rbx2) - a protein with a RING domain - mediates binding to E2-ubiquitin. A cullin protein (Cul1, Cul2, Cul3, Cul4A/4B, Cul5 or Cul7) acts as a scaffold. Cul4A and Cul4B mainly differ by 149 additional amino acids at the N-terminus (harbors a NLS) of Cul4B (Zou et al. 2009). CRLs are named based by their cullin protein, e.g. CRL2, if it contains Cul2. In addition, there is a substrate receptor that recognize the target protein as well as an adaptor protein that bridges the

substrate receptor to the cullin. Whereas the C-terminus of a cullin interacts with Rbx1 or Rbx2, the N-terminus binds to the adaptor. The adaptor proteins contain one of two common folds that mediate interaction with cullins: a WD40 ß-propeller fold, which is used by the DDB1-Cul4-associated factor (DCAF) family as well as a BTB fold that is used for instance by Skp1. The adaptors are linked to members of several substrate receptor families that contain typically 30-70 proteins (Sarikas et al. 2011). For instance, the adaptor Skp1 connects the F-box substrate receptor family (over 60 members) to a CRL1 (Skaar et al. 2013). The naming of a CRL complex not only refers to the cullin subunit, but also to the substrate receptor, e.g. CRL7-Fbw8. Substrate receptors contain domains that mediate recognition of substrates by degron motifs, which are specific amino acid sequences that are often post-translationally modified (Bulatov and Ciulli 2015; Lydeard et al. 2013).

The best-characterized CRL is CRL1, which is also often referred to as Skp1-Cul1-F-box (SCF) complex. The architecture of CRL1 is representative for all CRLs. The helical N-terminal domain (NTD) of Cul1 interacts with both Skp1 and the F-box domain of Skp2 in case of SCF-Skp2 (**Figure 4A**). The F-box motif is a three-helix bundle that packs along the helices of Skp1. At the other end of the complex, the globular C-terminal domain (CTD) of Cul1 creates a V-shaped binding pocket for Rbx1. The RING domain of Rbx1 binds three zinc ions (Zheng et al. 2002).

CRL4s uses the adaptor damaged DNA binding protein 1 (DDB1). This adaptor is special, since it does not contain the BTB fold found in the adaptors of CRL1/2/3/5. Instead, DDB1 comprises three WD40 ß-propeller domains (BPA, BPB, BPC) as well as a helical C-terminal domain. While only the BPB domain interacts with Cul4, BPA and BPC form a cleft, which acts as a binding site for the DCAF substrate receptors. CRL4s are the only CRLs known until know, which cannot only recognize proteins as substrates, but also DNA. CRL4-DDB2 is recruited to UV-induced lesions in DNA and then ubiquitinates nearby proteins to facilitate direct nucleotide excision repair (Fischer et al. 2011).

A)

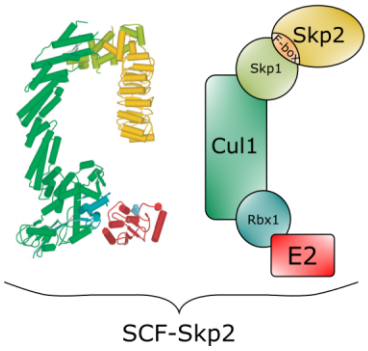

B)

Cullin	Adaptor	Substrate Receptor	RING protein
Cul1	Skp1	F-box proteins	Rbx1
Cul2	EloBC	VHL box proteins	Rbx1
Cul3	BTB proteins	BTB proteins	Rbx1
Cul4A/B	DDB1	DCAF proteins	Rbx1
Cul5	EloBC	SOCS box proteins	Rbx2
Cul7	Skp1	Fbw8	Rbx1

Figure 4 | Structure and composition of CRL complexes
A) Ribbon presentation of SCF-Skp2 generated from PDB ID 1LDK. Only the F-box domain of Skp2 is included in this 3D structure. The zinc ions in Rbx1 are depicted as spheres. Colors in the ribbon presentation correspond to colors in the schematic presentation to the right. The architecture of other CRL complexes is very similar to SCF-Skp2. **B)** Composition of CRL complexes. For each cullin, different adaptors, substrate receptors and RING proteins are used. Substrate receptors are grouped in families, which contain several proteins (e.g. approx. 60 members for the F-box family). However, for Cul7 only one substrate receptor (Fbw8) is known. Figure assembled from data in (Nguyen et al. 2017) and (Morgan 2007).

2.5 Regulation of CRL E3 ubiquitin ligases

The activity of CRL complexes is regulated by post-translational modifications as well as by alterations to the subunit composition (**Figure 5**).

For the activation of a CRL the covalent attachment of the protein Nedd8 to a cullin subunit – termed neddylation - is needed (Pan et al. 2004). Like ubiquitination, neddylation is dependent on a cascade of enzymes. While NAE acts as the E1, Ubc12 and Ube2F are NEDD8 E2s. In contrast to ubiquitination, beside a NEDD8 E3 a "co-E3" is required for neddylation. The RING protein of the CRL (Rbx1 or Rbx2) is the NEDD8 E3, while the protein DCN1 is used as a co-E3 (Kurz et al. 2005). The E2 is recruited by means of DCN1 and correctly positioned by the RING protein (Scott et al. 2014). Thereafter, NEDD8 can be transferred on the cullin CTD, which leads to a conformational change of the cullin winged helix B motif and the cullin-RING interface. This causes the displacement of Rbx1 from the cullin allowing to bring the E2 closer to the target substrate (Nguyen et al. 2017).

In addition, NEDD8 can be removed by the COP9 Signalosome (CSN) that is a complex of eight subunits (CSN1-8), which shows similarity to the 19S lid of the proteasome (Pick et al. 2009). CSN5 is the catalytic subunit, a zinc metalloproteinase, which cleaves NEDD8. Besides regulation by deneddylation, CSN can also regulate CRLs by interacting with unneddylated CRLs and thereby block binding of both an E2 and substrates. (Enchev et al. 2012; Cavadini et al. 2016). The association rate of CSN with unneddylated Cul1 is reduced by around twofold in comparison to neddylated Cul1 (Bennett et al. 2010). Electron microscopy

images of SCF-Skp2-Cks1 bound to CSN suggest that the subunit CSN2 binds the cullin-Rbx module, whereas other CSN subunits bind to the variable SR arm. Since the structure of these SR modules differs greatly, it is surprising that CSN interacts with multiple SRs. On the other hand, this could at least partly explain why different CRLs associate to variable rates with CSN. For instance, 40% of Cul4 was found associated with CSN, whereas this rate is < 5% for Cul2 and Cul3 (Bennett et al. 2010). When preformed CSN-CRL complexes are incubated with a substrate *in vitro*, the substrate displaces CSN from CRL (Bennett et al. 2010; Fischer et al. 2011; Emberley et al. 2012). This suggests that high substrate levels out-compete CSN for CRL. In addition, inositol hexakisphosphate can regulate the binding between CSN and CRL (Scherer et al. 2016).

CRLs can also be regulated by the protein CAND1 that facilitates the dissociation of a bound SR from a cullin to allow the binding of a new SR. Without CAND1 the exchange of SR modules would hardly be possible, since Skp1-Fbxw7 (probably representative for other SRs) binds extremely tightly to unneddylated or neddylated Cul1-Rbx1 (dissociation rate approx. 10^{-6}). CAND1 can only stimulate SR exchange for unneddylated CRLs, since Nedd8 blocks the access of CAND1 to the cullin scaffold (Pierce et al. 2013). Interestingly, CAND1 seems to have some specificity in terms of the SR that it can exchange (Pierce et al. 2013). CAND1 reversibly wraps around both the NTD and CTD of deneddylated cullin (Goldenberg et al. 2004). It is assumed that at least for Cul1 a meta-stable Cand1-SR-Cul1 complex is formed, which would either expel Cand1 or the SR (Pierce et al. 2013). However, further studies are necessary to elucidate the molecular basis of this exchange reaction.

Another regulation mechanism for CRLs is mediated by the protein Glomulin, which interacts with Rbx1, but not Rbx2 (Tron et al. 2012). Through this interaction, the E2-binding site is obscured, preventing both ubiquitination and neddylation (Nguyen et al. 2017).

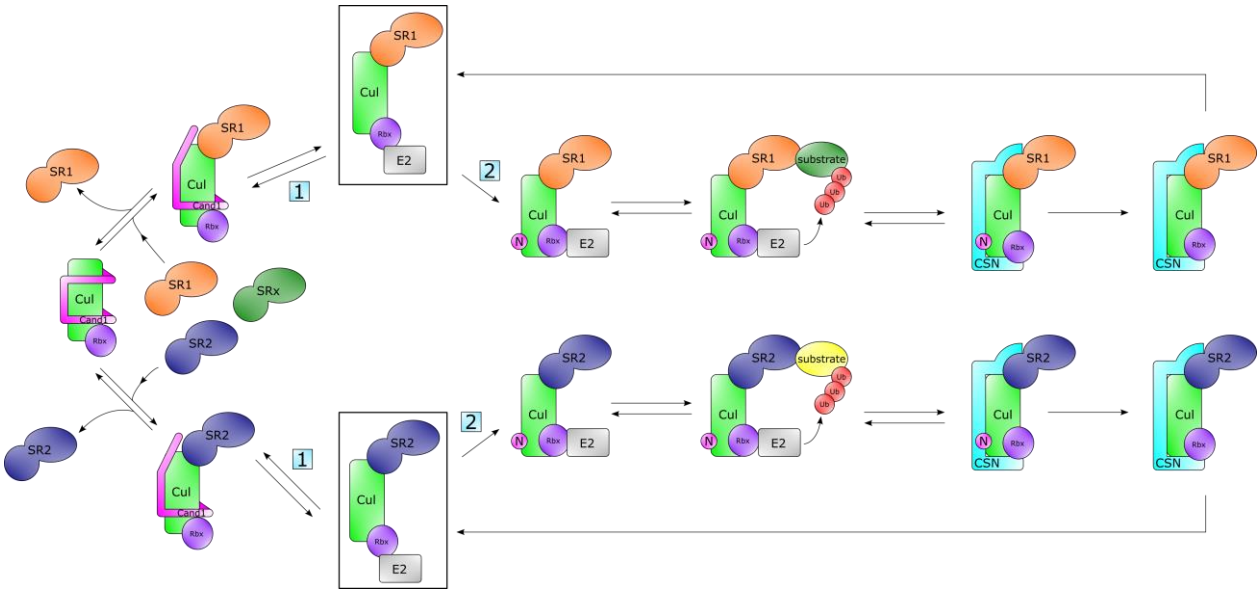

Figure 5 | Regulation of CRL E3 ubiquitin ligases
Starting from a Cul-Rbx-SR complex (marked with a black rectangle), CRLs can be regulated in several ways (direction 1 or 2). For simplicity in this figure SR (substrate receptor) refers to adaptor plus substrate receptor, since for some CRLs both subunits are one and the same. **1)** If Cand1 binds to Cul-Rbx-SR the SR can be split off. After that Cand1 can be replaced by another SR. **2)** In addition, Cul-Rbx-SR can be neddylated by means of proteins, which function like E1, E2 and E3 enzymes in the ubiquitination cascade. Once CRLs are neddylated, Cand1 can no longer bind to CRLs, which prevents the path via 1). The neddylation leads to a conformational change in the cullin and a rearrangement of Rbx1. Only after this shift, the E2, which binds to Rbx, can reach the substrate for ubiquitination. Neddylation can be reversed by CSN. Interestingly, CSN also regulates CRLs independent of Nedd8: CSN can bind stably to parts of Cul and the substrate receptor thereby preventing binding of both an E2 and substrates. However, high substrate levels can out-compete CSN for CRL. After the dissociation of CSN, the initial situation (black rectangle) is restored. Figure assembled from data in (Lydeard et al. 2013).

2.6 Substrate recruitment to SCF complexes

SCF complexes use F-box proteins as substrate recognition modules. These proteins contain the 40-amino-acid F-box domain, which was first identified in cyclin F. In humans approximately 70 F-box proteins are used to target hundreds of proteins for degradation (Jin et al. 2004; Skaar et al. 2009). F-box proteins can be subdivided into three families based on specific domains beyond the F-box domain: FBXW (F-box and WD40 domain), FBXL (F-box and Leu-rich repeat), FBXO (F-box only) (Jin et al. 2004; Cenciarelli et al. 1999; Winston et al. 1999). However, the name of FBXO is misleading, since also this family contains additional conserved homology domains (at least 21), but they are either not present in many F-box proteins or were not recognized. Therefore, the description “F-box and other domains” would be more suitable for FBXO (Skaar et al. 2013).

In response to stimuli, target proteins must be bound by their corresponding F-box protein or this interaction must be prevented. To this end, both F-box proteins as well as F-box protein-substrate interfaces are tightly regulated (Skaar et al. 2013) (**Figure 6**).

One way of regulation is via canonical phosphodegrons in substrates (**Figure 6A**). For instance, the F-box protein βTrCP binds the consensus degron Asp-Ser-Gly-Xaa-Ser (Xaa represents any amino acid and both Ser residues are phosphorylated). There may be deviations from the consensus sequence, e.g. replacing Ser and Thr residues or the inclusion of phosphomimicking amino acids. Whereas simple phosphodegrons can be phosphorylated by a single kinase, some degrons with multiple phosphorylation sites can be targeted by multiple kinases. For instance, the kinases Cdk2 and GSK3 phosphorylate different residues of the cyclin E degron (Welcker et al. 2003; Skaar et al. 2013).

In addition, priming phosphorylation can add an additional layer of complexity (**Figure 6B**). For example, GSK3 can phosphorylate the JUN degron only after it was phosphorylated by another kinase (Wei et al. 2005). Furthermore, it must be considered that in some cases priming phosphorylations are not always directly at the F-box protein-substrate interface, but only near it (Liu et al. 2002). Beside this regulation via canonical phosphodegrons, there are a couple of other regulation mechanisms some of which are described below. These mechanisms can be combined in different ways and thereby allow a more precise regulation of substrate targeting:

Regulation of substrate binding can also be dependent on cofactors (**Figure 6C**). For example, SCF-Skp2 requires the binding of the cofactor Cks1 to allow efficient ubiquitination of p27. Cks1, but not Skp2 binds to phosphorylated Thr187 of p27 and thereby contributes to substrate recognition (Ganoth et al. 2001; Spruck et al. 2001).

In addition, the access of degrons can be restricted (**Figure 6D**). For instance, when Cdk activity is low Thr33 - which is not part of the degron of RRM2 - is not phosphorylated and therefore the degron is obscured. However, in G2 Cdk activity enables phosphorylation of Thr33, which in turn allows access to the degron. Often it is not easy to determine, whether phosphorylation events beyond the degron are priming events for the degron, control degron access, or both (Duan et al. 2011; Gao et al. 2011; Zhao et al. 2011).

Beside phosphorylation there are also other covalent modifications for degrons (**Figure 6E**). For instance, the F-box proteins FBXO2 and FBXO6 bind glycosylated substrates via F-box-associated (FBA) domains. Interestingly not only covalent modifications can regulate substrate recruitment, but also non-covalent binding of regulators (**Figure 6F**). For instance, interaction with iron or plant hormones like auxin and jasmonate can trigger the binding between F-box proteins and substrates by filling the gaps between these proteins (Sheard et al. 2010; Tan et al. 2007). Although modifications often play an activating role in substrate recruitment, there are also cases where the opposite is true (**Figure 6G**). For example, Cdt2 and

p85β cannot be recognized by their corresponding F-box proteins as long their degrons are phosphorylated (Shafi Kuchay et al.; Skaar et al. 2013).

Furthermore, not all substrates are recognized by F-box proteins via short degron motifs. Instead recognition can also be mediated by conserved domain structures (**Figure 6H**). For instance, FBXO4 binds its substrates cyclin D1 and TRF1 in a domain-dependent manner. TIN2 can bind TRF1 via the same domain and thereby can block the access of TRF1 to FBXO4 (Skaar et al. 2013).

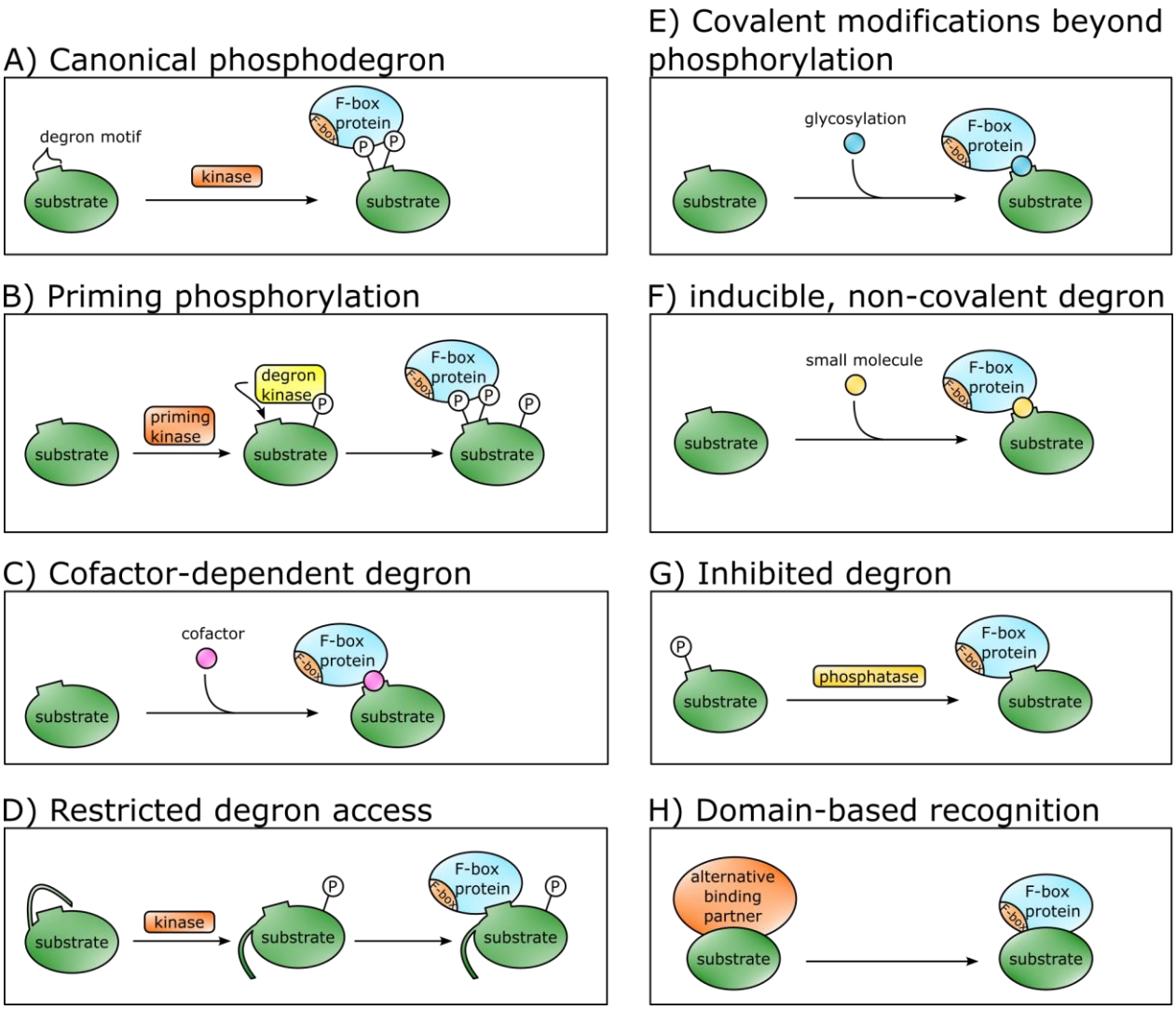

Figure 6 | Substrate recognition mechanisms of SCF complexes
Substrates are recognized by F-box proteins in different ways. **A)** Recognition of substrates can be mediated by canonical motifs, in which certain amino acids are phosphorylated, which allows binding of F-box proteins. **B)** In some cases, a priming kinase phosphorylates substrates, which in turn allows phosphorylation of other amino acids by a degron kinase. Only then recognition by an F-box protein is possible. **C)** Cofactors such as Cks1 can be a precondition for efficient recognition of substrates by F-box proteins. **D)** Some substrates initially adopt a tertiary structure, which shields a degron motif. After phosphorylation of specific amino acids, the structure changes and the degron is accessible for the F-box protein. **E)** Not only phosphorylation, but also other covalent modifications such as glycosylation can mediate substrate recognition. **F)** Even non-covalent binding of small molecules such as iron or plant hormones can arrange the interaction between substrates and F-box proteins. **G)** Although phosphorylation is frequently a requirement for substrate recognition, in some cases it acts in the opposite way by preventing binding of substrates to F-box proteins. **H)** Substrate recruitment can not only be mediated by short degron motifs. Also, domains are used, which sometimes can not only bind to the F-box protein, but to alternative binding partners as well. Figure assembled from data in (Skaar et al. 2013).

2.7 The Anaphase-promoting complex/cyclosome (APC/C)

The anaphase-promoting complex/cyclosome (APC/C) is a large E3 ubiquitin ligase that belongs to the RING class. The APC/C is essential for regulation of the mitotic cell cycle. It controls the onset of anaphase as well as mitotic exit. In addition, it is also plays a role for entry into S phase and for meiosis (Irniger et al. 1995; King et al. 1995; Sudakin et al. 1995; Tugendreich et al. 1995). Also, cell cycle independent APC/C functions such as dendrite formation in neurons are known (Alfieri et al. 2017; Herrero-Mendez et al. 2009).

The APC/C of vertebrates has a molecular weight of 1.22 MDa and consists of 14 different subunits (**Figure 7**). Since 5 subunits are present in 2 copies, the total number of subunits is 19. The complex can be structured into three domains: the platform, the catalytic core and the tetratricopeptide repeat (TPR) lobe (Sivakumar and Gorbsky 2015). The platform serves as a base for joining other subunits of the APC/C. The catalytic core is involved in substrate recruitment. However, also other proteins, namely co-activators are needed for this process. Part of the catalytic core are Apc11, the RING domain subunit (ortholog of Rbx1 in CRLs) and Apc2, the cullin subunit (Zachariae et al. 1998b; Alfieri et al. 2017). The TPR lobe comprises multiple structurally related proteins with numerous TPRs. In addition, this lobe contains TPR accessory factors, which stabilize APC/C subunits in the TPR lobe. The functions of this lobe are assembly of the APC/C as well as interactions with regulatory proteins (Herzog et al. 2009; Zhang et al. 2013).

In vertebrates, the initiating E2 UBCH10 mediates binding of the first ubiquitin to APC/C substrates by binding to the RING domain of the APC/C subunit APC11 (Brown et al. 2014; Williamson et al. 2011). The E2 UBCH5 can also have this function, at least *in vitro* (Williamson et al. 2011; Sivakumar and Gorbsky 2015). Thereafter, the elongating E2 UBE2S catalyzes attachment of further ubiquitins to the already bound ubiquitin. To this end, UBE2S binds to APC11 as well as to other components of the catalytic core and platform (Sivakumar and Gorbsky 2015; Brown et al. 2014). In higher eukaryotes, the APC/C generates by means of UBE2S K11-linked or mixed K11- and K48-linked chains that are both recognized and degraded by the 26S proteasome (Matsumoto et al. 2010; Jin et al. 2008a; Wu et al. 2010).

For full activity of the APC/C binding of co-activators – Cdc20 (Fzy in *Drosophila*) or Cdh1 (Fzr in *Drosophila*) is needed. Both co-activators contain a WD40 domain in their C termini, which is essential for recruitment of APC/C substrates (Kraft et al. 2005; Kimata et al. 2008). However, Cdc20 and Cdh1 also enhance the interaction of the APC/C with E2-ubiquitin and can therefore promote ubiquitination (Brown et al. 2014; van Voorhis and Morgan 2014; Sivakumar and Gorbsky 2015). Cdc20 and Cdh1 interact and activate the APC/C at different time periods as discussed below.

APC/C substrates contain short linear motifs (SLiMs) known as degradation sequences (degrons), through which they specifically interact with the APC/C-co-activator complex (Bansal and Tiwari 2019). The most

common degrons are the D-box (RxxLx[D/E][Ø]xN[N/S]) and the KEN-box (KENxxx[N/D]), where "Ø" is a hydrophobic and "x" is any amino acid (Bansal and Tiwari 2019; Sivakumar and Gorbsky 2015). Substrates with a D-box bind to both the WD40 domain (between the blades of the propeller) of the co-activator and to the APC/C subunit APC10. By this bipartite binding, interaction with the substrate is increased and the processivity of the ubiquitination reaction is enhanced (He et al. 2013; da Fonseca et al. 2011). On the other hand, the KEN-box only binds to the WD40 domain (top of the propeller) of the co-activator (He et al. 2013; Chao et al. 2012). Beside the D- and KEN-box, there are other APC/C degrons such as the ABBA motif or the O-, G-, A- and the CRY-box (Pines 2011; Sivakumar and Gorbsky 2015; Di Fiore et al. 2015). Strikingly, the degrons alone are not sufficient for recognition (Matyskiela et al. 2009; He et al. 2013). Substrates also contain additional non-conserved sequences that mediate finetuned timing of substrate degradation (Matsusaka et al. 2014). Not only the amino acid sequence, but also post-translational modifications (PTMs) regulate the timing of APC/C substrate degradation. For instance, phosphorylation sites are often present near or in the D-box of APC/C substrates and seem to be essential for finetuning the degradation time (Holt et al. 2009). Ubiquitination is usually promoted by phosphorylation of the acidic residue at position +6 of the D-box, whereas phosphorylation of the basic residue at position +2 of the D-box inhibits degradation (Alfieri et al. 2017).

A brief overview of APC/C regulation during the cell cycle is given below. First, predominantly Cdk1-cyclin B phosphorylates APC/C subunits, which allows binding and activation by Cdc20 (Yang and Ferrell 2013; Sivakumar and Gorbsky 2015). APC/C-Cdc20 can now target Nek2A and cyclin A for degradation in prometaphase. However, other APC/C-Cdc20 substrates such as cyclin B and securin are initially protected against degradation by the spindle assembly checkpoint (SAC). The exact mechanism of the SAC will not be described here. How prometaphase targets such as Cyclin A and Nek2 are not affected by the SAC, is currently under investigation. However, it seems that the primary mechanism is the ability of prometaphase substrates to use not the D- and KEN-box, but other sequences to bind to the APC/C (Sivakumar and Gorbsky 2015). Only after all sister chromatids are properly attached to the kinetochore in metaphase, the SAC is silenced. Degradation of Securin frees Separase, which can cleave the cohesin subunit kleisin on the sister chromatids (Uhlmann et al. 2000). Degradation of Cyclin B reduces the kinase activity of Cdk1, which in turn allows dephosphorylation and thus activation of Separase (Stemmann et al. 2001; Gorr et al. 2005; Holland and Taylor 2006). This allows the separation of sister chromatids and therefore anaphase can be initiated. Reduced kinase activity also allows dephosphorylation of Cdh1, which is a requirement for binding to the APC/C. APC/C-Cdh1 targets Cdc20 for ubiquitination. By this mechanism

APC/C-Cdc20 is replaced by APC/C-Cdh1 at the end of mitosis. APC/C-Cdh1 has the same substrates as APC/C-Cdc20, but can also recognize additional substrates (Alfieri et al. 2017; Floyd et al. 2008).

To exit mitosis also other substrates such as PLK1 and Aurora kinases are ubiquitinated by APC/C-Cdh1 after they have fulfilled their functions in telophase and cytokinesis (Lindon and Pines 2004; Littlepage and Ruderman 2002). APC/C-Cdh1 also targets S and M cyclins as well as regulators of replication such as ORC1, CDC6 and Geminin. This prevents premature entry into S phase (Araki et al. 2003; Pines 2011) . APC/C-Cdh1 stays active until the end of G1 phase and is then inactivated by different mechanisms: 1) APC/C-Cdh1 can inactivate itself by ubiquitination of the E2 UbcH10 (Rape and Kirschner 2004). 2) In addition, Cdh1 can be auto-ubiquitinated by APC/C-Cdh1 (Listovsky et al. 2004) . 3) cyclin E- or cyclin A-Cdks can phosphorylate Cdh1 and prevent it from binding to the APC/C (Zachariae et al. 1998a; Jaspersen et al. 1999). 4) Furthermore, inhibitors such as Emi1 in vertebrates and Rca1 in *Drosophila* can bind and inhibit APC/C-Cdh1 (Grosskortenhaus and Sprenger 2002; Reimann et al. 2001).

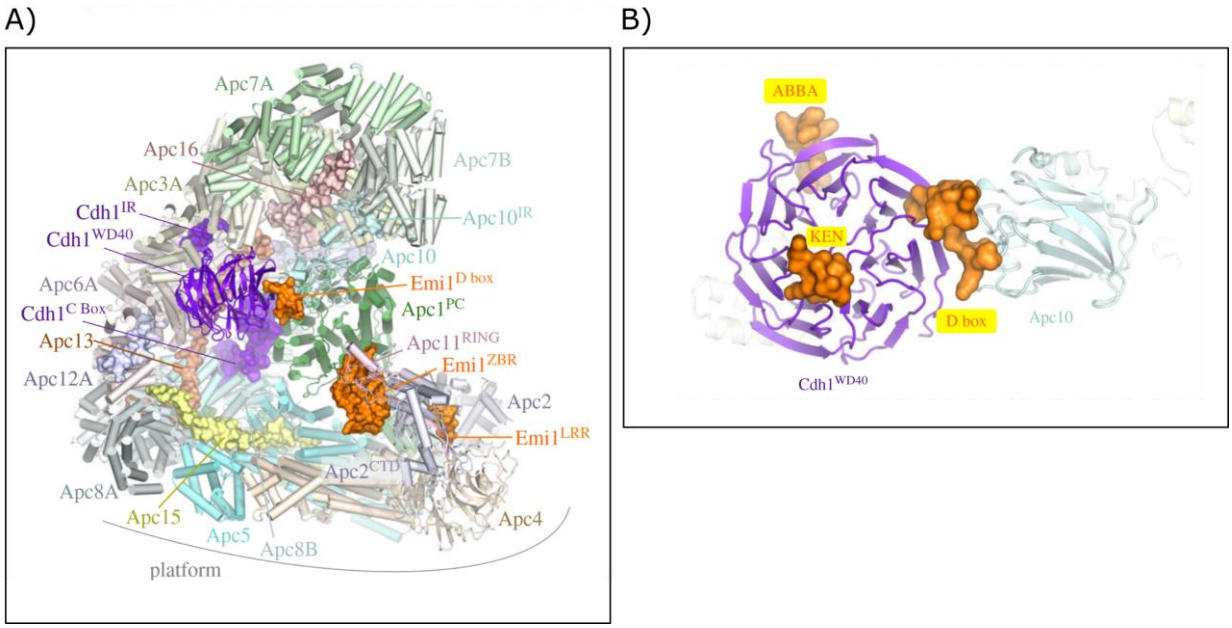

Figure 7 | Structure and substrate recognition of the APC/C
A) Structure of the human APC/C-Cdh1-Emi1 complex. Emi1, parts of Cdh1 and APC10 as well as small APC/C subunits (APC12, APC13, APC15, APC16) are represented as space filling depictions. Large APC/C subunits are shown as cartoons. The TPR subunits APC3, APC6, APC7, APC8 and APC12 exist as homodimers and are marked accordingly with the suffixes "A" and "B". The catalytic module of the APC/C consists of $APC2^{CTD}$ and $APC11^{RING}$, whereas the substrate recognition module is formed by Cdh1 and APC10. PDB 4UI9. **B)** Close-up representation of the D-box co-receptor, which is generated by Cdh1 and APC10. The D-box is recognized by both the WD40 domain of Cdh1 ($Cdh1^{WD40}$) as well as APC10. In contrast, the KEN-box and the ABBA motif are solely recognized by $Cdh1^{WD40}$. Figure modified from (Alfieri et al. 2017).

2.8 Emi1

Emi1 (early mitotic inhibitor 1) is an inhibitor of the APC/C-Cdh1 during S and G2. This leads to the stabilization of geminin, cyclin A and cyclin B thereby promoting S phase and preventing prereplication (Di Fiore and Pines 2007; Machida and Dutta 2007). Although Emi1 can also inhibit the APC/C-Cdc20 *in vitro*, *in vivo* data suggests that the inhibition of the APC/C-Cdh1 is more prominent and important. In addition, Emi1 has a second function as an F-box protein, where it targets Rad51 for degradation (Marzio et al. 2019).

Emi1 inhibits the APC/C-Cdh1 by means of the interplay of several domains in its C-terminus: D-box, linker, zinc binding region (ZBR) as well as an RL tail (**Figure 8A**). The D-box binds in the vicinity of Cdh1 and APC10 and thereby blocks the access of APC/C substrates (Frye et al. 2013). In this manner the D-box gives Emi1 the function as a pseudo substrate inhibitor. However, the D-box has only a modest effect on substrate competition in comparison to other substrates such as Hsl1 and securin. Only the contribution of the other mentioned domains in the C-terminus makes Emi1 a strong inhibitor (Frye et al. 2013; Wang and Kirschner 2013).

The ZBR can inhibit Ubch10 catalyzed multiple monoubiquitylation as well as chain elongation, and the latter can be inhibited more efficiently. An Emi1 mutant, which still contained the ZBR domain but not a C-terminal part beyond also failed to inhibit ubiquitination by either Ubch10 or UbcH5. Therefore, the C-terminal tail of Emi1 is might crucial to position the ZBR in the right place (Wang and Kirschner 2013). The linker between the D-box and the ZBR is also essential for inhibition, and it is assumed that this is due to the right positioning of the ZBR (Yamano 2013).

The RL-tail inhibits chain elongation by Ube2S (and UbcH10). Kinetic analyzes suggests that this inhibition occurs in a competitive manner. Both the RL-tail of Emi1 and Ube2S C terminus can interact with the APC/C subunit APC2. Furthermore, the RL-tail and the C terminus of Ube2S are rich in basic residues and are similar in their amino acid sequence. Therefore, it is assumed that the RL tail inhibits the activity of Ube2S by abolishing the interaction between Ube2S and APC2 (Wang and Kirschner 2013).

Summarized, Emi1 protects APC/C substrates from degradation mainly by inhibiting ubiquitin chain elongation. It is thought that DUBs synergize with this mechanism, since many of them seem to prefer monoubiquitinated substrates (Wang and Kirschner 2013).

Emi1 also has a F-box domain (**Figure 8A**). Although most F-box proteins act as substrate receptors of SCF complexes, this is not always the case. Instead, some (e.g. FBXW8, FBXL10, FBXL11) are incorporated into atypical protein complexes and show enzymatic activities distinct from that of E3 ubiquitin ligases (e.g. histone de-methylase activity for FBXL10 and FBXL11) (Skaar et al, 2013; Marzio). Since the discovery of Emi1, the function of Emi1´s F-box was not known for almost 20 years. In 2019 it was finally found out that

Emi1 is indeed part of an SCF complex that targets Rad51 for degradation. Skp1, Cul1 and Rbx1 co-precipitate with Emi1 in an F-box dependent manner. In addition, Emi1 only interacts with Cul1, but not with other members of the cullin family. Emi1 is a substrate of SCF-βTrCP (see below). To exclude that the interaction of Emi1 with Cul1 is dependent on SCF-βTrCP, Emi1(ΔDSG) – a mutant that lacks the βTrCP recognition motif - was used for co-IP experiments. Emi1(ΔDSG) is still able to efficiently co-immunoprecipitate Cul1. Furthermore, only immunoprecipitated Emi1, but not Emi1(ΔFbox) produces polyubiquitin chains *in vitro*. By means of mass spectrometry Rad51 was identified as a potential substrate of SCF-Emi1. To confirm this, co-IP experiments were conducted. Amongst 14 different F-box proteins only Emi1 can co-immunoprecipitate endogenous Rad51, which confirms the specificity of the binding. In addition, expression of Emi1 promotes Rad51 degradation and knockdown of Emi1 leads to higher levels of Rad51 *in vivo*. In contrast, expression of Emi1(ΔFbox) has no significant influence on Rad51 levels. Finally, it could be shown that Rad51 can be ubiquitinated by Emi1 in an F-box dependent manner *in vivo*. SCF-Emi1 targets Rad51 in a constitutive manner. However, upon genotoxic stress Rad51 is phosphorylated on Thr309 by Chk1, which increases its affinity for BRCA2. This in turn, protects Rad51 from SCF-Emi1 dependent degradation. This causes accumulation of Rad51 allowing efficient homologous recombination repair (HRR) (Marzio et al. 2019).

Emi1 activity during the cell cycle is regulated by transcription, stabilization, deactivation as well as degradation of Emi1 (**Figure 8B**). At the G1/S transition Emi1 is transcriptionally induced by the transcription factors E2F-1 and E2F-3 (Hsu et al. 2002). This initiates the inhibition of the APC/C-Cdh1 during S and G2 phase. This inhibition as well as transcriptional upregulation of cyclin A allows cyclin A accumulation, which activates Cdk2. CycA/Cdk2 then phosphorylates Cdh1, which in turn contributes to the inactivation of the APC/C-Cdh1 (Hsu et al. 2002).

Emi1 is a target of SCF-βTrCP. However, Emi1 degradation via this E3 is prevented in S and G2 by Evi5. Evi5 binds to a site adjacent to the DSGxxS phosphodegron thereby blocking phosphorylation by Polo-like kinases, which is a requirement for subsequent binding to βTrCP. Evi5 accumulates in early G1 and is degraded in early mitosis by an unknown E3 (Eldridge et al. 2006). Degradation of Evi5 is dependent on Plk1, just like for Emi1. Interestingly, stabilized Evi5 mutants cannot stabilize Emi1 in mitosis. This suggests that an additional inactivation step, for instance phosphorylation of Emi1 or Evi5 abolish the interaction between these proteins allowing phosphorylation by Plk1 (Eldridge et al. 2006).

In prophase, SCF- βTrCP can start to target Emi1 for degradation. To this end, Plk1 directly binds Emi1, likely through the S-pS_{149} sequence (PBD; Polo Box domain) of Emi1´s phosphodegron. It is assumed that S149 as well as other amino acids of Emi1 are phosphorylated by Cdk1 and possibly other kinases, which

contribute to binding of Plk1. In addition, Plk1 phosphorylates Emi1, likely amongst others on serine 145. All these binding and phosphorylation events by Cdk1, Plk1 and possibly other mitotic factors allow binding of Emi1 to βTrCP. It is assumed that these events occur simultaneously rather than in a processive manner. Furthermore, there are hints that some amino acids within the phosphodegron of Emi1 are helpful, but not essential. For instance, mutation of glutamate-143 only has a mild influence on the destruction of Emi1. Interestingly, overexpression of Plk3 can cause reduction of Emi1 levels. Therefore, it seems that Plk1 is supported by Plk3. On the other hand, Plk2 has no influence on Emi1 (Hansen et al. 2004).

The influence of Plk1 on Emi1 is also regulated in a spatial manner. Plk1 is recruited to the centrosome, whereas Emi1 is directed to the spindle poles, which are in the immediate vicinity. It was suggested that Emi1 could be actively transported along spindle microtubules to a "destruction center" at the centrosome, where phosphorylation and ubiquitination of Emi1 takes place. As an alternative, it was considered whether Emi1 could be a more static and functional component of the mitotic spindle. At first glance, it is counterintuitive that Emi1 should persist on the spindle when Plk1 is active and the majority of Emi1 is destroyed (Hansen et al. 2004). However, there is a similar example with cohesin, which is removed from chromatin whereas a small pool of cohesin is maintained at kinetochores (Waizenegger et al, 200 in Hansen). Indeed, spindle-associated Emi1 plays a role in protecting cyclin B from degradation at mitotic spindles. The mechanisms, which play a role in this, are summarized in the term "END network" (Emi1/NuMA/dynein-dynactin). First, Cdk1 phosphorylates NuMA, which is a dynein cargo protein. This enables NuMA to bind Emi1 and transport it to spindle poles by means of the dynein-dynactin motor complex. It is important to mention that also a part of APC/C complexes is localized at the poles. Emi1 in this pool is protected from bulk destruction after nuclear envelop breakdown. This leads to APC/C inhibition and in turn to protection of spindlepole-associated cyclin B. Cdk1/cyclin B can than sustain the phosphorylated state of NuMA, which is a requirement for its function (integration of microtubule arrays at the poles). Therefore, the Cdk1/cyclin B dependent assembly of the END network and the stabilization of cyclin B by the END network create a positive feedback loop to enable NuMA-dependent anchoring of microtubules at spindle poles (Ban et al. 2007).

Besides the degradation of Emi1 by SCF-βTrCP another degradation pathway via the APC/C-Cdh1 itself was proposed. In this model Emi1 switches from being a substrate to an inhibitor of the APC/C-Cdh1 in a concentration dependent manner. First, it was found out that low levels of Emi1 in G1 phase are due to degradation of Emi1 since treatment with the proteasome inhibitor MG132 increases Emi1. It is unlikely that this degradation is mediated by SCF-βTrCP considering that this E3 is active in pro-metaphase and not in G1 phase (Margottin-Goguet et al. 2003; Cappell et al. 2018). Instead, both *in vivo* and *in vitro*

experiments showed that Emi1 is a direct target of the APC/C-Cdh1. In *in vitro* ubiquitination assays APC/C-Cdh1 can ubiquitinate Emi1 if its concentration is low (23 nM). Among other things based on structural data and computational models the following model for the switch was proposed: Emi1 reversibly binds to a low-affinity substrate-binding site of the APC/C-Cdh1. Here mono- and poly-ubiquitination of Emi1 can take place in a non-processive manner. In this context it is important to mention that Emi1 is a distributive substrate meaning that poly-ubiquitination requires several encounters of Emi1 with APC/C-Cdh1. In addition, Emi1 reversibly binds to an inhibitory site of the APC/C-Cdh1 with higher affinity to suppress poly-ubiquitination of substrates. If Emi1 levels are lower than APC/C-Cdh1 levels Emi1 as well as other substrates can be ubiquitinated by APC/C-Cdh1, which is not inhibited by Emi1. With increasing levels of Emi1, the inhibitory site is progressively inhibited so that poly-ubiquitination of Emi1 and other substrates is hardly possible. The fact that Emi1 acts as both substrate and inhibitor of the APC/C-Cdh1 creates a dual-negative feedback loop, which is required for rapid and irreversible inactivation of the APC/C-Cdh1 and therefore cell-cycle commitment. In contrast, cyclin E/Cdk2 alone is at least in some cell lines not sufficient to inhibit the APC/C-Cdh1 so strongly that irreversibility is achieved. Interestingly, *in vitro* ubiquitination assays showed a concentration-dependent ubiquitination for Emi1 also using APC/C-Cd20 indicating that Emi1 is a substrate of the APC/C-Cdc20 as well (Cappell et al. 2018).

Emi1 activity cannot only be abolished through degradation, but also inactivating phosphorylation of Emi1 by Cdks. Notably, this phosphorylation was only observed in mitotic but not S phase cell extracts. By Cdks phosphorylated Emi1 can neither form a stable complex with the APC/C nor inhibit it. Furthermore, the addition of S-phase cell extracts to mitotic cell extracts can protect Emi1 from Cdk-mediated inactivation. This suggests that there is a protective factor in S phase cells. However, the identity of this factor is not known so far (Moshe et al. 2011).

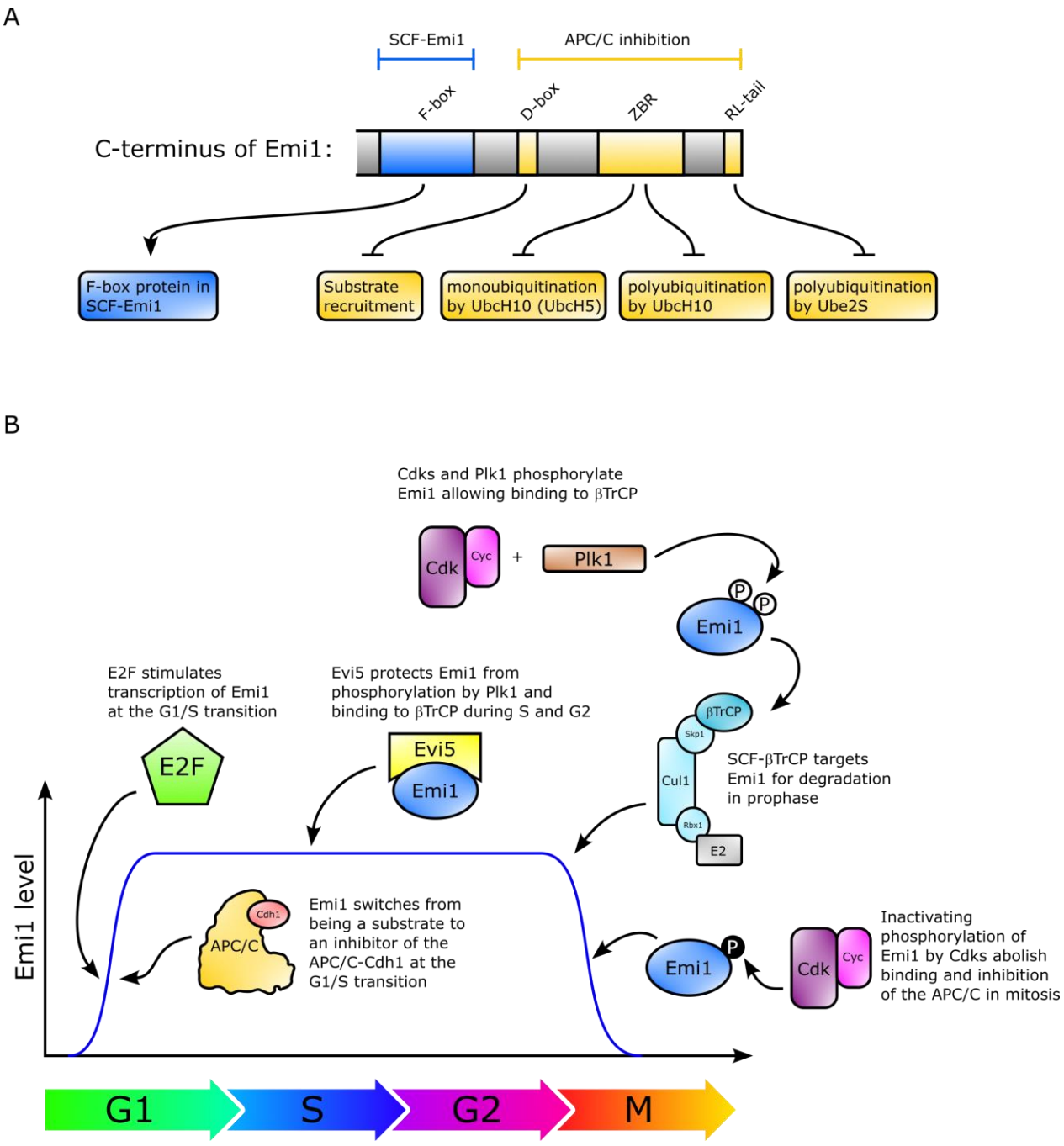

Figure 8 | Function and regulation of Emi1

A) Functions of Emi1: Emi1 is an inhibitor of the APC/C. Several domains mediate this inhibition by different mechanisms. In addition, Emi1 can act as a F-box protein in SCF-Emi1 via its F-box domain. So far, the only known substrate of SCF-Emi1 is Rad51. **B)** Regulation of Emi1: Emi1 is only active in S and G2 of the cell cycle. This is ensured by numerous mechanisms such as transcriptional control, degradation, and deactivation of Emi1. Figure assembled from data in (Yamano 2013; Marzio et al. 2019; Hsu et al. 2002; Eldridge et al. 2006; Hansen et al. 2004; Cappell et al. 2018; Moshe et al. 2011)

2.9 Rca1 – the *Drosophila* homolog of Emi1

Rca1 (Regulator of cyclin A1) is the homolog of Emi1 in *Drosophila* and shares 16 % amino acid sequence identity (25% similarity) with it. Both proteins have a similar size and placement of functional domains is comparable (Reimann et al. 2001) (**Figure 9**). Like Emi1 Rca1 is both an inhibitor and a substrate of APC/C-Fzr (Fzr = *Drosophila* homolog of Cdh1) (Grosskortenhaus and Sprenger 2002; Polz 2021). In addition, Rca1 also contains an F-box for which it was shown that it is essential for the interaction with SCF components and it was postulated that Rca1 is involved in regulating the G1/S transition (Zielke et al. 2006). However, no substrate of SCF-Rca1 could be identified so far.

In *Drosophila* Cdk activity in G2 is very low. Consequently, Fzr cannot be efficiently phosphorylated and would activate the APC/C. However, APC/C-Fzr activity in G2 is restricted by Rca1. This allows accumulation of CycA and therefore entry into mitosis. Rca1 also enables enrichment of CycB. However, only supplying additional CycA but not CycB is able to rescue the mitotic failure of Rca1 mutants. This could indicate that CycA and not CycB is the essential factor for triggering mitosis. However, CycB also disappears in CycA mutants and Rca1 can restore mitosis in CycA mutants (Dienemann and Sprenger 2004). This indicates that CycA is not essential for triggering mitosis, but CycA is required to inhibit Fzr activity (Dienemann and Sprenger 2004). There are indications that Rca1 specifically inhibits APC/C-Fzr and not APC/C-Fzy (Fzy = *Drosophila* homolog of Cdc20): Overexpression of Rca1 during the first 16 cell cycles in *Drosophila* where mainly Fzy is the main activator of the APC/C has no influence on cell cycle progression or cyclin degradation. Furthermore, coimmunoprecipitation showed that only Fzr but not Fzy can interact with Rca1 (Grosskortenhaus and Sprenger 2002).

In *Drosophila* embryos the role of Rca1 strongly alters during development. During the first 15 divisions CycE/Cdk2 is active throughout the cell cycle, including G2 (Knoblich et al. 1994). In cell cycle 16 CycE mRNA is downregulated and Dacapo, which is an inhibitor of CycE/Cdk2, is upregulated (de Nooij et al, 1996; Knoblich et al., 1994; Lane et al., 1996). This leads to an abolishment of CycE/Cdk2 activity in G2. In addition, Cdk1 is inhibited during G2 (Edgar et al., 1994). Therefore, Cdk1 and Cdk2 cannot phosphorylate Cdh1 in G2, which would prevent association with the APC/C. Thus, from G2 of cell cycle 16, Rca1 becomes essential replacing the inhibition mechanism via phosphorylation of Fzr. In agreement to this, Rca1 was dispensable when CycE was overexpressed during cell cycle 16 (Grosskortenhaus and Sprenger 2002).

Overexpression of Rca1_Del-1-203, which lacks the whole N terminus including the F-box, can restore mitosis of cell cycle 16 in Rca1 mutant cells. The same is true when Rca1 with a small deletion, removing the F-box domain, is overexpressed. This suggests that neither the N terminus (aa 1-203) nor the F-box are essential for inhibition of the APC/C-Fzr. In contrast, Rca1_Del-1-255 and Rca1_C346S (mutation in the ZBR) abolished Rca1 activity arguing that a C-terminal fragment (aa 255-411) with intact ZBR is sufficient

for APC/C inhibition (Zielke et al. 2006). In the C-terminus of Rca1 similar domains are involved in APC/C inhibition as for Emi1, namely a KEN- and a D-box as well as the ZBR and the RL tail. Mutation of the KEN- or D-box only have a modest effect on APC/C inhibition, whereas the ZBR (strong effect) and the RL tail (complete abolishment of the APC/C) are more important (Polz 2021). This suggests that the mechanisms for APC/C inhibition could be similar as for Emi1. However, to elucidate the concrete molecular mechanisms that are involved here, further experiments such as an *in vitro* ubiquitination assay are required.

At the end of mitosis APC/C-Cdc20 (Fzy) is replaced by APC/C-Cdh1 (Fzr), which stays active until the end of G1 (Sivakumar and Gorbsky 2015). Therefore, in this period, Rca1 must not be present or at least not be active. For Emi1 this problem is mainly solved by degradation via SCF-βTrCP at the beginning of mitosis (see chapter 2.8). In contrast, Rca1 seems not to be a substrate of SCF- βTrCP since mutations of putative phosphorylation sites in the respective predicted phosphodegron of Rca1 do not influence Rca1 stability (Radermacher 2007; Zielke et al. 2006; Morgenthaler 2013; Polz 2021). Furthermore, degradation of Rca1 only begins in early G1 and not at the entry into mitosis (Morgenthaler 2013; Grosskortenhaus and Sprenger 2002). Rca1 shows a similar degradation kinetic than APC/C-Fzr substrates such as geminin (Morgenthaler 2013; Polz 2021). This gave rise to the hypothesis that Rca1 could not only be an inhibitor but also a substrate of the APC/C-Fzr. In agreement to this, Rca1 stability decreases after overexpression of Fzr and inreases after knockdown of Fzr. In addition, mutation of sequences that are known to be important for APC/C degradation (degrons) leads to stabilization of Rca1 in G1. More precisely, two D-boxes, two KEN-boxes (one of which is non-canonical) and possibly an ABBA motif were found to mediate degradation of Rca1. Interestingly, also the RL-tail of Rca1 contributes to its degradation since mutation of this motif causes a complete stabilization of a C-terminal Rca1 fragment and a partial stabilization of full-length Rca1. Therefore, the RL-tail seems to have a dual role in both APC/C inhibition and degradation (Polz 2021).

For Emi1 it was shown that the switch between inhibitor and substrate of the APC/C-Cdh1 is dependent on its own concentration (see chapter 2.8). After initial degradation of Emi1 by SCF-βTrCP the concentration of Emi1 is low enough to allow further degradation via the APC/C-Cdh1 in G1. For Rca1 this kind of switch is not plausible since Rca1 levels are very high at the beginning of G1 when APC/C-Fzr dependent degradation starts. In addition, in the studies in which APC/C-Fzr dependent degradation of Rca1 was seen, Rca1 was overexpressed. Initial studies showed that phosphorylation, interaction with the protein 14-3-3 as well as nuclear localization of Rca1 play a role in mediating the switch. However, further experiments are needed to elucidate the exact process (Polz 2021).

Rca1, like Emi1, harbors an F-box, enabling its coprecipitation with the SCF component SkpA (= *Drosophila* homolog of Skp1). This interaction is F-box dependent since Rca1_ΔFbox failed to do so. Furthermore, co-IPs revealed that also Cul1 interacts with Rca1 in an F-box dependent manner (Zielke et al. 2006). In addition, SkpA and Cul1 were identified as interaction partners of Rca1 by means of mass spectrometry (M. Kies 2017). Taken together, this suggests the existence of an SCF-Rca1 complex.

Overexpression of Rca1 can induce ectopic S phase during eye development, causing a "rough eye" phenotype in flies. It is noteworthy that while Rca1_Del-1-203 and Rca1_ΔFbox retain the ability to inhibit the APC/C, they were unable to induce such ectopic S phases. This suggests that SCF-Rca1 mediates the degradation of a negative regulator of S phase entry. A potential candidate for this regulator was Fzr. Since APC/C-Fzr is essential for the establishment of G1, degradation of Fzr caused by overexpressed Rca1 could lead to premature S phase entry. However, no changes in Fzr levels were observed upon coexpression of Rca1 indicating that Fzr is not a substrate of SCF-Rca1 (Zielke et al. 2006). Another potential substrate of SCF-Rca1 is spn-A (*Drosophila* homolog of Rad51) since Rad51 is targeted by the human homolog SCF-Emi1 (Marzio et al. 2019). However, analysis in Schneider cells shows that spn-A levels are not influenced by overexpression or knockdown of Rca1 (Richard Bach 2023). In addition, since spn-A is needed for DNA repair it is unlikely that degradation of this protein would cause S phase induction (Staeva-Vieira et al. 2003).

A promising candidate for SCF-Rca1 mediated degradation is the CycE/Cdk2 inhibitor Dacapo (Dap) (see chapter 2.12). In *Drosophila* eye discs the G1/S transition is mediated by CycE/Cdk2 (Richardson et al. 1995). Degradation of Dap could allow CycE/Cdk2 to become active thereby enabling the G1/S transition. Initially, it was observed that Dap levels do not decrease after overexpression of Rca1 which would speak against Dap being a substrate of SCF-Rca1 (Zielke et al. 2006). However, this result must be questioned since the anti-Dap staining used for the underlying experiment could have been unspecific. Furthermore, there are several hints that Dap is indeed a substrate of SCF-Rca1: For instance, co-IPs revealed that Rca1 and Dap constructs can interact with each other (M. Kies 2017). However, it must be emphasized that this alone is no proof that Dap is a substrate of SCF-Rca1. The interaction between these proteins could also rely on other functions of Dap or Rca1. In addition, flow cytometry analysis of Schneider cells suggested that Rca1 causes instability of Dap_dCDI_dPIPa in an F-box dependent manner (M. Kies 2017). The dCDI mutation abolishes interaction with CycE/Cdk2 rendering Dap cell cycle inert. The dPIPa mutation blocks degradation via the E3 ubiquitin ligase CRL4-Cdt2 (see chapter 2.10), for which it is already known that Dap is a substrate of it (Swanson et al. 2015). However, for these stability analyzes the reference protein GFP and Dap_dCDI_dPIPa fused to CHE were expressed from different promotors. This leads to non-

stoichiometrically expression of these proteins and therefore a high variance of the obtained results. This in turn, makes a reliable statement difficult. In addition, ligase trapping – a method, which enables the co-precipitation of ubiquitinated substrates of E3 ubiquitin ligases – was not successful for Dap so far. Taken together, there are promising hints that Dap is indeed a substrate of SCF-Rca1, but more experiments are needed to confirm this hypothesis.

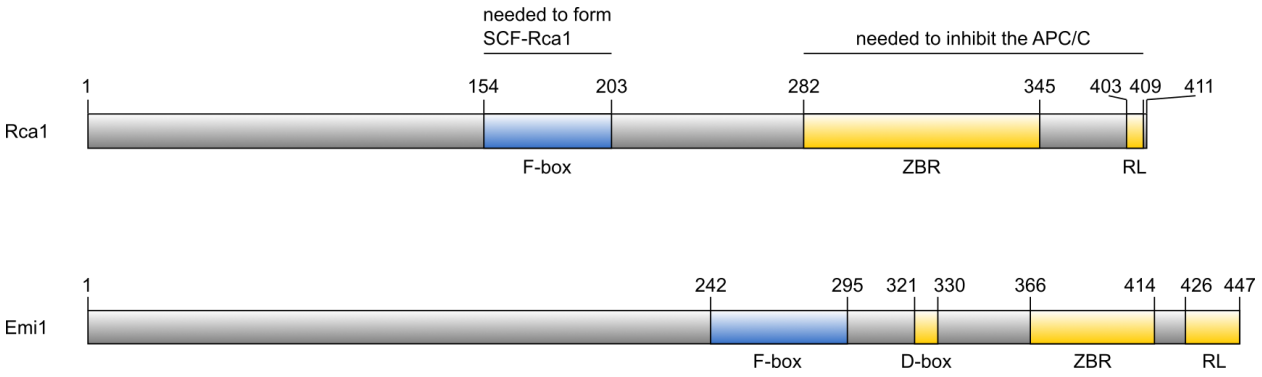

Figure 9 | Schematic illustration of Rca1 and its human homolog Emi1
Rca1 and Emi1 share similar domains and functions. Both can be incorporated into an SCF complex via their F-boxes (depicted in blue). In addition, they can inhibit the APC/C via domains in the C-terminus (depicted in yellow). For simplicity, in case of Rca1 only the Zinc binding region (ZBR) and the RL-tail, which are involved in APC/C inhibition are shown. However, there are a couple of other domains in Rca1, which mediate inhibition of the APC/C (not depicted). The location of the D-box and the ZBR in Emi1 was derived from (Frye et al. 2013). For the RL-tail the suggested location of (Yamano 2013) was used. The F-box was defined using the SMART database (M. Kies 2017). The domains, which are involved in APC/C inhibition in case of Rca1 were elucidated by (Polz 2021).

2.10 CRL4-Cdt2

The E3 ubiquitin ligase CRL4-Cdt2 contributes to genomic integrity by degrading essential proteins during S phase and after DNA damage. Amongst others Dap as well as its human homolog p21 are substrates of it.

CRL4 complexes use CUL4A or CUL4B as a scaffold, DDB1 as an adaptor, Rbx1 as well as one of 90 substrate receptors (also referred to as DCAF; DDB1-CUL4-associated factor). CRL4-Cdt2 uses Cdt2 as substrate receptor (Mazian et al. 2022).

CRL4-Cdt2 only can recognize its substrates in conjunction with PCNA loaded onto DNA ($PCNA^{DNA}$) (Kim et al. 2010; Havens et al. 2012). PCNA is a sliding clamp that anchors polymerases onto the DNA thereby increasing their processivity (Boehm et al. 2016). In addition, PCNA fulfils many other functions. For instance, its involved in Okazaki fragment maturation or mismatch repair (Levin et al. 1997; Umar et al.

1996). PCNA is a homotrimer with each monomer consisting of two similarly folded domains, which are connected by an interdomain-connecting loop (Krishna et al. 1994). The three monomers form a ring that can enclose DNA. This is made possible by positively charged residues, which can form electrostatic interactions with DNA (Boehm et al. 2016). PCNA is loaded onto chromatin during S phase and upon DNA damage (Shiomi and Nishitani 2017; Havens and Walter 2009).

Most proteins that interact with PCNA use a hydrophobic pocket near the interdomain-connecting loop of PCNA for this purpose (Gulbis et al. 1996; Bruning and Shamoo 2004; Hishiki et al. 2009). In addition, this interaction is normally mediated by a PCNA-interacting protein (PIP) motif located on the protein that binds PCNA (Jónsson et al. 1998; Warbrick 2000; Maga and Hubscher 2003). These motifs are sequences of eight amino acids. At position 1 a conserved glutamine is located, at position 4 a conserved aliphatic residue (leucine, isoleucine, methionine), and at positions 7 and 8 two conserved aromatic residues (phenylalanine or tyrosine). However, substrates of CRL4-Cdt2 do not contain a PIP box but a so-called PIP degron, which is needed for efficient ubiquitination. In addition to the conserved amino acids of the PIP box, the PIP degron harbors a TD motif (threonine and aspartate) at position 5 and 6 as well as a basic residue (lysine or arginine) at the fourth amino acid position downstream of the PIP box. The TD motif enables particularly strong binding to PCNA (Nakanishi et al. 1995; Warbrick et al. 1995; Chuang et al. 2005; Havens and Walter 2009). CRL4-Cdt2 substrates that lack the TD motif (e.g. Dup (*Drosophila* homolog of Cdt1) likely achieve strong PCNA binding by means of other residues (Havens and Walter 2011). The basic residue (referred to as B+4) is surface-exposed in the p21-PCNA cocrystal structure (Gulbis et al. 1996). Mutation of this residue prevents docking of CRL4-Cdt2 onto the PCNA-Cdt1 complex and abolishes degradation of Cdt1. However, the mutation does not influence the interaction between Cdt1 and PCNA (Havens and Walter 2009; Michishita et al. 2011). This suggests that B+4 mediates contact with Cdt2. Interestingly, proteins containing a PIP box can be converted into substrates of CRL4-Cdt2 by introducing the TD motif and B+4 into its PIP box (Havens and Walter 2009; Michishita et al. 2011). Furthermore, fusion of a short peptide (approx. 25 aa), which harbors the PIP-degron of human Cdt1 to GST can convert this protein into a substrate of CRL4-Cdt2 (Nishitani et al. 2006; Senga et al. 2006). This indicates that the PIP degron alone is necessary and sufficient to promote CRL4-Cdt2 dependent degradation.

For some CRL4-Cdt2 substrates also other amino acids in or next to the PIP box are crucial. For instance, in numerous substrates such as the CDK inhibitors p21 and Dap basic residues are located at the positions +3 and +5. These amino acids interact with acidic residues within PCNA in the p21-PCNA crystal structure (Gulbis et al. 1996). In agreement to this, destruction of human p21 and *Xenopus* Cdt1 was reduced in a

PCNA binding dependent manner, if B+5 was mutated (Nishitani et al. 2008; Havens and Walter 2009). It seems that only basic or polar amino acids are tolerated at this position (Havens and Walter 2011). Furthermore, in several substrates a cluster of positively charged amino acids upstream of the PIP box is located. Although these amino acids are apparently important, the underlying reason is not clear yet (Chuang and Yew 2005; Nishitani et al. 2008; Michishita et al. 2011).

CRL4-Cdt2 recognizes substrates via a bipartite surface composed of PCNA and the substrate. More precisely, B+4 in the substrate as well as D122 and E124 in PCNA contact CRL4-Cdt2. It was speculated that the PCNA-PIP-degron complex interacts with a surface of Cdt2, which harbors an arrangement of positive and negative charges. However, this was not proven so far (Havens et al. 2012).

In higher eukaryotes the N-terminus of Cdt2 contains seven WD-40 repeats that form a β-propeller structure (Panagopoulos et al. 2020; Jin et al. 2006). The C-terminus of Cdt2 harbors phosphorylation sites, the DNA binding domain (DBD) as well as a PIP-box (Mazian et al. 2022). So far, the structure of the N-terminus of Cdt2 has not been elucidated. However, it is assumed that it resembles that of another DCAF, namely DDB2 (Mazian et al. 2022). Based on the known structure of DDB2, one side of the Cdt2 N-terminus is predicted to interact with BPA and BPC, which are subunits of the adapter DDB1. The other side is thought to mediate substrate recognition (Fischer et al. 2011; Havens and Walter 2011). After the PIP degron of p21 binds to PCNA, the surface charge of the interdomain connecting loop of PCNA changes from negative to positive (Michishita et al. 2011). It is assumed that this positive charge mediates interaction with the negatively charged surface of Cdt2 (Mazian et al. 2022). It was tried to investigate the interaction between substrates and the N-terminus of Cdt2 by means of simulation with ZDOCK (Mazian et al. 2022). The results suggest that four amino acid residues (K144, R161, D381, E362) at the center of the β-propeller structure of Cdt2 interact with p21 (via S153, T148, D149, H152 and K154 (B+3)) (Pierce et al. 2014). One additional amino acid (K271) in the Cdt2 β-propeller was predicted to be involved in substrate interaction by the WDSPdb database (Wang et al. 2015). By mutating the amino acids in Cdt2 that are potentially involved in substrate recognition, the electrostatic potential of the β-propeller is highly altered. It is likely that Cdt2 with mutations of these amino acids can no longer recognize substrates. However, to confirm these predictions mutation analysis must be conducted. Interestingly, simulations also predicted that R155 (B+4) on p21 interacts with E124 on PCNA, but not on Cdt2 (Mazian et al. 2022). Although simulations indicate that the N-terminus (aa 45-400) of Cdt2 is sufficient for recruitment to the PIP-degron with bound $PCNA^{DNA}$, wet lab experiments showed that the Cdt2 N-terminus (aa 1-417) alone does not bind to this location (Hayashi et al. 2018). Consequently, substrates were not degraded without the C-terminus of Cdt2 (Mazian et al. 2019; Centore et al. 2010; Kim et al. 2008).

The C-terminus of Cdt2 contains a PIP box, which is conserved in higher eukaryotes and harbors the consensus sequence M-x-x-L/V/I/M-x-x-F/Y-F/Y) (Hayashi et al. 2018; Abbas and Dutta 2011; Leng et al. 2018). Interestingly, in *Drosophila* the first amino acid of this sequence is a glutamate (E712) instead of a methionine. This PIP box mediates interaction with PCNA and is essential for the efficient degradation of Cdt2 substrates (Havens et al. 2012; Hayashi et al. 2018; Leng et al. 2018). Only the C-terminus (aa 390-730), but not the N-terminus of Cdt2 (1-417) is crucial for recruitment of Cdt2 to PCNA (Hayashi et al. 2018). Therefore, the N-terminus of Cdt2 only seems to contact PCNA in context with substrate recognition but not with recruitment of Cdt2.

The C-terminus of Cdt2 can be phosphorylated by CDKs and this reduces binding of Cdt2 to $PCNA^{DNA}$ during late S phase (Nukina et al. 2018; Panagopoulos et al. 2020; Mazian et al. 2019). In accordance with that, Cdt2 hyperphosphorylation correlate with re-accumulation of substrates. The C-terminus (aa 420-730) of Cdt2 contains 18 S/T-P sites, which are consensus sites for CDK phosphorylation (Nukina et al. 2018). A Cdt2 mutant in which these sites were mutated (Cdt2-18A) was phosphorylated to a less content than the wildtype version. In addition, Cdt2-18A blocks re-accumulation of CRL4-Cdt2 substrate from late S phase to G2 phase (Rizzardi et al. 2015). However, the essential phosphorylation sites within these 18 S/T-P sites are not identified yet (Mazian et al. 2022).

Binding of PCNA to DNA is a requirement for the recognition of substrates by Cdt2 (Panagopoulos et al. 2020). It was speculated that the reason for this requirement is that Cdt2 must bind to DNA via its DNA binding domain (DBD) (aa 460-580) and that this is facilitated by binding of Cdt2 to DNA-bound PCNA. The region for the DBD domain was defined since a peptide containing aa 460-580 of Cdt2 can bind to DNA. After binding of Cdt2 to DNA, the DBD can cause alterations in the structure of Cdt2 (Mazian et al. 2019). Therefore, proper function of Cdt2 could depend on bipartite binding to PCNA (via PIP box) and DNA (via DBD) (Mazian et al. 2022). Degradation of Cdt1 was delayed, if DBD was replaced by a linker peptide (Mazian et al. 2019). Phosphorylation of DBD can inhibit its binding to DNA (Hirata et al. 1993; Smykowski et al. 2015; Alexander and Rizkallah 2017). It is assumed that these phosphorylations lead to electrostatic repulsion between Cdt2 and DNA (Mazian et al. 2022). The exact phosphorylation sites in the DBD, which prevent binding to DNA, are not known yet. Interestingly, Cdt2 prefers single-stranded DNA over double-stranded DNA *in vitro* (Mazian et al. 2019). This makes sense from a mechanistic point of view since PCNA is loaded onto double strand-single-strand junctions (Shiomi and Nishitani 2017).

Based on the above, the following model for the ubiquitination of CRL4-Cdt2 substrates can be created (**Figure 10**): 1) Cdt2 binds to $PCNA^{DNA}$ via its PIP box. 2) This allows binding of the DBD domain to single-stranded DNA thereby stably anchoring Cdt2 for efficient substrate recognition. 3) A substrate is recruited

to PCNA via its PIP box and independently of CRL4-Cdt2. 4) The β-propeller of Cdt2 recognizes a composite surface consisting of PCNA (D122 and E124) and the PIP-degron (B+4) of the substrate. This allows ubiquitination of the substrate. 5) Cdt2 is phosphorylated by CDKs at the end of S phase. The negatively charged phosphate groups abolish both interaction between Cdt2 and DNA as well as between Cdt2 and $PCNA^{DNA}$. CRL4-Cdt2 dissociates from the DNA and substrates are no longer ubiquitinated (Mazian et al. 2022; Havens et al. 2012).

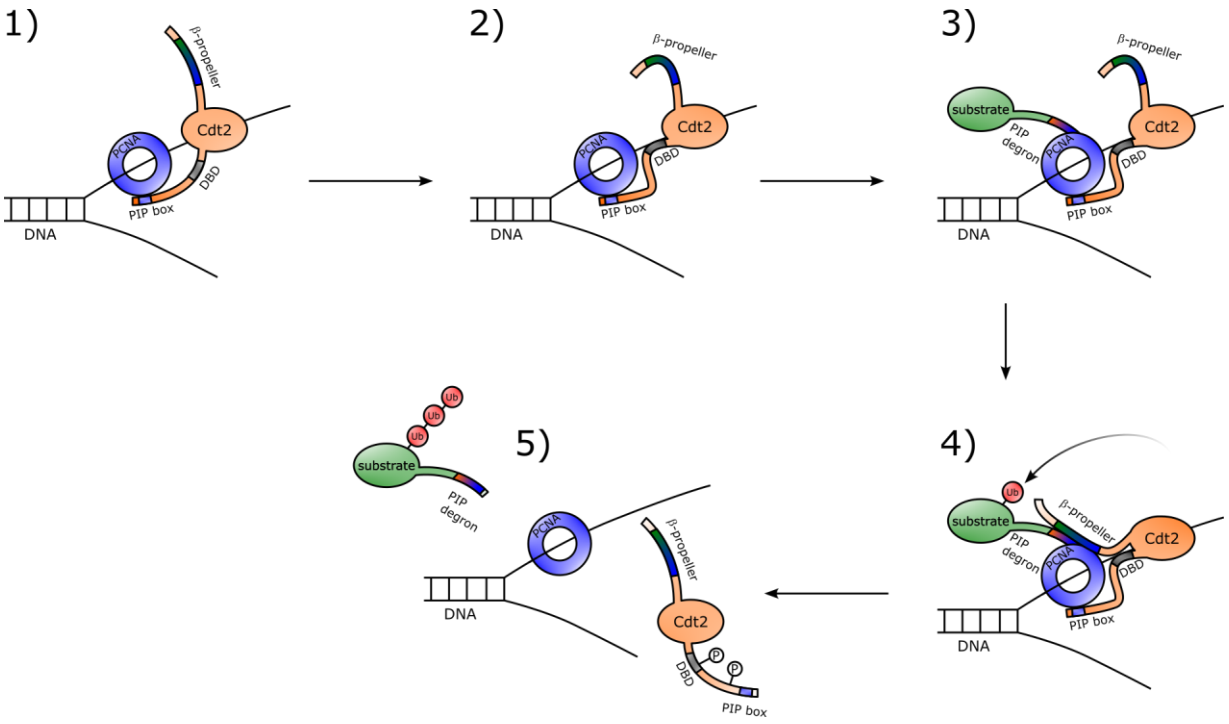

Figure 10 | Model for the recognition of substrates by CRL4-Cdt2
For clarity only the substrate recognition subunit Cdt2, but not the whole CRL4-Cdt2 complex, is shown. **1)** The PIP box of Cdt2 mediates binding to $PCNA^{DNA}$. **2)** This enables stable anchoring of Cdt2 to single-stranded DNA via the DNA binding domain (DBD). **3)** A substrate binds to PCNA via the PIP box within the PIP degron. This process is independent of CRL4-Cdt2. **4)** The center of the β-propeller of Cdt2 binds to a bipartite surface comprising PCNA and the PIP degron of the substrate (B+4). Thereafter, the substrate can be ubiquitinated by CRL4-Cdt2. **5)** At the end of S phase, the C-terminus of Cdt2 is phosphorylated. The negative charges of the phosphate groups lead to repulsion of both DNA and PCNA. This allows dissociation of the whole CRL4-Cdt2 complex. Figure assembled from data in (Mazian et al. 2022).

2.11 The CKI Dap and its human homologs p21, p27 and p57

p21 as well as p27 and p57 belong to the CIP/KIP family of cyclin-dependent kinase inhibitors (CKIs) (Murray 2004). Dacapo (Dap) is the homolog of human p21 and p27 in *Drosophila* .The amino acid sequence of Dap shares 20-27 % identity with its vertebrate CIP/KIP CKIs p21 and p27 (Lane et al. 1996).
Interestingly, these proteins are also involved in CDK-independent functions such as apoptosis, transcription and the cytoskeleton (Besson et al. 2008). Depending on the corresponding function and localization of the CIP/KIP CKIs they can act as tumor suppressors or oncogenes (Abukhdeir and Park 2008; Guo et al. 2010). CIP/KIP CKIs bind both the cyclin and the CDK subunit thereby modulating the activity of cyclin D-, E-, A-, and B-CDK complexes (Sherr and Roberts 1999). In contrast to its homologs, which can inhibit multiple Cyc/Cdk complexes, Dap specifically inhibits the CycE/Cdk2 complex. By co-IPs it was shown that Dap is only bound to CycE/Cdk2, but not Cdk1, CycA or CycB. Furthermore, addition of bacterial expressed and purified Dap to embryo extracts showed that Dap inhibited CycE/Cdk2 activity in a dose-dependent manner. A Dap version with deletions in the CycE binding domain (Dap_Del-39-43) was almost unable to inhibit CycE/Cdk2. Complexes consisting of Cdk1, CycA or CycB were not inhibited by Dap (Lane et al. 1996). Although it is unlikely that Dap interacts with Cdk4, Cdk6 or CycD as this would be untypical for CIP/KIPs, this was not tested so far to our knowledge.

p21, p27, p57 and Dap share conserved domains in the N-terminus, which mediate binding to CDKs and cyclins. However, otherwise their sequence differs greatly suggesting that the proteins have miscellaneous regulation and functions (Besson et al. 2008).
Indeed, p21, p27, p57 and Dap have different functions during the cell cycle: p21 can inhibit all cyclin/CDKs (Xiong et al. 1993). However, inhibition of CDK2 is most important (Abbas and Dutta 2009; Wade Harper 1993). p21 is expressed upon DNA damage and causes cell cycle arrest in G1 and G2 phase (Dulić et al. 1998). p21 is only essential for DNA damage response, but not for unperturbed cell cycles, at least in mice (Nakayama and Nakayama 1998).
Accumulation of p27 triggers cell cycle exit. As cells re-enter the cell cycle from G0 (quiescence) it is degraded (Chu et al. 2008). Accordingly, depletion of p27 leads to increased proliferation in mice (Nakayama and Nakayama 1998).
In contrast to p21 and p27, p57 is essential during embryonic development and regulates differentiation of tissues (Pateras et al. 2009; Nakayama and Nakayama 1998).
Dap is needed to arrest epidermal cells in the G1 phase followed by the terminal divisions (mitosis 16). Accordingly, Dap ensures that the epidermal cell proliferation is stopped at the correct developmental

stage. However, Dap is also crucial for the propriate development of other tissues such as neurons (Bivik Stadler et al. 2019).

A common feature of the CIP/KIP CKIs is that they are intrinsically unstructured proteins (IUPs) (Galea et al. 2008). It is assumed that this flexibility enables binding to many different proteins by forming various tertiary structures. Some E3s target CKIs only when they are bound to certain proteins, probably because only then a tertiary structure is acquired, which can be recognized. For instance, SCF-Skp2 recognizes CKIs only when they are bound to cyclin-CDK complexes (Abbas and Dutta 2009). There is a crystal structure for p27 bound to CycA/Cdk2 (Russo et al. 1996). Furthermore, kinetic data suggested that the binding of p27 to CycA/Cdk2 happens sequentially (Lacy et al. 2004). Highly disordered segments of the N-terminus of p27, which are highly conserved within the human CKIs mediate specific interactions with CycA/Cdk2. To describe the binding mechanism of p27 to CycA/Cdk2 the terms domain 1 (aa 27-37), linker helix (aa 38-59) as well as domain 2 (aa 60-88) are used. Amino acids in domain 1 are highly dynamic and bind to a hydrophobic patch on the surface of CycA. Domain 2, like domain 1, lacks secondary structure in solution. However, after binding to Cdk2, domain 2 forms a β-strand-rich structure. Amino acids in the linker helix are partially structured in solution. Interestingly, the amino acid sequence of the linker helix is poorly conserved, whereas the secondary structure seems to be conserved among the CKIs. The linker helix bridges a gap between domain 1 and domain 2. Only one amino acid of this helix (Leu 41) interacts specifically with CycA. Binding of p27 to either CycA or Cdk2 facilitates folding of the domain directly involved in the interaction (domain 1 or domain 2, respectively). However, also the folding of the otherwise partially structured linker helix is promoted after binding to domain 1 or 2. Kinetic data suggests that binding of p27 to CycA is strongly preferred in comparison to binding to Cdk2. In summary, first the disordered domain 1 binds rapidly to CycA. Thereafter, folding of the linker helix and then binding of domain 2 to Cdk2 takes place (Lacy et al. 2004).

In addition to binding of CKIs to Cyc/Cdk complexes, there are several other regulation mechanisms such as phosphorylation and subcellular localization, which mediate degradation of the CIP/KIP CKIs (Starostina and Kipreos 2012). The E3s that mediate degradation of p21, p27 and Dap are presented below.
SCF-Skp2 together with its cofactor Cks1 targets both p21 and p27 (and p57) for degradation. For Dap the results of different workgroup suggest either that it is a substrate of SCF-Skp2 or not, respectively. On the one hand, Dui et al. claimed that Dap is a substrate of SCF-Skp2 (Dui et al. 2013). Basis for this statement was the following: The F-box protein Skp2 interacted with Dap. Furthermore, the protein levels of Dap

were dependent on Skp2 activity. Knockdown of Skp2 lead to accumulation of Dap, whereas overexpression of Skp2 lowered Dap levels. Moreover, defects during the eye and wing development that were caused by knockdown of Skp2 could be rescued by knockdown of Dap. Finally, polyubiquitination of Dap *in vivo* was promoted by Skp2 (Dui et al. 2013).

However, the work of two other workgroups (including our own) suggest that Dap is not a substrate of SCF-Skp2 (Ghorbani et al. 2011; Rössler 2019). Ghorbani et al. reported that protein levels of Dap are not increased after knockdown of Skp2 (Ghorbani et al. 2011). In addition, overexpression of Skp2 slowed down the G1-S transition, whereas knockdown of Skp2 shortened G1 phase. This result is not in accordance with Dap being a substrate of SCF-Skp2 since degradation of Dap should result in more CycE/Cdk2 activity and consequently accelerated entry into S phase. Of course, the possibility remains open that overexpression/knockdown of Skp2 could also influence other substrates of SCF-Skp2, which would overcompensate the effects of altered Dap levels. However, it was also shown that upon overexpression of Skp2 the levels of three different Dap versions – Dap wildtype, a cell-cycle inert Dap version (Dap_dCDI) as well as a cell cycle and CRL4-Cdt2 inert version (Dap_dCDI_dPIPa) are not decreased (for Dap_dCDI and Dap_dCDI_dPIPa even increased). Furthermore, the interaction between Skp2 and Dap via co-IP seen by Dui et al. was not reproducible (Rössler 2019). Therefore, we assume that Dap is not a substrate of SCF-Skp2.

For p21 and p27, a requirement is that the CKIs are bound to CycE-Cdk2 or CycA-Cdk2 and are phosphorylated by the same CDKs on certain amino acids (S130 for p21; T187 for p27) (Lu and Hunter 2010). Furthermore, p27 is phosphorylated on Y74 and Y88 by the kinases ABL, SRC and LYN. This leads to a weakening of the interaction between p27 and Cyc-Cdk2 which in turn facilitates phosphorylation of T187. The degradation via SCF-Skp2 takes place in late G1 phase and early S phase. This allows activation of CDKs triggering S phase entry and preventing relicensing of DNA replication (Li and Jin 2010; Pospiech et al. 2010). The activity of SCF-Skp2 is controlled by the APC/C-Cdh1 and CycE-CDK2, among other things (Rodier et al. 2008).

p21 and Dap, but not p27 is a target of CRL4-Cdt2 (Abbas and Dutta 2011; Swanson et al. 2015). The general substrate recognition mechanism for CRL4-Cdt2 has already been described above (chapter 2.10). A special feature for p21 is that it must be phosphorylated on S114 by GSK3β to allow efficient ubiquitination by CRL4-Cdt2 (Abbas et al. 2008; Lee et al. 2007) . As for all other CRL4-Cdt2 substrates, degradation of p21 via this E3 is restricted to S phase and DNA damage (Abbas and Dutta 2011).

There is a crystal structure of a 22 residue peptide (aa 139-160) derived from the C-terminal region of p21 in complex with PCNA (Gulbis et al. 1996) (**Figure 10**). The peptide interacts with each of the three subunits of the ring. Residues in the N-terminal region of the peptide interact with the C-terminus of PCNA. Three residues in the center of the peptide (M147, F150, Y151) are anchored in a hydrophobic cleft between the connector loop and the C-terminus of PCNA. The C-terminal region of the peptide binds to the connector loop of PCNA. Furthermore, side chains in this region contact residues from the N-terminal domain of PCNA that are under the interdomain connector. The basic amino acids K154, R155, R156 of p21 interact with acidic amino acids of PCNA (Gulbis et al. 1996). Simultaneous mutation of these amino acids into alanine (K154A_R155A_R156A) prevented degradation of p21. In the N-terminus of p21 there is another basic cluster: R140_K141_R142_R143. Simultaneous mutation of these amino acids into alanine (R140A_K141A_R142A_R143A) abolished the degradation of p21 as well. Both the ^{154}KRR^{156} and the ^{140}RKRR^{143} mutant can still interact with PCNA. However, if both basic clusters were mutated at once (R140A_K141A_R142A_R143A_ K154A_R155A_R156A) p21 was not only stabilized, but interaction with PCNA was abolished (Nishitani et al. 2008). For Cdt1 – another well studied CRL4-Cdt2 substrate – it was suggested that the so-called B+4 (fourth amino acid after the PIP-box) is involved in interaction with Cdt2. For p21, this would be the amino acid R160. However, to our knowledge there is no study that would confirm or refute a role of this amino acid for p21 in Cdt2 interaction.

Beside p21, Dap is a substrate of CRL4-Cdt2 (Swanson et al. 2015). Three Dap mutants with different mutations in the predicted PIP degron (Dap_Q184A_I187A_T188A_E189A_F190A_K195A; Dap_ Dap_Q184A_I187A_T188A_E189A_F190A; Dap_K195A) were stabilized in S phase (all three to a similar extent) indicating that CRL4-Cdt2 mediated degradation was abolished. As already explained previously (chapter 2.9) data suggested that beside CRL4-Cdt2, Dap could also be a substrate of SCF-Rca1 (M. Kies 2017). However, more data is needed to confirm or refute this hypothesis. In addition, it is not known whether E3s other than CRL4-Cdt2 and SCF-Rca1 are involved in the degradation of Dap.

During prometaphase APC/C-Cdc20 mediates degradation of p21 (contains a D-box) (Amador et al. 2007). This facilitates the activation of mitotic Cyc-Cdk1 and thereby contributes to progression of mitosis (Starostina and Kipreos 2012). In addition, p21 degradation is mediated by the E3s MDM2/MDMX (Jin et al. 2003; Jin et al. 2008b), CRL2-LRR1 (Starostina et al. 2010) and MKRN1 (Lee et al. 2009). Further E3s that are involved in degradation of p27 are KPC (Kamura et al. 2004), PIRH2 (Hattori et al. 2007) and E6-AP (Mishra et al. 2009).

To understand how CKIs can mediate the development of tissues it is crucial to know how the expression and degradation of CKIs is regulated during different stages of the development of tissues. The mechanisms, which are involved here in case of Dap, are described below: Interestingly, CycE can activate the expression of Dap. However, this activation is restricted to a period during the final division cycle before cells enter mitotic quiescence. Before this period, developmental signals prevent the expression of Dap despite the presence of CycE. Finally, developmental constraints are relieved and CycE is able to induce expression of Dap beginning late in the G2 phase preceding the terminal division (mitosis 16) (Nooij et al. 2000; Lane et al. 1996). High activity of CycE may also promote degradation of Dap. This ensures that significant accumulation of Dap is restricted to the period when CycE levels begin to decline (phase IIb) (Nooij et al. 2000). In this period CycE/Cdk2 is inhibited by Dap, which leads to a G1 arrest after the terminal division of epidermal cells (mitosis 16). In addition to the upregulation of Dap, down-regulation of CycE transcriptions seems to contribute to the inactivation of CycE/Cdk2 activity in this phase (Knoblich et al. 1994). At the end of the IIb phase expression of Dap is reduced and the cells enter phase III (postmitotic) in which both Dap and CycE/Cdk2 levels are low (Lane et al. 1996). In some cells such as in the ovaries and salivary glands of *Drosophila*, endocycles take place at a later time. In endocycles, mitosis is circumvented so that the cell cycle only consists of a gap- and S phase (G1-S). As a result, polyploidy can be found in the corresponding cells. A requirement for endocycles is cycling CycE/Cdk2 activity. Dap ensures that the appropriate timing of cycling CycE/Cdk2 activity by accumulating in the G phase and being degraded in S phase via CRL4-Cdt2 (Swanson et al. 2015).

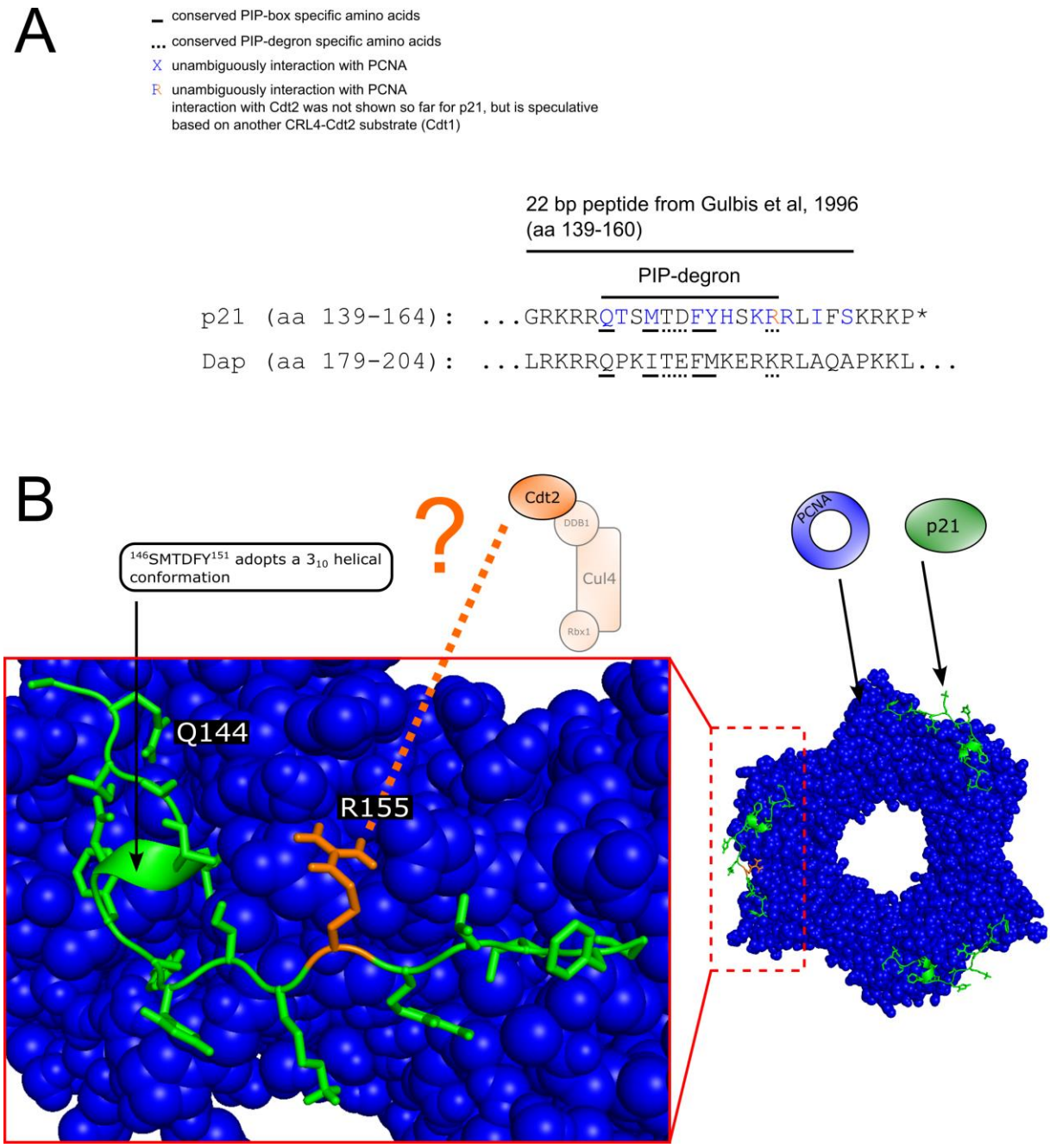

Figure 11 | PIP-degron of p21

A) Depiction of the amino acid sequence of the 22 bp peptide of p21 for which a crystal structure in complex with PCNA was obtained by (Gulbis et al. 1996). The amino acids, which are conserved in different PIP box substrates, are underlined with a continuous line. The amino acids that are specific for the PIP degron are underlined with a dashed line. Amino acids for which direct interaction with PCNA was shown are depicted in blue. For the last amino acid of the PIP degron of p21 (R155; right half shown in orange) interaction with Cdt2 was not shown, but was speculative based on another CRL4-Cdt2 substrate (Cdt1). The aligned amino acid sequence of Dap is shown under the sequence of p21. **B)** Crystal structure of the complex consisting of the 22 bp peptide of p21 (depicted in green) and PCNA (depicted in blue) obtained by (Gulbis et al. 1996). PDB code: 1AXC. The basic amino acid R155 (depicted in orange) makes contact to PCNA. However, it was speculated that R155 could also mediate interaction with Cdt2 based on the CRL4-Cdt2 substrate Cdt1. Figure assembled from data in (Gulbis et al. 1996) and (Havens and Walter 2011)

3 Aim

Previous work indicated that Dap could be a substrate of SCF-Rca1 (M. Kies 2017). However, the flow cytometry data, which supported this hypothesis, was relatively error-prone: S2R+ *Drosophila* cells were transfected with plasmids that used two separate and different promotors (metallothionein and actin promotor) to express Dap constructs fused to GFP and the reference protein (CHE) (M. Kies 2017). Therefore, stoichiometric expression of both proteins, which is a requirement for meaningful stability measurements, was questionable. At the beginning of this thesis, a more accurate and reliable method for relative protein stability measurement using flow cytometry – the RPS system – was developed in the Sprenger-lab (Polz 2021). The basis of this system is a T2A sequence, which allows stoichiometrical expression of two (or more) proteins under the control of one promotor.

To substantiate the hypothesis of Dap being a substrate of SCF-Rca1, we wanted to apply this RPS system and conduct further stability analysis of Dap constructs regarding Rca1 effects. In addition, to understand the interaction between Rca1 and Dap in more detail co-IPs were conducted. Furthermore, we wanted to apply different strategies to abolish or at least reduce CRL4-Cdt2 dependent degradation of Dap to exclude that Rca1 effects on Dap stability are indirectly caused by altered degradation via CRL4-Cdt2. We also wanted to analyze how mutations in the PIP degron of Dap do affect its degradation via CRL4-Cdt2 and wanted to elucidate the underlying mechanism. Although flow cytometry analysis is a powerful tool to analyze the degradation of proteins during the cell cycle it comes with some restrictions. For instance, flow cytometry does not allow to detect ubiquitination of proteins directly. To this end, we wanted to establish other methods - TUBE-ligase trapping and an *in vitro* SCF-Rca1 ubiquitination assay - to allow detection of ubiquitinated Dap by SCF-Rca1.

4 Results

4.1 Rca1 can influence the stability of Dap_dCDI

Previous experiments indicated that Dacapo (Dap) could be a substrate of SCF-Rca1 (M. Kies 2017; Herzinger 2019). To substantiate this hypothesis, effects of Rca1 on the stability of Dap were analyzed by a flow cytometry-based method outlined below. For this kind of analysis, *Drosophila* S2R+ cells were transfected with plasmids that coded for eGFP ("GFP") (Cormack et al. 1996) as a reference fluorescent protein as well as Dap constructs fused to the red fluorescent protein mCherry ("CHE") (Shaner et al. 2004). A T2A (thosea asigna virus 2A) sequence between the coding sequence for GFP and the Dap version fused to CHE enabled ribosome skipping. This allowed the stoichiometric expression of both proteins under the control of one promotor. The high efficiency and reliability of this T2A system in combination with flow cytometry (referred to as *R*elative *P*rotein *S*tability (RPS) system) was already shown before (Polz 2021). A detailed description of this method can be found in the methods part of this thesis (chapter 7.4).

Briefly, transfected cells were DNA-stained using Hoechst 33342, harvested and analyzed individually by flow cytometry in which fluorescent signal intensities of GFP, CHE and Hoechst-stained DNA were recorded. The ratio between CHE and GFP fluorescent intensities between different experimental conditions allowed to assess the relative stability of the CHE-tagged protein. In addition, the DNA content of the cells (measured by Hoechst staining) allowed the display of a cell cycle distribution curve. Individual cells can be assigned to different cell cycle phases and the relative stability of the CHE-tagged protein within an experimental condition can be determined for each cell cycle phase (G1, S, or G2/M) separately. In addition, cell cycle distribution changes induced by experimental conditions can be determined.

In most cases, the POI is fused to an HA-NLS-CHE tag to allow constitutive nuclear localization by the nuclear localization sequence (NLS) and detection of the POI on Western blots using the haemagglutinin tag (HA). For simplicity, the always present HA-NLS-CHE-tag on the different POIs is not explicitly mentioned. To study effects of different Rca1 variants, we expressed Rca1 constructs with a triple HA-tag, e.g. 3xHA-Rca1. Again, for simplification, the 3xHA-tag is not mentioned in most cases. To reduce the level of a certain protein, RNAi was performed by knockdown (KD) of the corresponding mRNA level. The knockdowns were conducted by expression of a short hairpin RNA based on the mir1 micro RNA (Nguyen and Frasch 2006; Ni et al. 2011).

For the analysis of Rca1 effects on the stability of Dap, we first analyzed a HA-NLS-CHE-tagged Dap version with deletions in the CDI domain (Dap_Del-38-44-RAR_Del-103-105-G; Dap_dCDI). This Dap construct cannot bind and inhibit CycE/Cdk2 (M. Kies 2017; Lane et al. 1996) and even after overexpression of this construct, the cell cycle distribution of the transfected cells did not change significantly (**Figure 12 B**).

Previously it was shown that Rca1 can trigger the G1/S transition of the cell cycle in an F-box dependent manner (Zielke et al. 2006). In addition, it was known that Dap is a substrate of CRL4-Cdt2 in S phase (Swanson et al. 2015). Although not shown explicitly for *Drosophila*, it was shown for other eukaryotes that CRL4-Cdt2 activity is dependent on DNA-bound PCNA and is therefore restricted to S phase (Havens and Walter 2011; Marzio et al. 2019). CyclinE/Cdk2 activity is required for triggering the G1/S transition but during G1, Cyclin E/Cdk2 is inhibited by Dap (Richardson et al. 1993; Lane et al. 1996).

One potential mechanism by which the G1/S transition can be facilitated is degradation of Dap at the end of G1 and thereby relieve of Cyclin E/Cdk2 inhibition. Based on previous analysis, Rca1 in an SCF complex would be a good candidate that mediates this degradation (Zielke et al. 2006; M. Kies 2017). Therefore, we wanted to analyze Rca1 effects on the stability of Dap especially in G1, but also in the phases S and G2. For this purpose, the examined cells were categorized based on their DNA content into G1, S, or G2 phases. Since the DNA content of cells in G1 and early S phase is almost the same, a small portion of early S phase cells is also present in the "G1" selection. In the "G2" selection, late S phase cells and some mitotic cells can also be present. This must be considered for the interpretation of the results. We have omitted the quotes when mentioning the different cell cycle gates mostly in the text.

The relative stability of Dap_dCDI was low in general (compare with relative stability of CHE), probably due to the strong degradation via CRL4-Cdt2 (**Figure 12 B-F**). Coexpression of Rca1 caused destabilization of Dap_dCDI in G1, S and G2, whereby the effect was significant in G1 and S. In contrast, knockdown against the endogenous Rca1 increased the stability of Dap_dCDI in all phases. This was in line with our hypothesis that Dap is targeted for degradation by SCF-Rca1. However, destabilization of Dap_dCDI by Rca1_dFbox was noticeable as well. In Rca1_dFbox, a deletion of aa 164-203 within the F-box domain (aa 154-203) destroys the F-box domain and no interaction with SkpA can be observed. Thus, Rca1_dFbox cannot be incorporated into an SCF complex, but is still able to inhibit the APC/C (Zielke et al. 2006; M. Kies 2017). APC/C inhibition could result in S phase induction and destabilization of Dap_dCDI by Rca1_dFbox could then be indirectly caused via CRL4-Cdt2. In this scenario, overexpression of Rca1_dFbox would increase the amount of early S phase cells in the "G1" selection so that more degradation of Dap_dCDI via CRL4-Cdt2 is observed. However, Rca1_dFbox cannot reduce the stability of Dap_dCDI as strong as Rca1. This indicates that the F-box function of Rca1 is required for robust destabilization of Dap_dCDI.

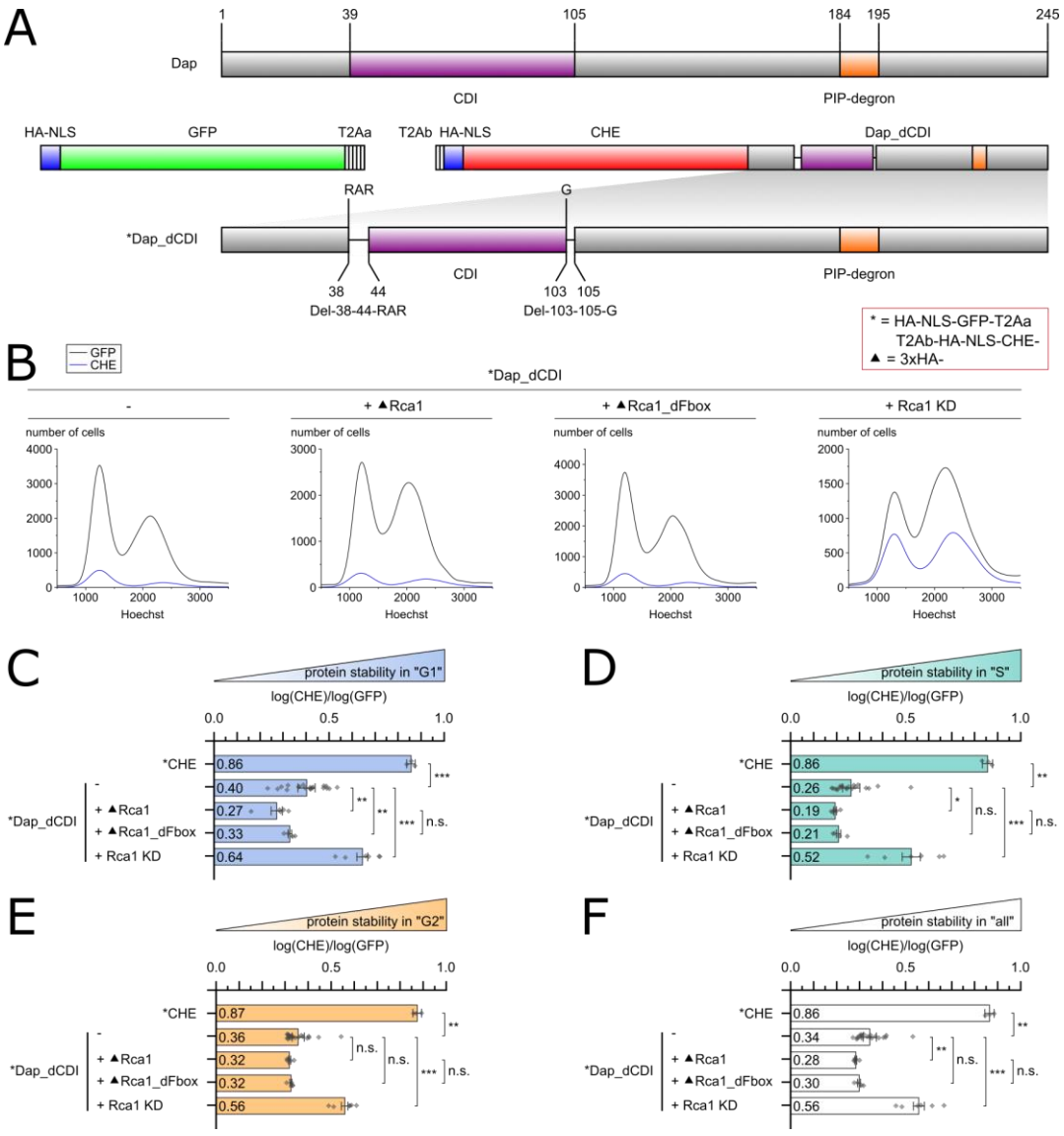

Figure 12 | Rca1 can destabilize Dap_dCDI

A) To analyze the relative stability of Dap_dCDI by flow cytometry it was expressed as a HA-NLS-CHE-tagged version using a T2A plasmid. This enabled stoichiometric expression of HA-NLS-GFP-T2Aa (reference) and T2Ab-HA-NLS-CHE-Dap_dCDI (protein of interest). In Dap_dCDI deletions in the CDI (*C*yclin-*d*ependent kinase *i*nhibitor) domain abolish the inhibition of CycE/Cdk2. Therefore, the G1/S transition is not affected when Dap_dCDI is overexpressed and cells maintain a normal cell cycle profile. The PIP degron by which Dap is recognized by CRL4-Cdt2 is still present. **B)** Flow cytometry DNA content distribution curves ("Cell cycle curves") of transfected cells (GFP positive in black) and CHE-Dap_dCDI positive cells (in blue). The barplots (**C-F**) represent the relative stability of Dap_dCDI in G1 (**C**), S, (**D**), G2 (**E**) and all cells ("all") (**F**). In addition, the relative stability of CHE alone (HA-NLS-CHE) is shown. HA-NLS-CHE-Dap_dCDI was significantly more instable in all phases than HA-NLS-CHE. Coexpression of Rca1 tended to decrease the stability of Dap_dCDI in G1, G2 and S, whereas knockdown (KD) of Rca1 caused stabilization. The destabilization of Dap_dCDI by Rca1_dFbox tended to be less than by Rca1, at least in G1. Statistical significance was evaluated by Welch two sample test in case of normal distributed data sets or Wilcoxon rank sum test in case of not normal distributed data sets. * = $p < 0.05$, ** = $p < 0.01$, *** = $p < 0.001$, n.s. = not significant. For the analysis, only cells with a medium GFP fluorescent level (56-316; loc-scale: 1.75-2.25) were selected to avoid strong overexpression artefacts. Abbreviations: HA: haemagglution-tag (YPYDVPDY), NLS: nuclear localization sequence (PKKKRKV), T2A: *thosea asigna virus 2A* sequence (EGRGSLLTCGDVEENPG|PGS). The "cleavage" site is indicated by a straight line. PIP degron (QPKITEFMKERK): sequence that targets PCNA-interacting proteins for proteasomal degradation via the E3 ubiquitin ligase CRL4-Cdt2. Rca1_dFbox: Rca1 with deletion of aa 164-203. Rca1 KD: knockdown of Rca1 using a mir1-based construct targeting the 5´UTR of endogenous Rca1. Hoechst: Hoechst 33342 DNA staining dye. The abbreviations listed here and the execution of statistical tests as well as the expression level 1.75-2.50 also applies to all of the following figures, but is no longer mentioned.

4.2 Rca1 causes instability of Dap_dCDI even after CRL4-Cdt2 knockdown

The reduced "G1" stability of Dap_dCDI after overexpression of 3xHA-Rca1_dFbox could result from APC/C inhibition and subsequent acceleration of the G1/S transition. In S phase, Dap_dCDI would then be the target of the CRL4-Cdt2 ubiquitin ligase. To eliminate this effect, we wanted to abolish or at least reduce the activity of CRL4-Cdt2 by knockdowns of its subunits Cul4 and Cdt2. Cul4 acts as a scaffold, whereas Cdt2 is the substrate recognition module of CRL4-Cdt2 (Havens and Walter 2011). The stability of Dap_dCDI in S phase increased after knockdown of Cul4 or Cdt2, indicating that the knockdowns worked (**Figure 13 A**). The knockdown for Cdt2 caused more stabilization of Dap_dCDI than the knockdown for Cul4. Therefore, the effect of Rca1 on the stability of Dap_dCDI was analyzed after knockdown of Cdt2.

After knockdown of Cdt2, the stability of Dap_dCDI in G1 was higher than without knockdown of Cdt2 (**Figure 13 C; compare with Figure 12 C**). If the degradation of Dap_dCDI is impeded in S, the initial Dap_dCDI level is also higher in the following G1. In addition, as mentioned above early S phase cells are also present in the "'G1" selection. Both effects can contribute to the stabilization of Dap_dCDI in G1 after knockdown of Cdt2. After Cdt2 knockdown, co-overexpression of Rca1 caused instability of Dap_dCDI in "G1" and "G2" (**Figure C, D**). The Rca1_dFbox destabilization in G1 and G2 tended to be weaker than Rca1 but was not eliminated. Since Dap_dCDI was not completely stabilized in S after Cdt2 knockdown (log(CHE)/log(GFP) = 0.77), any remaining CRL4-Cdt2 might still be responsible for the induced Dap_dCDI instability after Rca1_dFbox expression. Nevertheless, Rca1 shows a stronger destabilization of Dap_dCDI in this experimental setup, indicating an F-box dependent role of Rca1.

It must be emphasized that the knockdown of Cdt2 led to a cell cycle profile in which the proportion of G1 cells is increased. (**compare Figure 13 B with Figure 12 B**). The overexpression of Rca1 resulted in the change of the cell cycle profile with less G1 cells and this effect was stronger than with coexpression of Rca1_dFbox. This indicates again that the F-box function of Rca1 is responsible for the G1/S induction, also after Cdt2 knockdown. However, the induced cell cycle changes make the interpretation of the Dap_dCDI destabilization more difficult.

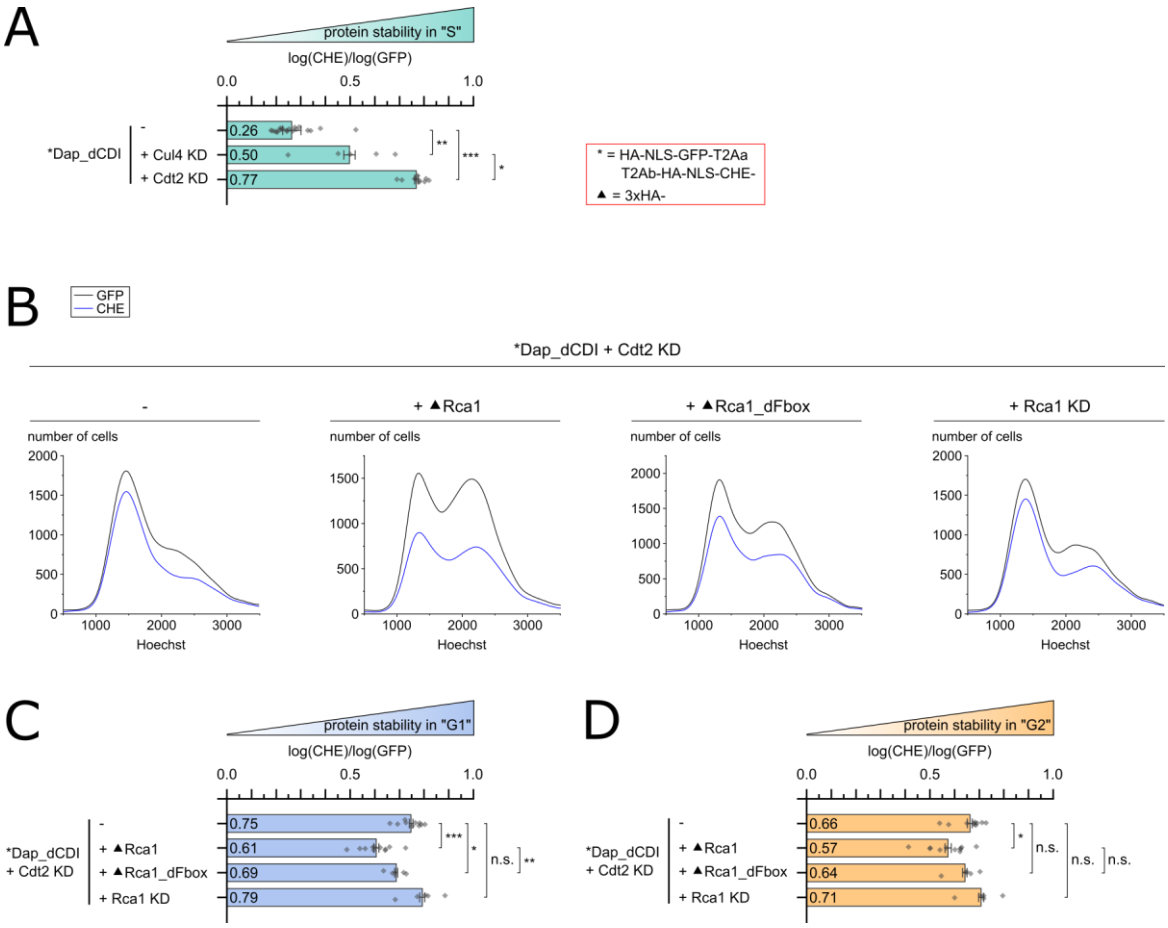

Figure 13 | Rca1 can influence the stability of Dap_dCDI despite knockdown of Cdt2

A) Barplots representing the relative stability of Dap_dCDI. The data was obtained by flow cytometry. Knockdown of the CRL4-Cdt2 subunits Cul4 or Cdt2 increased the stability of Dap_dCDI in S phase. The knockdown of Cdt2 stabilized Dap_dCDI to a higher extent than the one for Cul4. Since Dap_dCDI was not completely stabilized it might be that some residual activity of CRL4-Cdt2 remained. **B, C, D)** Cell cycle curves (**B**) and barplots (**C, D**) representing the relative stability of Dap_dCDI after knockdown of Cdt2. Coexpression of Rca1 could destabilize Dap_dCDI in G1 and G2. In addition, coexpression of Rca1_dFbox tended to decrease the stability of Dap_dCDI in G1 and G2. However, the destabilizing effect of Rca1_dFbox on Dap_dCDI tended to be weaker than that of Rca1.

4.3 Residual Cdt2 is likely responsible for the destabilization of substrates containing a PIP degron after Cdt2 knockdown

Overexpression of Rca1_dFbox resulted in destabilization of Dap_dCDI even after RNAi based knockdown of Cdt2. This could be caused by the promotion of G1/S transition that can be induced by Rca1 mediated APC/C inhibition for which Rca1_dFbox is capable of. Residual Cdt2 protein levels could then be responsible for early S phase destabilization of Dap_dCDI. To investigate this further, we employed an extra CRL4-Cdt2 substrate that we anticipate not being targeted by SCF-Rca1.

We used the CRL4-Cdt2 substrate Dup, which is the *Drosophila* homolog of Cdt1 (**Figure 14 A**). To prevent confusion between Dup and Dap, Dup is referred to as Cdt1 if not mentioned otherwise. Cdt1 (Dup) facilitates the recruitment of the MCM-complex to origins of replication (Whittaker et al. 2000). In S phase and after DNA damage Cdt1 is ubiquitinated by CRL4-Cdt2 in all metazoans (Havens and Walter 2011). Cdt1 knockdown in cells typically leads to the inhibition or reduction of DNA replication initiation (Braun et al. 2012). Cdt1 would therefore not be considered an SCF-Rca1 target, since downregulation of Cdt1 would result in less S phases. Thus, Cdt1 is unlikely an SCF-Rca1 substrate and can be used to evaluate CRL4-Cdt2 activity changes after Rca1 expression.

Like Dap, Cdt1 contains a PIP degron, which mediates degradation via CRL4-Cdt2. In addition, Cdt1 contains two functional domains: The MCM-binding domain mediates recruitment of the MCM helicase to the origin of replication. Furthermore, Cdt1 contains a domain for binding of Geminin, which is an inhibitor of Cdt1 (Pozo and Cook 2016). To avoid cell cycle changes by overexpression of functional Cdt1, a truncated Cdt1 version (Cdt1_1-101) was used. Cdt1_1-101 contains the PIP degron but no functional domains and is therefore cell cycle inert. Like Dap_dCDI, Cdt1_1-101 is instable in S. The trend of Cdt1_1-101 stabilization during S phase after knockdown of Cul4 or Cdt2 is shown in **Figure 14 B**.

After knockdown of Cdt2 (**Figure 14 C, D, E**), coexpression of Rca1 decreased the stability of Cdt1_1-101 in G1, whereas knockdown of Rca1 tended to stabilize it. Coexpression of Rca1_dFbox could not significantly influence the stability of Cdt1_1-101 in G1 and G2. In both cases – coexpression of Rca1 or Rca1_dFbox, a change in the cell cycle profile is visible with less cells in the G1 state compared to cells in which only Cdt2 was knocked down. This indicates that Rca1 and Rca1_dFbox can induce G1/S transition and residual Cdt2 is likely responsible for the destabilization of Cdt1. Since both Rca1 and Rca1_dFbox can inhibit the APC/C (Zielke et al. 2006) but Rca1 does induce more G1/S transition, it is likely that the different effects of Rca1 and Rca1_dFbox are dependent on the F-box function and would trigger the G1/S transition. Degradation of Dap could facilitate this G1/S transition. However, it is also conceivable that other SCF-Rca1 substrates could trigger the seen effects. Therefore, more experiments (see below) are needed to prove that Dap is a substrate of SCF-Rca1.

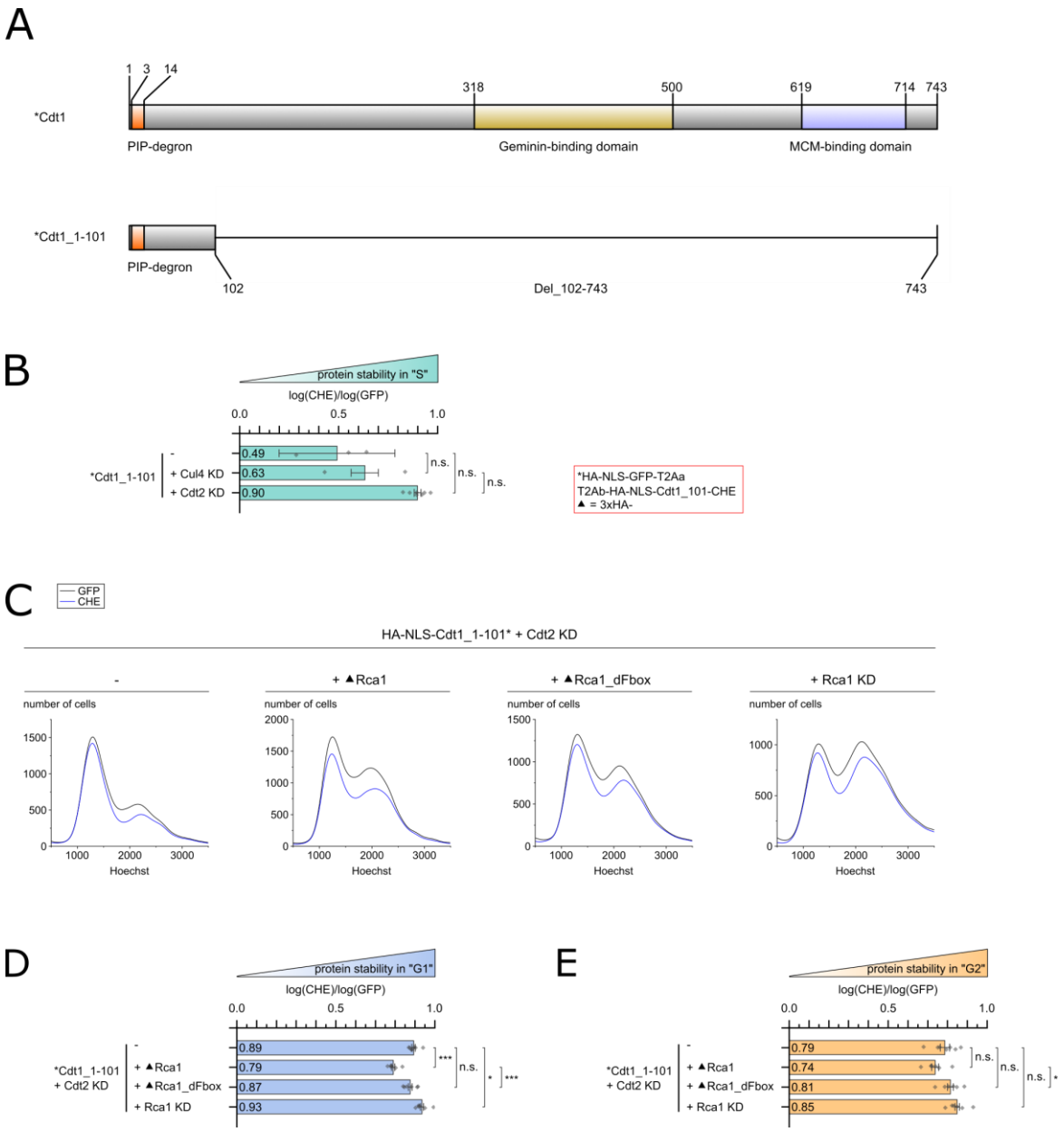

Figure 14 | Cdt1_1-101 stability is affected by Rca1 despite knockdown of Cdt2

A) Protein schemes of Cdt1 and Cdt1_1-101. Cdt1_101 still contains the PIP degron for CRL4-Cdt2 dependent degradation. However, the functional domains (Geminin- and MCM-binding domains) are not included. Therefore, Cdt1_1-101 is cell cycle inert in case of overexpression, which makes flow cytometric analysis easier to interpret. **B)** Barplots representing the relative stability of Cdt1_1-101 in S phase. The data was obtained by flow cytometry. Both knockdown of Cul4 or Cdt2 tended to stabilize Cdt1_1-101. **C, D, E)** Cell cycle curves (**C**) and barplots (**D, E**) representing the relative stability of Cdt1_101 after knockdown of Cdt2. Overexpression of Rca1 tended to destabilize Cdt1_1-101 in G1 and G2, whereas knockdown of Rca1 tended to stabilize it. Overexpression of Rca1_dFbox could not influence the stability of Cdt1_1-101 significantly.

4.4 Dap_dCDI can be stabilized in S phase by mutations in its PIP-degron

Rca1 can induce the G1/S transition and degradation of PIP degron containing substrates in S phase can occur; to a certain extent even after Cdt2 knockdown. This makes the interpretation of direct Rca1 effects difficult. Another problem is that reduced CRL4-Cdt2 activity leads to less degradation of a number of different CRL4-Cdt2 substrates, which could lead to unwanted effects such as changes in the cell cycle profile. Thus, in order to exclusively observe potential direct impacts of Rca1 on Dap_dCDI through SCF-Rca1, we pursued an alternative approach to eliminate the CRL4-Cdt2 mediated degradation of Dap_dCDI. Previously it was shown that mutation of amino acids in Dap, which are conserved in PIP degron sequences of other CRL4-Cdt2 substrates can cause stabilization in S phase (Swanson et al. 2015). Thus, our strategy was to use Dap versions with mutated PIP degron to analyze effects of Rca1 on Dap. The role of the individual amino acids in the PIP degron of Dap for the degradation via CRL4-Cdt2 was not studied so far. Thus, we realized that we must first understand the degradation mechanism of Dap via CRL4-Cdt2 to interpret Rca1 effects on Dap correctly.

First, we analyzed the stability of the following Dap constructs with mutations in the PIP degron in S phase (the mutations are highlighted in bold face): Dap_dCDI_**Q184A**, Dap_dCDI_**Q184A_I187A_T188A**, Dap_dCDI_**K195A**, Dap_dCDI_**Q184A_K195A**, Dap_dCDI_**dPIPa**, Dap_dCDI_**PIP-6A** and Dap_dCDI_**R194A_L197A** (**Figure 15 A**). Dap versions with a single mutation in conserved amino acids, i.e. Dap_dCDI_Q184A and Dap_dCDI_K195A showed already stabilization in S phase (**Figure 15 B**). However, only after combining several mutations or deletion of several amino acids, strong stabilization of Dap was observed. This indicates that Q184 and K195 are important, but not essential for ubiquitination of Dap by CRL4-Cdt2. In p21 – the human homolog of Dap – several amino acids including the corresponding amino acids of Q184 and K195 interact directly with PCNA (Gulbis et al. 1996). Therefore, it is conceivable that in Dap other amino acids partially compensate for the loss of Q184 or K195. For Cdt1 there are indications that the corresponding amino acid of K195 is essential for the interaction with Cdt2 (Michishita et al. 2011; Havens and Walter 2009). Therefore, it is conceivable that K195 in Dap might be also involved in the interaction with Cdt2. The double mutant Dap_dCDI_Q184A_K195A was more stable than the corresponding mutants with one single mutation. However, it was not as stable as Dap_dCDI_Q184A_I187A_T188A, Dap_dCDI_dPIPa and Dap_dCDI_PIP-6A. In addition to conserved amino acids in the PIP degron, a potential D-box motif (RXXL; aa 194-197) for the recognition by the APC/C is located in Dap. Dap_dCDI_R194A_L197A was weakly stabilized. It cannot be said with certainty whether this effect raised from altered degradation via APC/C or CRL4-Cdt2 or both.

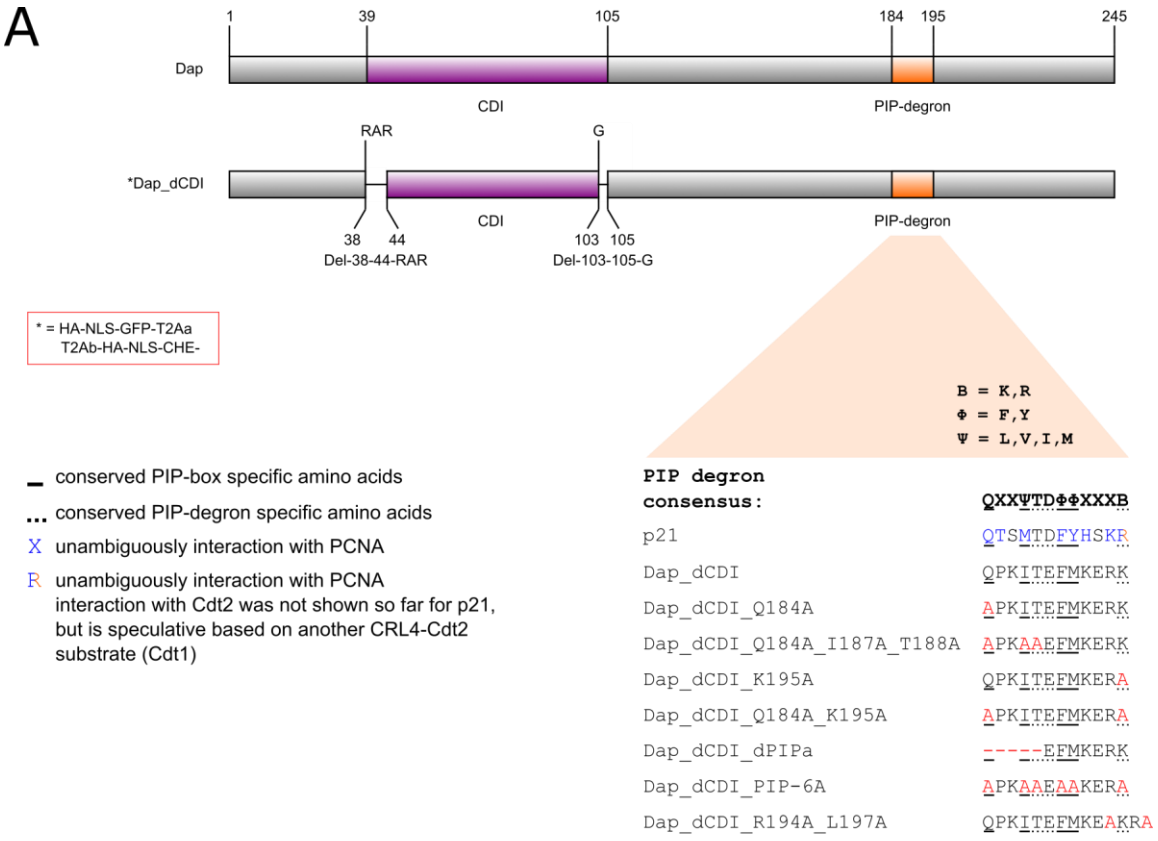

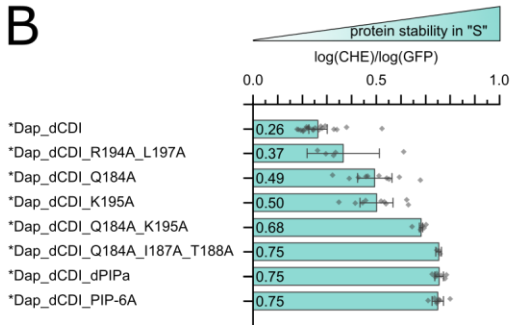

Figure 15 | Stability of Dap_dCDI constructs with mutations in the PIP degron
A) Tested Dap_dCDI constructs with mutations in the PIP degron. Underlined amino acids are conserved PIP box specific amino acids, whereas dotted underlined amino acids are conserved PIP degron specific amino acids. The amino acids in p21, for which Gulbis et al showed that they interact with PCNA, are depicted in blue. For the last basic amino acid of the PIP degron of p21 (right half depicted in orange) interaction with Cdt2 was not shown, but is speculative based on the corresponding amino acid of the well-studied CRL4-Cdt2 substrate Cdt1. **B**) Barplots representing the relative stability of Dap_dCDI constructs with mutations in the PIP degron in S phase. In general, the more conserved amino acids were mutated, the stronger the stabilization in S phase. Mutation of Q184 or K195 alone led to medium stabilization indicating that these amino acids are important, but not essential. Probably other amino acids can partially compensate for their loss.

4.5 Q184 in Dap_dCDI is needed for interaction with PCNA

For other substrates of CRL4-Cdt2 it was already known that interaction with the substrate recognition unit Cdt2 as well as with PCNA is needed for recognition and ubiquitination by this E3 (Havens and Walter 2011; Mazian et al. 2022) . To understand the underlying mechanism of the stabilization of Dap_dCDI by mutations in the PIP degron, co-immunoprecipitations (co-IPs) were conducted. Different 4xFLAG tagged Dap constructs with mutations in the PIP degron were precipitated and it was analyzed, if 3xHA-PCNA can coprecipitate (**Figure 16**).

Like other CRL4-Cdt2 substrates 4xFLAG-Dap_dCDI interacted with PCNA. 4xFLAG-Dap_dCDI_dPIPa in which three amino acids that are predicted to interact with PCNA (based on comparison with p21-PCNA structure; (Gulbis et al. 1996)) were deleted could not coprecipitate PCNA. Interestingly, also with 4xFLAG-Dap_dCDI_Q184A coprecipitation of PCNA was not possible. As seen in the flow cytometric analysis (chapter 4.4), the stabilization of Dap_dCDI_Q184A was comparatively weaker than Dap_dCDI variants possessing additional mutations in the PIP degron. This could indicate that Dap_dCDI_Q184A can still interact with PCNA weakly to allow reduced degradation via CRL4-Cdt2. However, this interaction might be too weak to be detected via co-IPs. 4xFLAG-Dap_dCDI_K195A was able to coprecipitate PCNA as strong as Dap_dCDI. This indicates that K195 is dispensable for the interaction with PCNA. PCNA also cannot be coprecipitated using 4xFLAG-Dap_dCDI_Q184A_K195A, which is as expected, since the Q184A mutation is already sufficient to abolish the interaction with PCNA.

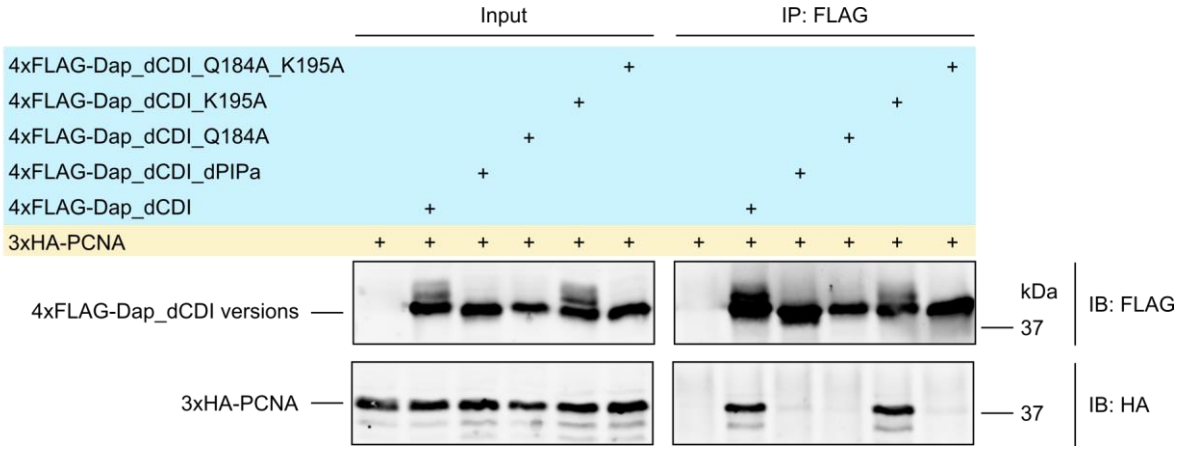

Figure 16 | Q184 in Dap_dCDI is needed for interaction with PCNA

The interaction of Dap_dCDI constructs with mutations in the PIP degron and PCNA was analyzed by co-IPs. 4xFLAG-Dap_dCDI was able to coprecipitate 3xHA-PCNA. Deletion of the amino acids 184-188 (4xFLAG-Dap_dCDI_dPIPa) as well as a single mutation of Q184 into alanine abolished this interaction. 4xFLAG-Dap_dCDI_K195A could coprecipitate PCNA as strong as 4xFLAG-Dap_dCDI. As expected 4xFLAG-Dap_dCDI_Q184A_K195A was also not able to coprecipitate 3xHA-PCNA, since the mutation of Q184A alone was already sufficient to abolish this interaction.

4.6 N-terminus of Dap mediates interaction with Cdt2

Substrates of CRL4-Cdt2 interact with the substrate recognition module Cdt2. To test, which amino acids in Dap_dCDI mediate this interaction, co-IPs were conducted. Different 4xFLAG tagged Dap_dCDI constructs with mutations in the PIP degron were precipitated and it was tested if 3xHA-Cdt2 can be coprecipitated (**Figure 18 A**). 4xFLAG-Dap_dCDI was able to coprecipitate 3xHA-Cdt2. The quantity of coprecipitated 3xHA-Cdt2 was low. Nevertheless, this outcome is anticipated, as the interaction between substrates and the substrate recognition module of E3 ubiquitin ligases is usually weak and transient (Watanabe et al. 2020). Interestingly, 4xFLAG-Dap_dCDI_Q184A, 4xFLAG-Dap_dCDI_K195A and 4xFLAG-Dap_dCDI_Q184A_K195 were able to coprecipitate 3xHA-Cdt2 as well. Therefore, neither Q184 nor K195 in Dap_dCDI are essential for the interaction with Cdt2. As seen previously, the K195A mutation stabilized Dap_dCDI noticeably (chapter 4.4). Therefore, K195 seems to have an important role, although it is not essential for the interaction with PCNA and Cdt2. Further experiments were conducted to determine the function of K195 (chapter 4.8).

Since the interaction with Cdt2 was present for all tested Dap constructs, we considered that domains other than the PIP degron mediate this interaction. To test this, different N- and C-terminal truncated Dap versions (with and without functional CDI) were tested for interaction with Cdt2 (**Figure 17, 18 B**): 4xFLAG-Dap, 4xFLAG-Dap_dCDI, 4xFLAG-Dap_160-245, 4xFLAG-Dap_126-245, 4xFLAG-Dap_126-245_dPIPa, NLS-4xFLAG-Dap_1-160, NLS-4xFLAG-Dap_1-160_dCDI, NLS-4xFLAG-Dap_1-125, NLS-4xFLAG-Dap_1-125_dCDI. For the Dap constructs that included a functional CDI domain HA-CycE/Cdk2-T18A_Y19F-HA ((T18A_Y19F to prevent inhibitory phosphorylation; hereinafter referred to as HA-CycE/Cdk2-HA) was coexpressed to overcome the G1/S transition. For the N-terminal Dap fragments an NLS domain was fused to compensate the loss of the predicted NLS-sequences of Dap, which are located in the C-terminal part of Dap (NLS-01: aa 192-214; NLS-02: aa 178-199).

4xFLAG-Dap was able to coprecipitate 3xHA-Cdt2 only slightly more efficient than 4xFLAG-Dap_dCDI (**Figure 18 B, lanes 3, 4**). The difference is too small to safely conclude that the CDI domain plays a role here. When HA-CycE/Cdk2-HA was coexpressed with 4xFLAG-Dap, the precipitation of 4xFLAG-Dap did result in coprecipitation of HA-CycE and Cdk2-HA (**lane 2**), indicating that Dap interacted with CycE and Cdk2. The amount of Cdt2 coprecipitation was not changed, suggesting that Dap-Cdt2 interaction is not dependent on Dap interaction with CycE/Cdk2. Interestingly, 4xFLAG-Dap_160-245, which contained the whole PIP-degron sequence (aa 184-195) could not coprecipitate 3xHA-Cdt2, even though this fragment is a target of CRL4-Cdt2 (**lane 5**) (chapter 4.22). In contrast, interaction between 4xFLAG-Dap_126-245 and 4xFLAG-Dap_126-245_dPIPa with 3xHA-Cdt2 could be detected, albeit it is very weak (**lane 6,7**). It is slightly higher for 4xFLAG-Dap_126-245_dPIPa, presumably by higher expression and precipitation of this

Dap construct. For NLS-4xFLAG-Dap_1-160_dCDI and NLS-4xFLAG-Dap_1-160, interaction with 3xHA-Cdt2 was detected (**lane 8-10**), whereby the amount of coprecipitated 3xHA-Cdt2 in case of NLS-4xFLAG-Dap_1-160 was comparable to that of the full-length Dap versions. It made no significant difference whether HA-CycE/Cdk2-HA was coexpressed with NLS-4xFLAG-Dap_1-160 or not. Both NLS-4xFLAG-Dap_1-125_dCDI and NLS-4xFLAG-Dap_1-125 were able to coprecipitate 3xHA-Cdt2 but only weakly (**lane 11, 12**). In summary, the results suggest that the N-terminal part of Dap (aa 1-160) mediates binding to Cdt2 and the region between aa 125-160 apparently is required for a more robust interaction. In contrast, interaction of the C-terminal part of Dap including the PIP degron (aa 160-245) with Cdt2 cannot be detected by co-IP experiments.

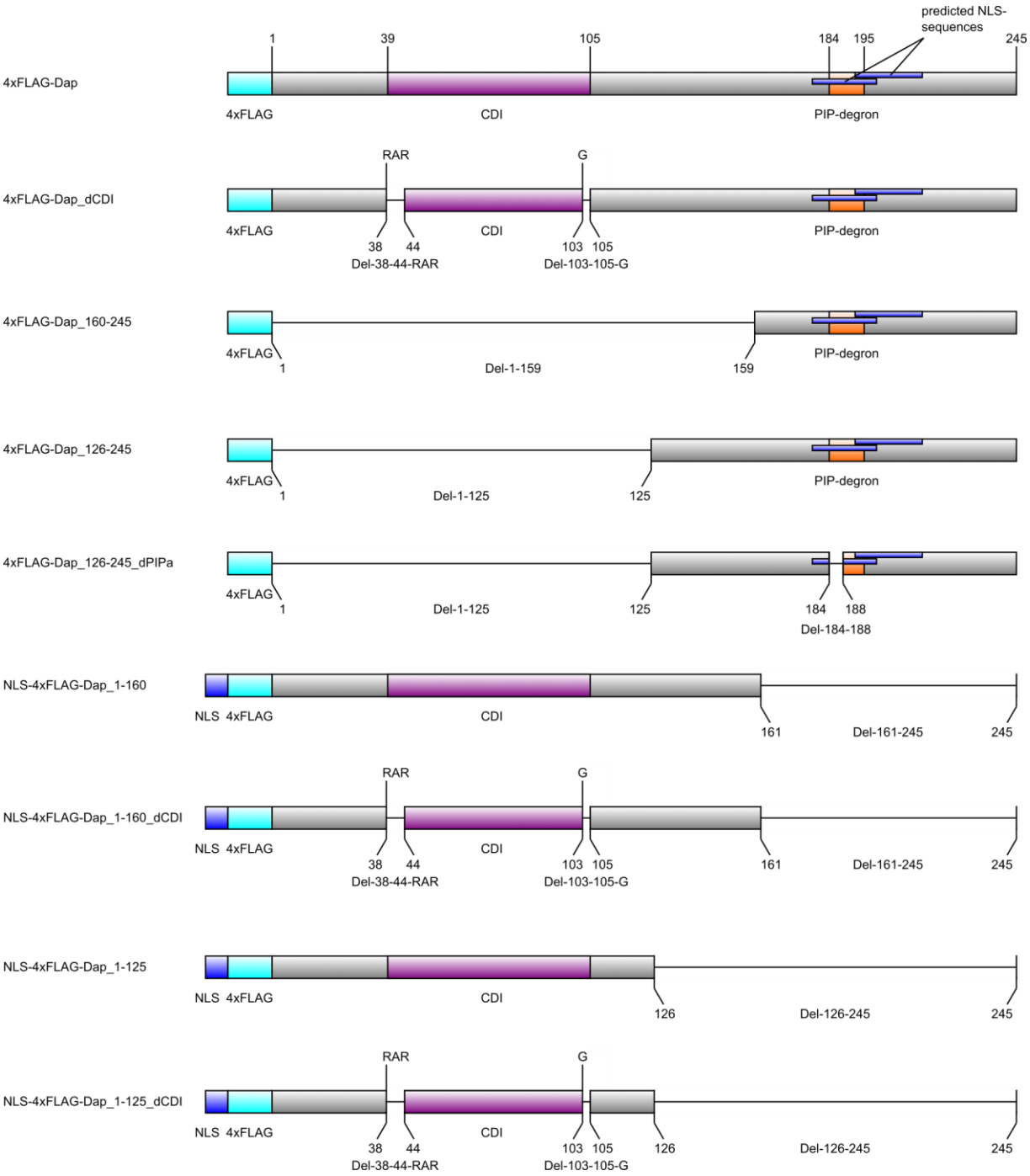

Figure 17 | Dap constructs used for co-IPs

The depicted Dap constructs were used for co-IP analysis with 3xHA-Cdt2 (see Figure 18) and 3xHA-Rca1 (see Figure 35). Dap contains two sequences, which are predicted to be NLS sequences: NLS-01: aa 192-214, NLS-Mapper Score: 15; NLS-02: aa 178-199, NLS-Mapper Score: 5.2. Since the depicted N-terminal fragments of Dap did not contain these predicted NLS-sequences, an artificial NLS-sequence was fused at the N-terminus. The NLS-Mapper Scores were determined using the cNLS Mapper based on Kosugi et al. (https://nls-mapper.iab.keio.ac.jp/cgi-bin/NLS_Mapper_form.cgi).

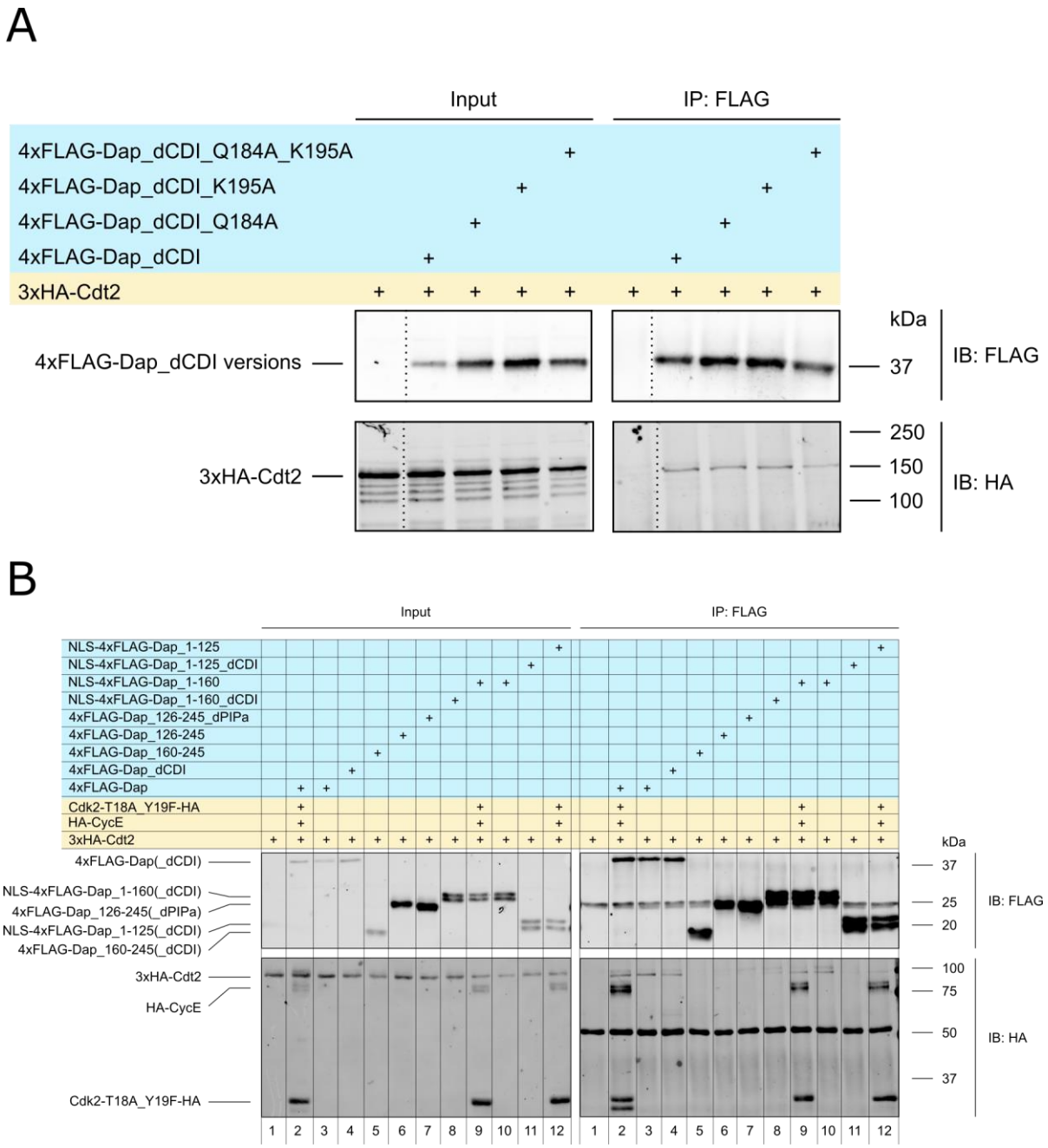

Figure 18 | The N-terminal part of Dap mediates interaction with Cdt2

A) The interaction of Dap_dCDI constructs with mutations in the PIP degron and Cdt2 was analyzed by co-IPs. All tested constructs (4xFLAG-Dap_dCDI, 4xFLAG-Dap_dCDI_Q184A, 4xFLAG-Dap_dCDI_K195A and 4xFLAG-Dap_dCDI_Q184A_K195A) were able to coprecipitate Cdt2. Therefore, neither Q184 nor K195 in Dap_dCDI are needed for the interaction with Cdt2. **B)** To find out, which domains in Dap mediate interaction with Cdt2, different N- and C-terminal fragments of Dap were used. The N-terminal fragments of Dap, which lacked predicted NLS-sequences were fused with an artificial NLS-sequence. Dap constructs that included a functional CDI domain were expressed together with HA-CycE/Cdk2-T18A_Y19F-HA to facilitate the G1/S transition. Coprecipitation of 3xHA-Cdt2 with NLS-4xFLAG-Dap_1-160 (lane 10) was almost as efficient as with the full-length Dap constructs 4xFLAG-Dap and 4xFLAG-Dap_dCDI (lane 2-4). Moreover, the Dap_1-125 constructs (lane 11, 12) were able to coprecipitate 3xHA-Cdt2, albeit less efficient than the Dap_1-160 fragments (lane 8-10). This indicates that the N-terminal part of Dap (aa 1-160) is important for binding to Cdt2. In contrast, C-terminal fragments of Dap showed either no (4xFLAG-Dap_160-245) (lane 5) or weak (4xFLAG-Dap_126-245(_dPIPa)) (lane 6, 7) interaction with 3xHA-Cdt2.

4.7 PCNA and Cdt2 interact with each other

For the human system it was shown that the C-terminal part of Cdt2 contains a PIP box that mediates binding of Cdt2 to PCNA (Hayashi et al. 2018). We were interested, whether interaction between PCNA and Cdt2 can also be detected for the *Drosophila* system. To test this, co-IPs were conducted. On the one hand, it was tested whether 3xHA-PCNA can be coprecipitated using 4xFLAG-Cdt2. On the other hand, the opposite direction – coprecipitation of 3xHA-Cdt2 using 4xFLAG-PCNA – was also tested. The amount of coprecipitated 3xHA-PCNA using 4xFLAG-Cdt2 was very small (**Figure 19**). Coprecipitation of 3xHA-Cdt2 using 4xFLAG-PCNA did not show any coprecipitated 3xHA-Cdt2. This indicates that the interaction between PCNA and Cdt2 is weak, at least in this experimental setup. An analysis of the Cdt2 sequence of different organisms revealed an important difference in the first amino acid of the PIP box in *Drosophila*. In contrast to most organisms where methionine is present, *Drosophila* Cdt2 contains a glutamate (**Figure 19 A**). A crystal structure of human Cdt2 C-terminal PIP box peptide in complex with PCNA indicates that this methionine (M706) makes contact with PCNA (Hayashi et al. 2018) (**Figure 19 B**). Methionine contains a short hydrophobic side chain, whereas glutamate harbors a much longer and hydrophilic sidechain. This could disturb the proposed binding to PCNA. Therefore, we speculated that it might be possible to increase the interaction between PCNA and Cdt2 by changing the glutamate into methionine (Cdt2_E712M). Again, both precipitation directions were tested with 4xFLAG-Cdt2_E712M or 3xHA-Cdt2_E712M, respectively. However, neither coprecipitation of 3xHA-PCNA using 4xFLAG-Cdt2_E712M nor coprecipitation of 3xHA-Cdt2_E712M using 4xFLAG-PCNA showed interaction between PCNA and Cdt2 with this mutation. Therefore, the glutamate at the first position of the PIP-box is not the reason for the weak interaction between PCNA and Cdt2 in coprecipitation experiments using *Drosophila* proteins.

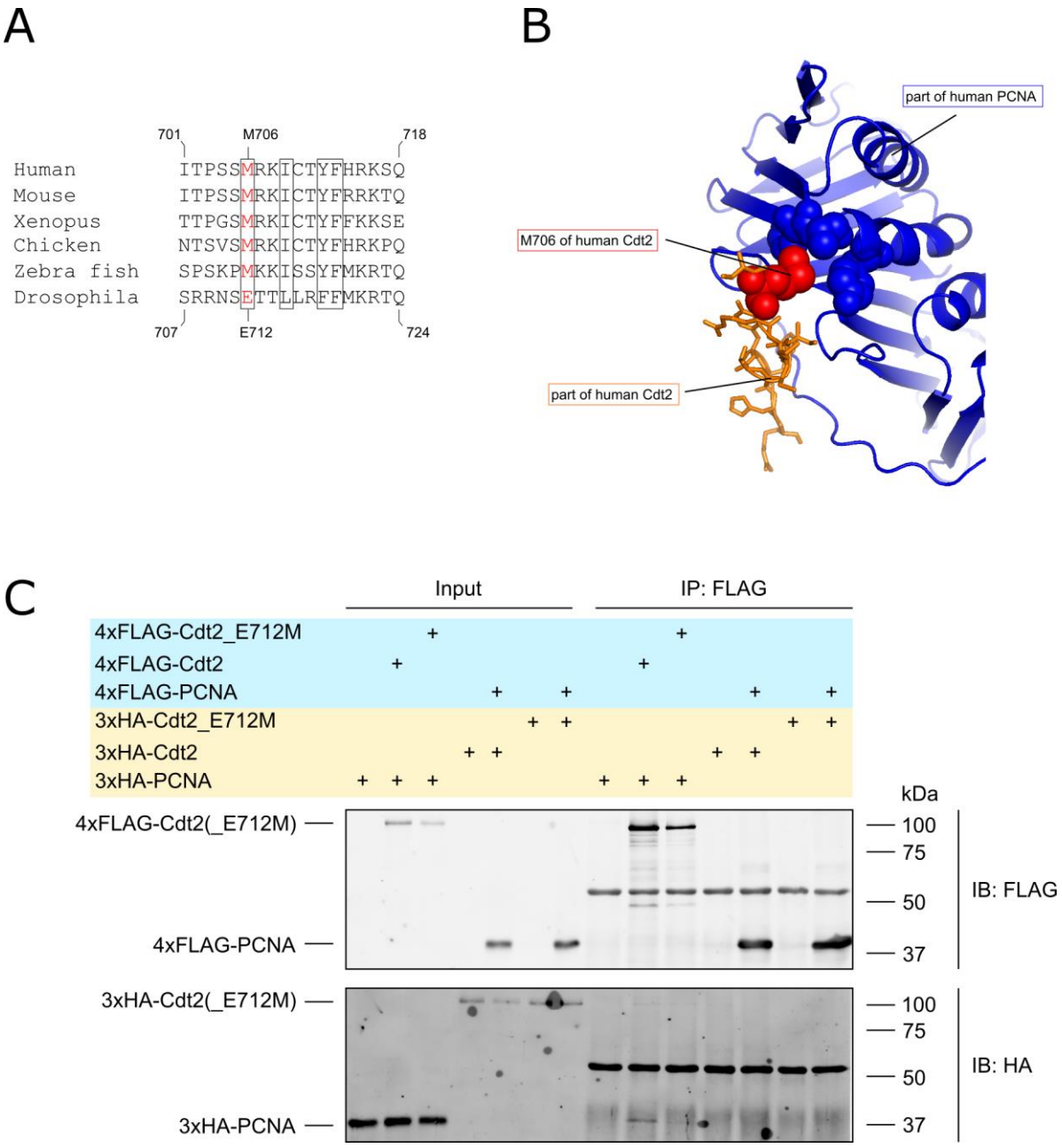

Figure 19 | Weak PCNA and Cdt2 interaction in co-IP experiments
A) Sequence alignment of the PIP box region of Cdt2 in different organisms. In contrast to many vertebrates, *Drosophila* harbors a glutamate instead of a methionine at the first position of the PIP box. **B)** M706 – the first amino acid of the PIP box in human Cdt2 – makes contact to PCNA. The corresponding amino acid in *Drosophila* (E712) harbors a hydrophilic side chain instead of a hydrophobic one. Therefore, we speculated, whether the interaction between *Drosophila* Cdt2 and PCNA can be increased, if E712 is mutated into methionine. **C)** The interaction between PCNA and Cdt2 or Cdt2_E712M was studied by co-IP. 3xHA-PCNA was coprecipitated in low amounts using 4xFLAG-Cdt2. Using 4xFLAG-Cdt2_E712M for precipitation no 3xHA-PCNA was coprecipitated. In addition, no 3xHA-Cdt2 or 3xHA-Cdt2_E712M was coprecipitated using 4xFLAG-PCNA. Therefore, the mutation of glutamate into methionine was not able to increase the interaction between Cdt2 and PCNA.

4.8 A basic cluster in the PIP degron of Dap is essential for CRL4-Cdt2 dependent degradation

Dap_dCDI_K195A was noticeably more stable as Dap_dCDI (chapter 4.4), but K195 was neither needed for interaction with PCNA (chapter 4.5) nor Cdt2 (chapter 4.6). Therefore, we speculated whether K195 acts as a ubiquitination site for CRL4-Cdt2. Lysines as well as the N-terminus of a protein are the only locations where a protein can be ubiquitinated (Komander and Rape 2012). In case that K195 is an important ubiquitin acceptor site, mutation to arginine (K195R) should stabilize Dap_dCDI to the same extent as the previously tested K195A mutation. On the other hand, arginine as chemically similar amino acid might be able (at least partially) to fulfill the role of K195 if this is not a ubiquitin acceptor site.

The results in **Figure 20** show that Dap_dCDI_K195R was not as much stabilized in S phase as Dap_dCDI_K195A indicating that the arginine at position 195 can partially compensate for the loss of lysine. Therefore, K195 is not an essential ubiquitination site. K195 could play a role in protein-protein or protein-DNA interaction. Both to the left and to the right of K195 are two basic amino acids (R194 and R196). In many other CRL4-Cdt2 substrates such as human p21 and Cdt1 from human and *Drosophila* there are also basic amino acids at the corresponding positions (B + 3 and B + 5; the number refers to the distance from the PIP box) (**Figure 20 A**). At least for p21 it is known that the basic amino acids at the positions B + 3 and B + 5 interact with acidic residues within PCNA (Gulbis et al. 1996). In addition, mutation of B + 5 in human p21 and in *Xenopus* Cdt1 lead to reduced destruction due to impeded binding to PCNA (Havens and Walter 2009; Nishitani et al. 2008). Therefore, we were interested whether mutation of R194 and R196 in Dap_dCDI also affects its stability in S phase. Dap_dCDI_R194A_R196A was similar stable as Dap_dCDI_K195A (**Figure 20 B**). Therefore, R194 or/and R196 play a role for the degradation of Dap_dCDI. Furthermore, Dap_dCDI_R194A_K195A_R196A was even more stable as Dap_dCDI_K195A or Dap_dCDI_R194A_R196A. Similar trends for the stabilization by these basic amino acids were also observed for Dap constructs with functional CDI domain (**Figure 20 C**).

To figure out the mechanism for the stabilization of Dap by mutation of R194, K195 and R196 co-IPs were conducted (**Figure 20 D**). It was tested, whether 4xFLAG-Dap_dCDI_R194A_R196A and 4xFLAG-Dap_dCDI_R194A_K195A_R196 can coprecipitate 3xHA- PCNA. Although previously tested (chapter 4.5), 4xFLAG-Dap_dCDI, 4xFLAG-Dap_dCDI_K195A and 4xFLAG-Dap_dCDI_Q184A were included as controls. In accordance with previous experiments, the Q184A mutation almost completely abolished interaction with 3xHA-PCNA. However, all Dap_dCDI versions with mutations in R194A, K195A or R196A could coprecipitate 3xHA-PCNA as good as Dap_dCDI. Therefore, these basic amino acids are not essential for binding to PCNA. We refrained from investigating the interaction between Cdt2 and Dap constructs with

mutations of these basic amino acids via co-IP, since we already knew that the N-terminus of Dap (aa 1-160) is most important for binding to Cdt2 (chapter 4.6).

In summary, the basic amino acids cluster consisting of R194, K195 and R196 is essential for the degradation of Dap. However, these residues neither act as ubiquitination sites (K195) nor are they essential for binding to PCNA or Cdt2.

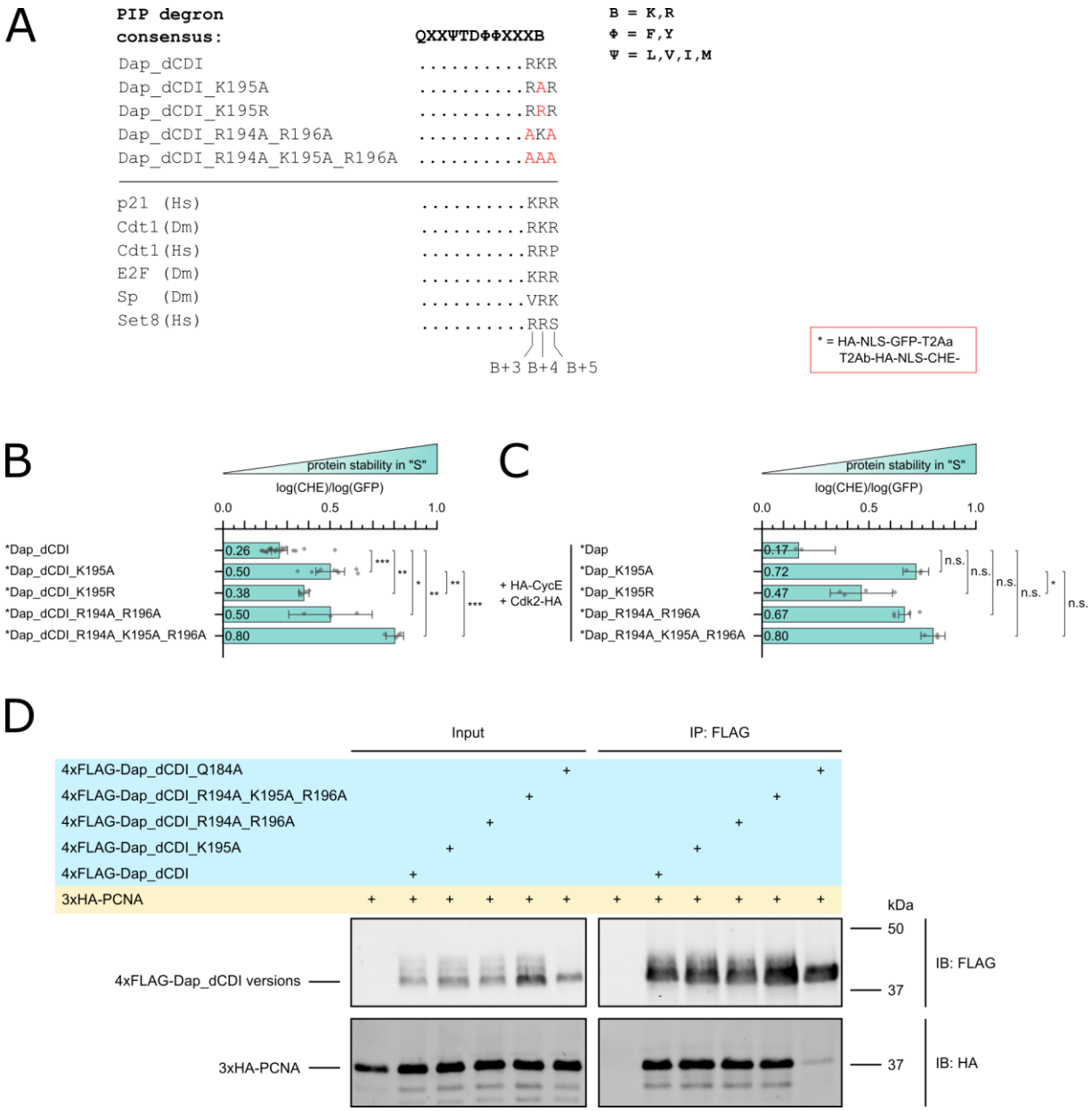

Figure 20 | A basic cluster in the PIP degron of Dap is essential for CRL4-Cdt2 dependent degradation

A) In Dap and several other substrates of CRL4-Cdt2 both left and right to the basic amino acid of the PIP degron consensus sequence (B+4; the number refers to the distance to the PIP box), there are neighboring basic amino acids (B+3 and B+5). To analyze the role of K195 as well as the neighboring basic amino acids R194 and R196, the shown Dap constructs were analyzed. Dm = *Drosophila melanogaster*, Hs = *Homo sapiens*. **B, C)** Barplots representing the relative stability of Dap_dCDI (**B**) and Dap (**C**) constructs with different mutations in the basic cluster (aa 194-196) in S phase. The data was obtained by flow cytometry. In case of the Dap constructs with functional CDI domain, HA-CycE and Cdk2-HA were coexpressed to facilitate the G1/S transition. For both Dap_dCDI and Dap the stabilization in S phase caused by K195R was not as strong as with K195A. This indicates that K195 does not act as a ubiquitination site, but is probably involved in protein-protein or protein-DNA interactions, which can be partially restored by the chemically similar amino acid arginine. The double mutation R194A_R196A stabilized Dap_dCDI and Dap to a similar extent as K195A. The triple mutation R194A_K195A_R196 led to the strongest stabilization. **D)** It was analyzed by co-IP whether mutation of R194, K195 or R196 affects interaction with Cdt2. 4xFLAG-Dap_dCDI_Q184 served as a negative control and, as expected, could hardly coprecipitate 3xHA-PCNA. In contrast, 4xFLAG-Dap_dCDI_K195A, 4xFLAG-Dap_dCDI_R194A_R196A and 4xFLAG-Dap_dCDI_R194A_K195A_R196 coprecipitated 3xHA-PCNA as efficient as Dap_dCDI.

4.9 Rca1 can destabilize Dap_dCDI_Q184A and Dap_Q184A in an F-box dependent manner

The degradation of Dap_dCDI_Q184A by CRL4-Cdt2 is strongly reduced, but not completely abolished (chapter 4.4). We were intrigued to investigate whether Rca1 could affect the stability of Dap_dCDI_Q184A, particularly in this scenario where the impact of CRL4-Cdt2 is significantly diminished. Overexpression of Rca1 led to destabilization of Dap_dCDI_Q184A in "G1" and G2", whereas knockdown of Rca1 increased its stability (**Figure 21 B, D, E**). In contrast, overexpression of Rca1_dFbox had no significant effect on Dap_dCDI_Q184A in G1 and G2. If the CRL4-Cdt2 dependent degradation of Dap_dCDI_Q184A was additionally reduced by a knockdown of Cdt2, the overall stability of this construct was increased (**Figure 21 C, F, G**). Under these conditions, overexpression of Rca1 still caused significant destabilization of Dap_dCDI_Q184A at least in G1 phase. Overexpression of Rca1_dFbox had no significant effect on Dap_dCDI_Q184A.

We also wanted to make sure that Dap constructs with functional CDI domain are influenced by Rca1 in the same manner as Dap_dCDI constructs. Dap_Q184A can inhibit CycE/Cdk2, which leads to a strong delay of the G1/S transition (data not shown). To avoid this G1 arrest, CycE and Cdk2 were coexpressed with Dap_Q184A. Under these conditions, overexpression of Rca1 tended to destabilize Dap_Q184A in G1 and G2 (**Figure 22 B, D, E**). Overexpression of Rca1_dFbox had no significant influence on Dap_Q184A both in G1 and G2. Knockdown of Rca1 tended to stabilize Dap_Q184A in G1 and G2. In another experiment, a knockdown of Cdt2 was additionally carried out (**Figure 22 C, F, G**). Here, a similar trend as without knockdown of Cdt2 were observed.

As previously noted, we assumed that some Rca1 effects on the stability of Dap constructs could be indirectly caused by changes in the cell cycle distribution and then CRL4-Cdt2 dependent degradation. Therefore, to reduce changes in the cell cycle distribution we enriched cells in G2 phase by using a more active CycE version with NLS sequence (NLS-4xFLAG-CycE). In addition, to increase the accumulation in G2 even more, less Dap_Q184A plasmid (20 ng instead of 40 ng) was used for transfection (**Figure 23**). Indeed, the cell cycle distributions were similar no matter whether Dap_Q184A was expressed alone or together with Rca1 constructs. Despite the similar cell cycle distributions, there was still the trend that Rca1 caused instability and Rca1 knockdown caused stabilization of Dap_Q184A in G1 and G2 (**Figure 23 C, D**). If a knockdown of Cdt2 was additionally conducted, it was not possible to achieve similar cell cycle distributions (**Figure 23 B**). Here, overexpression of Rca1 tended to reduce the stability of Dap_Q184A in G1 and G2. In contrast, knockdown of Rca1 had no noticeable effect on the stability of Dap_Q184A. In conclusion, these data show that Rca1 can destabilize a Dap mutant that is comprised in the CRL4-Cdt2 dependent degradation. Yet, even under these circumstances, residual degradation via CRL4-Cdt2 also contributes to Dap destabilization.

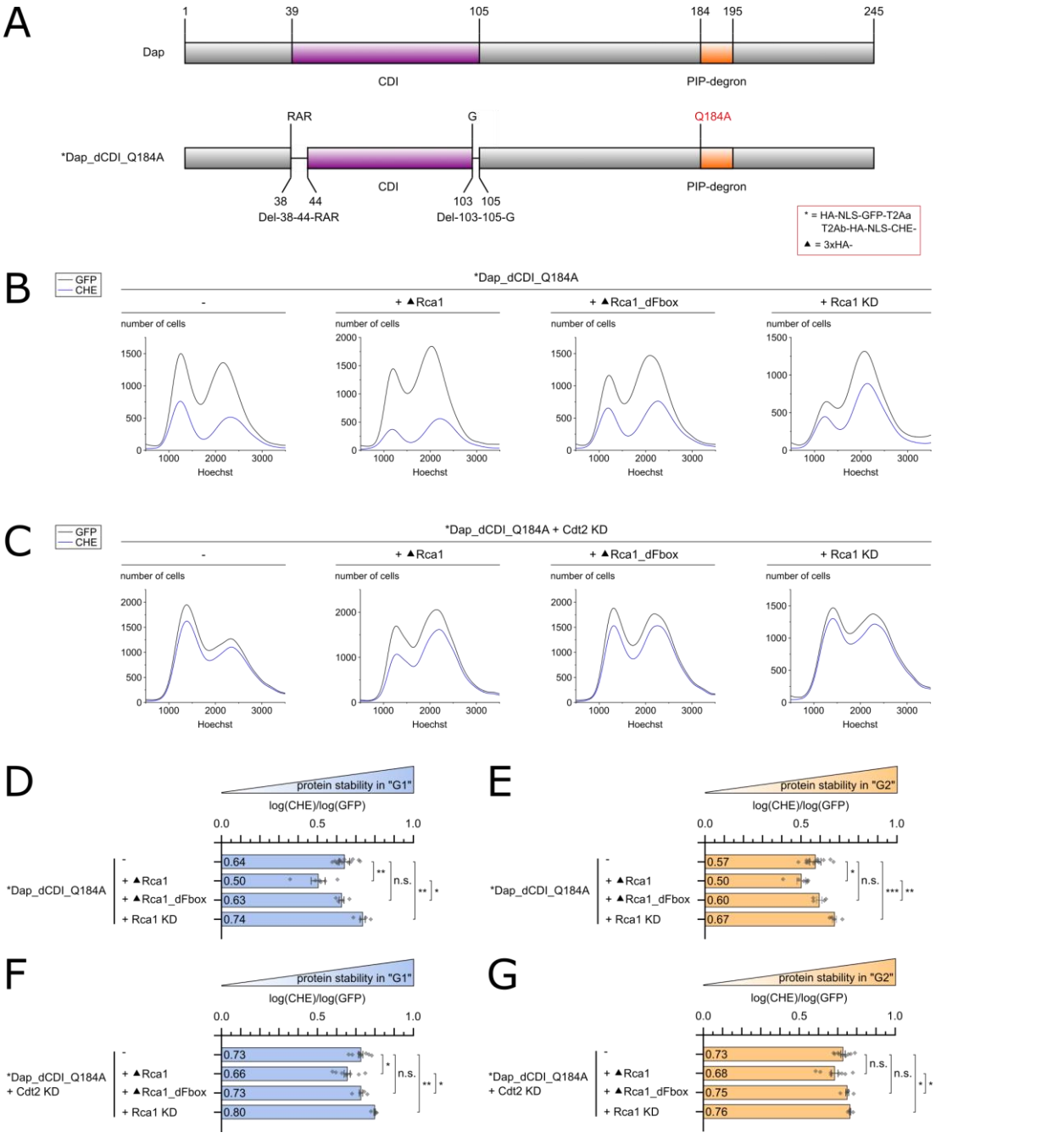

Figure 21 | Rca1 can influence the stability of Dap_dCDI_Q184A

A) Schematic representation of Dap_dCDI_Q184A. **B, D, E)** Cell cycle curves (**B**) and barplots (**D, E**) representing the relative stability of Dap_dCDI_Q184A. The data was obtained by flow cytometry. Coexpression of Rca1 destabilized Dap_dCDI_Q184A, whereas knockdown of Rca1 increased its stability in G1 and G2. Coexpression of Rca1_dFbox had no significant influence on the stability of Dap_dCDI_Q184A. **C, F, G)** Cell cycle curves (**B**) and barplots (**F, G**) representing the relative stability of Dap_dCDI_Q184A, when a knockdown of Cdt2 was applied. Coexpression of Rca1 tended to reduce the stability of Dap_dCDI_Q184A in G1 and G2. Coexpression of Rca1_dFbox had no significant influence on the stability of Dap_dCDI_Q184A. Both in G1 and G2, knockdown of Rca1 led to stabilization of Dap_dCDI_Q184A.

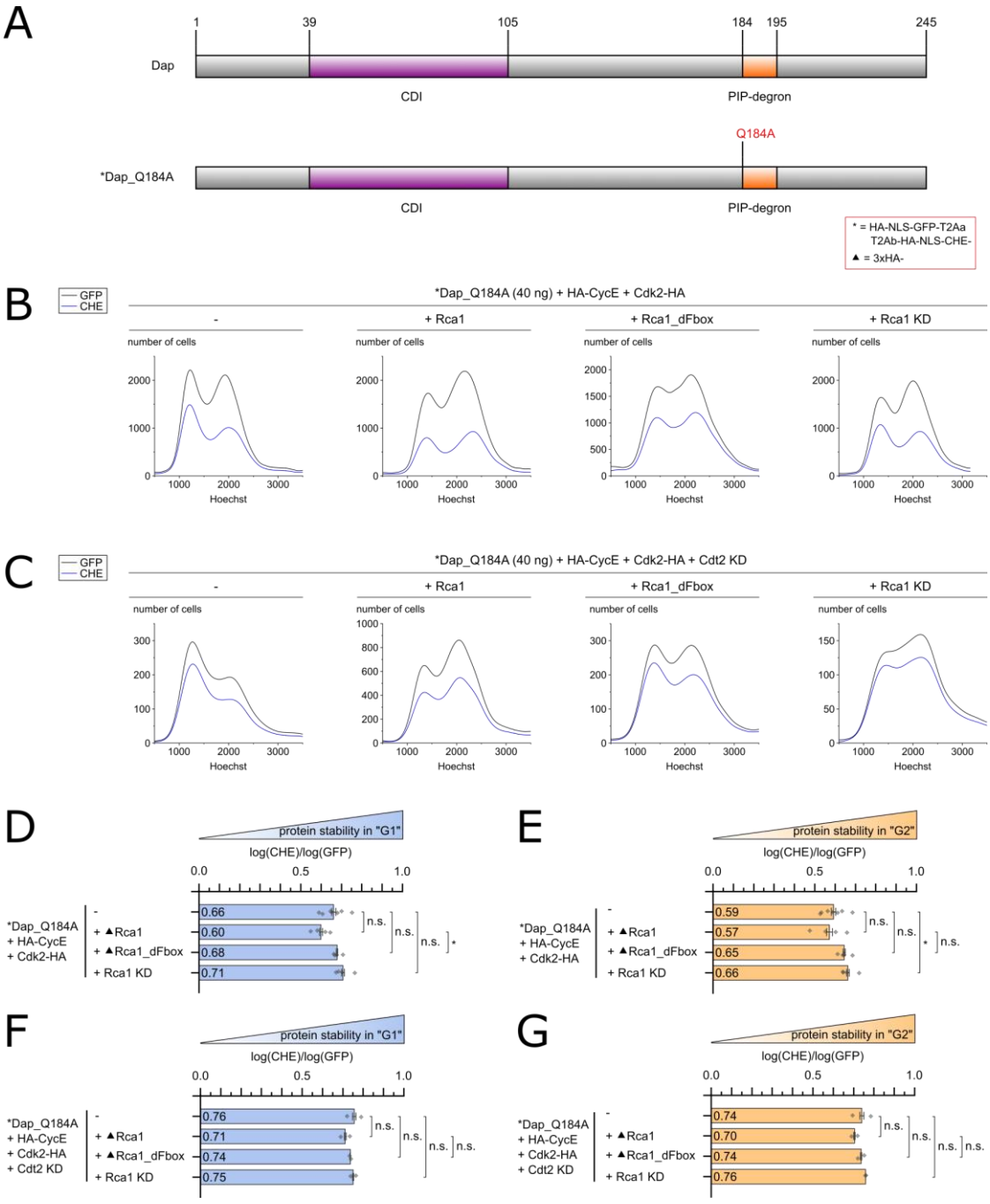

Figure 22 | Stability of Dap_Q184 can be influenced by Rca1

A) Schematic representation of Dap_Q184A. **B, D, E)** Cell cycle curves (**B**) and barplots (**D, E**) representing the relative stability of Dap_Q184A coexpressed with HA-CycE and Cdk2-HA. The data was obtained by flow cytometry. There was the tendency that coexpression of Rca1 led to destabilization of Dap_Q184A in G1 and G2. Coexpression of Rca1_dFbox tended to increase the stability of Dap_Q184A in G1 and G2. Knockdown of Rca1 tended to cause stabilization of Dap_Q184A in G1 and G2. **C, F, G**) Cell cycle curves (**C**) and barplots (**F, G**) representing the relative stability of Dap_Q184A coexpressed with HA-CycE and Cdk2-HA. In addition, a knockdown of Cdt2 (Cdt2 KD) was conducted. The trend of Rca1 effects on the stability of Dap_Q184A was similar compared to the setup without knockdown of Cdt2.

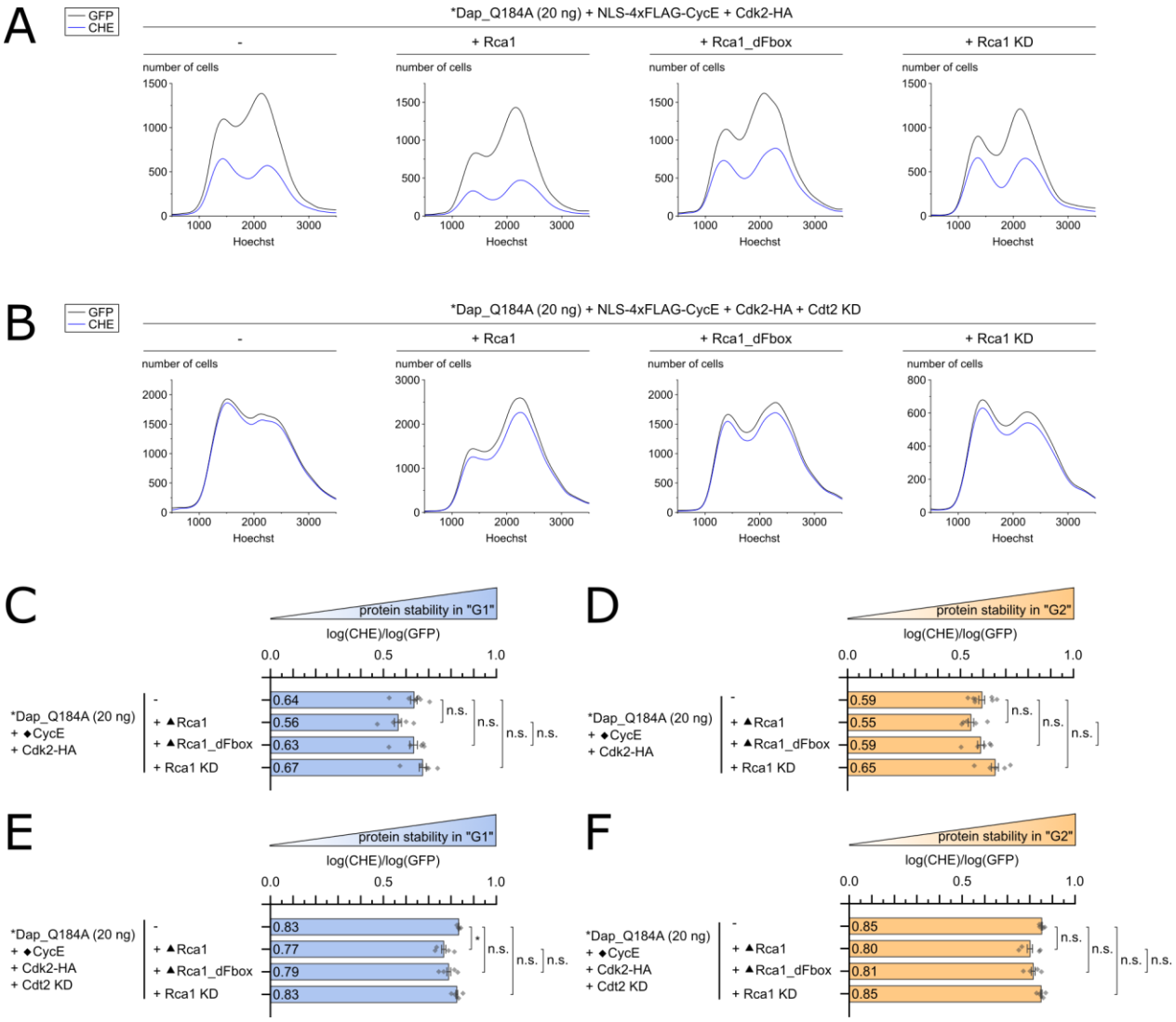

Figure 23 | Stability of Dap_Q184A can be influenced by Rca1 despite similar cell cycle profiles

A, C, D) Cell cycle curves (**A**) and barplots (**C, D**) representing the relative stability of Dap_Q184A (20 ng instead of the previously used 40 ng) coexpressed with NLS-4xFLAG-CycE and Cdk2-HA. The data was obtained by flow cytometry. By using less Dap_Q184 and a more active CycE version (NLS-4xFLAG-CycE) similar cell cycle profiles were achieved no matter, if Rca1/Rca1_dFbox were coexpressed or a knockdown of Rca1 was conducted. Especially, the cell cycle curves for Rca1 and Rca1_dFbox looked very similar. Despite that, there was the tendency that Rca1 caused destabilization and Rca1 knockdown stabilization of Dap_Q184A in G1 and G2. This indicates that the stability difference of Dap_Q184A by Rca1 is not only dependent on changes in cell cycle distribution.
B, E, F) Cell cycle curves (**B**) and barplots (**E, F**) representing the relative stability of Dap_Q184A (20 ng instead of the previously used 40 ng) coexpressed with NLS-4xFLAG-CycE and Cdk2-HA. In addition, a knockdown of Cdt2 was conducted. Under these conditions it was not possible to achieve similar cell cycle profiles for all samples. Coexpression of Rca1 tended to reduce the stability of Dap_Q184 in G1 and G2. However, knockdown of Rca1 had no noticeable effect on the stability of Dap_Q184A.

4.10 Rca1 can influence the stability of Dap constructs in which CRL4-Cdt2 dependent degradation is greatly reduced

Rca1 was able to influence the stability of Dap constructs with the PIP degron mutation Q184A (chapter 4.9). We now wanted to analyze if Rca1 can destabilize Dap containing other PIP degron mutations.

In particular, our focus was on determining whether the effects of Rca1 persist in Dap constructs where the degradation dependent on CRL4-Cdt2 is not only diminished (e.g. Dap(_dCDI)_Q184A), but also in those where such degradation is nearly eliminated (e.g. Dap(_dCDI)_dPIPa). The subsequent constructs were examined in this context: Dap(_dCDI)_K195A (**Figure 24**), Dap(_dCDI)_K195R (**Figure 25**), Dap(_dCDI)_R194A_R196A (**Figure 26**), Dap(_dCDI)_R194A_K195A_R196A (**Figure 27**), Dap(_dCDI)_Q184A_K195A (**Figure 28**) and Dap(_dCDI)_dPIPa (**Figure 29**). For three Dap constructs with functional CDI domain (Dap_K195A, Dap_Q184A_K195A and Dap_dPIPa) we coexpressed NLS-4xFLAG-CycE and used less plasmid DNA (20 ng instead of 40 ng) to avoid a G1 arrest caused by these Dap constructs.

As seen previously, the mutations K195A, K195R or R194A_R196A caused moderate S phase instability, respectively, but did not completely stabilize Dap_dCDI (**Figure 15, 20**). For these constructs, Rca1 effects were in general comparable to that of Dap(_dCDI)_Q184A: Overexpression of Rca1 led to destabilization in “G1” and “G2”, whereas knockdown of Rca1 caused stabilization. Overexpression of Rca1 was consistently more potent in destabilizing these Dap constructs than overexpression of Rca1_dFbox. The general stability and the extent of Rca1 effects was largely independent on whether a functional CDI domain was present or not. However, for Dap_K195A, the Rca1 effects were weaker than for Dap_dCDI_K195A.

With the Q184A_K195A double, R194A_K195A_R196A triple or dPIPa-deletion mutation, the general stability of Dap_dCDI was much higher than of previously described Dap versions. In general, overexpression of Rca1 or knockdown of Rca1 tended to influence the stability of these constructs. The stability values in the barplot charts are presented on a logarithmic scale (chapter 7.4.4). This presentation allows a good comparison of relative protein stability within an experiment when a single Dap construct is examined. When comparing various Dap constructs with differing initial stabilities and subsequently assessing the impact of Rca1 on their stability, representing the relative protein stabilities on a linear scale may be easier to interpret. These are shown in **Figure 30 and 31**, in which the differences are represented on a linear scale. These barplots with linear scale show that Rca1 knockdown results in stabilization of almost all constructs in “G1” as well as in “G2” to variable extent. Rca1 overexpression did result in destabilization of all Dap constructs with intact CDI domain in “G1”. There was no correlation with the starting stability of the different constructs, indicating that Rca1 can induce destabilization independent

of the PIP degron, but these effects of Rca1 on Dap with compromised PIP degron remained rather weak. When Dap constructs with mutated CDI domain and various PIP degron mutations were analyzed, Rca1 overexpression was only showing destabilizing effects in G1 with either no PIP degron mutation or the Q184A or K195A mutation. This could indicate that overexpressed Rca1 has restricted ability to destabilize Dap constructs with mutated PIP degron, when Dap is not associated with CycE/Cdk2. However, the observation that Rca1 knockdown still results in stabilization of all constructs shows that (endogenous) Rca1 is involved in Dap protein level regulation.

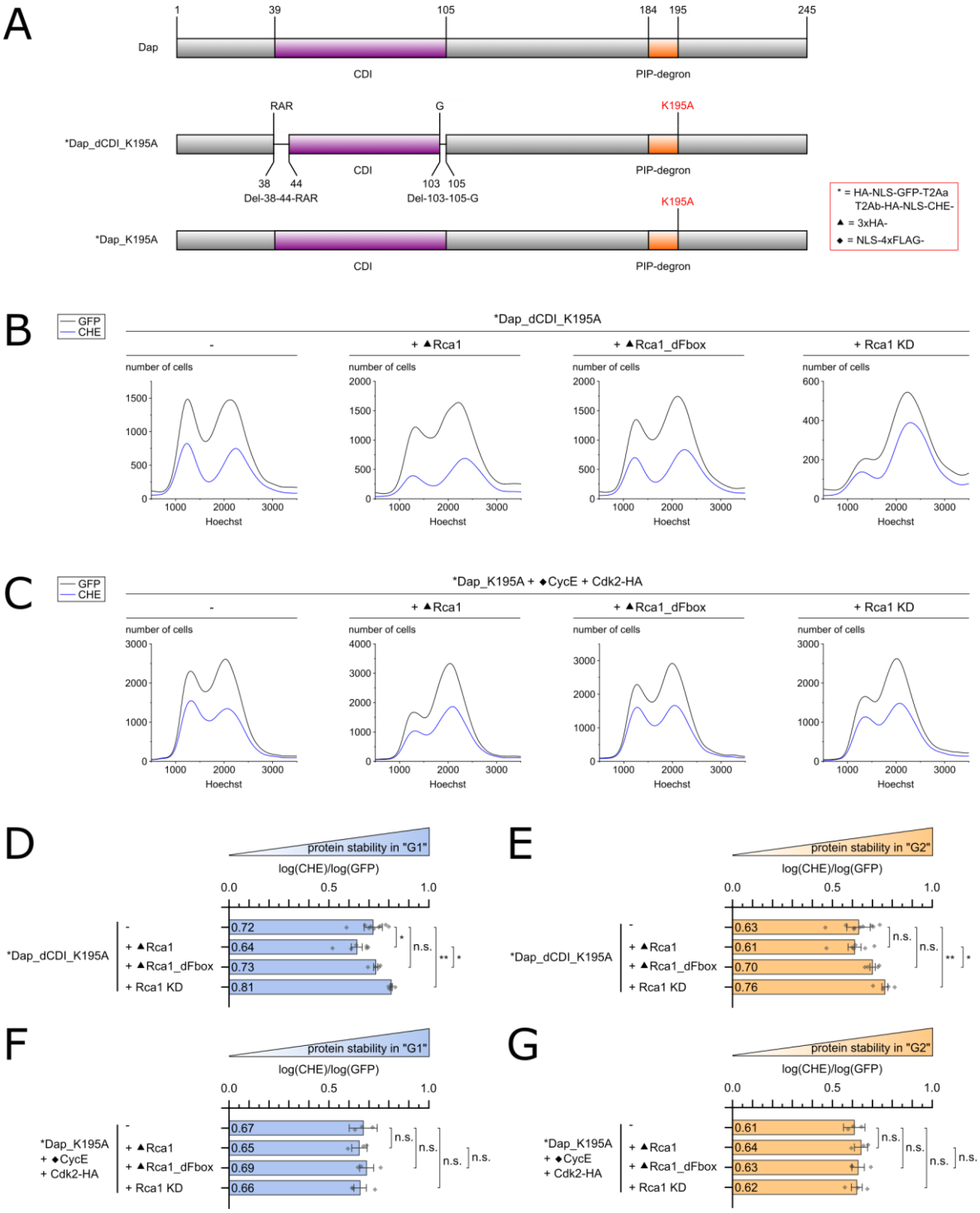

Figure 24 | Influence of Rca1 on the stability of Dap_dCDI_K195A and Dap_K195A

A) Schematic representation of Dap_dCDI_K195A and Dap_K195A. **B, D, E)** Cell cycle curves (**B**) and barplots (**D, E**) representing the relative stability of Dap_dCDI_K195A. The data was obtained by flow cytometry. Coexpression of Rca1 tended to destabilize Dap_dCDI_K195A in G1 and G2, whereas knockdown of Rca1 (Rca1 KD) caused stabilization in G1 and G2. Rca1_dFbox had no significant influence on the stability of Dap_dCDI_K195 in G1 and G2 **C, F, G**) Cell cycle curves (**C**) and barplots (**F, G**) representing the relative stability of Dap_K195A coexpressed with NLS-4xFLAG-CycE and Cdk2-HA. Effects of Rca1/Rca1_dFbox coexpression or knockdown of Rca1 on the stability of Dap_K195A were not significant.

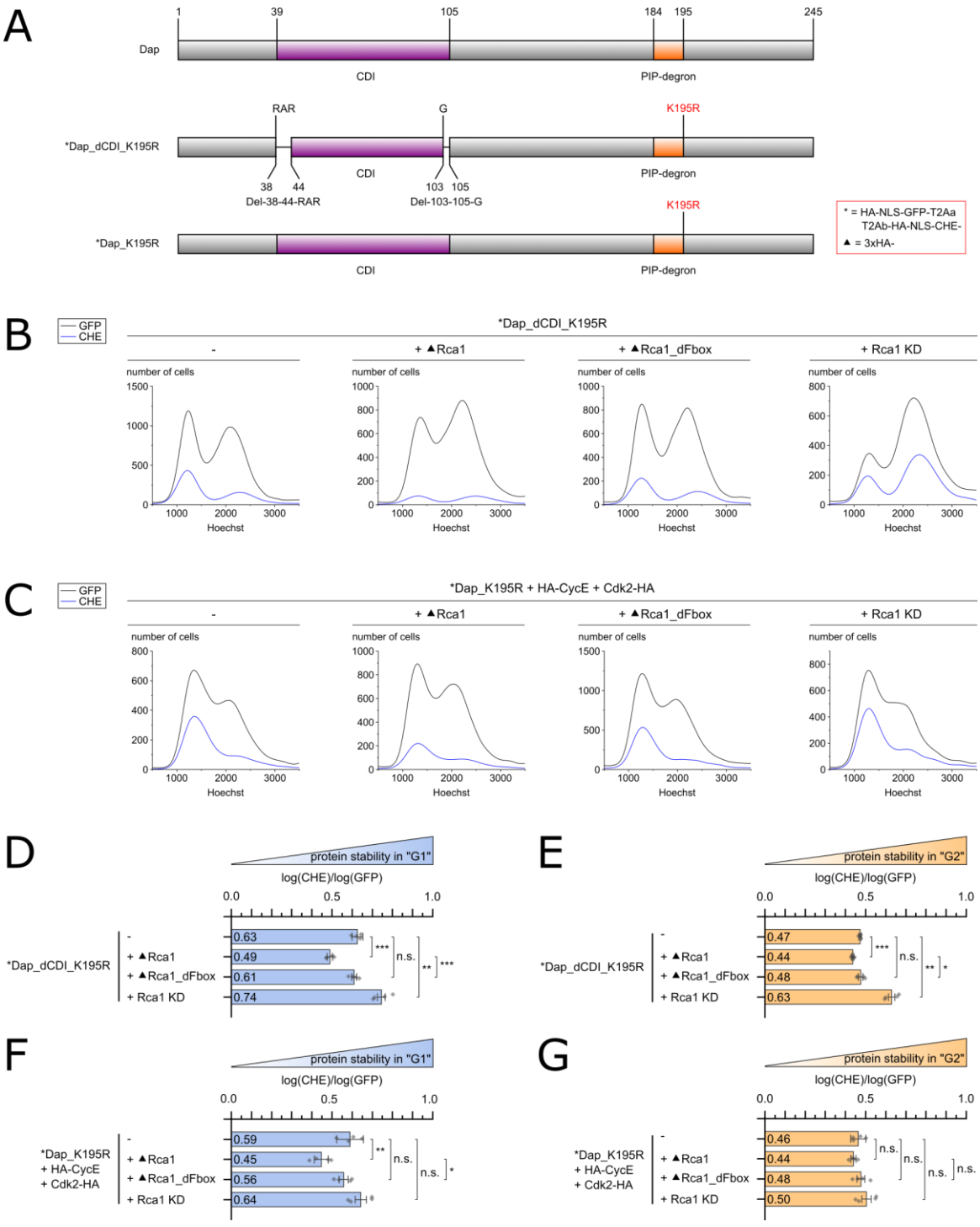

Figure 25 | Influence of Rca1 on the stability of Dap_dCDI_K195R and Dap_K195R

A) Schematic representation of Dap_dCDI_K195R and Dap_K195R. **B, D, E)** Cell cycle curves (**B**) and barplots (**D, E**) representing the relative stability of Dap_dCDI_K195R. The data was obtained by flow cytometry. Coexpression of Rca1 caused a destabilization of Dap_dCDI_K195R in G1 and G2, whereas knockdown of Rca1 (Rca1 KD) caused stabilization. Coexpression of Rca1_dFbox did not significantly influence the stability of Dap_dCDI_K195R. **C, F, G)** Cell cycle curves (**C**) and barplots (**F, G**) representing the relative stability of Dap_K195R coexpressed with HA-CycE and Cdk2-HA. Coexpression of Rca1 caused destabilization of Dap_K195R in G1. Knockdown of Rca1 tended to increase the stability Dap_K195R in G1 and G2. Coexpression of Rca1_dFbox had no significant influence on the stability of Dap_K195R.

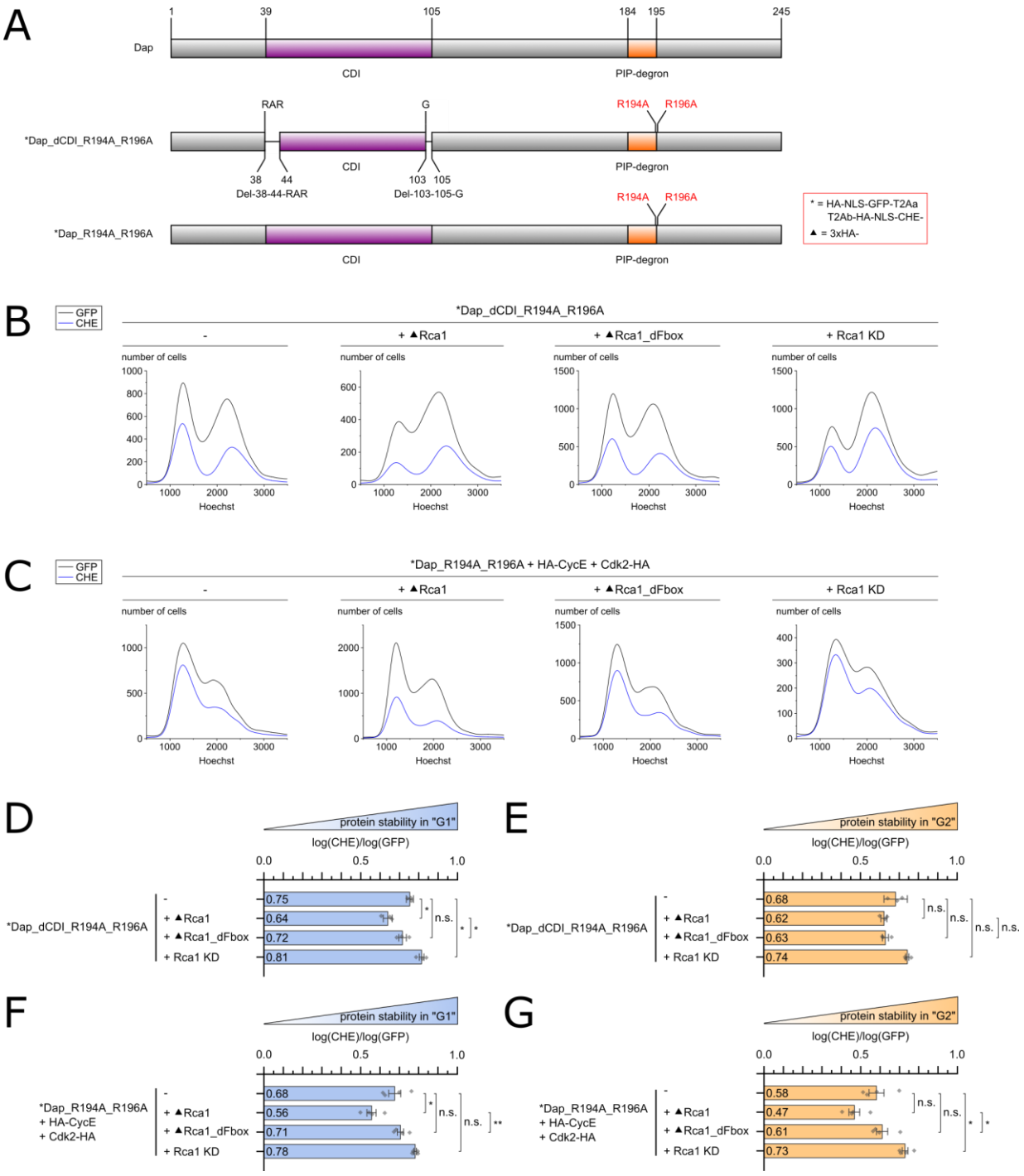

Figure 26 | Influence of Rca1 on the stability of Dap_dCDI_R194A_R196A and Dap_R194A_R196A

A) Schematic representation of Dap_dCDI_R194A_R196A and Dap_R194A_R196A. **B, D, E)** Cell cycle curves (**B**) and barplots (**D, E**) representing the relative stability of Dap_dCDI_R194A_R196A. The data was obtained by flow cytometry. Coexpression of Rca1 tended to decrease the stability of Dap_dCDI_R194A_R196A in G1 and G2, whereas knockdown of Rca1 (Rca1 KD) tended to stabilize it. At least in G1, coexpression of Rca1_dFbox tended to have a weaker destabilizing effect on Dap_dCDI_R194A_R196A than Rca1. **C, F, G**) Cell cycle curves (**C**) and barplots (**F, G**) representing the relative stability of Dap_R194A_R196A coexpressed with HA-CycE and Cdk2-HA. Coexpression of Rca1 tended to cause destabilization of Dap_R194A_R196A in G1 and G2, whereas knockdown of Rca1 tended to increase its stability. Coexpression of Rca1_dFbox had no significant influence on the stability of Dap_R194A_R196A.

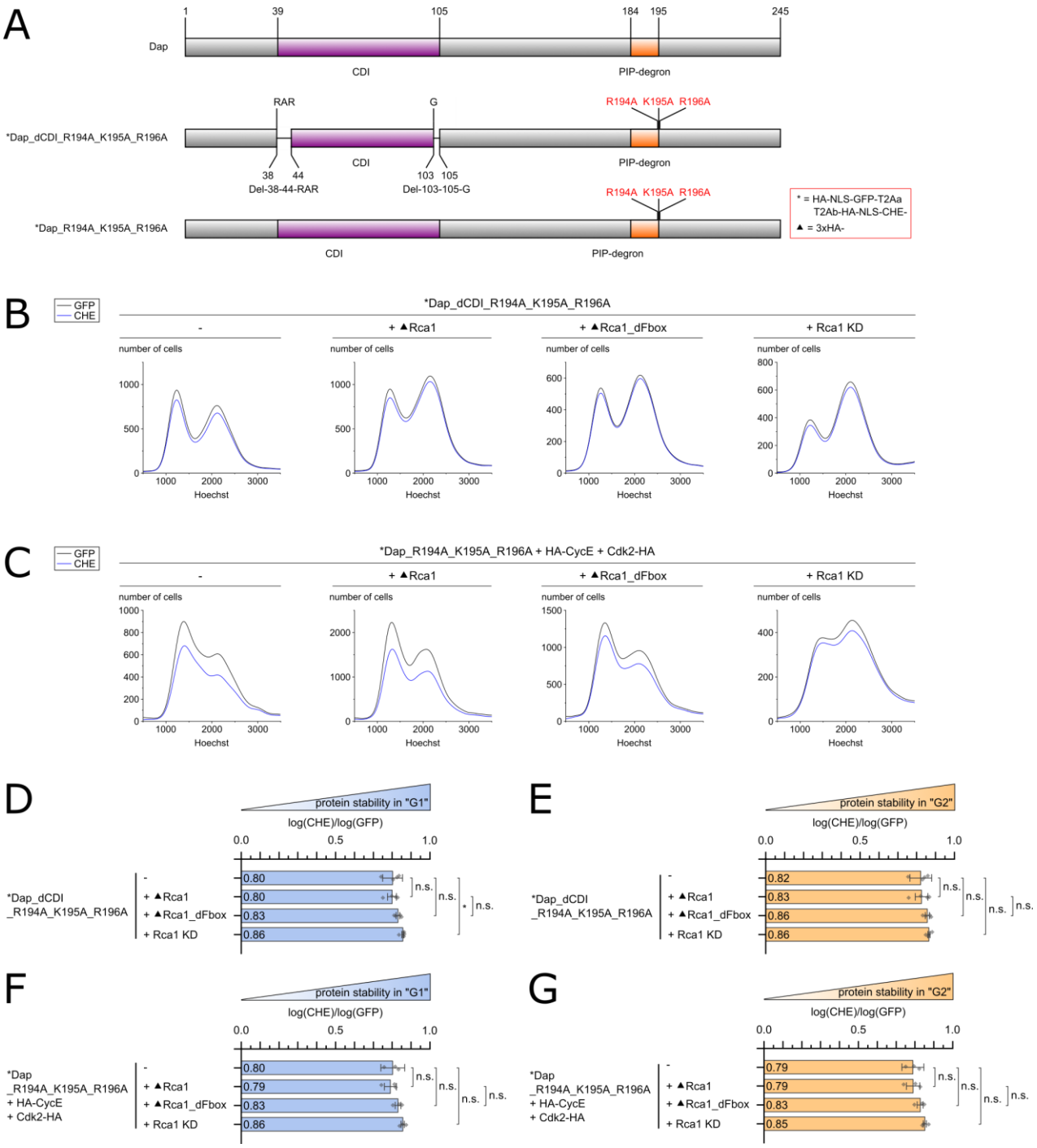

Figure 27 | Influence of Rca1 on the stability of Dap_dCDI_R194A_K195A_R196A and Dap_R194A_K195A_R196A
A) Schematic representation of Dap_dCDI_R194A_K195A_R196A and Dap_R194A_K195A_R196A. **B, D, E)** Cell cycle curves (**B**) and barplots (**D, E**) representing the relative stability of Dap_dCDI_R194A_K195A_R196A. The data was obtained by flow cytometry. Coexpression of Rca1 had no significant effect on the stability of Dap_dCDI_R194A_K195A_R196A in G1 and G2. In contrast, knockdown of Rca1 and coexpression of Rca1_dFbox tended to cause stabilization of Dap_dCDI_R194A_K195A_R196A in G1 and G2.. **C, F, G**) Cell cycle curves (**C**) and barplots (**F, G**) representing the relative stability of Dap_R194A_K195A_R196A coexpressed with HA-CycE and Cdk2-HA. Knockdown of Rca1 and coexpression of Rca1_dFbox tended to cause stabilization of Dap_R194A_K195A_R196A in G1 and G2.

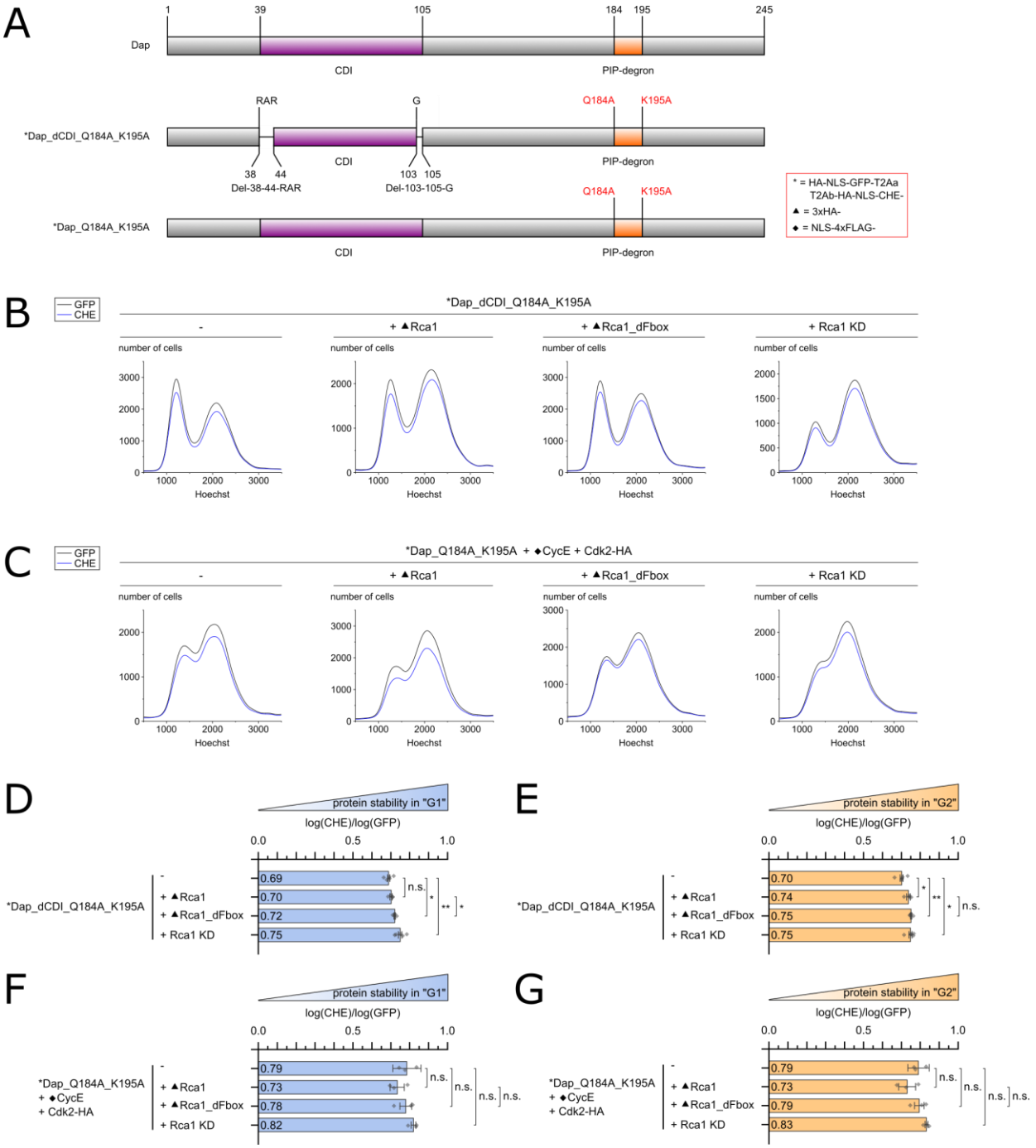

Figure 28 | Influence of Rca1 on the stability of Dap_dCDI_Q184A_K195A and Dap_Q184A_K195A

A) Schematic representation of Dap_dCDI_Q184A_K195A and Dap_Q184A_K195A. **B, D, E)** Cell cycle curves (**B**) and barplots (**D, E**) representing the relative stability of Dap_dCDI_Q184A_K195A. The data was obtained by flow cytometry. Coexpression of Rca1 had no significant effect on the stability of Dap_dCDI_Q184A_K195A in G1. In contrast, coexpression of Rca1_dFbox or knockdown of Rca1 caused stabilization of Dap_dCDI_Q184A_K195A in G1. In G2, both coexpression of Rca1 or Rca1_dFbox as well as knockdown of Rca1 significantly increased the stability of Dap_dCDI_Q184A_K195A. **C, F, G**) Cell cycle curves (**C**) and barplots (**F, G**) representing the relative stability of Dap_Q184A_K195A coexpressed with NLS-4xFLAG-CycE and Cdk2-HA. Coexpression of Rca1 tended to decrease the stability of Dap_Q184A_K195A in G1 and G2, whereas knockdown of Rca1 tended to increase its stability. Coexpression of Rca1_dFbox had no significant influence on the stability of Dap_Q184A_K195A.

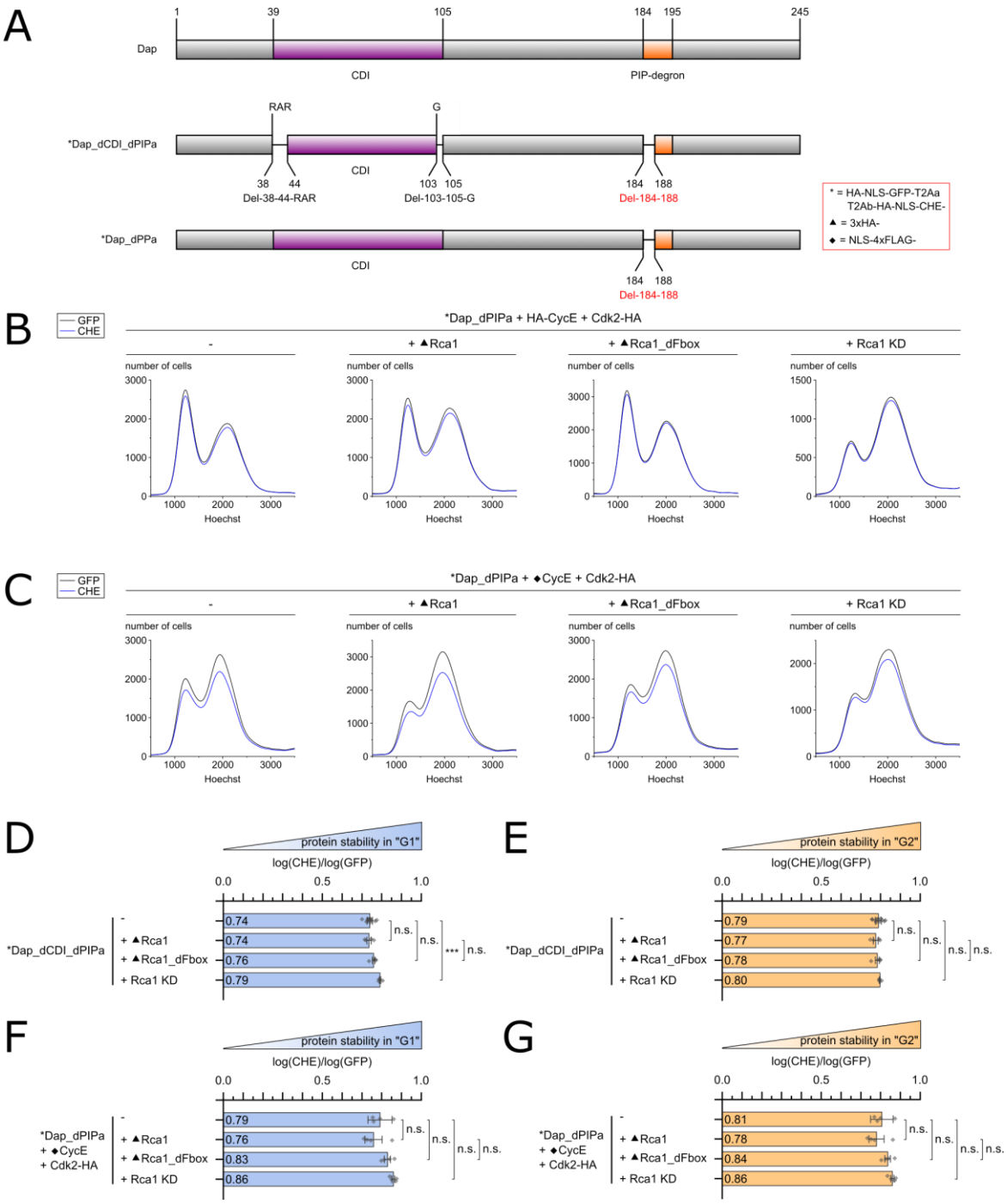

Figure 29 | Influence of Rca1 on the stability of Dap_dCDI_dPIPa and Dap_dPIPa

A) Schematic representation of Dap_dCDI_dPIPa and Dap_dPIPa. **B, D, E)** Cell cycle curves (**B**) and barplots (**D, E**) representing the relative stability of Dap_dCDI_dPIPa. The data was obtained by flow cytometry. Coexpression of Rca1 had no effect on the stability of Dap_dCDI_dPIPa in G1 and G2. In contrast, knockdown of Rca1 tended to stabilize Dap_dCDI_dPIPa, at least in G1. **C, F, G)** Cell cycle curves (**C**) and barplots (**F, G**) representing the relative stability of Dap_dPIPa coexpressed with NLS-4xFLAG-CycE and Cdk2-HA. Coexpression of Rca1 tended to destabilize Dap_dPIPa in G1 and G2. Knockdown of Rca1 and coexpression of Rca1_dFbox tended to stabilize Dap_dPIPa in G1 and G2.

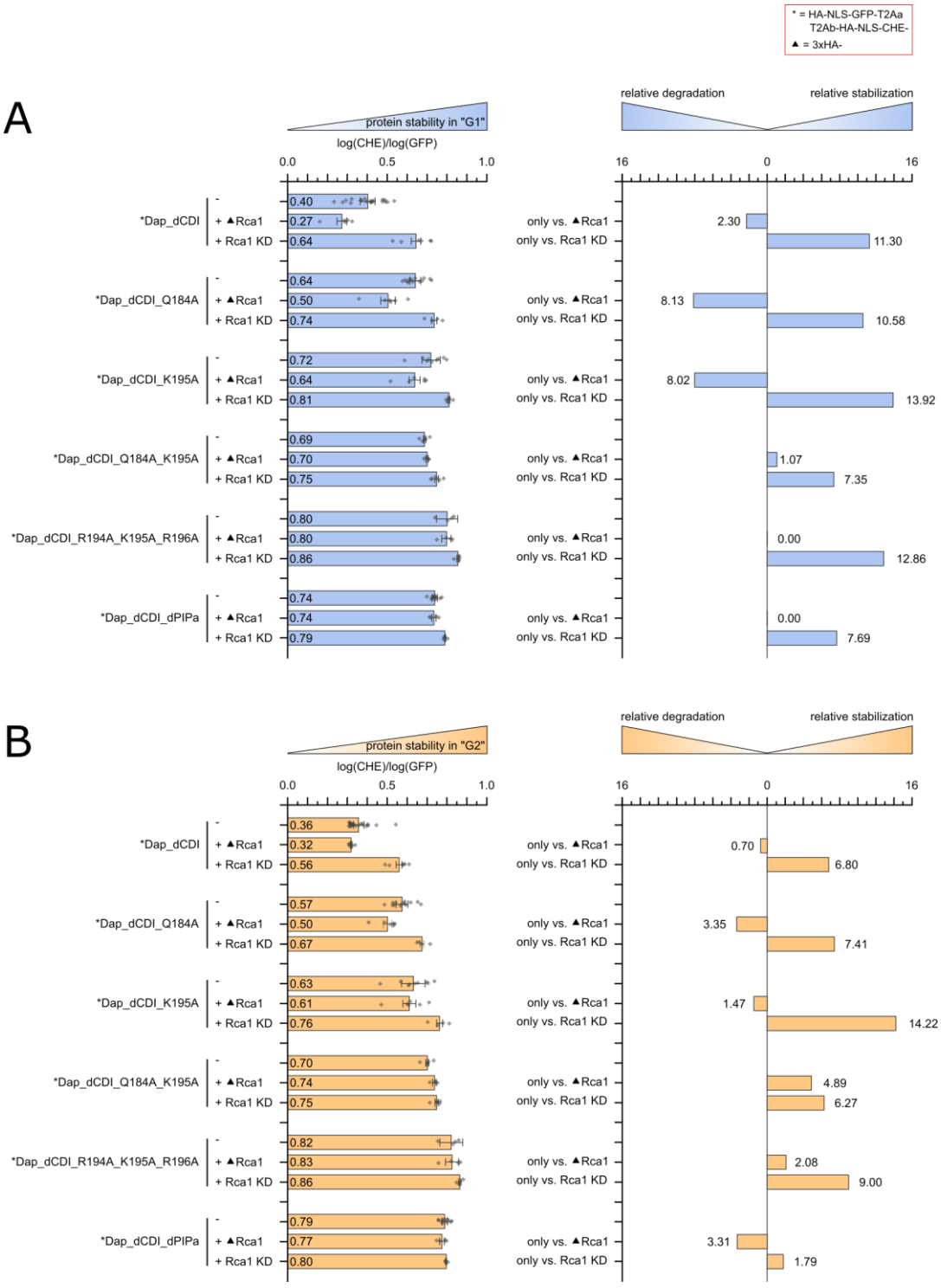

Figure 30 | Relative degradation and stabilization of Dap_dCDI constructs with mutations in the PIP degron

A, B) On the left side barplots representing the relative stability of Dap_dCDI constructs with mutations in the PIP degron in G1 (**A**) and G2 (**B**) are shown. To visualize the extent of degradation or stabilization of Dap constructs by overexpression or knockdown of Rca1 for the chart to the right a linear scale was chosen. The extent of Rca1 effects does not clearly correlate with the general stability of Dap_dCDI constructs. However, it becomes clear that the stability of highly stabilized Dap constructs (R194A_K195A_R196A, Q184A_K195A, dPIPa) is often influenced to a similar extent as of the more instable Dap versions (Q184A, K195A, K195R).

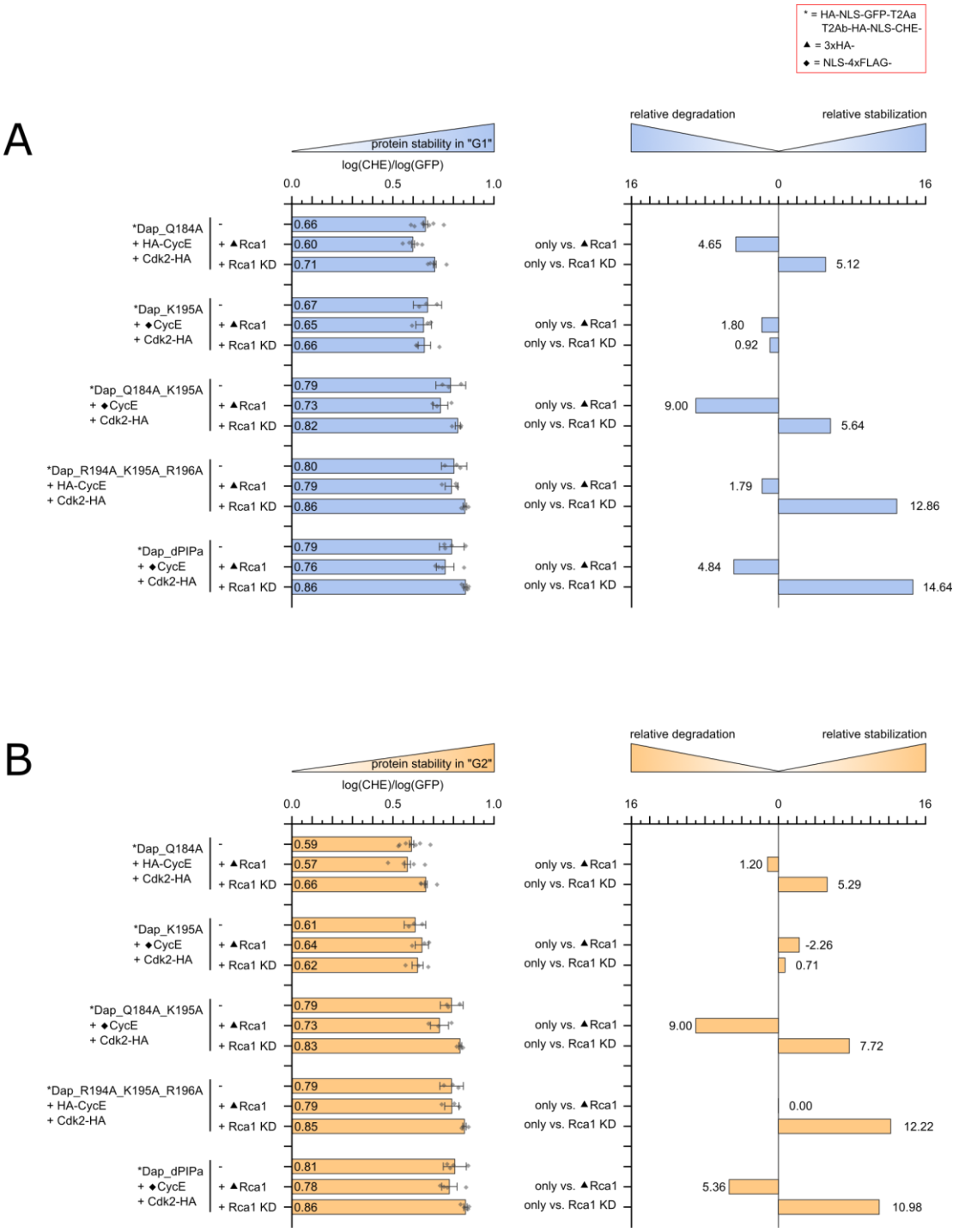

Figure 31 | Relative degradation and stabilization of Dap constructs with mutations in the PIP degron
A, B) On the left side barplots representing the relative stability of Dap constructs with mutations in the PIP degron in G1 (**A**) and G2 (**B**) are shown. To visualize the extent of degradation or stabilization of Dap constructs by overexpression or knockdown of Rca1 for the chart to the right a linear scale was chosen. The extent of Rca1 effects does not clearly correlate with the general stability of Dap constructs. However, it becomes clear that the stability of highly stabilized Dap constructs (R194A_K195A_R196A, Q184A_K195A, dPIPa) is often influenced to a similar extent as of the more instable Dap versions (Q184A, K195A, K195R).

4.11 Degradation of Dap via CRL4-Cdt2 cannot be reduced by mutation of S154

Although there was the tendency that Rca1 could influence the stability of strongly stabilized Dap constructs (e.g. Dap_dPIPa) the effect size was variable and not strong enough to obtain statistical significance for several conditions (chapter 4.10). We speculated that mutations in the PIP degron could not only affect recognition of Dap by CRL4-Cdt2, but also by SCF-Rca1 and that this could lead to small effect sizes. We therefore aimed for a strategy to specifically abolish or at least reduce CRL4-Cdt2 dependent degradation, while retaining degradation via SCF-Rca1.

For p21 it was shown that S114 is phosphorylated by GSK3β (Lee et al. 2007; Abbas et al. 2008). In addition, a phosphomimetic substitution (S114E) strongly promoted polyubiquitination of p21 via CRL4-Cdt2 *in vitro* (Abbas et al. 2008). Therefore, we wondered whether we can reduce the degradation of Dap via CRL4-Cdt2, if we mutate the corresponding amino acid in Dap into alanine (no phosphorylation possible). Sequence alignment of p21 and Dap indicated that S154 in Dap corresponds to S114 in p21 (**Figure 32 A**). The distance of S154 to the PIP degron (aa 184-195) is large. Therefore, we expected that potential effects of S154A would be independent of the PIP degron function. Dap_S154A was as stable in S phase as Dap (**Figure 32 C and E**). This indicates that CRL4-Cdt2 can target Dap_S154A efficiently despite mutation of S154 into alanine. If constructs such as Dap and Dap_S154A are very instable, differences in stabilities may be masked in flow cytometry analysis. Therefore, in another approach the stability of both constructs was elevated by applying a knockdown of Cdt2 (**Figure 32 D and F**). Since the knockdown of Cdt2 is not complete, we expected that remaining CRL4-Cdt2 activity would still allow degradation of both constructs to some extent. However, despite increased stability in S phase, the stability of Dap and Dap_S154A was the same. Therefore, no further analysis with Dap_S154A in combination with Rca1 constructs was conducted.

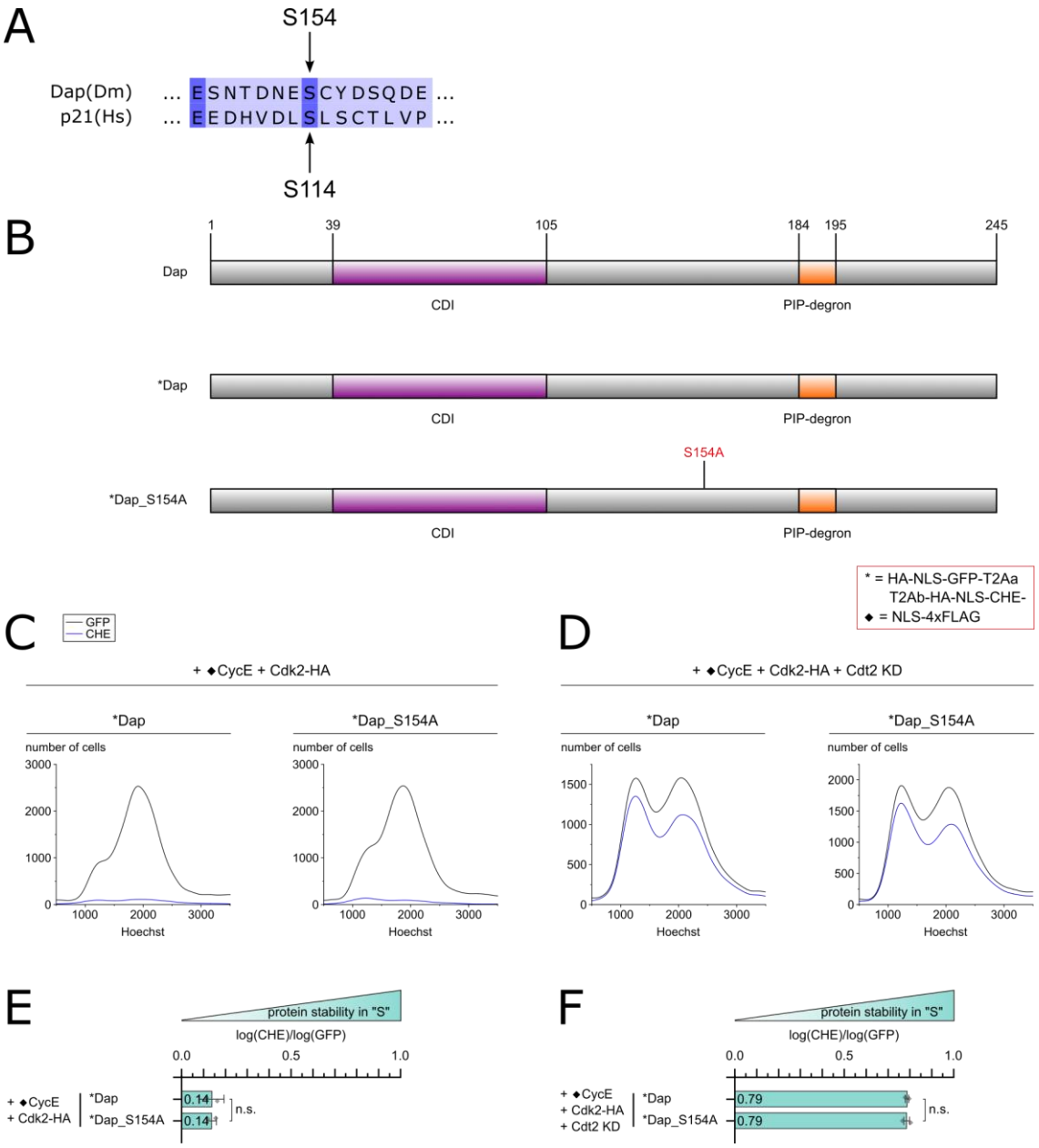

Figure 32 | Mutation of S154 in Dap does not affect its stability in S phase

A) For p21 there is evidence that phosphorylation of S114 enhances its degradation via CRL4-Cdt2 (Abbas et al. 2008). We wanted to mutate the corresponding amino acid in Dap into alanine so that potential phosphorylation would be abolished and CRL4-Cdt2 dependent degradation may be reduced. A sequence alignment between Dap and human p21 was conducted using Jalview with the alignment option "Clustal with Defaults". This alignment suggested that S154 in Dap is the corresponding amino acid of S114 in p21. **B)** Schematic representation of Dap and Dap_S154A. The distance between S154 and the PIP degron (aa 184-195) is large. Therefore, we did not expect that S154A would impede the function of the PIP degron. **C and E)** Cell cycle curves (**C**) and barplots (**E**) representing the relative stability of Dap or Dap_S154A coexpressed with NLS-4xFLAG-CycE/Cdk2-HA. In S phase the stability of Dap and Dap_S154A was the same indicating that CRL4-Cdt2 targeted Dap_S154A efficiently for degradation. **D and F)** Cell cycle curves (**D**) and barplots (**F**) representing the relative stability of Dap or Dap_S154A when NLS-4xFLAG-CycE/Cdk2-HA was coexpressed and a knockdown of Cdt2 was conducted. We speculated that a small difference between the stability of Dap and Dap_S154A may be better detectable, if the stability of both constructs is elevated by means of a knockdown of Cdt2. Since the Cdt2 knockdown is not complete, we expected residual CRL4-Cdt2 activity. However, even after knockdown of Cdt2, the stability of Dap and Dap_S154A in S phase was the same.

4.12 Rca1 APC/C inhibition mutants can destabilize Dap_Q184A

The degradation of Dap by CRL4-Cdt2 interferes with the analysis of Rca1 effects on Dap and neither knockdown of Cdt2 nor mutation of the PIP degron or the S154 site in Dap were able to eliminate these effects. Therefore, we aimed for another strategy to abolish indirect Rca1 effects on the stability of Dap without affecting the potential degradation via SCF-Rca1: Instead of abolishing or at least reducing the degradation of Dap via CRL4-Cdt2 directly, we wanted to abolish the inhibitory function of Rca1 towards the APC/C. Since we assumed that the indirect Rca1 effects via CRL4-Cdt2 are caused by altered APC/C activity in the first place, this strategy should allow to influence the stability of Dap only via the F-box, but not the APC/C inhibitory domains of Rca1.

Previously it was shown that mutations in the ZBR domain (S285R and A344T) or deletion in the RL tail (aa 403-409) of Rca1 almost completely abolish its function as APC/C inhibitor (Polz 2021). Therefore, it was tested whether Rca1_A344T, Rca1_S285R and Rca1_dRL can induce instability of Dap constructs (**Figure 33, 34)**. Since the stability of Dap is very low and this would mask potential Rca1 effects, Dap_Q184A was used for this experiment. In addition, NLS-4xFLAG-CycE/Cdk2-HA was coexpressed to facilitate the G1/S transition.

Although the effects were not significant, the extent of destabilization of Dap_Q184A in G1 and G2 by overexpression of Rca1_A344T and Rca1_S285R was comparable to that by Rca1 (**Figure 34 A, C, D**). The destabilizing effect was weaker for Rca1_dRL, but still present. This indicates that the destabilizing effect on Dap by Rca1 is at least not solely dependent on its function as APC/C inhibitor. We were interested, whether the Rca1 APC/C inhibition mutants can destabilize Dap_Q184A after knockdown of Cdt2. The cell cycle profiles using the different Rca1 APC/C inhibition mutants in combination with knockdown of Cdt2 contain more cells in G1 than the one using Rca1 (**Figure 34 B**). This reflects the fact that in cells with the Rca1 APC/C inhibition mutants, cyclin A and B (APC/C substrates) cannot accumulate as much as in cells with overexpression of Rca1. A slight destabilization of Dap_Q184A in G1 and G2 was observed for all Rca1 APC/C inhibition mutants, albeit the effect was not quite as strong as for Rca1 and not significant. In summary, the results indicate that Rca1 can influence the stability of Dap independent of its function as APC/C inhibitor. However, these APC/C independent Rca1 effects are weak making it difficult to detect and to demonstrate statistical significance.

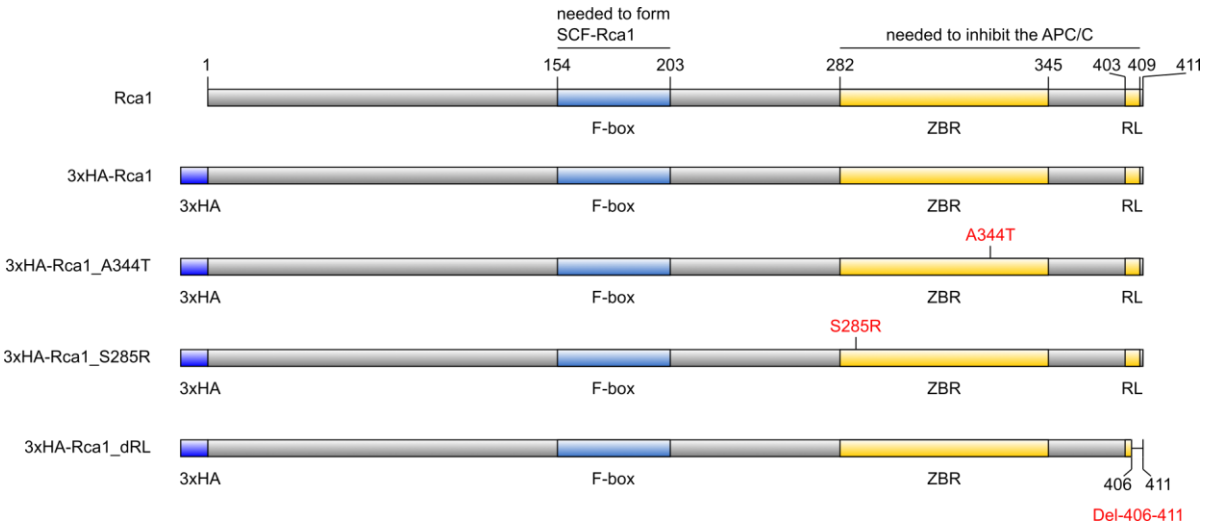

Figure 33 | Rca1 APC/C inhibition mutants used for flow cytometry analysis
Schematic representation of Rca1, Rca1_A344T, Rca1_S285R and Rca1_dRL. APC/C inhibition of these Rca1 mutants is almost abolished (Polz 2021). These constructs were used to analyze the F-box effect of Rca1 on Dap_Q184A without the disturbing influence of the APC/C inhibition by Rca1.

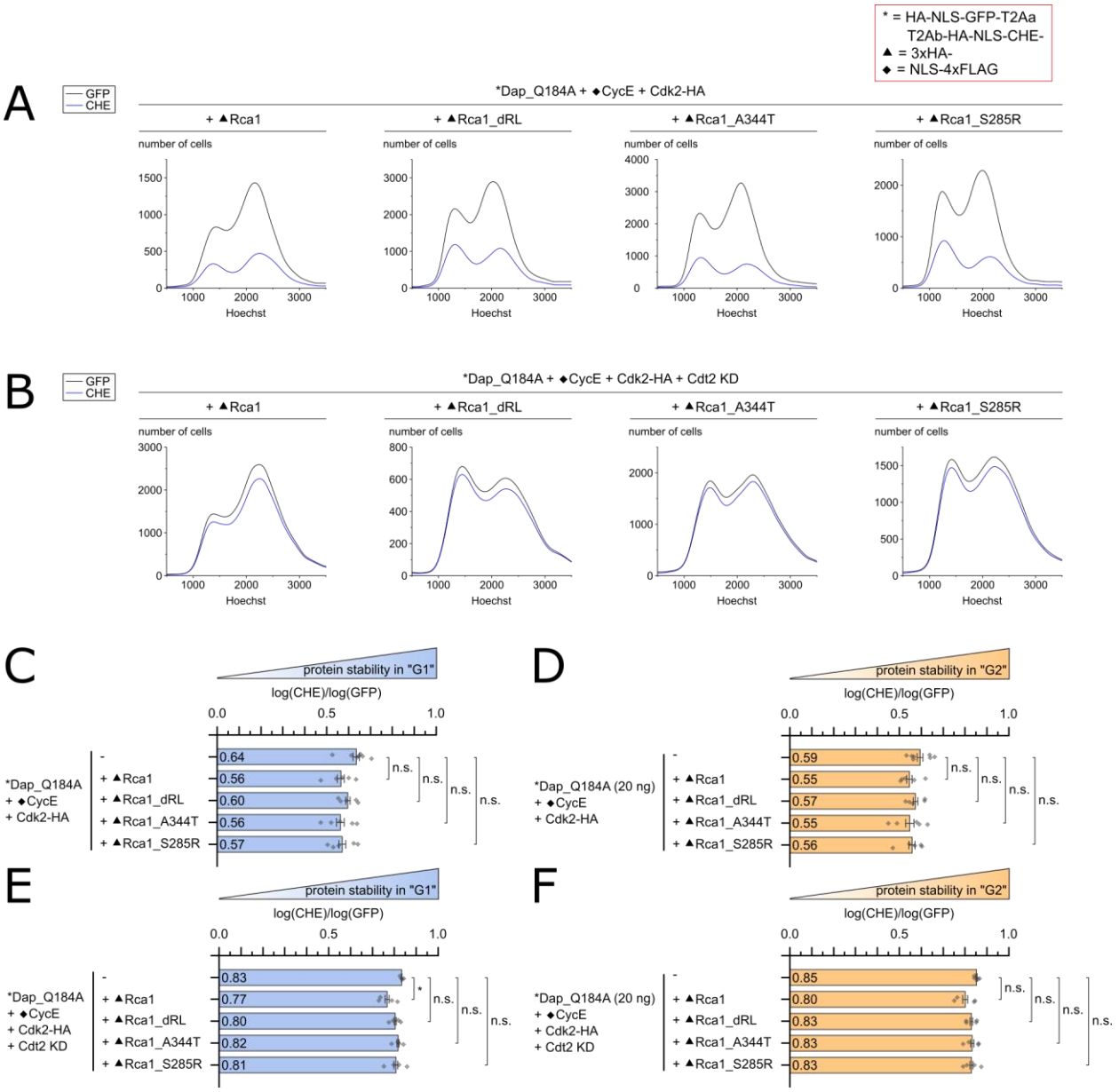

Figure 34 | Rca1 APC/C inhibition mutants can destabilize Dap_Q184A

A, C, D) Cell cycle curves (**A**) and barplots (**C, D**) representing the relative stability of Dap_Q184A coexpressed with NLS-4xFLAG-CycE/Cdk2-HA. Coexpression of Rca1_A344T or Rca1_S285R tended to reduce the stability of Dap_Q184A in G1 and G2 to a similar extent as overexpression of Rca1. Destabilization of Dap_Q184A by coexpression of Rca1_dRL was not as strong as for Rca1, Rca1_A344T and Rca1_S285R. **B, E, F)** Cell cycle curves (**C**) and barplots (**E, F**) representing the relative stability of Dap_Q184A, when NLS-4xFLAG-CycE/Cdk2-HA was coexpressed and a knockdown of Cdt2 was conducted. Coexpression of Rca1_dRL, Rca1_A344T or Rca1_S285R tended to destabilize Dap_Q184A in G1 and G2 even after knockdown of Cdt2. However, the effects were not as strong as for Rca1.

4.13 Rca1 interacts with the N-terminal half of Dap in a CDI dependent manner

Previous work in the Sprenger-lab indicated that overexpression of Rca1 can cause instability of Dap_1-125 (Herzinger 2019). This N-terminal fragment of Dap contains the CDI domain (aa 38-105), but lacks the PIP degron (aa 184-195). Therefore, we do not assume that Dap_1-125 can be targeted by CRL4-Cdt2. Based on comparison with the crystal structure of p27 bound to CycA/Cdk1, it was expected that the region 1-125 in Dap should allow binding to CycE/Cdk2. This was the reason why exactly this region was chosen. Subsequent experiments confirmed that Dap_1-125 can interact with CycE and Cdk2 (Herzinger 2019). Interaction between Rca1 and different Dap fragments was already studied previously (M. Kies 2017). However, for most Dap constructs either the CDI and/or the PIP-degron was deleted. For Dap_1-125_dCDI no interaction with Rca1 was detected (M. Kies 2017). To analyze, which regions in Dap mediate interaction with Rca1 and whether the CDI domain or the PIP degron is needed for this purpose, the following Dap constructs were used: 4xFLAG-Dap, 4xFLAG-Dap_dCDI, 4xFLAG-Dap_160-245, 4xFLAG-Dap_126-245, 4xFLAG-Dap_126-245_dPIPa, NLS-4xFLAG-Dap_1-160, NLS-4xFLAG-Dap_1-160_dCDI, NLS-4xFLAG-Dap_1-125, NLS-4xFLAG-Dap_1-125_dCDI (**Figure 17**). For the Dap constructs that included a functional CDI domain and that would cause a G1 arrest, CycE and Cdk2 was coexpressed to facilitate the G1/S transition. Dap contains nuclear localization sequences in the C-terminus. To maintain a nuclear localization, the N-terminal Dap fragments were fused to an NLS.

To test the interaction between Rca1 and Dap, first 4xFLAG-Dap and 4xFLAG-Dap_dCDI were precipitated and tested for coprecipitation of 3xHA-Rca1. In both cases, Rca1 coprecipitation was observed to a similar extent (**Figure 35 A, lane 3,4**). In addition, in case of 4xFLAG-Dap it made no difference for the coprecipitation of 3xHA-Rca1, whether CycE/Cdk2 was coexpressed or not (**lane 2,3**). NLS-4xFLAG-Dap_1-160_dCDI was able to coprecipitate 3xHA-Rca1 only in low amounts (**lane 5**). In contrast, the efficiency for coprecipitation of 3xHA-Rca1 was higher for NLS-4xFLAG-Dap_1-160 (**lane 6**), albeit it was not as good as for the full-length Dap constructs (**lane 6 vs lane 2**). This indicates that at least for the N-terminal half of Dap the CDI domain plays an important role for the interaction with Rca1. Coprecipitation of 3xHA-Rca1 was hardly detectable using NLS-4xFLAG-Dap_1-125_dCDI (**lane 8**). This is in line, with previously conducted co-IPs (M. Kies 2017). In contrast, NLS-4xFLAG-Dap_1-125 was able to coprecipitate 3xHA-Rca1 (**lane 9**), albeit the efficiency was not quite as good as for NLS-4xFLAG-Dap_1-160. In case of NLS-4xFLAG-Dap_1-160 and NLS-4xFLAG-Dap_1-125 the additional overexpression of CycE/Cdk2 resulted in some increase in Rca1 coprecipitation (**lane 6,9**), probably allowing more Dap to associate with CycE/Cdk2. In conclusion, this substantiates that the interaction of the N-terminal half of Dap with Rca1 is dependent on the CDI domain.

Previously it was shown that the C-terminal Dap fragments 4xFLAG-Dap_140-245_dPIPa as well as 4xFLAG-Dap_160-245 cannot coprecipitate 3xHA-Rca1 (M. Kies 2017). We speculated that the PIP degron is not only needed for the recognition by CRL4-Cdt2, but also SCF-Rca1. Therefore, we were interested, whether coprecipitation of 3xHA-Rca1 is possible with C-terminal Dap fragments that contain a functional PIP degron (**Figure 35 B**). 4xFLAG-Dap_160-245 could not coprecipitate 3xHA-Rca1 (**lane 3**). However, both 4xFLAG-Dap_126-245 and 4xFLAG-Dap_126-245_dPIPa could weakly coprecipitate 3xHA-Rca1 to a small extent (**lane 4, 5**). Therefore, the region 126-245 in Dap interacts weakly with Rca1 and this interaction is not dependent on the PIP degron.

In summary, primarily the N-terminus of Dap (aa 1-125/160) is involved in the interaction with Rca1. However, for this interaction it is important that the CDI domain is intact. The C-terminal half of Dap (aa 126-245) mediates weak interaction with Rca1. This interaction is not dependent on the PIP degron. Although the C-terminal half of Dap only weakly interacts with Rca1 it seems to be important, since full-length Dap constructs interacted much stronger with 3xHA-Rca1 as the N-terminal half of Dap alone.

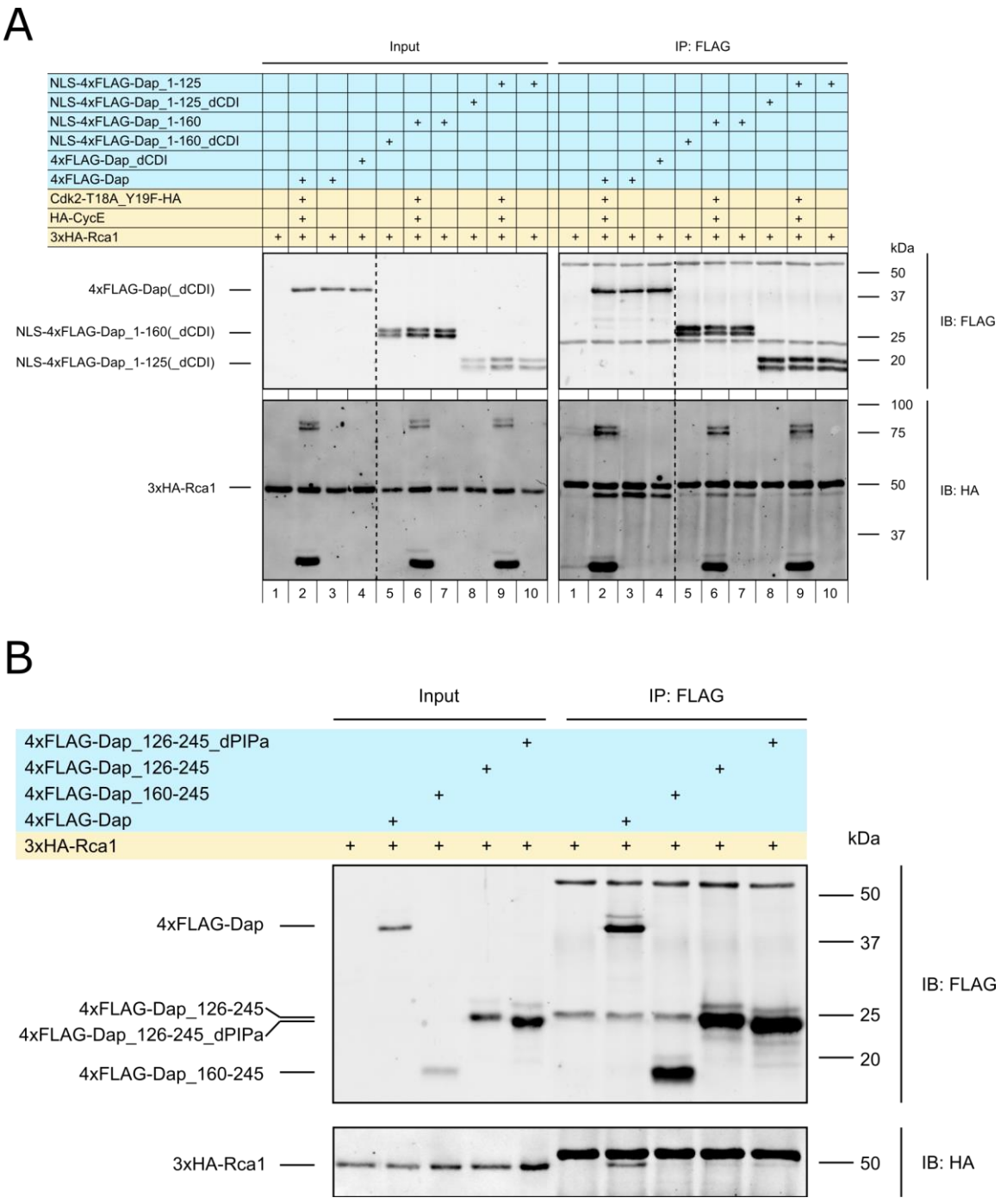

Figure 35 | Rca1 interacts with the N-terminal half of Dap in a CDI dependent manner
A) The interaction between N-terminal Dap fragments and Rca1 was tested via co-IP. The full-length Dap constructs 4xFLAG-Dap and 4xFLAG-Dap_dCDI could coprecipitate 3xHA-Rca1 to a similar extent. It made no notable difference in case of 4xFLAG-Dap, whether CycE/Cdk2 was coexpressed or not. Both NLS-4xFLAG-Dap_1-160 and NLS-4xFLAG-Dap_1-125 could coprecipitate 3xHA-Rca1, albeit the efficiency was not as good as for the full-length Dap constructs. The amount of coprecipitated Rca1 was slightly increased, when CycE/Cdk2 was coexpressed with NLS-4xFLAG-Dap_1-160 or NLS-4xFLAG-Dap_1-125. Interaction with 3xHA-Rca1 was greatly reduced, when the CDI domain was deleted in the 1-125 and 1-160 Dap constructs. **B)** The interaction between C-terminal Dap fragments and Rca1 was tested via co-IP. Coprecipitation of 3xHA-Rca1 using 4xFLAG-Dap worked and served as a positive control. Coprecipitation of 3xHA-Rca1 was not detected using 4xFLAG-Dap_160-245. However, 4xFLAG-Dap_1-126-245 and 4xFLAG-Dap_1-126-245_dPIPa could weakly coprecipitate 3xHA-Rca1. Therefore, this interaction is independent of a functional PIP degron.

4.14 Dap_1-125 can be destabilized by Rca1

As seen previously, Dap_1-125 interacted with Rca1 (chapter 4.13). In addition, initial work indicated that overexpression of Rca1 can destabilize Dap_1-125 in an F-box dependent manner (Herzinger 2019). This made Dap_1-125 a promising candidate for further analysis in relation to Rca1 effects. First, it was tested whether the previously seen destabilization can be reproduced. In addition, it was tested, whether knockdown of Rca1 can influence the stability of Dap_1-125. Since the PIP degron (aa 184-195) is not part of Dap_1-125 we did not expect any degradation of this construct via CRL4-Cdt2.

To allow the G1/S transition, Dap_1-125 was coexpressed with NLS-4xFLAG-CycE and Cdk2-HA. This resulted in similar cell cycle profiles where most cells are in the G2 phase of the cell cycle. Interestingly, the stability of Dap_1-125 was lowest in G2 (**Figure 36 E**). This could indicate that Dap_1-125 is specifically targeted for degradation in G2. Alternatively, the degradation of Dap_1-125 may occur throughout the cell cycle, with lower stability values becoming imminent in G2, given that cells predominantly reside in this phase for the majority of their time. Coexpression of Rca1 tended to destabilize Dap_1-125 in G1 and G2 (**Figure 36 C, D**) and knockdown of Rca1 tended to stabilize Dap_1-125 in G1 and G2. Therefore, Rca1 might impact the stability of Dap irrespective of the PIP-degron, albeit these effects are weak and lack statistical validation.

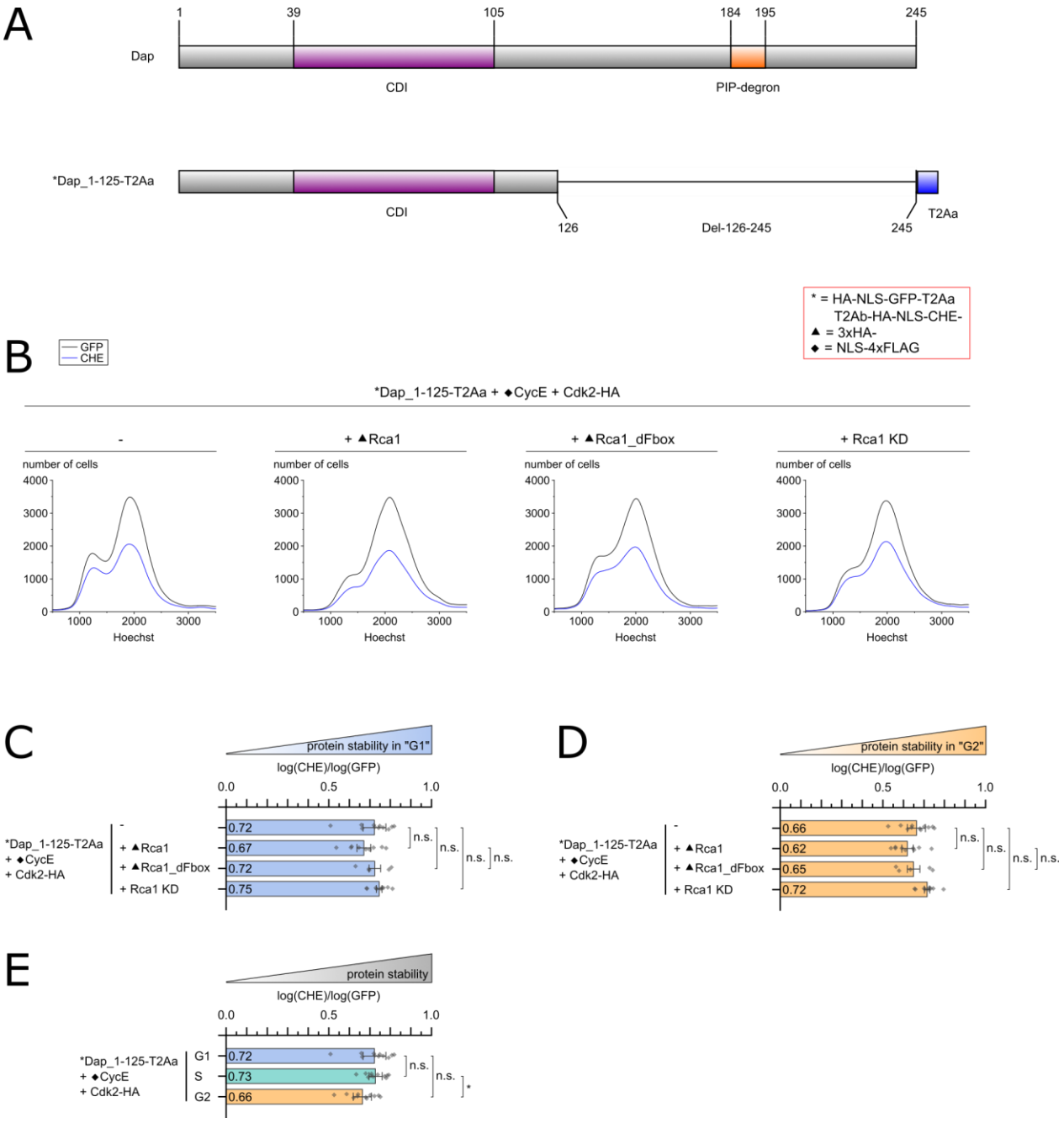

Figure 36 | Rca1 can destabilize Dap_1-125

A) Schematic representation of Dap_1-125. For cloning reasons, a short T2A sequence (T2Aa) was fused to the C-terminus of Dap_1-125. **B-E)** Cell cycle curves (**B**) and barplots (**C, D, E**) representing the stability of Dap_1-125 coexpressed with NLS-4xFLAG-CycE/Cdk2-HA. The data was obtained by flow cytometry. **C, D)** Coexpression of 3xHA-Rca1 tended to destabilize Dap_1-125 in G1 and G2, whereas knockdown of Rca1 tended to stabilize it. Coexpression of Rca1_dFbox had no significant influence on the stability of Dap_1-125. **E)** Dap_1-125 showed a similar stability in S as in G1. However, its stability in G2 was significantly lower than in S.

4.15 Dap_1-125 is stabilized by deletions in its CycE binding domain

As previously noted, the strength of the interaction beween Dap_1-125_dCDI and Rca1 is significantly lower compared to that of Dap_1-125 (chapter 4.13). Therefore, we were interested in the stability of Dap_1-125_dCDI during the cell cycle and whether it can be influenced by Rca1. Due to the deletions in the CDI domain, Dap_1-125_dCDI is not able to inhibit CycE/Cdk2. Therefore, overexpression of Dap_1-125_dCDI did not lead to an arrest in G1 and coexpression of CycE/Cdk2 was not conducted (**Figure 37 B**). Dap_1-125_dCDI was almost completely stable during the whole cell cycle (**Figure 37 E**) and the increased degradation visible in G2, which was observed for Dap_1-125, was not present for Dap_1-125_dCDI. Coexpression of Rca1 or Rca1_dFbox had no noticeable influence on the stability of Dap_1-125 in G1 and G2 (**Figure 37 B-D**). Knockdown of Rca1 tended to stabilize Dap_1-125_dCDI in G1 and G2, although the effect was not significant.

The CDI domain of Dap and its human homologs p21 and p27 contains two separate regions responsible for the binding to the cyclin and to Cdk. The dCDI deletion in Dap_1-125_dCDI is designed to abolish binding to CycE via the deletion Del-38-44-RAR (dCyc) and to Cdk2 via the deletion Del-103-105-G (dCDK). For p27 it is known that it preferentially binds first to CycA before it binds to Cdk2 (Lacy et al. 2004). Therefore, we wondered whether stabilization of Dap_1-125 could also be achieved, if only binding to CycE is abolished. Indeed, Dap_1-125_dCyc was almost as stable as Dap_1-125_dCDI (**Figure 38**). As for Dap_1-125_dCDI, overexpression of Rca1 or Rca1_dFbox could not influence the stability of Dap_1-125_dCyc. Knockdown of Rca1 tended to stabilize Dap_1-125_dCyc in G1 and G2, although the effect was not significant. Furthermore, the increased instability in G2, which was observed for Dap_1-125, was not observed for Dap_1-125_dCyc.

In summary, the results suggest that binding of Dap_1-125 to CycE is essential for its degradation. In addition, overexpression of Rca1 tend to decrease the stability of Dap_1-125 solely when the domain responsible for binding CycE remains present.

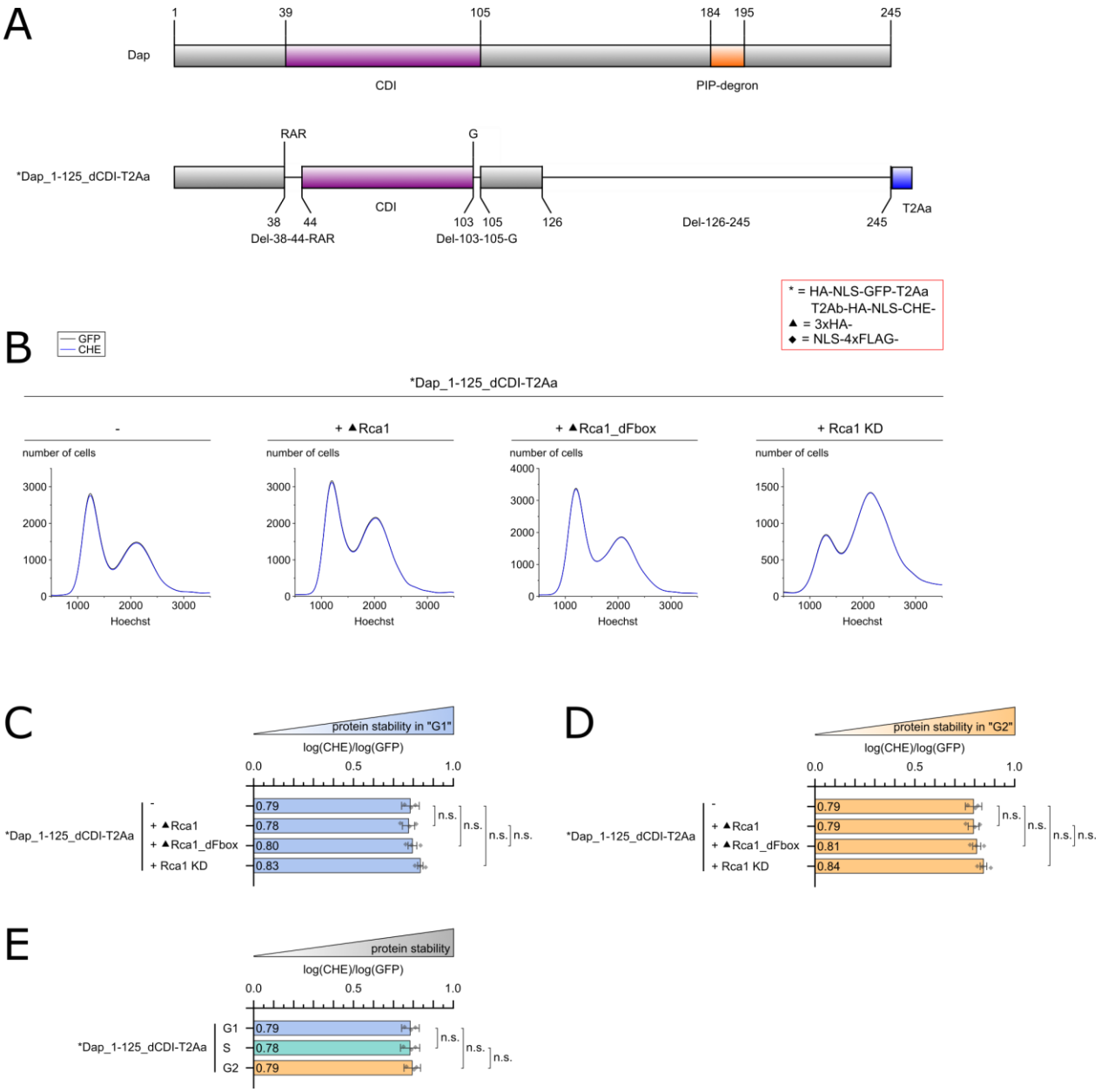

Figure 37 | Dap_1-125 is stabilized by deletion of the domains responsible for binding CycE and Cdk2
A) Schematic representation of Dap_1-125_dCDI. For cloning reasons, a short T2A sequence (T2Aa) was fused to the C-terminus of Dap_1-125_dCDI. **B-E)** Cell cycle curves (**B**) and barplots (**C-E**) representing the stability of Dap_1-125_dCDI. The data was obtained by flow cytometry. CycE/Cdk2 was not coexpressed, since overexpression of Dap_dCDI_1-125 did not lead to a G1 arrest. **C, D)** Coexpression of Rca1 and Rca1_dFbox had no significant influence on the stability of Dap_1-125_dCDI in G1 and G2. Knockdown of Rca1 tended to stabilize Dap_1-125_dCDI in G1 and G2. **E)** The stability of Dap_1-125_dCDI was similar in G1, S and G2.

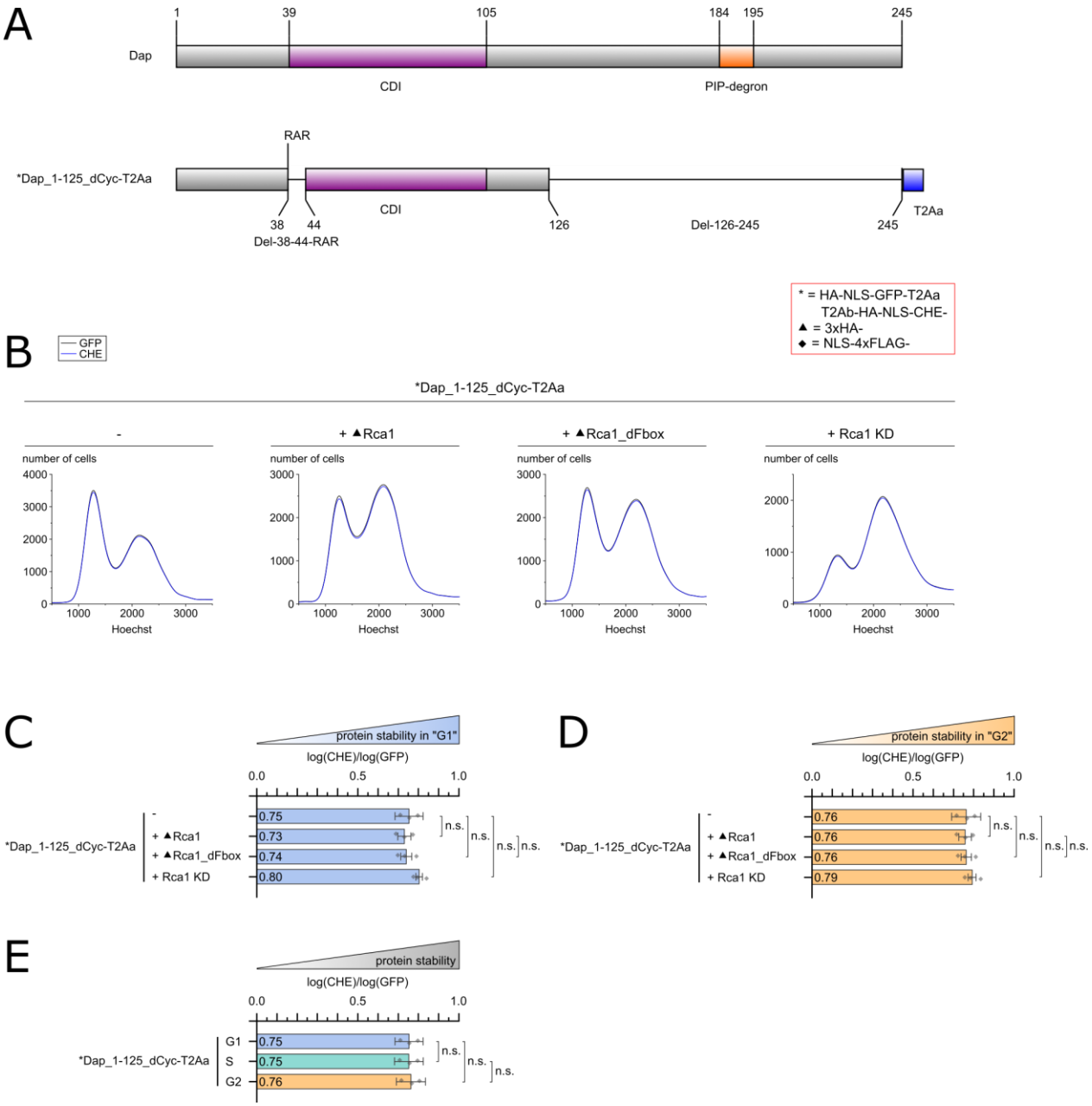

Figure 38 | Deletion of the domain responsible for binding CycE is sufficient to stabilize Dap_1-125
A) Schematic representation of Dap_1-125_dCyc. For cloning reasons, a short T2A sequence (T2Aa) was fused to the C-terminus of Dap_1-125_dCyc. **B-E)** Cell cycle curves (**B**) and barplots (**C-E**) representing the stability of Dap_1-125_dCyc. The data was obtained by flow cytometry. CycE/Cdk2 was not coexpressed, since overexpression of Dap_dCyc_1-125 did not lead to a G1 arrest. **C, D)** Coexpression of Rca1 and Rca1_dFbox had no significant influence on the stability of Dap_1-125_dCyc in G1 and G2. Knockdown of Rca1 tended to stabilize Dap_1-125_dCyc in G1 and G2. **E)** The stability of Dap_1-125_dCyc was similar in G1, S and G2.

4.16 Dap_1-125 is not stabilized by the mutation dCDK

Dap_1-125 with mutation of the Cyclin binding domain or lacking the cyclin binding and Cdk binding domain were stable throughout the cell cycle and Rca1 had neglectable effects on their stability (chapter 4.15). We now analyzed what effect the mutation in the Cdk binding domain (Del-103-105-G) has on the stability of Dap_1-125.

Expression of Dap_1-125_dCDK resulted in an accumulation of cells in G1 and early S phase (**Figure 39 B**). Therefore, this mutation is able to inhibit CycE/Cdk2 when overexpressed. However, titration experiments indicated that Dap_1-125_dCDK was a weaker inhibitor of CycE/Cdk2 than Dap_1-125 (Bach 2021). To analyze the cell cycle stability of Dap_1-125_dCDK, we coexpressed CycE/Cdk2. Using the 80 ng plasmid DNA of CycE/Cdk2 resulted in a cell cycle distribution with almost all cells in G2 (data not shown). We therefore used less CycE/Cdk2 to obtain a cell cycle distribution with all cell cycle phases.

Rca1 knockdown tended to stabilize Dap_1-125_dCDK in G1 and G2 (**Figure 39 C, D**). However, Rca1 overexpression could not noticeably destabilize Dap_1-125_dCDK in G1. In G2, there was even the tendency that Rca1 stabilized Dap_1-125_dCDK.

To visualize the effect of the different mutations in the CDI domain of Dap_1-125, the stability of the corresponding Dap constructs is summarized in one chart (**Figure 40**). For a better comparison, the stability of CHE alone is represented as well in this chart. Dap_1-125 was significantly more instable than CHE in G1 and G2. Compared to Dap_1-125, Dap_1-125_dCDK tended to be less stable in G1 and G2. In contrast, Dap_1-125_dCDI and Dap_1-125_dCyc tended to be more stable in G1 and G2 than Dap_1-125.

In summary, Dap_1-125_dCDK was less stable than Dap_1-125, especially in G2 phase. Rca1 knockdown resulted in higher stability, consistent with the idea that Rca1 can trigger Dap degradation. On the other hand, overexpression of Rca1 was unable to destabilize Dap_1-125_dCDK in contrast to Dap_1-125, which was at least weakly destabilized by Rca1 overexpression.

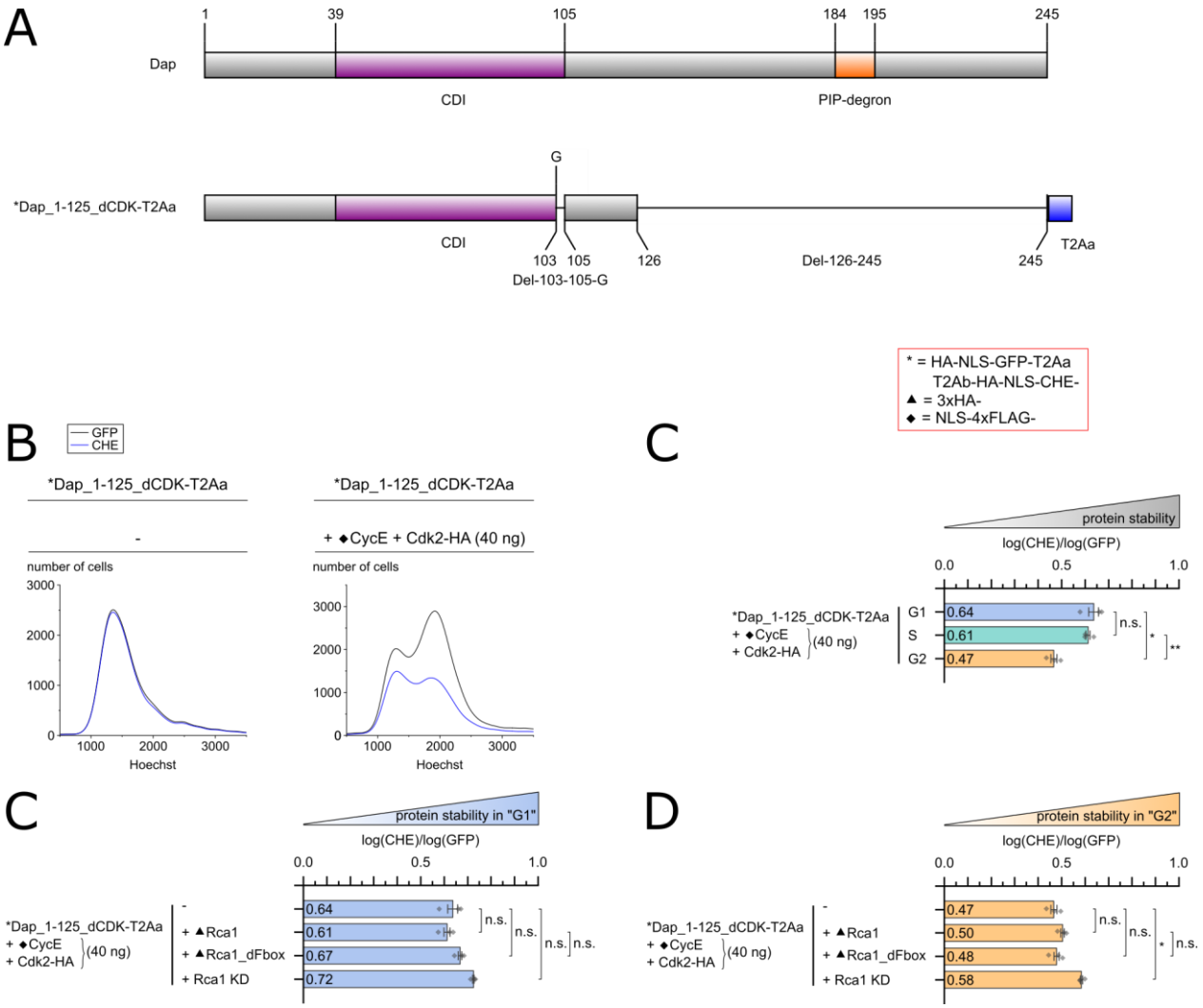

Figure 39 | Knockdown of Rca1 can affect the stability of Dap_1-125_dCDK

A) Schematic representation of Dap_1-125_dCDK. For cloning reasons, a short T2A sequence (T2Aa) was fused to the C-terminus of Dap_1-125_dCDK. **B)** Cell cycle curves representing the relative stability of Dap_1-125_dCDK either coexpressed with no (left chart) or NLS-4xFLAG-CycE/Cdk2 (40 ng plasmid) (right chart). The data was obtained by flow cytometry. Without coexpression of NLS-4xFLAG-CycE/Cdk2, the cells accumulated in G1 indicating that Dap_1-125_dCDK can inhibit CycE/Cdk2. Coexpression of NLS-4xFLAG-CycE/Cdk2 (40 ng plasmid) allowed similar cell cycle distributions as for Dap_1-125. **C)** Barplots representing the relative stability of Dap_1-125_dCDK in G1, S and G2, when NLS-4xFLAG-CycE/Cdk2 (40 ng plasmid) was coexpressed. The stability of Dap_1-125_dCDK was significantly lower in G2 than in G1 or S. **C, D)** Barplots representing the relative stability of Dap_1-125_dCDK in G1 and G2, when NLS-4xFLAG-CycE/Cdk2 (40 ng plasmid) was coexpressed. Coexpression of Rca1 or Rca1_dFbox had no noticeable influence on the stability of Dap_1-125_dCDK in G1 and G2. Knockdown of Rca1 tended to stabilize Dap_1-125_dCDK in G1 and G2.

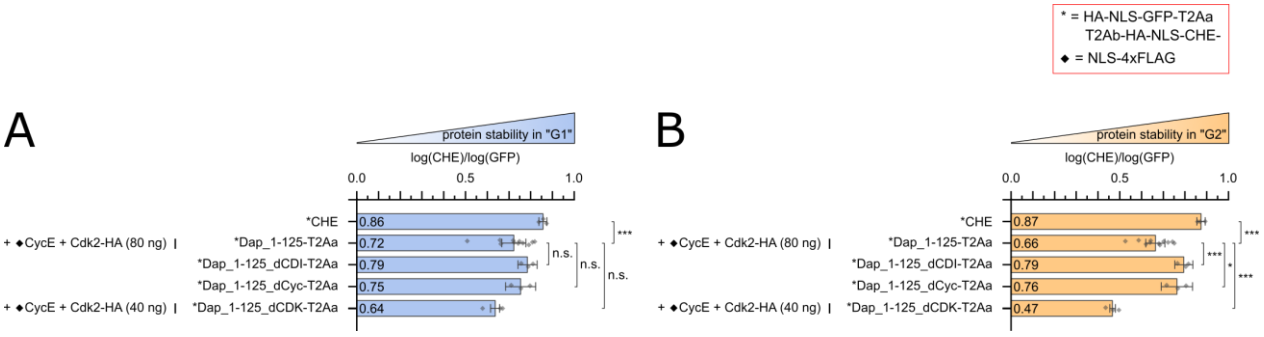

Figure 40 | Stability of Dap_1-125 constructs with different mutations in the CDI domain

A, B) Barplots representing the relative stability of Dap_1-125 constructs with different mutations in the CDI domain in G1 (**A**) and G2 (**B**). The data was obtained by flow cytometry. Dap_1-125 and Dap_1-125_dCDK were coexpressed with 4xFLAG-NLS-CycE/Cdk2-HA to facilitate the G1/S transition. In G1 and G2, Dap_1-125 (fused to CHE) was significantly more instable than CHE alone. Dap_1-125_dCDI and Dap_1-125_dCyc tended to be more stable than Dap_1-125 in G1 and G2, whereas Dap_1-125_dCDK tended to be more instable.

4.17 Influence of the dCDK mutation on full-length Dap constructs

Since Dap_1-125_dCDK was less stable in G2 and was stabilized by Rca1 knockdown, we analyzed this mutation in the full-length Dap construct. Since this contains the PIP degron, we analyzed the dCDK mutation in the background of PIP degron mutations (Q184A, K195A and dPIPa) and also applied Cdt2 knockdown. All these should reduce the contribution of CRL4-Cdt2 to the degradation of Dap.

We used the following constructs for flow cytometry analysis: Dap_dCDK_Q184A (**Figure 41**), Dap_dCDK_K195A (**Figure 42**), Dap_dCDK_Q184A_K195A (**Figure 43**) as well as Dap_dCDK_dPIPa (**Figure 44**). In addition, we coexpressed HA-CycE/Cdk2-HA to facilitate the G1/S transition. In the case of Dap_dCDK_dPIPa, we even had to use less Dap plasmid and the more active NLS-4xFLAG-CycE/Cdk2-HA to allow cells to escape the G1 arrest.

The stability of Dap_dCDK_Q184A coexpressed with HA-CycE/Cdk2-HA in G1 was comparable to that of Dap_Q184A coexpressed with HA-CycE/Cdk2-HA (**compare Figure 41 with Figure 22**). Coexpression of both Rca1 and Rca1_dFbox tended to cause destabilization of Dap_dCDK_Q184A in G1 and G2. In addition, the destabilization of Dap_dCDK_Q184A in G1 and G2 tended to be stronger for Rca1 than for Rca1_dFbox. Therefore, coexpression of Rca1 did not cause stabilization in G2 like it was observed for Dap_1-125_dCDK. Knockdown of Rca1 led to stabilization of Dap_dCDK_Q184A in G1 and G2.

Coexpression of Rca1 caused stronger destabilization in G1 for Dap_dCDK_Q184A (stability value: 0.66 → 0.49; 10.2 % degradation) than for Dap_Q184A (stability value: 0.66 → 0.60; 4.6 % degradation) (**compare Figure 41 with Figure 22**). In case of Dap_dCDK_Q184A, degradation via CRL4-Cdt2 could still lead to indirect Rca1 effects. Thus, we were interested, whether the effect of Rca1 coexpression on the stability of Dap_dCDK_Q184A remains, when a knockdown of Cdt2 is conducted in parallel. Indeed, coexpression of Rca1 still caused noticeable destabilization of Dap_dCDK_Q184A both in G1 and G2.

For Dap_dCDK_K195A the effects of coexpression/knockdown of Rca1 on its stability were similar as for Dap_dCDK_Q184A. Also Dap_dCDK_Q184_K195A as well as Dap_dCDK_dPIPa tended to be affected by coexpression of Rca1 or knockdown of Rca1. Especially for Dap_dCDK_dPIPa, the general stability in G1 and G2 was high. Therefore, mutation of the binding domain for Cdk2 in Dap can only trigger strong degradation for the N-terminal Dap fragment Dap_1-125, but not full-length Dap constructs.

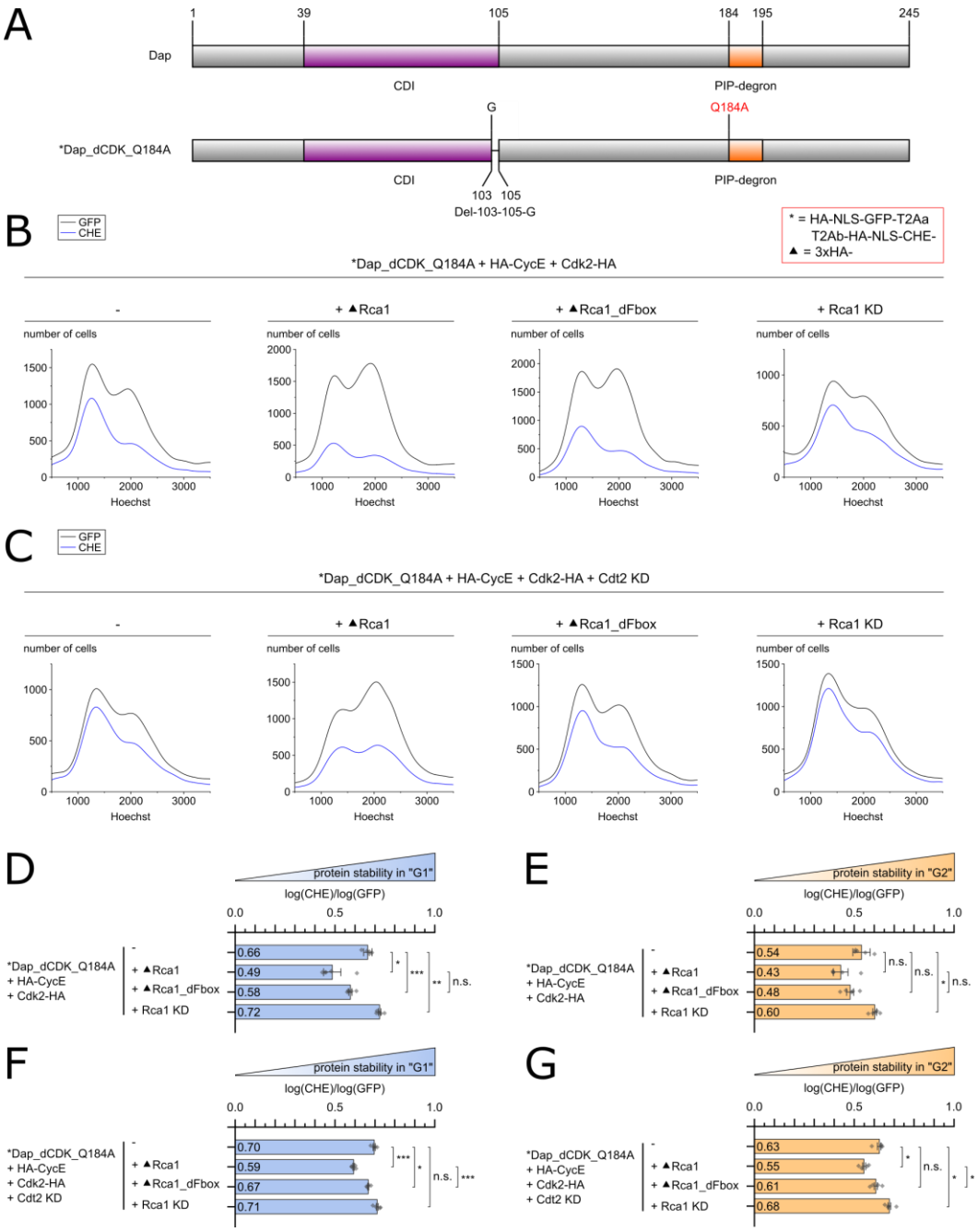

Figure 41 | Influence of Rca1 on the stability of Dap_dCDK_Q184A

A) Schematic representation of Dap_1-125_dCDK_Q184A. **B, D, E)** Cell cycle curves (**B**) and barplots (**D, F**) representing the relative stability of Dap_dCDK_Q184A coexpressed with HA-CycE/Cdk2-HA. The data was obtained by flow cytometry. Coexpression of HA-CycE/Cdk2-HA facilitated the G1/S transition. Coexpression of Rca1 or Rca1_dFbox tended to cause destabilization of Dap_dCDK_Q184A in G1 and G2. Destabilization of Dap_dCDK_Q184A tended to be stronger for Rca1 than for Rca1_dFbox. Knockdown of Rca1 led to stabilization of Dap_dCDK_Q184A in G1 and G2. **C, F, G**) Cell cycle curves (**C**) and barplots (**F, G**) representing the relative stability of Dap_dCDK_Q184A, when HA-CycE/Cdk2-HA was coexpressed and a knockdown of Cdt2 was conducted. Even after knockdown of Cdt2, coexpression of Rca1 was able to destabilize Dap_dCDK_Q184A in G1 and G2. Destabilization of Dap_dCDK_Q184A in G1 and G2 was weaker for Rca1_dFbox than for Rca1. Knockdown of Rca1 hardly affected the stability of Dap_dCDK_Q184A in G1, but led to stabilization in G2.

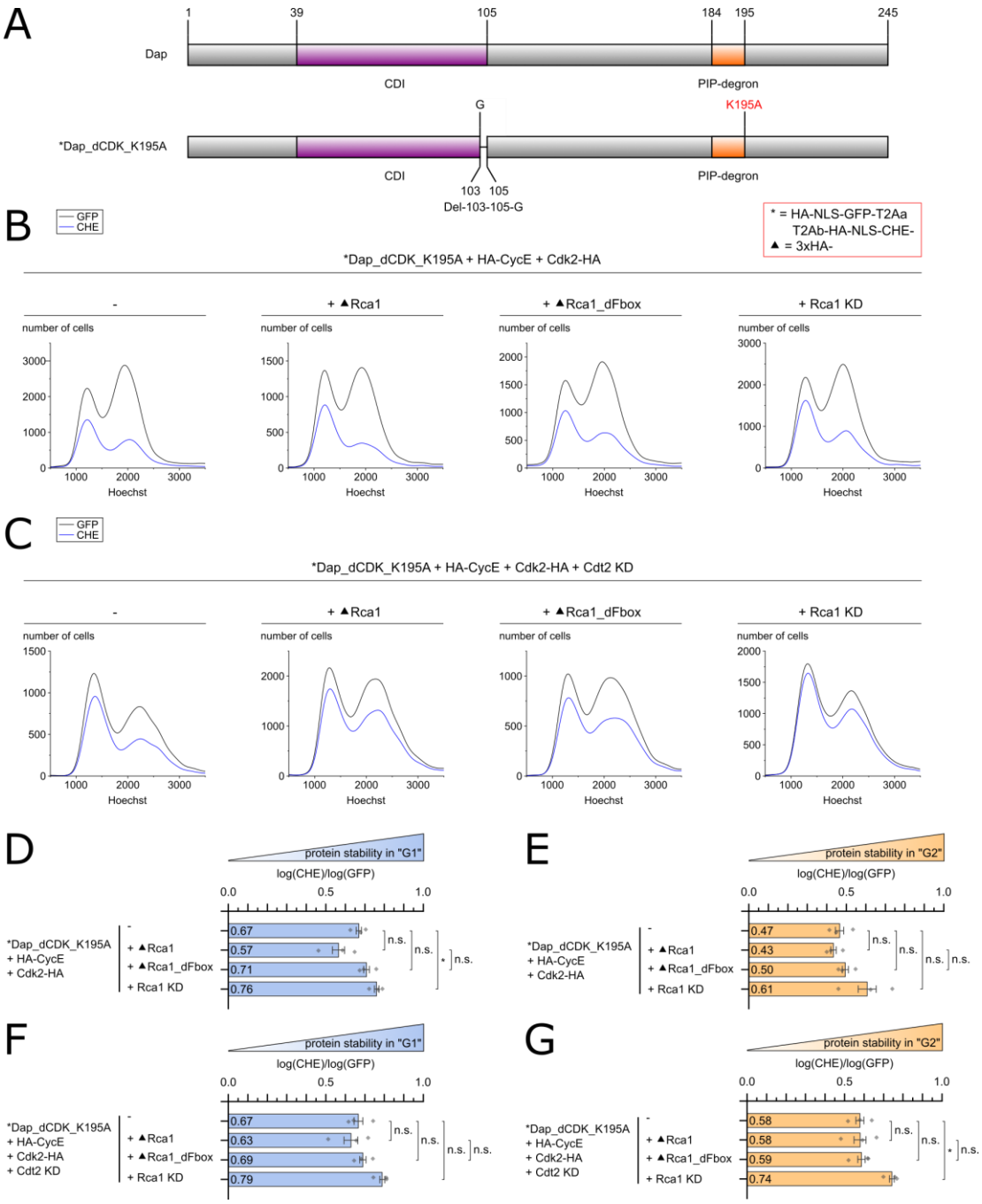

Figure 42 | Influence of Rca1 on the stability of Dap_dCDK_K195A

A) Schematic representation of Dap_1-125_dCDK_K195A. **B, D, E)** Cell cycle curves (**B**) and barplots (**D, E**) representing the relative stability of Dap_dCDK_K195A coexpressed with HA-CycE/Cdk2-HA. The data was obtained by flow cytometry. Coexpression of HA-CycE/Cdk2-HA facilitated the G1/S transition. Coexpression of Rca1 tended to cause destabilization of Dap_dCDK_K195A in G1 and G2. In contrast, coexpression of Rca1_dFbox tended to cause stabilization in G1 and G2. Knockdown of Rca1 tended to stabilize Dap_dCDK_K195A in G1 and G2. **C, F, G**) Cell cycle curves (**C**) and barplots (**F, G**) representing the relative stability of Dap_dCDK_K195A, when HA-CycE/Cdk2-HA was coexpressed and a knockdown of Cdt2 was conducted. Even after knockdown of Cdt2, coexpression of Rca1 caused destabilization of Dap_dCDK_K195A in G1. However, coexpression of Rca1 did not influence the stability of Dap_dCDK_K195A in G2. Coexpression of Rca1_dFbox had hardly any effect on the stability of Dap_dCDK_K195A in G1 and G2. Knockdown of Rca1 tended to increase the stability of Dap_dCDK_K195A in G1 and G2.

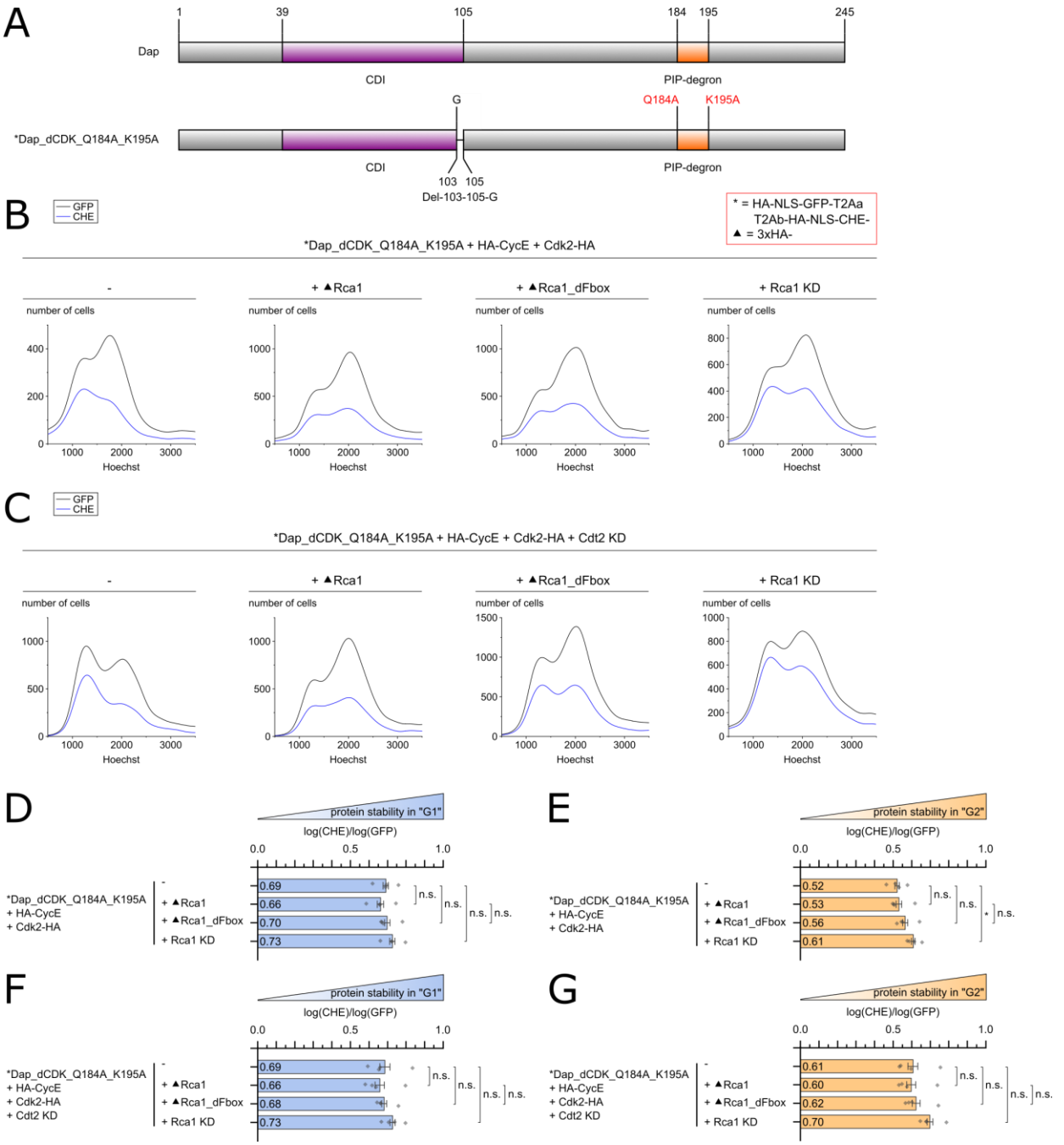

Figure 43 | Influence of Rca1 on the stability of Dap_dCDK_Q184A_K195A

A) Schematic representation of Dap_1-125_dCDK_Q184A_K195A. **B, D, E)** Cell cycle curves (**B**) and barplots (**D, E**) representing the relative stability of Dap_dCDK_Q184A_K195A coexpressed with HA-CycE/Cdk2-HA. The data was obtained by flow cytometry. Coexpression of HA-CycE/Cdk2-HA facilitated the G1/S transition. Coexpression of Rca1 tended to destabilize Dap_dCDK_Q184A_K195A in G1, whereas it hardly influenced its stability in G2. In contrast, coexpression of Rca1_dFbox had hardly any effect in G1 and tended to stabilize Dap_dCDK_Q184A_K195A in G2. Knockdown of Rca1 tended to stabilize Dap_dCDK_Q184A_K195A in G1 and G2. **C, F, G**) Cell cycle curves (**C**) and barplots (**F, G**) representing the relative stability of Dap_dCDK_Q184A_K195A, when HA-CycE/Cdk2-HA was coexpressed and a knockdown of Cdt2 was conducted. Coexpression of Rca1 tended to cause a slight destabilization of Dap_dCDK_Q184A_K195A in G1 and had hardly any effect in G2. Coexpression of Rca1_dFbox had hardly any effect on the stability of Dap_dCDK_K195A in G1 and G2. Knockdown of Rca1 tended to increase the stability of Dap_dCDK_K195A in G1 and G2.

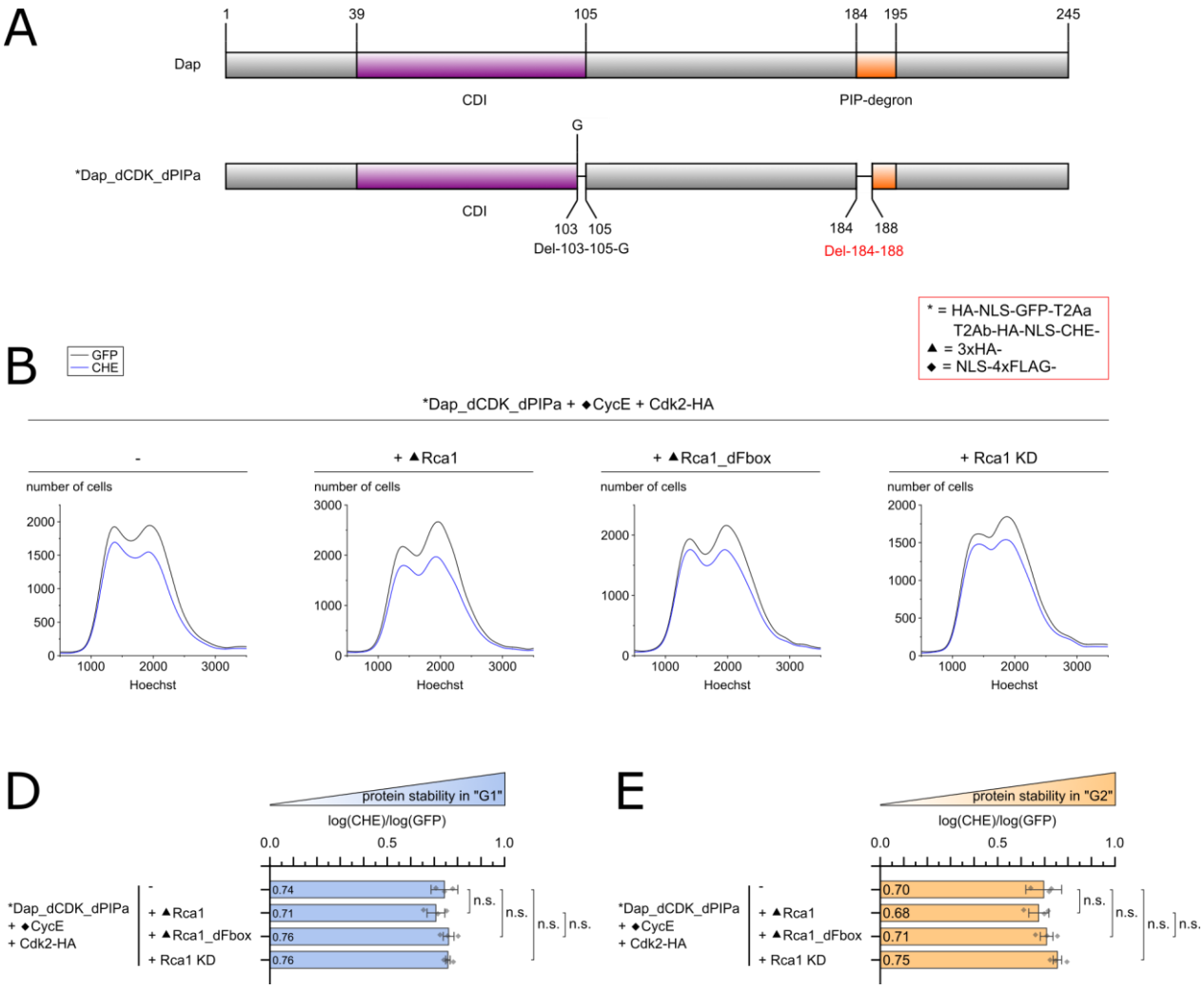

Figure 44 | Influence of Rca1 on the stability of Dap_dCDK_dPIPa

A) Schematic representation of Dap_1-125_dCDK_dPIPa. **B, D, E)** Cell cycle curves (**B**) and barplots (**D, E**) representing the relative stability of Dap_dCDK_dPIPa coexpressed with NLS-4xFLAG-CycE/Cdk2-HA. The data was obtained by flow cytometry. Coexpression of NLS-4xFLAG-CycE/Cdk2-HA facilitated the G1/S transition. Coexpression of Rca1 tended to cause destabilization of Dap_dCDK_dPIPa in G1 and G2. In contrast, coexpression of Rca1_dFbox tended to cause stabilization of Dap_dCDK_dPIPa in G1 and had hardly any effect in G2. Knockdown of Rca1 tended to stabilize Dap_dCDK_dPIPa in G1 and G2.

4.18 C-terminal extensions stabilize Dap_1-125

Neither Dap_1-125 nor Dap_dPIPa contain a functional PIP degron. Therefore, both constructs should not be targeted by CRL4-Cdt2. However, Dap_1-125 and Dap_1-125_dCDK are destabilized during the cell cycle, whereas Dap_dPIPa and Dap_dCDK_dPIPa are much more stable. This indicates that the C-terminal fragment of Dap (aa 126-245) impedes the destabilization of the N-terminal fragment of Dap (aa 1-125). Thus, we were interested, which part of the C-terminal region is responsible for the stabilization. We conducted experiments with various Dap constructs containing additional C-terminal amino acids beyond residue 125. We used the following constructs (with functional CDI or with the dCDK deletion) for relative stability analysis: Dap(_dCDK)_1-125, Dap(_dCDK)_1-140, Dap(_dCDK)_1-160 and Dap(_dCDK)_1-180 (**Figure 45, 46**). All of these constructs do not contain the PIP degron (aa 184-195). Therefore, potential effects by these extensions should be independent of the PIP degron. To facilitate the G1/S transition, NLS-4xFLAG-CycE/Cdk2-HA was coexpressed with each Dap construct.

Due to cloning constraints, the C-terminus of Dap_1-125 constructs (Dap_1-125, Dap_1-125_dCDI, Dap_1-125_dCyc and Dap_1-125_dCDK) contains a small T2A sequence. This was not present in the constructs coding for full-length Dap or Dap_1-140/160/180. We considered it as unlikely that this T2A sequence significantly influences the stability of these proteins. Nevertheless, we tested the stability of Dap_1-125 and compared it to Dap_1-125-T2Aa. Indeed, the stability values for Dap_1-125 and Dap_1-125-T2Aa in G1 and G2 were similar (**Figure 46 A, C, D**).

For the other C-terminal extended Dap constructs, similar cell cycle profiles were obtained (**Figure 46 A and B**). Dap_1-140, Dap_1-160 and Dap_1-180 tended to be more stable in G1 than Dap_1-125 (**Figure 46 C**). In G2, a clear stabilization of all constructs that contained additional amino acids beyond amino acid 125 was seen (**Figure 46 D**). With mutation of the Cdk binding domain, Dap_1-140 and Dap_1-160 showed a significant stabilization both in G1 and G2.

In summary, the extension of amino acids beyond amino acid 125 resulted in a marked increase in the stability of Dap constructs, indicating that the region between amino acids 125 and 140/160 is somehow impeding the degradation of Dap.

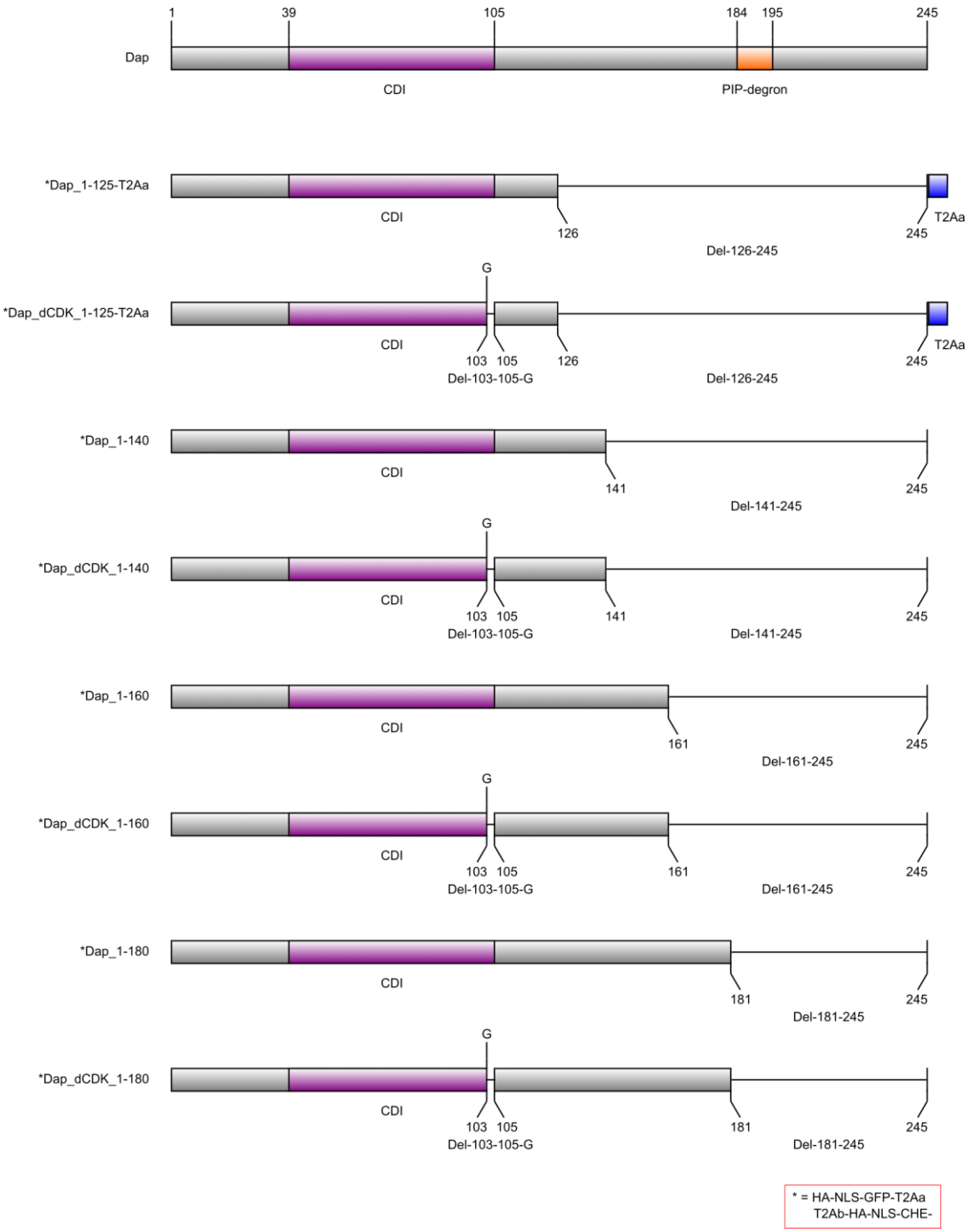

Figure 45 | Dap constructs that were used to analyze the effect of C-terminal extensions on the stability of Dap_125 and Dap_1-125_dCDK

Schematic representation of Dap constructs that were used to analyze how C-terminal extensions can influence the stability of Dap_1-125 and Dap_1-125_dCDK. For cloning reasons, a short T2A sequence (T2Aa) was fused to the C-terminus of Dap_1-125 and Dap_1-125_dCDK.

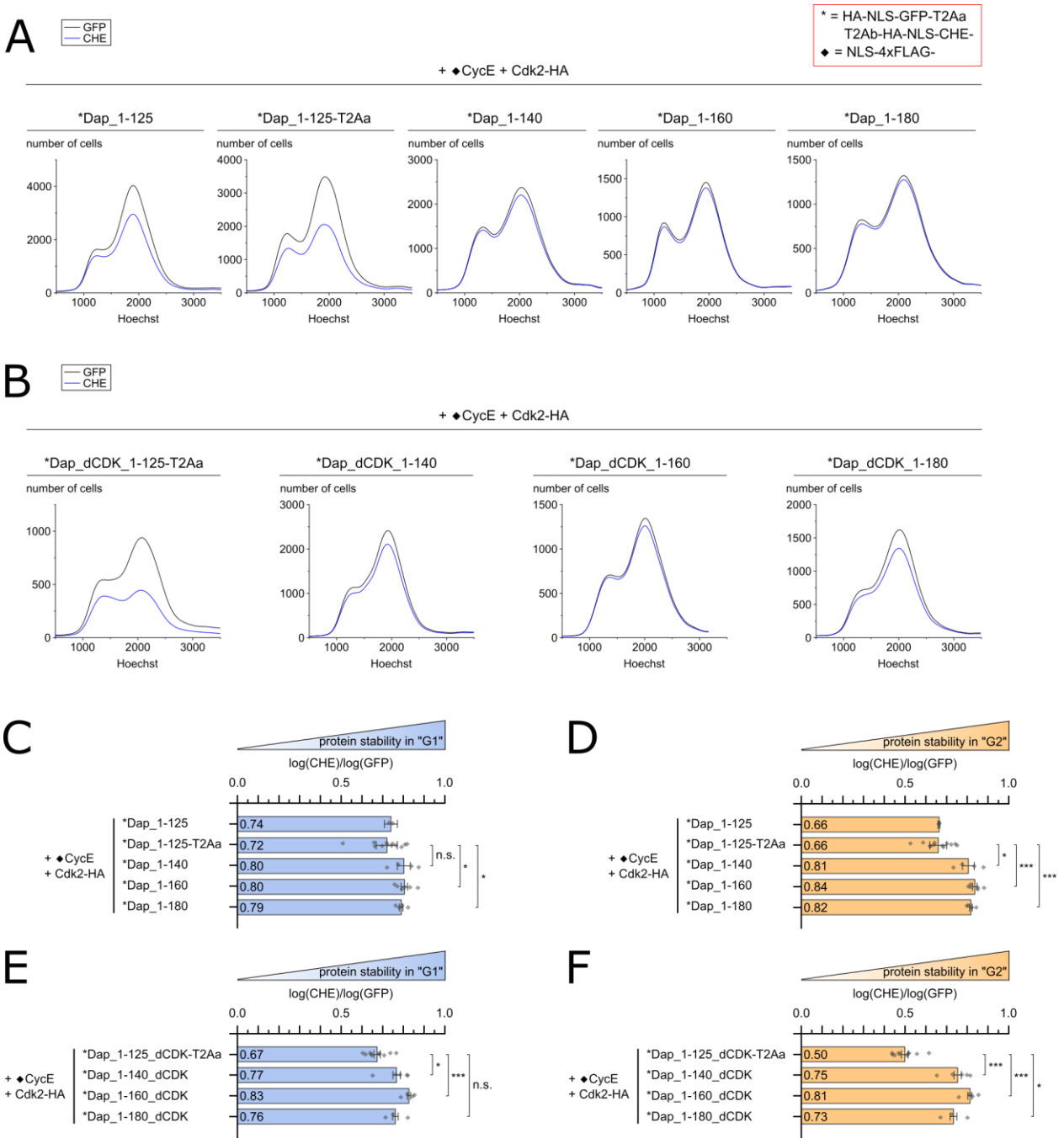

Figure 46 | Dap_1-125 and Dap_1-125_dCDK are stabilized by C-terminal extensions

A, C, D) Cell cycle curves (**A**) and barplots (**C, D**) representing the relative stability of Dap_1-125, Dap_1-125-T2Aa, Dap_1-140, Dap_1-160 and Dap_1-180 each coexpressed with NLS-4xFLAG-CycE/Cdk2-HA. The data was obtained by flow cytometry. The cell cycle profile was similar for all Dap constructs. Dap_1-125 and Dap_125-T2Aa had almost the same stability in G1 and G2 indicating that the small T2Aa sequence did not affect the stability of Dap constructs. Dap_1-140, Dap_1-160 and Dap_1-180 tended to be more stable in G1 and G2 than Dap_1-125. Dap_1-140, Dap_1-160 and Dap_1-180 showed similar stability in G1 and G2. **B, E, F)** Cell cycle curves (**B**) and barplots (**E, F**) representing the relative stability of Dap_1-125_dCDK, Dap_1-140_dCDK, Dap_1-160_dCDK and Dap_1-180_dCDK each coexpressed with NLS-4xFLAG-CycE/Cdk2. The cell cycle profile was similar for all Dap constructs. Dap_1-140_dCDK, Dap_1-160_dCDK and Dap_1-180_dCDK tended to show higher stability in G1 and G2 compared to Dap_1-125_dCDK. Dap_1-160_dCDK tended to be more stable in G1 and G2 than Dap_1-140_dCDK and Dap_1-180_dCDK.

4.19 Influence of N-terminal truncations of CycE on the stability of Dap_1-125 and Dap_dCDK_1-125

Dap_1-125_dCDI and Dap_1-125_dCyc were noticeably more stable than Dap_1-125. This indicates that binding of Dap_1-125 to CycE is essential for its destabilization. We were interested in the underlying mechanism of this destabilization.

As part of another work, which was conducted during this thesis in the Sprenger-lab, the stability of CycE was analyzed. Here, it was found out that deletions of the first 235 amino acids of CycE cause stabilization of CycE. This truncated CycE construct was still able to trigger the G1/S transition when overexpressed and therefore must be able to bind to and to activate Cdk2 (Engelhardt 2022). When Dap_1-125 was coexpressed with the truncated CycE, less degradation of Dap_1-125 was observed than with full-length CycE (Bach 2021). Therefore, we were interested in the link and molecular mechanisms between Dap degradation and CycE truncation and/or stabilization. We cloned several CycE constructs into suitable plasmids for coexpression and coexpressed them with Dap_1-125 or Dap_1-125_dCDK, respectively (**Figure 47, 48**). In addition, Cdk2 was coexpressed in all cases to allow CycE/Cdk2 complex formation.

Besides the CycE lacking the first 235 amino acids, two additional N-terminal deletions were tested, CycE with deletions of the first 202 and 143 amino acids, respectively. The deletion of the first 143 amino acids did not change the stability of CycE, while deletion of the first 202 amino acids resulted in partial stabilization of CycE (Engelhardt 2022). Degradation of CycE depends on a phosphodegron in the C-terminus of CycE (Ye et al. 2004; Hao et al. 2007). Mutations of T544_S548 to alanine prevents phosphorylation and renders CycE stable (personal communication with Sebastian Sigl). Thus, a stable CycE in an otherwise full-length context could be tested as well.

We coexpressed Dap_1-125 with the different CycE versions and Cdk2 and analyzed the stability of Dap_1-125 in G1 and G2. Dap_1-125 tended to be stabilized, especially in G2, when truncated CycE versions were coexpressed. In general, the stabilization was the stronger the larger the truncation in CycE was.

However, no stabilization was observed when coexpressed with the stable full-length CycE construct CycE_T544A_S548A. Thus, stabilization of Dap_1-125 is not a consequence of the stabilization of CycE. Rather, the N-terminus of CycE seems to be essential for the destabilization of Dap_1-125 in a different way. Similar to Dap_1-125, coexpression of CycE_236-602 also caused the strongest stabilization of Dap_1-125_dCDK in G1 and G2 (**Figure 48 B, E, F**). The cell cycle profiles at least in case of coexpressed CycE compared to CycE_236-602 look very similar for both Dap_1-125 and Dap_1-125_dCDK. This indicates that the differences in the stability of Dap_1-125 and Dap_1-125(_dCDK) are not caused by different cell cycle profiles. Like for Dap_1-125, CycE_ T544A_S548A was not able to stabilize Dap_1-125_dCDK.

We wondered whether coexpression of Rca1 can destabilize Dap_1-125 or Dap_1-125_dCDK, when coexpressed with CycE_236-602. Rca1 had no significant effect on the stability of Dap_1-125 or Dap_1-125_dCDK under these conditions (**Figure 49**).

In summary, the N-terminus (aa 1-235) of CycE is essential for the destabilization of Dap_1-125(_dCDK). While CycE lacking the first 235 amino acids is stable, the stability of Dap_1-125 is not correlated with CycE stability. Rather, the N-terminus of CycE is somehow required for destabilization of Dap_1-125 in a different way.

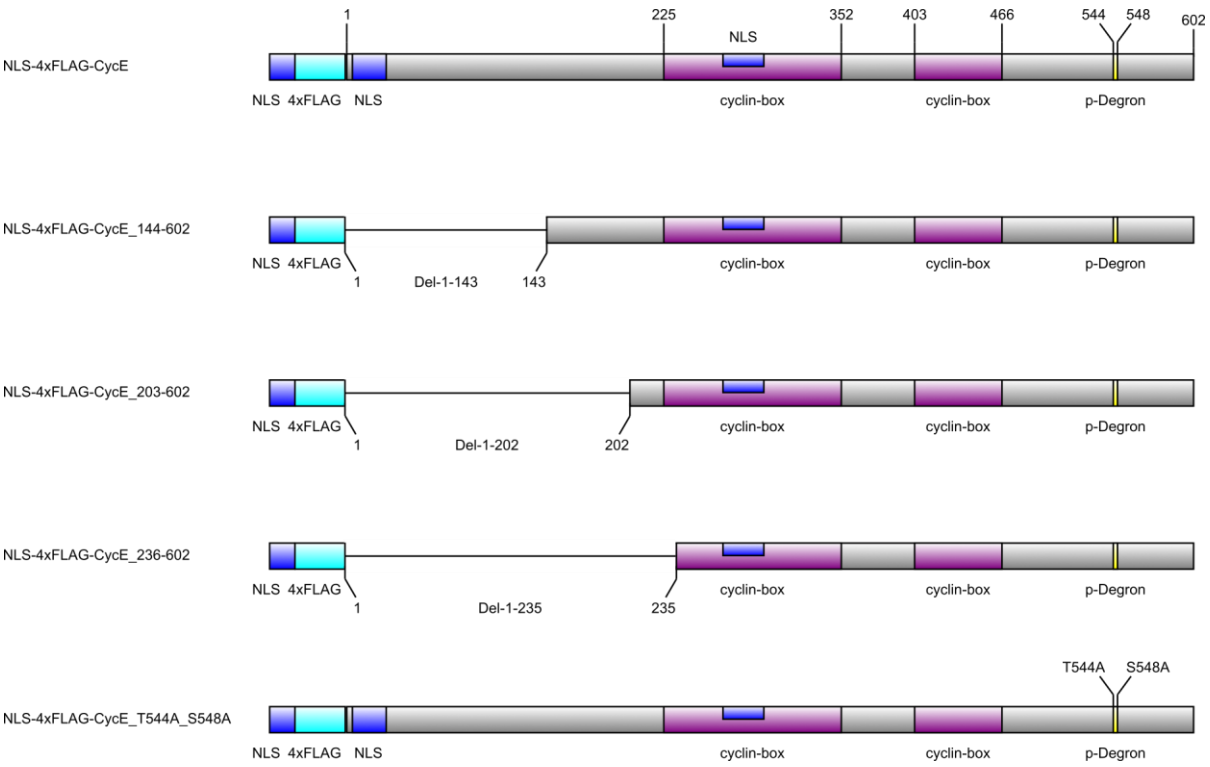

Figure 47 | CycE constructs used for flow cytometry analysis
Schematic representation of CycE constructs that were coexpressed with Dap_1-125 or Dap_1-125_dCDK, respectively. Previously, these CycE constructs were present in T2A plasmids to analyze their stability during the cell cycle (Engelhardt 2022). To analyze their influence on the stability of Dap constructs they were cloned into plasmids suitable for coexpression.

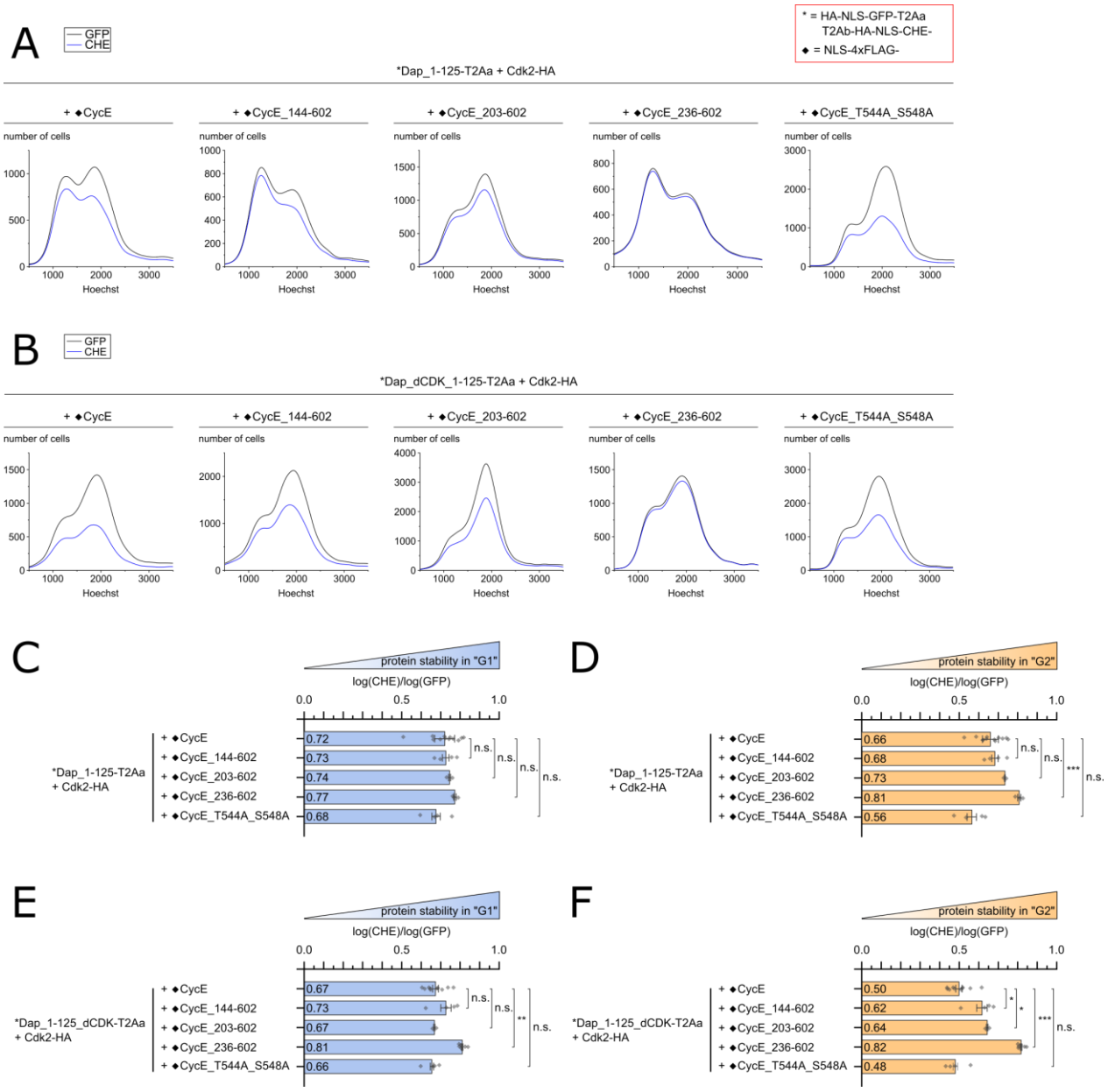

Figure 48 | N-terminal truncations of CycE correlate with the stability of Dap_1-125 and Dap_1-125_dCDK
A, C, D) Cell cycle curves (**A**) and barplots (**C, D**) representing the relative stability of Dap_1-125 coexpressed with the indicated CycE versions and Cdk2. The longer the N-terminal truncation of the coexpressed CycE construct, the more Dap_1-125 tended to be stabilized in G1 and G2, whereby the effect was stronger in G2. CycE_236-602 tended to cause the strongest stabilization of Dap_1-125 in G1 and G2. Although CycE_T544A_S548A is similar stable as CycE_236-602 (personal communication with Sebastian Sigl), CycE_T544A_S548A was not able to cause stabilization of Dap_1-125 in G1 and G2. Rather, CycE_T544A_S548A tended to cause even stronger destabilization of Dap_1-125 than CycE. **B, E, F)** Cell cycle curves (**B**) and barplots (**E, F**) representing the relative stability of Dap_1-125_dCDK coexpressed with the indicated CycE versions and Cdk2. In general, the stability of Dap_1-125_dCDK in G1 and G2 tended to increase the longer the N-terminal truncation of the coexpressed CycE construct was. The only exception was CycE_203-602 that was not able to cause stronger stabilization of Dap_1-125_dCDK in G1 than CycE_144-602. The cell cycle profiles for coexpressed CycE and CycE_236-602 look very similar. Thus, the stabilization of Dap_1-125_dCDK seems to be independent of cell cycle shifts. Like for Dap_1-125, CycE_T544A_S548A was again not able to cause stabilization of Dap_1-125_dCDK.

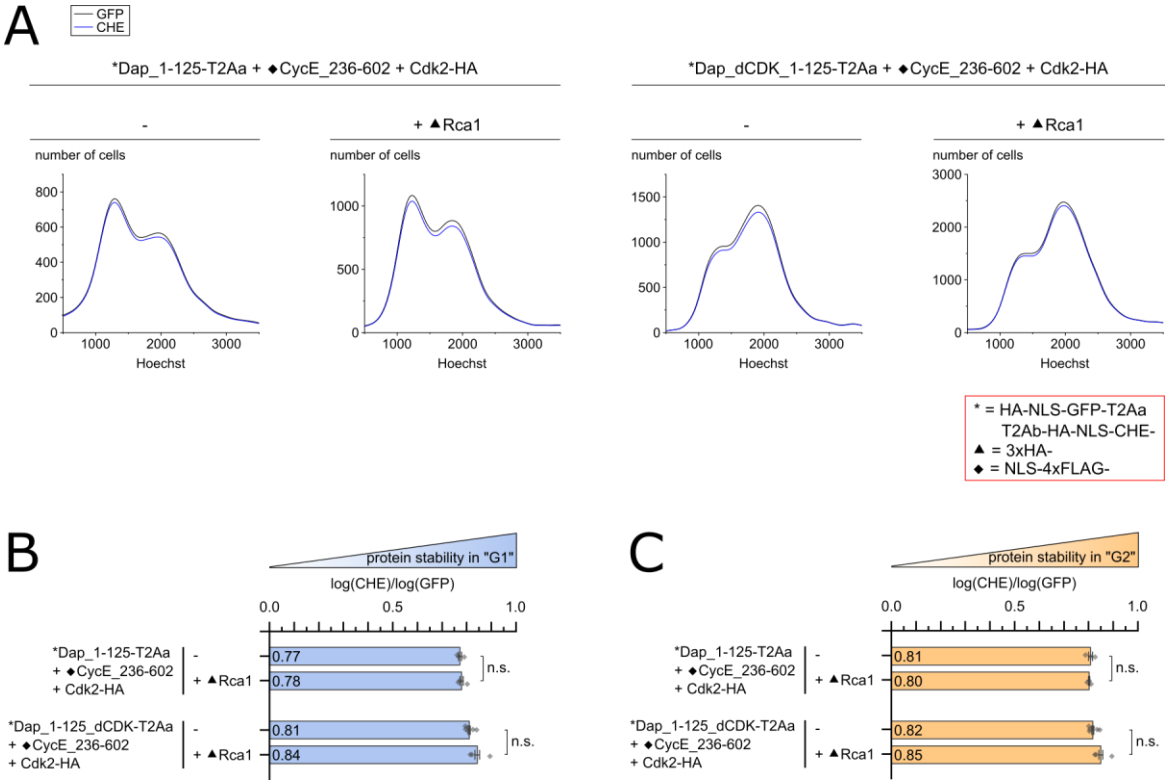

Figure 49 | Rca1 does not influence the stability of Dap_1-125 or Dap_dCDK_1-125 when coexpressed with CycE_236-602
A, B, C) Cell cycle curves (**A**) and barplots (**B, C**) representing the relative stability of Dap_1-125 and Dap_1-125_dCDK, when coexpressed with CycE_236-602 and Cdk2. The data was obtained by flow cytometry. Coexpression of Rca1 had hardly any influence on the stability of Dap_1-125 and Dap_1-125_dCDK in G1 and G2.

4.20 Influence of Ago knockdown on the stability of Dap_1-125 and Dap_dCDK_125

As previously noted, CycE is similarly stabilized by either deletion of the N-terminal fragment 1-235 or by the mutation T544A_S548A. However, Dap_1-125(_dCDK) is only stabilized, when coexpressed with CycE_236-602, but not when coexpressed with CycE_T544A_S548A. This indicated that not the stability of CycE is linked to the stability of Dap_1-125(_dCDK), but that the N-terminus of CycE regulates destabilization of Dap_1-125(_dCDK) in a different manner. We wanted to substantiate our hypothesis that the stability of CycE is not directly linked to the stability of Dap by knockdown of the ubiquitin ligase SCF-Ago that is responsible for the ubiquitination of CycE (Moberg et al. 2001). Previously it was shown that knockdown of Ago results in strong stabilization of CycE (Engelhardt 2022; Moberg et al. 2001). If our hypothesis is right, we expected that the stability of Dap_1-125(_dCDK) is not directly affected by a knockdown of Ago. However, knockdown of Ago could result in indirect effects since it hinders the G1/S transition. Similar to knockdown of Ago, knockdown of Cdt2 results in a different cell cycle profile (**Figure 50 A, B**), presumably by an increase in G1 and early S phase cells. Knockdown of Cdt2 should not have any direct effects on the stability of Dap_1-125(_dCDK) since the PIP degron is missing.

Both Dap_1-125 and Dap_1-125_dCDK tended to be stabilized in G1 and G2 by knockdown of Ago and Cdt2 to a similar extent (**Figure 50**). This suggests that accumulation of cells in G1 or early S phase indirectly influences the stability of Dap_1-125_dCDK. In contrast, we considered direct effects of the Ago knockdown on the stability of Dap_1-125(_dCDK) to be unlikely.

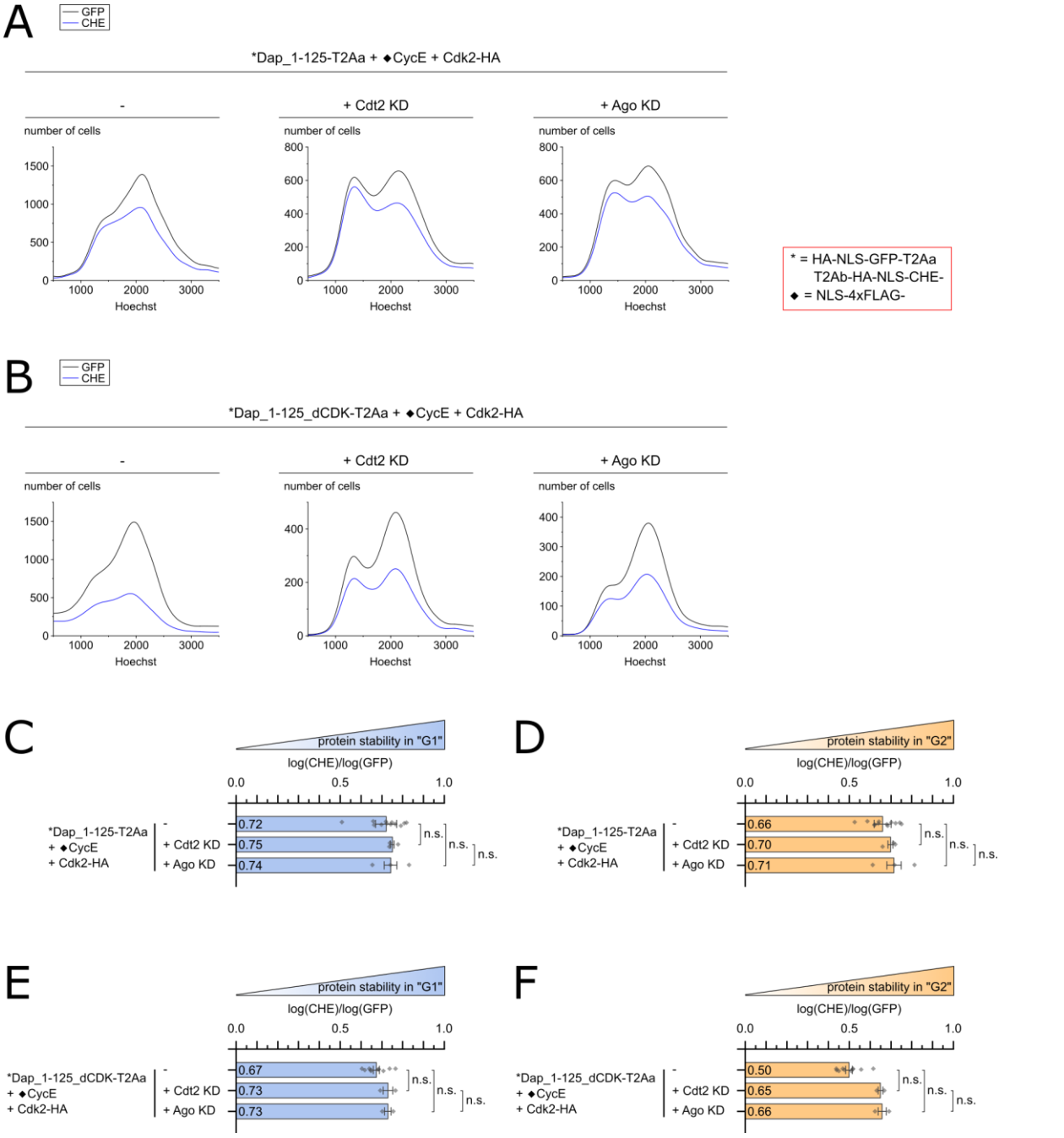

Figure 50 | Influence of Ago knockdown on the stability of Dap_1-125

A, C, D) Cell cycle curves (**A**) and barplots (**C, D**) representing the relative stability of Dap_1-125. The data was obtained by flow cytometry. Both knockdown of Cdt2 and Ago impeded accumulation of cells in G2. In addition, both knockdowns tended to cause stabilization of Dap_1-125 in G1 and G2 to a similar extent. **B, E, F)** Cell cycle curves (**B**) and barplots (**E, F**) representing the relative stability of Dap_1-125_dCDK. Both knockdown of Cdt2 and Ago impeded accumulation of cells in G2. In addition, both knockdowns tended to cause stabilization of Dap_1-125_dCDK in G1 and G2 to a similar extent. This could indicate that this effect was not direct, but indirectly caused by hindering the transition into G2.

4.21 Deletion of the amino acids 1-17 does not stabilize Dap constructs

Although the results above (chapter 4.19, chapter 4.20) suggested that degradation of CycE is not linked to degradation of Dap_1-125, we conducted one additional experiment to directly target this question: Based on crystal structures for the human CycE/Cdk2 complex as well as p27 bound to CycA/Cdk2 it was assumed that the N-terminal region 1-17 of Dap, which harbors a lysine at postion 17, is in proximity of the ubiquitination site of CycE. We wondered whether this region in Dap could be ubiquitinated by SCF-Ago, while it ubiquitinates CycE. To test this hypothesis, we analyzed the stability of Dap_18-125 and Dap_18-125_dCDK by flow cytometry. The deletion of 1-17 in Dap_1-125(_dCDK) would cause stabilization, when the region 1-17 is needed for ubiquitination by SCF-Ago. However, Dap_18-125 and Dap_18_125_dCDK were even less stable than Dap_1-125 or Dap_1-125_dCDK, respectively (**Figure 51**). Therefore, the region 1-17 is not needed for destabilization of Dap_1-125.

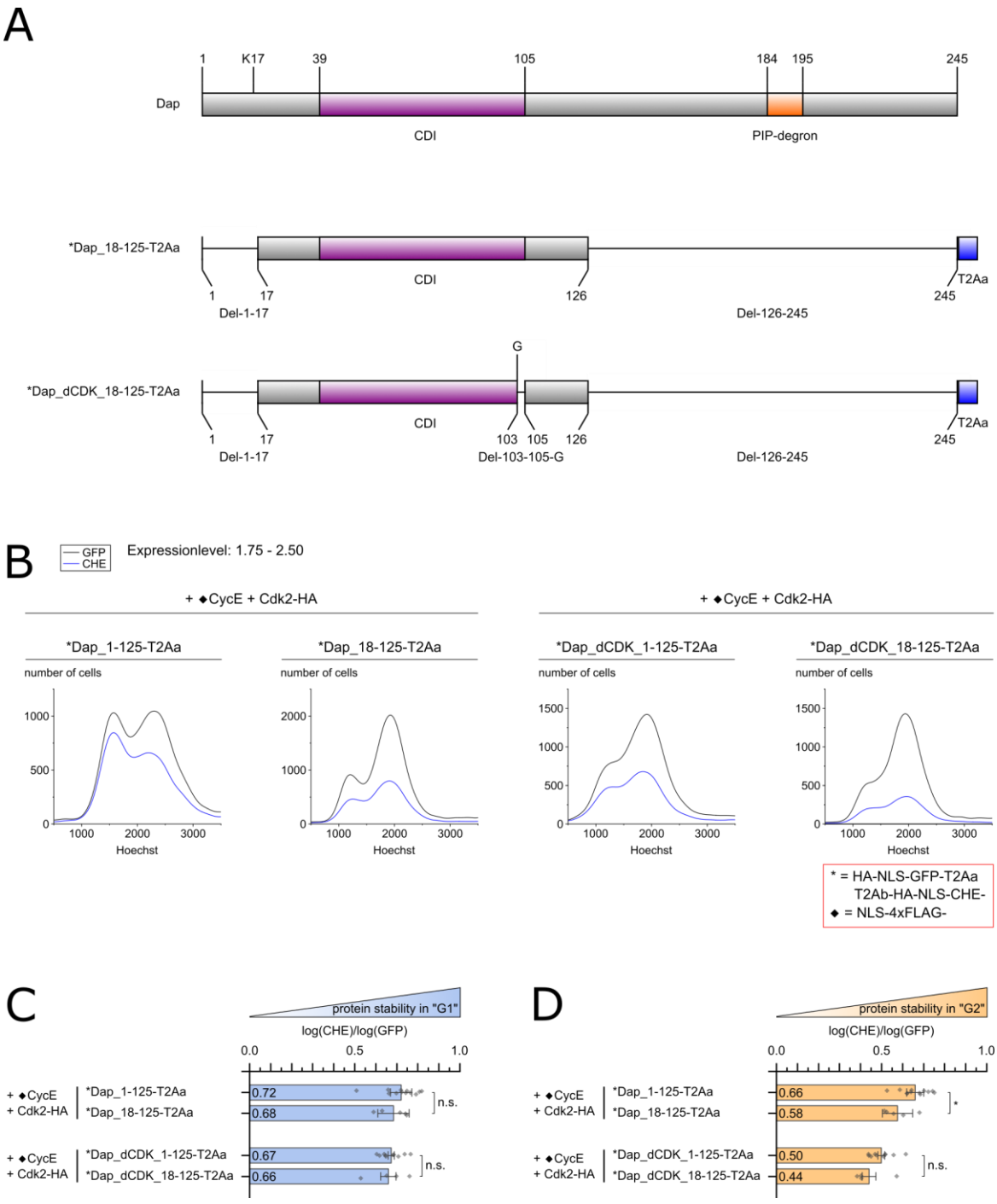

Figure 51 | Deletion of the amino acids 1-17 does not stabilize Dap constructs

A) Schematic representation of Dap_1-125_dCDK_dPIPa. **B, C, D)** Cell cycle curves (**A**) and barplots (**C, D**) representing the stability of Dap_1-125 or Dap_1-125_dCDK, respectively. Neither Dap_1-125 nor Dap_125_dCDK was stabilized in G1 and G2 by deletion of the amino acids 1-17. This indicates that this region in Dap is dispensable for its instability during the cell cycle and not targeted for ubiquitination by SCF-Ago. However, it cannot be ruled out that other regions in Dap are ubiquitinated by SCF-Ago by this experiment.

4.22 The C-terminus of Dap is sufficient for degradation via CRL4-Cdt2

Degradation of Dap and p21 via CRL4-Cdt2 is mediated via their PIP degrons in the C-terminal half (aa 184-195 in case of Dap). To our knowledge, it was not described so far that regions in the N-terminal half of Dap or p21 also contribute to recognition by CRL4-Cdt2. However, as previously noted, co-IPs showed that the N-terminus of Dap (aa 1-160 and aa 1-125) interact with Cdt2. In contrast, interaction of Cdt2 was weak for Dap_126-245 and even not detectable for Dap_160-245 (chapter 4.6). Therefore, we wondered whether Dap constructs lacking the N-terminal half can still be degraded via CRL4-Cdt2 (**Figure 52**). To address this question, we analyzed Dap_126-245 and Dap_160-245 by flow cytometry. To assess whether potential destabilization of these constructs is dependent on CRL4-Cdt2 we analyzed their stability with and without knockdown of Cdt2. Furthermore, in case of Dap_126-245 we introduced mutations in the PIP degron (Q184A_K195A and dPIPa) and observed whether and to which extent this would cause stabilization.

Both Dap_126-245 and Dap_160-245 were very instable in S and knockdown of Cdt2 caused strong stabilization (**Figure 52 B**). This indicates that both Dap constructs are targeted by CRL4-Cdt2 for degradation. Thus, the N-terminal half of Dap, which mediates interaction with Cdt2, seems to be dispensable for recognition by CRL4-Cdt2. Like knockdown of Cdt2, Dap_126-245 tended to be stabilized in S by the PIP degron mutations Q184A_K195A and dPIPa (**Figure 52 C**).

We were interested whether coexpression of Rca1 can cause destabilization of Dap_126-245 or Dap_160-245 (**Figure 53, 54**). Both Dap_1-126-245 and Dap_160-245 tended to be destabilized by coexpression of Rca1 in G1 and G2, whereby the effect was more pronounced in G1. In contrast, coexpression of Rca1_dFbox tended to destabilize Dap_126-245 in G1 and G2 to a smaller extent than Rca1. Coexpression of Rca1_dFbox even tended to cause stabilization of Dap_160-245. Knockdown of Rca1 tended to cause stabilization of Dap_126-245 and Dap_160-245 in G1 and G2.

After knockdown of Cdt2, coexpression of Rca1 and Rca1_dFbox as well as knockdown of Rca1 had similar effects on the stability of Dap_126-245 and Dap_160-245 in G1 and G2 compared to the set without knockdown of Cdt2.

We were also interested whether Rca1 can influence the stability of Dap_126-245 with mutations in its PIP degron. In case of Dap_126-245_Q184A_K195A, coexpression of Rca1 or Rca1_dFbox tended to cause destabilization of Dap_126-245_Q184A_K195A in G1 and G2, whereby the effect was stronger for Rca1_dFbox. However, for Dap_126-245_dPIPa, coexpression of Rca1 or Rca1_dFbox led to increased stability in G1 and G2.

In summary, the results above indicate that both Dap_126-245 and Dap_160-245 are efficiently targeted for degradation by CRL4-Cdt2. If degradation of these Dap constructs via CRL4-Cdt2 is reduced by

knockdown of Cdt2, Rca1 can still destabilize them. In contrast, Rca1 effects on Dap_126-245 with mutations in the PIP degron were ambiguous.

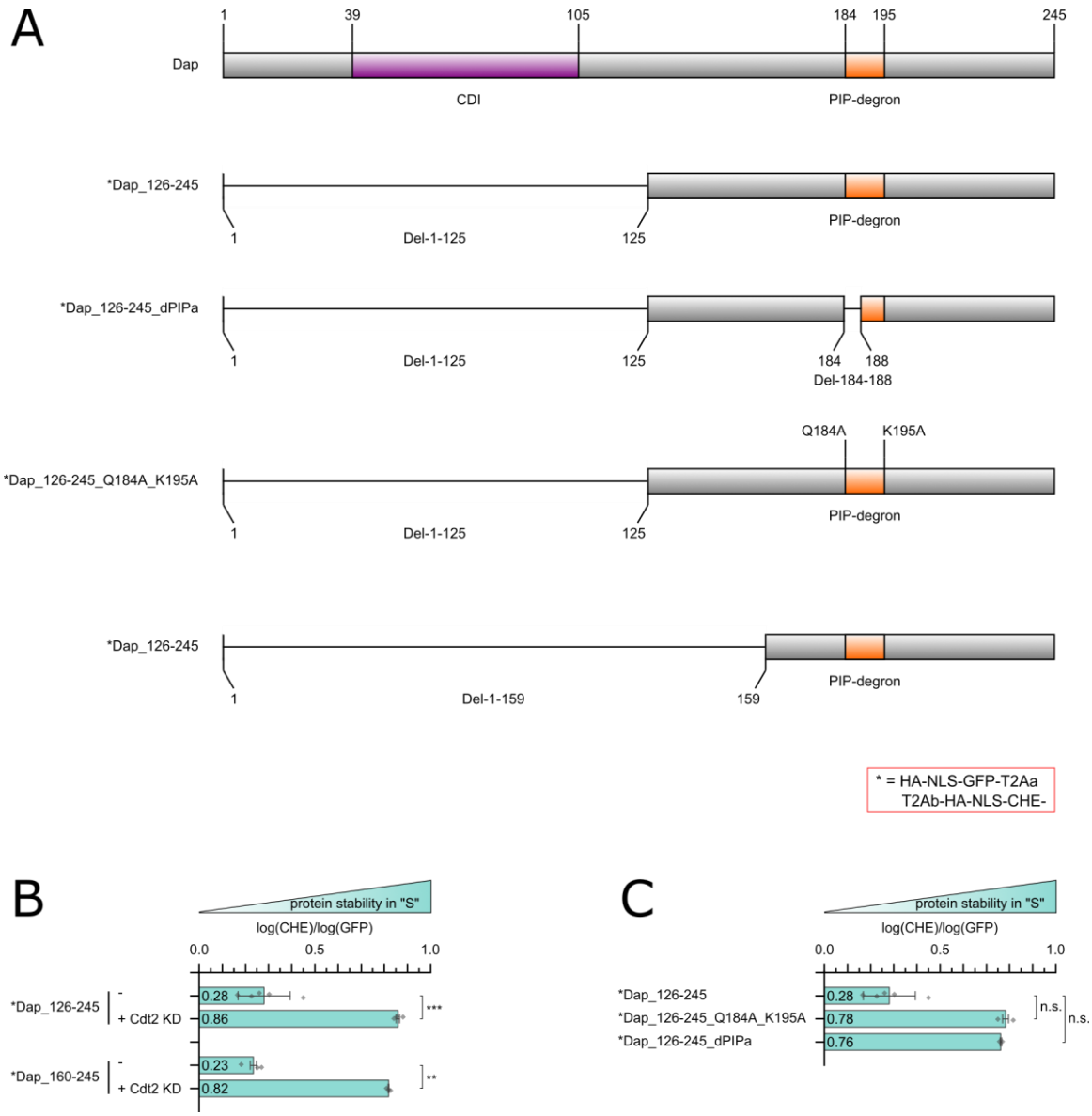

Figure 52 | The C-terminus of Dap is sufficient for its degradation via CRL4-Cdt2
A) Schematic representation of Dap constructs lacking different parts of the N-terminal region. In case of Dap_126-245, two versions were included that harbored mutations in the PIP degron: Dap_126-245_Q184A_K195A and Dap_126-245_dPIPa. **B)** Barplots representing the relative stability of Dap_1-126-245 or Dap_160-245 in S with or without knockdown of Cdt2. Both Dap_126-245 and Dap_160-245 showed high instability in S. However, after knockdown of Cdt2, their stability in S increased significantly. This indicates that the N-terminus of Dap (aa 1-159) is not needed for sufficient degradation via CRL4-Cdt2 **C)** Barplots representing the relative stability of Dap_126-245, Dap_126-245_Q184A_K195A and Dap_126-245_dPIPa in S. The Dap constructs with mutations in the PIP degron tended to be more stable than Dap_126-245. This is in line with the fact that also full-length Dap constructs can be stabilized in S by the mutations Q184A_K195A or dPIPa.

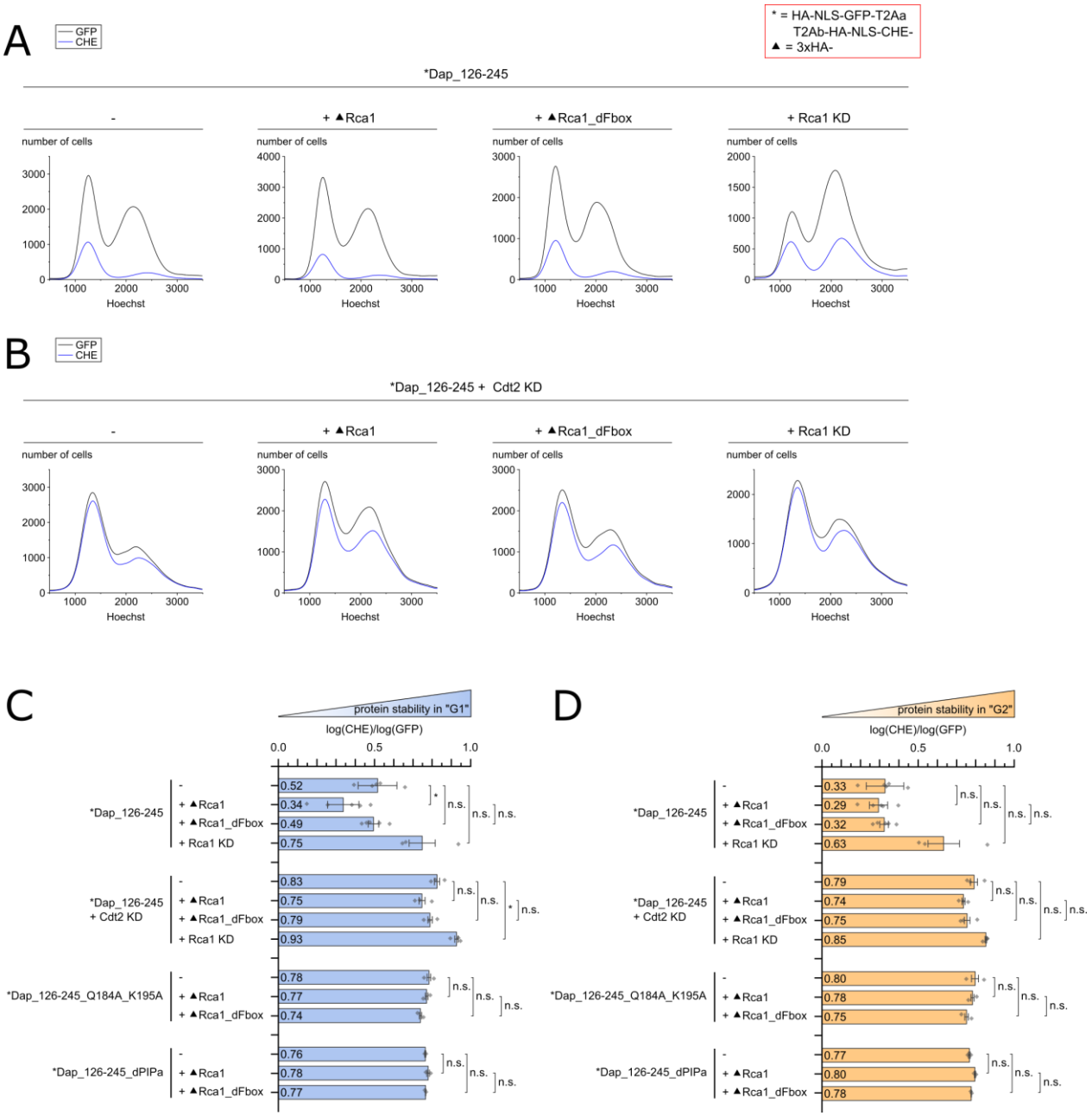

Figure 53 | Rca1 can influence the stability of of Dap_126-245 versions

A-D) Cell cycle curves (**A, B**) and barplots (**C, D**) representing the relative stability of Dap_126-245, Dap_126-245_Q184A_K195A and Dap_126-245_dPIPa. Coexpression of Rca1 tended to destabilize Dap_126-245 in G1 and G2. In G1 and G2, destabilization of Dap_126-245 by Rca1_dFbox tended to be weaker than by Rca1. Knockdown of Rca1 tended to cause stabilization of Dap_126-245 in G1 and G2. After knockdown of Cdt2, coexpression of Rca1 or Rca1_dFbox as well as knockdown of Rca1 tended to influence the stability of Dap_126-245 in G1 and G2 in a similar manner as without knockdown of Cdt2. Dap_126-245_Q184A_K195A tended to be destabilized by Rca1 and Rca1_dFbox in G1 and G2, whereby the effect tended to be more pronounced for Rca1_dFbox. In contrast, coexpression of Rca1 and Rca1_dFbox caused stabilization of Dap_126-245_dPIPa in G1 and G2.

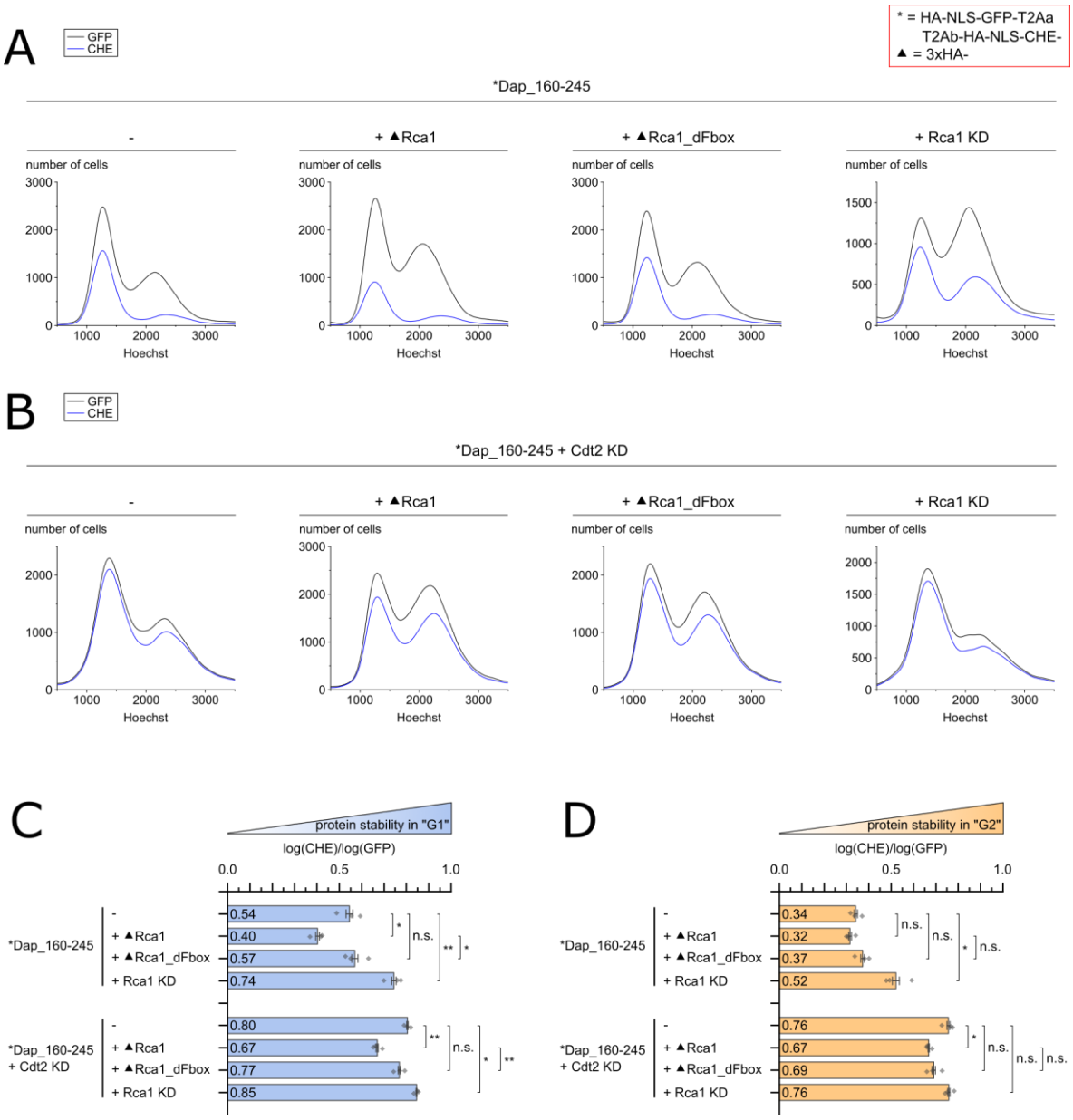

Figure 54 | Rca1 can influence the stability of Dap_160-245

A-D) Cell cycle curves (**A, B**) and barplots (**C, D**) representing the relative stability of Dap_160-245 with or without knockdown of Cdt2. Coexpression of Rca1 tended to cause destabilization of Dap_160-245 in G1 and G2, whereby the effect was stronger in G1. Coexpression of Rca1_dFbox tended to cause stabilization of Dap_160-245 in G1 and G2. Knockdown of Rca1 tended to stabilize Dap_160-245 in G1 and G2. After knockdown of Cdt2, Rca1 effects in G1 and G2 were similar as without knockdown of Cdt2.

4.23 Establishment of TUBE-ligase trapping and an *in vitro* ubiquitination assay to allow detection of ubiquitination of Dap by SCF-Rca1

Dap is a target of the E3 ubiquitin ligase CRL4-Cdt2 (Swanson et al. 2015). As previously noted, we have indications that coexpression/knockdown of Rca1 can cause destabilization/stabilization of Dap indirectly via CRL4-Cdt2. This is a problem for the relative protein stability analysis using flow cytometry since changes in the cell cycle status by Rca1 overexpression can influence the amount of Dap degradation by the CRL4-Cdt2 pathway. Above, several strategies were applied to reduce these indirect Rca1 effects on Dap destabilization in a cellular system. To avoid these changes in cell cycle distributions, we tried to establish other methods that would show more directly that Dap is ubiquitinated by SCF-Rca1. To this end, we focused on two approaches: TUBE-ligase trapping as well as an *in vitro* ubiquitination assay.

TUBE-ligase trapping is a recently described method to allow identification of substrates of E3 ubiquitin ligases (Watanabe et al. 2020). The principle behind this method is the following: The interaction between E3 ubiquitin ligases and their substrates is usually transient. This means that substrates immediately dissociate from the corresponding E3 after they have been ubiquitinated. Therefore, ubiquitinated substrates usually do not coprecipitate, when the E3 is precipitated. To prevent dissociation between ubiquitinated substrate and E3, TUBE-ligase trapping makes use of so-called UBA domains, which can strongly bind ubiquitin. These UBA domains are fused to the substrate recognition module (e.g. Rca1) of the E3. Four UBA domains are fused together in a row (4xUBA), which protects the substrate from proteasomal degradation. As soon as the substrate (e.g. Dap) is ubiquitinated it binds strongly to the substrate recognition module with fused UBA domains (e.g. Rca1-4xUBA-4xFLAG). When ubiquitinated Dap can be coprecipitated, when UBA fused Rca1 is precipitated, this would indicate that Dap is a substrate of SCF-Rca1.

To apply this TUBE-ligase method, we constructed and overexpressed Rca1-4xUBA-4xFLAG together with HA-Dap in S2R+ cells. Then, we precipitated Rca1-4xUBA-4xFLAG using an anti-FLAG antibody coupled to agarose beads. Unfortunately, it could not be assessed whether (ubiquitinated) Dap was coprecipitated since a diffuse band on the western blot resulting from the antibody used for precipitation ran at the same height as HA-Dap (data not shown). To avoid this problem, we fused GFP at the N-terminus of Rca1-4xUBA-4xFLAG, which resulted in GFP-Rca1-4xUBA-4xFLAG. Then, we precipitated GFP-Rca1-4xUBA-4xFLAG using a GFP nanobody coupled to agarose beads. By means of that we could avoid the diffuse band mentioned above. However, 4xFLAG-Dap precipitated non-specifically even when GFP-Rca1-4xUBA-4xFLAG was not coexpressed (**Figure 55**). Nevertheless, the amount of 4xFLAG-Dap was higher, when GFP-Rca1-4xUBA-4xFLAG was precipitated. This could indicate that 4xFLAG-Dap interacted with GFP-Rca1-4xUBA-4xFLAG. Above the main band of 4xFLAG-Dap additional weaker bands were present both in the input and the IP

sample when coexpressed with GFP-Rca1-4xUBA-4xFLAG. These bands are likely posttranslationally modified versions of 4xFLAG-Dap, but it remains to be shown what kind of posttranslational modifications are present. As previously noted, binding of Dap_1-125 to CycE seems to be essential for its degradation. Therefore, in a second approach CycE/Cdk2 was additionally coexpressed with either 4xFLAG-Dap or NLS-4xFLAG-Dap_1-125. However, also here both 4xFLAG-Dap and NLS-4xFLAG-Dap_1-125 were non-specifically precipitated. Currently, optimization steps are conducted in our workgroup to unequivocally demonstrate ubiquitination of Dap by means of TUBE-ligase trapping.

We also tried to detect ubiquitination of Dap by means of an SCF-Rca1 *in vitro* ubiquitination assay. First, we wanted to establish a positive control for this assay. To this end, we wanted to use GFP as a substrate and the F-box protein Slmb fused to a GFP nanobody (4xFLAG-Slmb-vhh-GFP). We wanted to make sure that 4xFLAG-Slmb-vhh-GFP can be incorporated into an SCF complex. To test this, we tried to coprecipitate 3xHA-SkpA, 3xHA-Cul1 and 3xHA-Roc1a, when we precipitate 4xFLAG-Slmb-vhh-GFP using an anti-FLAG antibody coupled to agarose beads. 3xHA-SkpA was specifically coprecipitated in high amounts (**Figure 56**). However, 3xHA-Cul1 was only coprecipitated in low amounts, whereas coprecipitated 3xHA-Roc1a was not detectable at all. We wondered, whether we can increase the amount of coprecipitated 3xHA-Cul1, when we use 4xFLAG-SkpA for precipitation. Indeed, higher amounts of coprecipitated 3xHA-Cul1 could be achieved. We assume that also Roc1 coprecipitates with Cul1, although this was not directly shown so far.

In summary, the results indicate that the whole SCF-4xFLAG-Slmb-vhh-GFP complex can be coprecipitated, when 4xFLAG-Slmb-vhh-GFP is precipitated. This forms the basis for subsequent experiments. Currently, in our workgroup further establishment is conducted to enable the detection of ubiquitinated GFP constructs by Slmb-vhh-GFP. Once the positive control is established, it will be tried to detect ubiquitination of Dap by means of an SCF-Rca1 *in vitro* ubiquitination assay.

A

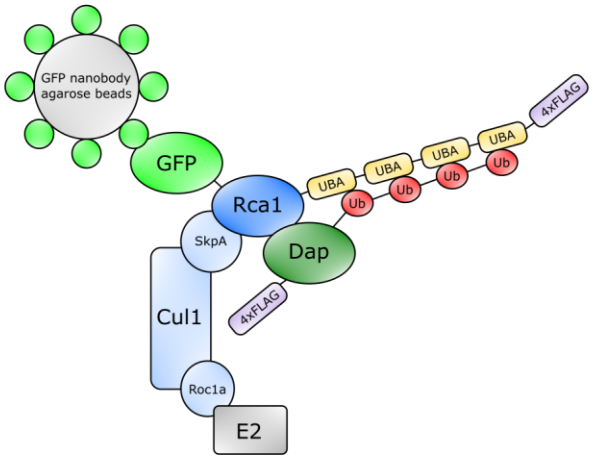

B

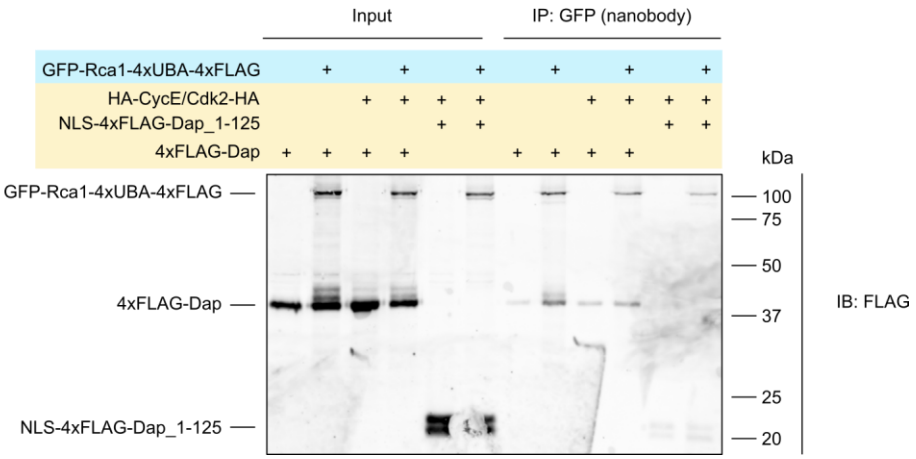

Figure 55 | Establishment of TUBE-ligase trapping to detect ubiquitination of Dap
A) Scheme illustrating the principle of TUBE-ligase trapping. If 4xFLAG-Dap is ubiquitinated by SCF-Rca1, the ubiquitin chain binds strongly to the UBA domains, which are fused to Rca1. In addition, GFP is fused to Rca1 to allow precipitation by GFP nanobodies, which are coupled to agarose beads. Detection of GFP-Rca1-4xUBA-4xFLAG and 4xFLAG-Dap on western blots is enabled by means of the 4xFLAG tag. If ubiquitinated 4xFLAG-Dap can be coprecipitated, when GFP-Rca1-4xUBA-4xFLAG is precipitated, this indicates that Dap is a substrate of SCF-Rca1. **B)** TUBE ligase trapping was conducted as described in (**A**). Unfortunately, 4xFLAG-Dap was precipitated non-specifically even in the absence of GFP-Rca1-4xUBA-4xFLAG. However, the amount of 4xFLAG-Dap increased in the IP samples, when GFP-Rca1-4xUBA-4xFLAG was coexpressed. This could indicate that 4xFLAG-Dap and GFP-Rca1-4xUBA-4xFLAG interacted with each other. When GFP-Rca1-4xUBA-4xFLAG was coexpressed with 4xFLAG-Dap, weak bands above the band containing 4xFLAG-Dap were present in both the input and IP sample. However, it cannot be said with certainty whether these bands resulted from ubiquitinated 4xFLAG-Dap or whether they were caused by other posttranslational modifications such as phosphorylation. Previous results indicated that binding of Dap_1-125 to CycE is essential for its degradation. Therefore, in a second approach HA-CycE/Cdk2-HA was additionally coexpressed. However, also here no clear ubiquitination bands were detected in the corresponding IP sample. Precipitation of NLS-4xFLAG-Dap_1-125 was not specific as well. In addition, ubiquitination could not be detected for NLS-4xFLAG-Dap_1-125.

A

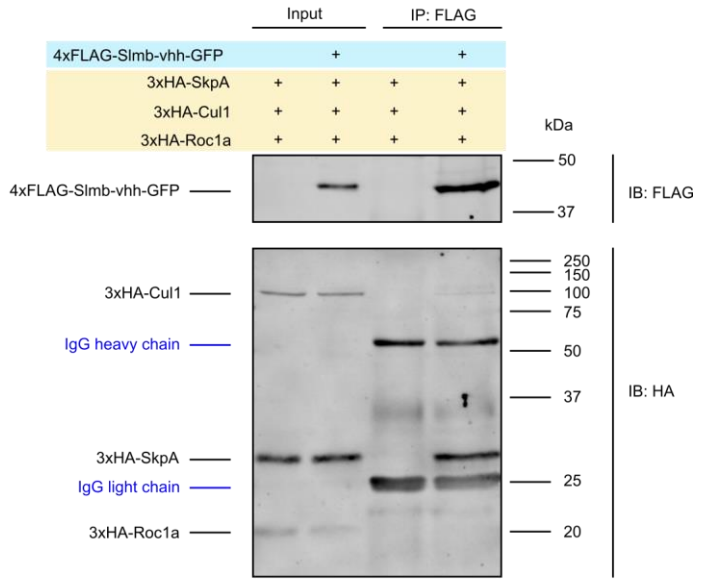

B

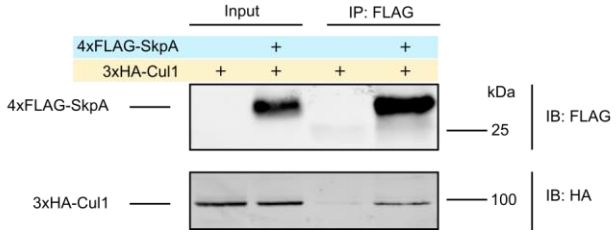

Figure 56 | Establishment of an *in vitro* ubiquitination assay to detect ubiquitination of GFP constructs
A) As a positive control an *in vitro* ubiquitination assay should be established with SCF-4xFLAG-Slmb-vhh-GFP to allow ubiquitination of GFP constructs. To this end, we were interested, whether the whole SCF-4xFLAG-Slmb-vhh-GFP can be obtained by precipitation of 4xFLAG-Slmb-vhh-GFP using anti-FLAG antibodies coupled to agarose beads. 3xHA-SkpA was coprecipitated in high amounts, whereas 3xHA-Cul1 coprecipitated in low amounts and 3xHA-Roc1a was not detectable at all in the IP sample. **B)** We were interested, whether higher amounts of coprecipitated 3xHA-Cul1 can be achieved, when we precipitate 4xFLAG-SkpA. Indeed, coprecipitation of 3xHA-Cul1 was more efficient in comparison to precipitation of 4xFLAG-Slmb-vhh-GFP. This is likely due to the higher amount of SkpA.

4.24 A fragment of Rca1 can be ubiquitinated *in vitro* by APC/C-Fzr

Rca1 is an inhibitor of the E3 ubiquitin ligase APC/C-Fzr (Grosskortenhaus and Sprenger 2002). Flow cytometry analysis indicated that Rca1 switches during the cell cycle from being an inhibitor to a substrate of APC/C-Fzr (Morgenthaler 2013; Polz 2021). However, flow cytometry analysis does not allow detection of ubiquitinated Rca1, which would be a more direct evidence that Rca1 is a substrate of APC/C-Fzr. Therefore, we wanted to detect ubiquitination of Rca1 by APC/C-Fzr by means of an *in vitro* APC/C ubiquitination assay. The following proteins needed for ubiquitination were heterologously expressed in *E. coli* and purified by means of an ÄKTA system: 6xHis-4xFLAG-Ubiquitin, 6xHis-Uba1 (E1) and 6xHis-Vihar (E2). APC/C-Fzr is a large complex consisting of several subunits and heterologous expression in *E. coli* would be difficult. Therefore APC/C-Fzr was obtained from *Drosophila* embryo mutants that expressed a tagged APC/C subunit: Cdc16-MYC-TEV-GFP. Previously it was shown that Cdc16-MYC-TEV-GFP can be incorporated into endogenous APC/C complexes (Berger 2017). Therefore, we precipitated Cdc16-MYC-TEV-GFP to coprecipitate APC/C-Fzr. APC/C can be activated by two different co-activators: Fzr (Cdh1 in human) and Fzy (Cdc20 in human). In order to enrich for APC/C-Fzr, but not APC/C-Fzy complexes, we used *Drosophila* embryos incubated for 17 hours at 18 °C before lysis. At these stages, most cells in the embryo are in the G1 state and the APC/C is mainly associated with Fzr, but not Fzy (Raff et al. 2002). The *Drosophila* embryos were homogenized and lysed, and Cdc16-MYC-TEV-GFP was precipitated using GFP nanobodies coupled to agarose beads (GFP nanobody beads). As a negative control, precipitation using GFP nanobody beads was also conducted with wildtype *Drosophila* embryos to exclude that E3s other than the APC/C are precipitated in a non-specific manner, which could ubiquitinate Rca1. Full-length Rca1 could not be obtained in sufficient amounts by expression in *E. coli*, *Drosophila*, or *Sf21* (using baculoviruses). Previous flow cytometry analysis indicated that the region 204-299 in Rca1 is sufficient to facilitate degradation of Rca1 via APC/C-Fzr (Morgenthaler 2013; Polz 2021). Expression of 6xHis-10xHA-CHE-Rca1_204-411 in *E. coli* was successful and the protein was purified by an ÄKTA system. To exclude that the tag 6xHis-10xHA-CHE but not Rca1_204-411 is ubiquitinated by APC/C-Fzr, 6xHis-10xHA-CHE was additionally expressed and purified to serve as a negative control. All purified/precipitated proteins were mixed and incubated for one hour at 30 °C in ubiquitination buffer (see material and methods). Only 6xHis-10xHA-CHE-Rca1_204-299, but not 6xHis-10xHA-CHE was ubiquitinated after addition of APC/C-Fzr (**Figure 57).** This indicates that specifically Rca1_204-299, but not the tag 6xHis-10xHA-CHE was ubiquitinated.

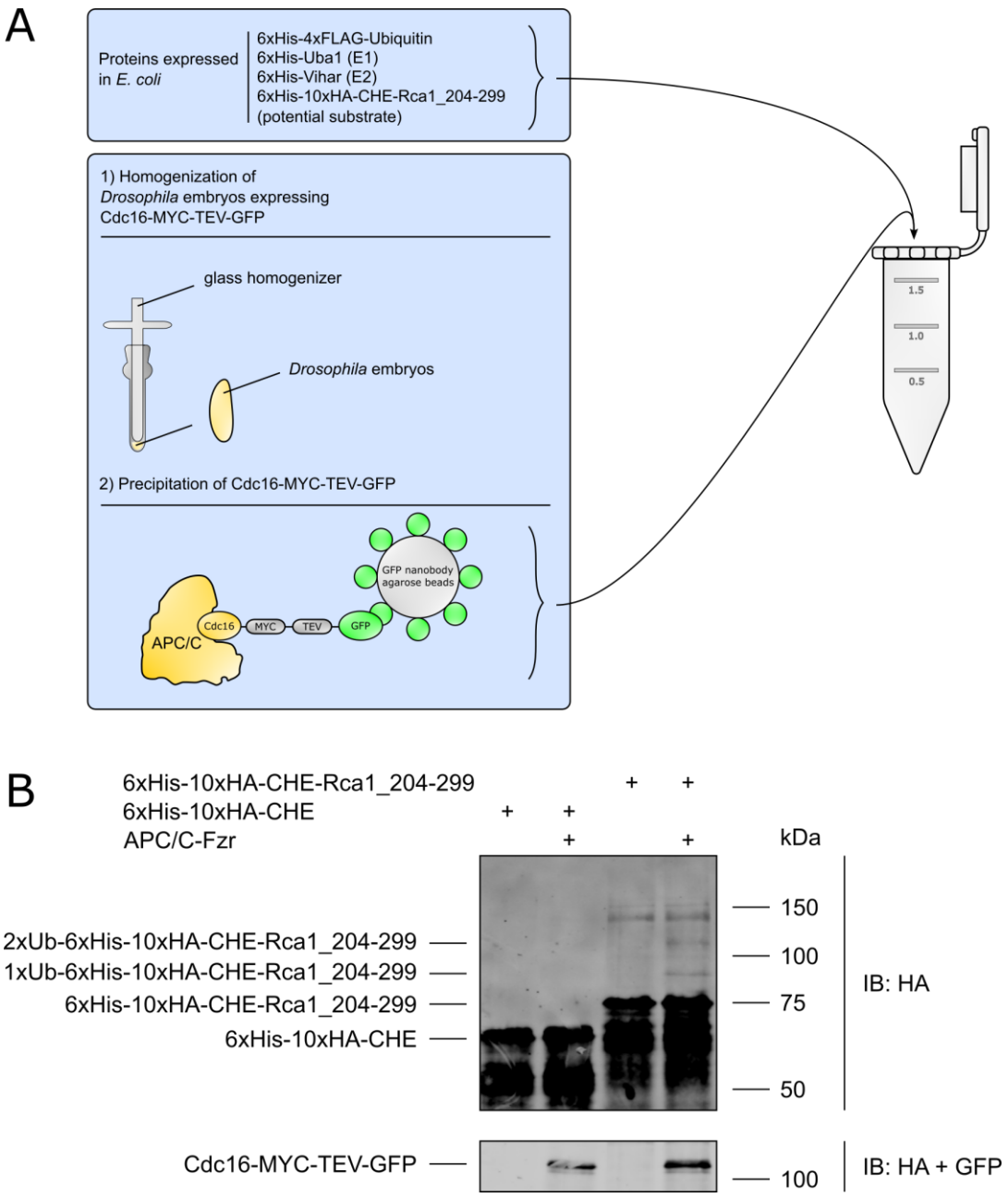

Figure 57 | Rca1_204-299 is ubiquitinated by APC/C-Fzr *in vitro*

A) Workflow for the APC/C *in vitro* ubiquitination assay. The following proteins needed for ubiquitination were expressed in *E. coli* and purified by an ÄKTA system: 6xHis-4xFLAG-Ubiquitin, 6xHis-Uba1 (E1), 6xHis-Vihar (E2), 6xHis-10xHA-CHE-Rca1_204-299 (potential substrate) and 6xHis-10xHA-CHE (negative control). APC/C-Fzr was obtained from transgenic *Drosophila* embryos that expressed a tagged APC/C subunit: Cdc16-MYC-TEV-GFP. Cdc16-MYC-TEV-GFP was precipitated using a GFP nanobody coupled to agarose beads. APC/C-Fzr was coprecipitated as it was previously shown that Cdc16-MYC-TEV-GFP is incorporated into APC/C-Fzr (Berger 2017). To ensure that mainly APC/C-Fzr, but not APC/C-Fzy is coprecipitated, the *Drosophila* embryos were incubated for 17 hour at 18 °C. All purified/precipitated proteins were mixed and incubated in ubiquitination buffer at 30°C for one hour. Thereafter, ubiquitination was detected by western blot. **B)** Presence of Cdc16-MYC-TEV-GFP (lower western blot) indicated that APC/C-Fzr was present (lane 2 and 4). In lane 1 and 3 wildtype *Drosophila* embryos were used for precipitation using GFP nanobody coupled agarose beads. This served as a negative control, if non-specifically precipitated E3s would have caused ubiquitination of substrates. 6xHis-10xHA-CHE-Rca1_204-299 but not 6xHis-10xHA-CHE was ubiquitinated when APC/C-Fzr was present. This indicates that Rca1_204-299 and not the tag 6xHis-10xHA-CHE was ubiquitinated.

5. Discussion

5.1 Rca1 can influence the stability of Dap_dCDI in an F-box dependent manner, but also indirectly via CRL4-Cdt2

The aim of this thesis was to understand the mechanisms, which regulate degradation of Dap during the cell cycle. Especially, we were interested whether Dap is targeted for degradation by SCF-Rca1. Previous work already suggested that Dap could act as a substrate of SCF-Rca1: It was shown that Rca1 can interact with the SCF components SkpA and Cul1 in an F-box dependent manner. This indicated that there is an SCF-Rca1 complex. Furthermore, Rca1 accelerated the G1/S transition in an F-box dependent manner. This suggested that SCF-Rca1 can promote S phase entry (Zielke et al. 2006). Dap blocks the G1/S transition by inhibiting CycE/Cdk2 (Lane et al. 1996). Thus, to overcome G1, degradation of Dap at the end of G1 would be a plausible mechanism. However, other mechanisms such as accumulation of CycE/Cdk2 so that the amount of Dap is exceeded at some point would also be conceivable. Also, a combination – Dap degradation and accumulation of CycE/Cdk2 – is imaginable. The human homologs of Dap – p21 and p27 – are targeted for degradation by SCF-Skp2 from the end of G1 to M phase (Starostina and Kipreos 2012). Initially, also for Dap it was claimed that it is a target of SCF-Skp2 (Dui et al. 2013). However, two other publications came to the conclusion that Dap is not a substrate of SCF-Skp2 (Ghorbani et al. 2011; Rössler 2019). The effects of Skp2 on Dap stability seen by Dui et al. were probably indirect and not interpreted correctly (Rössler 2019). In contrast, there is agreement that Dap is a substrate of CRL4-Cdt2 (Swanson et al. 2015; M. Kies 2017). However, degradation of substrates via CRL4-Cdt2 is restricted to S phase (or DNA damage) (Havens and Walter 2011). Therefore, we do not assume that CRL4-Cdt2 targets Dap for degradation at the end of G1 or in G2.

Rather, there are indications that Dap could be a substrate of SCF-Rca1: On the one hand, interaction between Rca1 and Dap constructs was shown by co-IP and mass spectrometry. In addition, flow cytometry analysis indicated that Rca1 can trigger the degradation of Dap_dCDI_dPIPa in an F-box dependent manner (M. Kies 2017). The dCDI and dPIPa mutation of this Dap construct should make the analysis easier, since the dCDI mutation should abolish binding to CycE/Cdk2 (→ cell cycle inert) and the dPIPa mutation should abolish degradation via CRL4-Cdt2. However, the effect of Rca1 on the stability of Dap_dCDI_dPIPa was weak. In addition, the variance of the measurements was high (M. Kies 2017). One problem of this flow cytometry analysis was that the stoichiometric expression of the reference protein CHE and the protein of interest (e.g. Dap constructs) fused to GFP was under the control of two separate and different promotors (methalothionin and actin promotor). Meanwhile a new approach – the so-called RPS system was

established in the Sprenger-lab – which allows accurate and reproduceable measurement of relative protein stabilities using flow cytometry (Polz 2021). Important in this system is the T2A sequence, which enables the expression of two proteins under the control of one promotor.

We used this RPS system to analyze effects of Rca1 on the stability of Dap constructs. If our hypothesis of SCF-Rca1 targeting Dap for degradation is correct, we would expect the following: Overexpression of Rca1 leads to more SCF-Rca1 complexes and therefore decreased stability of Dap. However, it should be cautioned that the amount of SCF complexes in which Rca1 can be incorporated might be limiting and the increase in SCF-Rca1 complexes by overexpression could be restricted.

In contrast, knockdown of Rca1 by RNAi approaches would reduce the number of SCF-Rca1 complexes and therefore the stability of Dap would increase. In this context, constraints arise from both the efficacy of RNAi and the stability of the Rca1 protein and SCF complexes, which may limit the overall response. We also overexpressed Rca1_dFbox, for which we already knew that it can still inhibit APC/C-Fzr, but cannot be incorporated into an SCF complex (Zielke et al. 2006). We expected that Rca1_dFbox does either not influence or could even increase the stability of Dap constructs: Rca1_dFbox is not incorporated into an SCF complex, but could bind Dap and thereby protect it from degradation via SCF-Rca1. Previously it was hypothesized that Dap could be degraded via SCF-Rca1 both at the end of G1 and G2 (M. Kies 2017). Therefore, Rca1 effects on the stability of Dap constructs were analyzed for G1 and G2.

We started our analysis with Dap_dCDI. In this Dap construct the CDI domain (aa 38-105), which is needed for inhibition of CycE/Cdk2, was mutated (M. Kies 2017). This rendered Dap_dCDI cell cycle inert, which made flow cytometry analysis easier to interpret. Overexpression of Rca1 reduced the stability of Dap_dCDI in G1 and G2, while knockdown led to stabilization. This supported our hypothesis. Coexpression of Rca1_dFbox was not as potent in destabilizing Dap_dCDI as Rca1. However, the destabilizing effect of Rca1_dFbox was relatively pronounced, which made us ask by which mechanism Rca1_dFbox can influence the stability of Dap_dCDI. We hypothesized that the destabilization of Dap_dCDI via Rca1_dFbox is caused indirectly via APC/C inhibition and then CRL4-Cdt2 dependent degradation in S phase: Since Rca1_dFbox can inhibit APC/C-Fzr, this in turn leads to an altered cell cycle distribution, which could influence the degradation of Dap via CRL4-Cdt2 or the detection of this degradation. One restriction of our flow cytometry analysis is that the classification of cells in G1, S and G2 phase is not perfectly accurate. Therefore, for instance some cells in the “G1” selection are actually cells in early S phase. It would be conceivable that coexpression of Rca1_dFbox increases the proportion of early S phase cells in the G1 selection by influencing the cell cycle distribution. Therefore, more degradation of Dap_dCDI by CRL4-Cdt2 would be detected in the G1 selection after coexpression of Rca1_dFbox. To abolish or at least reduce this

potential indirect effect we wanted to reduce the activity of CRL4-Cdt2. We achieved this by applying a knockdown of Cdt2. The significantly increased stability of Dap_dCDI in S phase indicated the high efficiency of this knockdown. Coexpression of Rca1 caused instability of Dap_dCDI in G1 and G2, while knockdown of Rca1 increased its stability. However, Rca1_dFbox was still able to cause noticeable instability of Dap_dCDI. Thus, we assumed that despite Cdt2 knockdown some residual activity of CRL4-Cdt2 remained.

To verify our hypothesis that Rca1 can influence the stability of Dap indirectly via CRL4-Cdt2 despite knockdown of Cdt2, we took the following approach: We tested whether the stability of the CRL4-Cdt2 substrate Cdt1 can be influenced by coexpression of Rca1/Rca1_dFbox or knockdown of Rca1, when additionally, a Cdt2 knockdown is conducted. We did not assume that Cdt1 is a substrate of SCF-Rca1, since downregulation of Cdt1 at the end of G1 would impede transition into S phase (Braun et al. 2012). Therefore, if Cdt1 would be influenced by Rca1 this would be an indication that this effect is indirect via CRL4-Cdt2 and not SCF-Rca1. Cdt1 contains functional domains (Geminin- and MCM-binding domains), which would influence the cell cycle in case of overexpression (Pozo and Cook 2016; Braun et al. 2012). To avoid this, we used the cell-cycle inert version Cdt1_1-101, which lacks the functional domains but still contains the PIP degron for degradation via CRL4-Cdt2. Expression of Cdt1_1-101 without knockdown of Cdt2 showed great instability of this construct indicating that it can be efficiently degraded via CRL4-Cdt2. Coexpression of Rca1 decreased the stability of Cdt1_1-101 in G1 and G2, whereas knockdown led to stabilization. A significant effect by coexpression of Rca1_dFbox was not observed. Both Rca1 and Rca1_dFbox induced changes in the cell cycle distribution so that less cells were in G1 phase compared to the cells where only Cdt2 was knocked down. However, Rca1 is more potent in triggering the G1/S transition than Rca1_dFbox (**Figure 12 C**; (Zielke et al. 2006)). It is likely that the induced G1/S transition can then influence the obtained stability values for Cdt1_1-101. Since the G1/S transition is more pronounced after Rca1 coexpression, also the stability of Cdt1 is decreased to a higher extent compared to Rca1_dFbox. Both Rca1 and Rca1_dFbox can inhibit the APC/C, which leads to the question what mechanism is responsible for the different stability of Cdt1_1-101 after Rca1 or Rca1_dFbox coexpression, respectively. One possible explanation would be that both Rca1 and Rca1_dFbox can induce the G1/S transition to a certain extent via inhibition of the APC/C. However, only coexpression of Rca1 causes a destabilization of endogenous Dap via SCF-Rca1, which would additionally accelerate the G1/S transition to a larger extent (**Figure 58**). However, it would be also conceivable that increased degradation of other SCF-Rca1 substrates are responsible for the destabilization of Cdt1_1-101 after coexpression of Rca1. In summary, as previous studies (Zielke et al. 2006) these experiments indicated that SCF-Rca1 targets

substrates for degradation, which facilitates the G1/S transition. However, it was also revealed that Rca1 can influence the stability of Dap indirectly via CRL4-Cdt2. Therefore, other strategies outlined below were applied to analyze potential direct Rca1 effects (via SCF-Rca1) on the stability of Dap without the disturbing influence of the indirect Rca1 effects via APC/C and then CRL4-Cdt2.

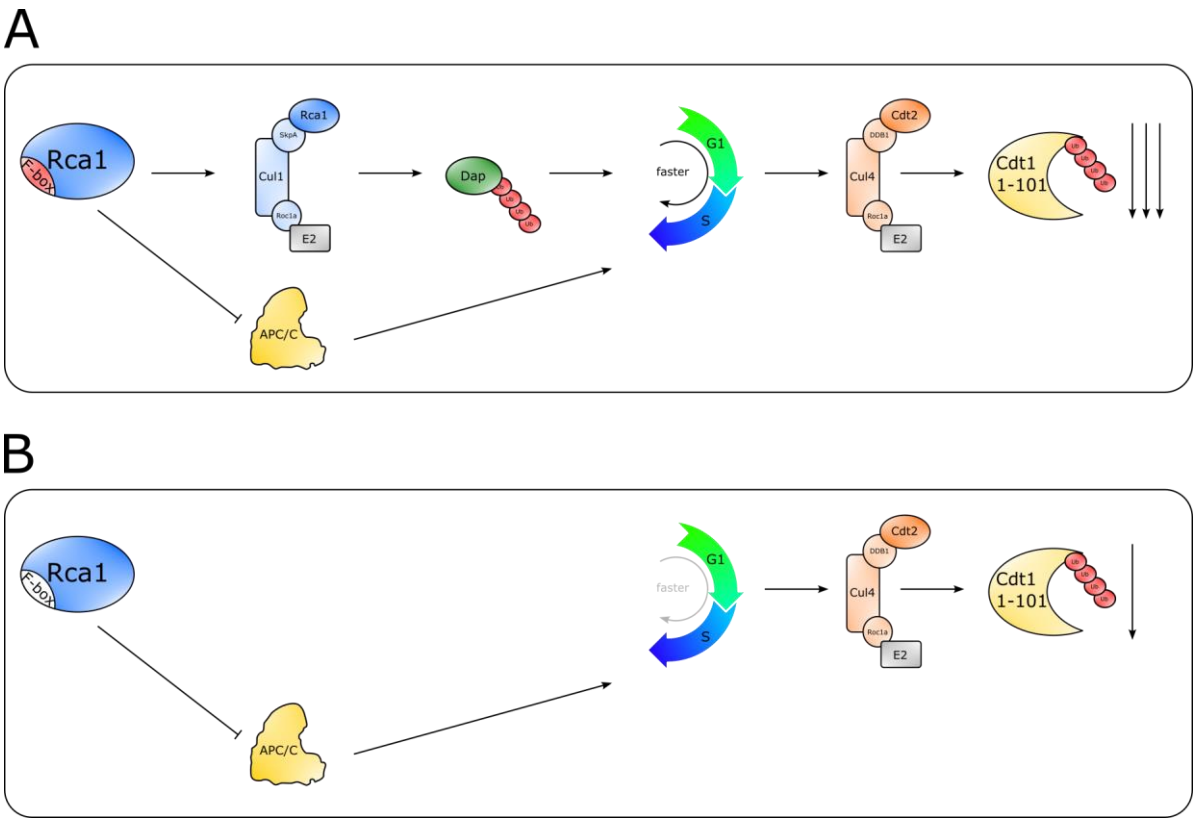

Figure 58 | Model for the Rca1 and F-box dependent degradation of Cdt1_1-101
Data in this thesis showed that overexpression of Rca1 can trigger the degradation of the overexpressed CRL4-Cdt2 substrate Cdt1_1-101 to a higher extent than overexpression of Rca1_dFbox. In addition, we considered it as unlikely that Cdt1_1-101 is a substrate of SCF-Rca1. Based on that we developed a model, which can explain why Rca1 can influence the stability of Cdt1_1-101 in an F-box dependent manner: **A)** Overexpression of Rca1 can influence the stability of overexpressed Cdt1_1-101 via two mechanisms: On the one hand, coexpression of Rca1 leads to more SCF-Rca1 complexes, which can increase degradation of endogenous Dap and thereby trigger the G1/S transition. This in turn, can cause either an alteration of CRL4-Cdt2 dependent degradation of Cdt1_1-101 and/or an alteration of the detection of this degradation. On the other hand, Rca1 can also inhibit APC/C, which can accelerate transition through S phase (via accumulation of CycA and CycB) and thereby influence the degradation of Cdt1_1-101 via CRL4-Cdt2 in a similar manner as the pathway via SCF-Rca1, but to a smaller extent. **B)** In contrast, Rca1_dFbox cannot be incorporated into an SCF complex. Rather, Rca1_dFbox can only inhibit APC/C and thereby only slightly influence the degradation of Cdt1_1-101 via CRL4-Cdt2.

5.2 Elucidation of the mechanism by which the PIP-degron of Dap mediates degradation via CRL4-Cdt2

The above-described strategy to apply a knockdown of Cdt2 to eliminate indirect Rca1 effects on the stability of Dap was not completely successful. One problem was the residual activity of CRL4-Cdt2, since the Cdt2 knockdown was not 100 % complete. In addition, knockdown of Cdt2 does not only reduce the degradation of Dap, but also other substrates of CRL4-Cdt2. This can lead to unwanted effects such as changes in the cell cycle distribution. Therefore, we aimed for another strategy to abolish degradation of Dap via CRL4-Cdt2. The C-terminus of Dap contains a PIP degron (aa 184-195), which mediates degradation via CRL4-Cdt2 (Swanson et al. 2015). Therefore, we wanted to inactive the PIP degron by mutations so that Dap is no longer targeted by CRL4-Cdt2. During our analysis we realized that it would be essential to understand the mechanism by which the PIP degron mediates this degradation to interpret Rca1 effects on the stability of Dap correctly. Previously it was shown that mutation of amino acids in Dap that are conserved in PIP degron sequences of other CRL4-Cdt2 substrates can cause stabilization in S phase (Swanson et al. 2015; M. Kies 2017). Swanson et al. analyzed the following Dap PIP degron mutants: Dap_Q184A_I187A_T188A_E189A_F190A (referred to as Dap (mPIP), where amino acids predicted to contact PCNA were mutated), Dap_K195A (referred to as Dap (mK + 4), where amino acids predicted to contact Cdt2 were mutated) and Dap_Q184A_I187A_T188A_E189A_F190A_K195A (referred to as Dap (mDeg); a combination of Dap (mPIP) and Dap (mK + 4)). All three PIP degron mutants accumulated during the cell cycle (Swanson et al. 2015). However, relative protein stability analysis such as with our RPS system was not conducted. In addition, the role of the mutated amino acids for interaction with PCNA or Cdt2 was not studied, but only predicted based on other CRL4-Cdt2 substrates. Also, Kies, 2017, made use of PIP degron mutants (e.g. with the mutations Del-184-188 (dPIPa) or Q184A_I187A_T188A_F190A_M191A_K195A (PIP-6A) (M. Kies 2017). However, neither the stability of these Dap constructs was analyzed with the more accurate and reliable RPS system nor was the mechanism by which these mutations stabilize Dap studied so far. The analysis with the RPS system in this thesis revealed that Q184A or K195A caused similar and mediocre stabilization of Dap_dCDI in S phase, while a combination of both (Q184A_K195A) led to higher stability. Nevertheless, other mutants such as Dap_dCDI_dPIPa showed even higher stability than Dap_dCDI_Q184A_K195A. This indicated that Q184 and K195 alone are important, but, when mutated, not sufficient to eliminate degradation via CRL4-Cdt2. It is likely that other amino acids in the PIP degron contribute to this. Based on the crystal structure of the Dap homolog p21 both Q184A and K195A were predicted to interact with PCNA (Gulbis et al. 1996). However, K195A was the only amino acid in the PIP degron for which interaction with Cdt2 was predicted

based on other CRL4-Cdt2 substrates (Havens and Walter 2011). Therefore, it was decided to focus on Q184 and K195 to elucidate the mechanism by which CRL4-Cdt2 recognizes Dap via its PIP degron.

Co-IPs indicated that Q184, but not K195 in Dap_dCDI is needed for the interaction with PCNA. Since Dap_dCDI_Q184A was not completely stabilized in our flow cytometry analysis, we assume that weak interaction of Dap with PCNA is still possible via other amino acids in the PIP degron, but that this interaction is too weak to detect it via co-IP. Alternatively, degradation without PCNA interaction might be possible. The interaction of Dap with Cdt2 was not affected in co-IPs by mutation of Q184 or K195. Thus, both residues are not essential for the interaction with Cdt2. Therefore, we wondered whether other regions in Dap are needed for the interaction with Cdt2. Surprisingly, we found out that especially the N-terminal part of Dap (aa 1-160) mediates interaction with Cdt2. To our knowledge, it was not described for other CRL4-Cdt2 substrates that interaction with Cdt2 is mediated by regions outside of the PIP degron. Therefore, for future investigations it would be interesting to elucidate whether this PIP degron independent interaction with Cdt2 also applies for other CRL4-Cdt2 substrates. In contrast, interaction of the C-terminal part of Dap (aa 160-245; including the PIP degron (aa 184-195) with Cdt2 could not be confirmed via co-IP. However, flow cytometry indicated that the C-terminal part of Dap (aa 160-245) is sufficient to be degraded by CRL4-Cdt2. Two possible explanations for that would be the following: **1)** The C-terminal part of Dap still weakly interacts with Cdt2, but that this interaction is too weak to detect it via co-IP. The observed interaction with the N-terminal part of Dap could still be important to facilitate a robust degradation *in vivo*. **2)** It could also be possible that Dap and Cdt2 do not interact via the C-terminal part of Dap at all. In the C-terminal part of Dap only the PIP degron is required that could create a structure when bound to PCNA that allows Cdt2 ubiquitination without previous Cdt2-Dap interaction.

It is already known for the human system that the C-terminal part of Cdt2 contains a PIP box that mediates binding of Cdt2 to PCNA (Hayashi et al. 2018). We wanted to analyze whether this is also true for the *Drosophila* system. Co-IPs revealed that PCNA and Cdt2 interact with each other. However, this interaction was very weak. By comparing the putative PIP box sequence of *Drosophila* Cdt2 with Cdt2 from other vertebrates, we noticed that the first amino acid of the "*Drosophila* PIP box" is a glutamate (E712) instead of the otherwise conserved methionine. Methionine harbors a short hydrophobic side chain, whereas glutamate contains a much longer and hydrophilic sidechain. It would be conceivable that the sidechain of glutamate impedes the binding to PCNA. Therefore, we wondered whether we could increase the interaction between PCNA and Cdt2, if we mutate E712 in *Drosophila* Cdt2 into methionine (E712M). However, this mutation could not increase, but in contrast even abolished interaction with PCNA completely. This indicates that E712 is not the reason for low affinity between Cdt2 and PCNA in

Drosophila. For the human system it is known that Cdt2 specifically recognize PCNA, which is bound to DNA (Havens and Walter 2011; Hayashi et al. 2018). We expect that not all PCNA proteins, which were overexpressed in our setup, were bound to DNA. This may have been a limiting factor in our experiments. As mentioned above, K195 – the last amino acid of the PIP degron in Dap – was neither needed for interaction with PCNA nor Cdt2. However, the K195A mutation stabilized Dap_dCDI to a similar extent as Q184A. Therefore, we speculated which function K195 could fulfill. One idea was that it could act as ubiquitination site for CRL4-Cdt2. Ubiquitination of substrates can only take place at lysines or the N-terminus of proteins (Komander and Rape 2012). Therefore, we took the following approach to elucidate whether K195 acts as a ubiquitination site: We mutated K195 into arginine (K195R). If our theory was correct, we would expect that K195R stabilizes Dap to the same extent as K195A, since both mutations would completely abolish ubiquitination of this site. Arginine (R) is chemically similar to lysine (K). Therefore, if stabilization by K195R is not as strong as by K195A this would indicate that arginine (R) can (partially) compensate for the loss of lysin (K) and the function of K195 would probably rely on protein-protein or protein-DNA interactions. Stabilization of Dap_dCDI (and Dap) by K195R in S phase was significantly less than by K195A indicating that K195 does not act as ubiquitination site but is important for protein-protein or protein-DNA interactions. Thereafter, we had a closer look at the PIP degron sequence of Dap and noticed that adjacent to K195 there are two more basic amino acids – R194A and R196A. Also, in other CRL4-Cdt2 substrates such as p21, Cdt1 or E2F the basic amino acid at position B + 4 (number indicates distance to PIP box) is flanked by basic amino acids (B + 3 and/or B + 5). In the p21-PCNA crystal structure from Gulbis et al. B + 3 and B + 5 of p21 interact with acidic residues within PCNA (Gulbis et al. 1996). Furthermore, mutation of B + 5 in *Xenopus* Cdt1 and human p21 impeded destruction due to impaired binding to PCNA (Nishitani et al. 2008; Havens and Walter 2009). Furthermore, studies that used chimera constructs composed of Cdt1 and ligase I revealed that an acidic amino acid at position B + 5 prevents destruction (Michishita et al. 2011). All these data indicate that a positively charged surface in the region B + 3-5 is essential for CRL4-Cdt2 dependent degradation. Therefore, we extended our analysis by testing the stability of Dap versions with R194A_R196A or R194A_K195A_R196A mutations, respectively. The mutation R194A_R196A stabilized Dap constructs to a similar extent as K195A. In addition, stabilization by the mutation R194A_K195A_R196A was noticeable higher than with K195A or R194A_R196A alone. This suggests that loss of one or two basic amino acids of the B + 3-5 cluster can be partially compensates by the other remaining basic amino acids. However, if all three basic amino acids are mutated, the function of this cluster is completely abolished. Interestingly, co-IPs revealed that Dap_dCDI_R194A_K195A_R196A can interact with PCNA as good as Dap_dCDI without mutations in the

PIP degron. This suggests that this basic cluster is not needed for interaction with PCNA. Up- and downstream of K195 (each within 10 AS range) there are additional basic amino acids: K186, K192, K202 and K203. Previous studies showed that amino acids flanking PIP motifs can strongly modulate the affinity to PCNA (Prestel et al. 2019). Therefore, to exclude that these basic amino acids still can compensate for the loss of the B + 3-5 cluster, corresponding mutants could be tested for interaction with PCNA in future experiments. However, we do not consider it as likely that these amino acids can compensate for the loss of B + 3-5, since the stabilization by R194A_K195A_R196A seen in the flow cytometry analysis was quite strong. The B + 3-5 cluster might also be needed for interaction with Cdt2. However, we already knew that the N-terminus of Dap is sufficient for interaction with Cdt2 and effects by mutating B + 3-5 would therefore be masked. We also observed no interaction of a C-terminal part of Dap with Cdk2, thus an analysis of the B + 3-5 cluster by co-IP was destined to give no further insights and were not followed up.

In summary, important insights into the mechanism how CRL4-Cdt2 recognizes Dap via its PIP degron were gained (**Figure 59**): Q184 is important for interaction with PCNA, which is in line with studies of other CRL4-Cdt2 substrates (Havens and Walter 2011). For K195 it was excluded that it acts as an essential site for ubiquitination. Instead K195 acts synergistically with R194 and R196 forming a basic cluster (B + 3-5), which probably plays a role for protein-protein or protein-DNA interactions. Although data from other CRL4-Cdt2 substrates suggest that this basic cluster is needed for interaction with PCNA, our data does not support that this is the case for Dap. It is also conceivable that the B + 3-5 cluster plays a role for interaction with Cdt2 or DNA. However, this theory could not be substantiated or refused during this thesis and requires further analysis. Furthermore, it was shown that the N-terminus of Dap is sufficient to interact with Cdt2. However, the N-terminus of Dap is not needed for degradation via CRL4-Cdt2 but weaker interactions with the C-terminal part of Dap (not detectable by co-IP) might be sufficient for degradation. Lastly, it was shown that Cdt2 interacts with PCNA like in the human system. However, this interaction was weak and could not be increased by adjusting the PIP box sequence of *Drosophila* Cdt2 so that it resembles the PIP box sequence of other vertebrates.

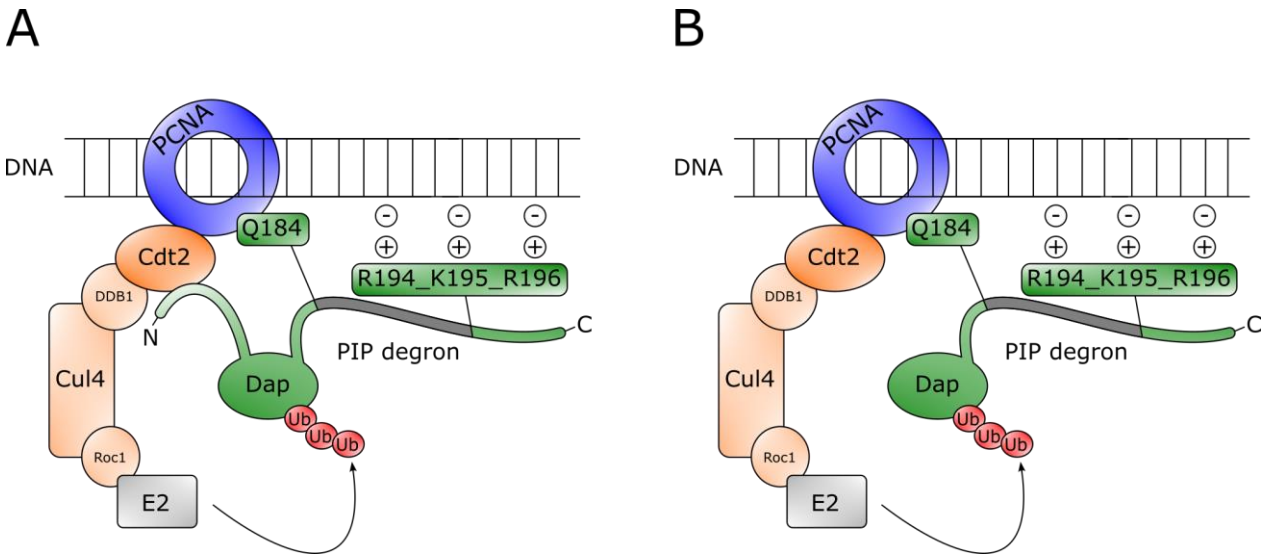

Figure 59 | Model illustrating how Dap is potentially targeted for degradation by CRL4-Cdt2
A) Based on data described in chapter 5.2 we propose the following model illustrating how Dap could be targeted for degradation by CRL4-Cdt2: CRL4-Cdt2 binds to PCNA (bound to DNA) via its substrate recognition module Cdt2. The N-terminal part of Dap mediates interaction with Cdt2, but is not essential for degradation (see **B)**). Q184 in Dap mediates interaction with PCNA. It is possible that the positive charges of B + 3-5 make contact to the negatively charged DNA. However, we have not performed experiments in this direction and B + 3-5 could also mediate degradation by another mechanism. **B)** Model illustrating how C-terminal Dap fragments (Dap_126-245 and Dap_160-245) can be targeted by CRL4-Cdt2. The interaction of the N-terminus of Dap with Cdt2 (shown in **A)**) is not essential for its degradation via CRL4-Cdt2. Two possible explanations would be the following: **1)** The C-terminal Dap fragments weakly interact with Cdt2 but this interaction was too weak to detect it via co-IP (not shown in model). **2)** C-terminal Dap fragments can be ubiquitinated by CRL4-Cdt2, although they do not directly interact with Cdt2. Interaction with PCNA and possibly also with DNA might be sufficient for this purpose (shown in model).

5.3 Rca1 effects on the stability of Dap are present, even if indirect effects via CRL4-Cdt2 are strongly reduced

After we gained insights into the mechanism by which the PIP degron of Dap mediates recognition by CRL4-Cdt2 (chapter 5.2), we had a good basis to continue analyzing Rca1 effects on the stability of Dap (see also chapter 5.1). We used Dap constructs with mutations in the PIP degron to reduce CRL4-Cdt2 dependent degradation and therefore indirect Rca1 effects via APC/C and then CRL4-Cdt2. If Rca1 would affect the stability of Dap solely or mainly indirectly via CRL4-Cdt2, but not via SCF-Rca1, we could assume the following: The effect size of Rca1 effects (coexpression/knockdown of Rca1) would decrease, the more Dap versions are stabilized by mutations in its PIP degron. Since we were not sure, whether the CDI domain in Dap is needed for recognition by SCF-Rca1 we always additionally analyzed Dap versions with functional CDI domain. However, in this case we had to coexpress CycE/Cdk2 to compensate for the inhibition of CycE/Cdk2 by these Dap versions. A clear trend that Rca1 effects decrease or increase the more the Dap constructs were stabilized by PIP degron mutations was not apparent. However, in G1 and G2 destabilization by Rca1 coexpression and stabilization by Rca1 knockdown of strongly stabilized Dap versions (with Q184A_K195A, R194A_K195A_R196A or dPIPa mutation) were often as strong or even

stronger compared to Dap versions with mediocre stabilization (with Q184A or K195A mutation). This could indicate that Dap is indeed targeted directly by SCF-Rca1 for degradation. However, the effect sizes were quite weak making it difficult to obtain significant effects by statistic evaluation.

It must be emphasized that even if the stabilization of Dap constructs by the mutations Q184A_K195A, R194A_K195A_R196A and dPIPa was quite strong, remaining rest instability was still present. For instance, for Dap_dCDI_dPIPa the relative stability value in S phase was 0.75 (**Figure 4**). This corresponds to a relative degradation rate (compared to GFP) of approximately 70 %. We consider it as likely that this degradation is largely dependent on cell cycle independent degradation. However, we can also not exclude that some amino acids of the PIP degron compensate for the loss of the corresponding mutated amino acids and that CRL4-Cdt2 dependent degradation still takes place to some extent. On the other hand, the fact that Dap_dCDI_PIP-6A (where even more conserved amino acids of the PIP degron were mutated) showed the same relative stability value as Dap_dCDI_dPIPa, make it unlikely that the stability of full-length Dap constructs can be further increased by deleting more or all amino acids of the PIP degron. Overall, based on these data, we were not confident enough to state with certainty that Dap is a substrate of SCF-Rca1. We were still considering that remaining CRL4-Cdt2 activity could lead to misinterpretations of our results. In addition, due to the small effect size of Rca1 effects we speculated whether the PIP degron might be not only needed for recognition by CRL4-Cdt2, but also by SCF-Rca1. This is not unreasonable, since it was shown that PIP motifs often fulfill multiple functions (Boehm and Washington 2016). Therefore, we tried to find other regions in Dap, which are needed for recognition by CRL4-Cdt2, but likely are not involved in recognition by SCF-Rca1. For p21 it was shown that S114 is phosphorylated by GSK3β and that phoshomimetic substitution (S114E) can promote polyubiquitination of p21 via CRL4-Cdt2 *in vitro* (Lee et al. 2007; Abbas et al. 2008). Thus, we tested if we could impede degradation of Dap via CRL4-Cdt2 by mutating the corresponding amino acid (S154; based on sequence alignment) into alanine. Unfortunately, the mutation S154A had no effect on the stability of Dap. Therefore, Dap_S154A was not suited for further analyses regarding Rca1 effects. Next, we wanted to reduce indirect Rca1 effects via CRL4-Cdt2 by means of another strategy: As previously mentioned we assume that inhibition of APC/C causes the indirect effects in the first place. Therefore, we wanted to try whether Rca1 versions, which cannot inhibit the APC/C anymore, still can destabilize Dap constructs. In previous work it was shown that mutations in the ZBR domain (Rca1_A344T, Rca1_S285R) or the RL tail (Rca1_dRL; Del-403-409) of Rca1 can strongly impede inhibition of APC/C. Since the stability of Dap is very low and this could mask potential Rca1 effects, Dap_Q184A was used for this analysis. All Rca1 APC/C inhibition mutants tended to destabilize Dap_Q184A in G1 and G2 even after additional knockdown of Cdt2. However, the

destabilization was weaker than with Rca1, especially after knockdown of Cdt2. This could indicate that the Rca1 APC/C inhibition mutants triggered weak destabilization of Dap_Q184A via SCF-Rca1. For wildtype Rca1 additionally to its direct influence on Dap stability, there could be indirect effects via APC/C and Cdt2, which is why the destabilizing effect of Rca1 is stronger than the Rca1 APC/C inhibition mutants. However, we cannot exclude with certainty that some remaining rest activity regarding APC/C inhibition, causes the weak effects of the Rca1 APC/C mutants. In addition, the APC/C inhibition mutants could also disturb the SCF-functions, for example by preventing substrate recognition of the F-box protein. The ZBR region is a well folded structure (Frye et al. 2013). Any alterations of this structure could result in misfolding and long-range structural changes of the Rca1 protein.

In summary, even if potential indirect Rca1 effects via CRL4-Cdt2 were strongly reduced by either mutating the PIP degron of Dap or using Rca1 versions, in which APC/C inhibition is greatly reduced, Rca1 effects were still present. This is in line with the hypothesis that Dap is directly targeted by SCF-Rca1 for degradation. However, since we are not sure whether we abolished CRL4-Cdt2 activity completely, it cannot be stated with certainty whether and to which extent Rca1 directly influences Dap stability via SCF-Rca1. However, the results indicate that if direct Rca1 effects on Dap are indeed present, they are weak making it difficult to obtain meaningful results. We also tried to enhance direct Rca1 effects via SCF-Rca1 by intervening in the regulation mechanism by which substrate recognition modules of CRL complexes are exchanged (Harper and Schulman 2021). We hoped that this would enhance the number of SCF-Rca1 complexes. To this end, we overexpressed/knocked down CSN5 or Cand1 to analyze whether Rca1 dependent degradation of Dap constructs can be increased. However, a meaningful and reproducible effect could not be achieved (data not shown).

From a biological point of view, it would not be surprising if degradation via SCF-Rca1 is much weaker than by CRL4-Cdt2: We assume that already a low degradation rate at the end of G1 would be sufficient to facilitate the G1/S transition, since Dap don't have to be removed completely but only must fall below the number of CycE/Cdk complexes. As soon as S phase starts, the rest of Dap can be degraded via CRL4-Cdt2. It was also speculated that SCF-Rca1 target Dap in G2 for degradation to inhibit APC/C by triggering phosphorylation of the APC/C coavtivator Fzr by CycE/Cdk2 (M. Kies 2017). Also here, a low degradation rate of Dap is probably sufficient, since CycE/Cdk2 levels are relatively low in G2 due to its degradation in S phase (Moberg et al. 2001; Engelhardt 2022). In addition, the APC/C is directly inhibited by Rca1 in G2, which could compensate, if the APC/C inhibition via Dap degradation is not complete.

5.4 Elucidation of the degradation mechanism of the N-terminal Dap fragment Dap_1-125

5.4.1 Degradation of Dap_1-125 is dependent on its CDI domain and can be influenced by Rca1

Previous work in the Sprenger lab indicated that coexpression of Rca1 can cause instability of Dap_1-125 (Herzinger 2019). Destabilization of Dap_1-125 in G1 and G2 by coexpression of Rca1 and stabilization by knockdown of Rca1 was also observed in this thesis (**Figure 25**). Dap_1-125 harbors the CDI domain (aa 38-105), but lacks the PIP degron (aa 184-195). Based on comparison with the crystal structure of p27 bound to CycA/Cdk1, we expected that the region 1-125 in Dap should allow binding to CycE/Cdk2. Thus, exactly this region of Dap was chosen. Dap_1-125 was able to interact with Cdt2, although the interaction was weaker than with Dap_1-160 and Dap full-length (**Figure 7**). Despite this interaction with Cdt2 we do not assume that CRL4-Cdt2 can target Dap_1-125 for degradation since the whole PIP degron (aa 184-195) including flanking regions, which might also contribute to CRL4-Cdt2 dependent degradation to some extent, are not present. This makes Dap_1-125 perfectly suited to analyze Rca1 effects without the disturbing indirect effects via CRL4-Cdt2.

The stability of Dap_1-125 – especially in G2 – was noticeably lower than the one of strongly stabilized full-length Dap constructs (e.g. Dap_dPIPa). This was surprising and we wanted to know whether this instability is indeed caused by Rca1 or other mechanisms. Protein fragments are sometimes degraded cell cycle independently (Goldberg 2003). However, since the degradation rate of Dap_1-125 was not evenly, but mainly in G2 and Rca1 was able to cause instability we considered it as unlikely that the degradation solely depends on cell cycle independent degradation.

In case of the Dap homologs p21 and p27 numerous E3 ubiquitin ligases mediate degradation of these CKIs at different or overlapping periods of the cell cycle (Starostina and Kipreos 2012). Work which was conducted in the Sprenger lab during this thesis, indicated that homologs of these E3s in *Drosophila*, which were considered to be involved in degradation of Dap_1-125, do actually not contribute to degradation of this Dap fragment (Camelo-Prieto 2022). Therefore, we had first indications that Rca1 influences the stability of Dap_1-125 directly via SCF-Rca1.

Previously, interaction between Dap_1-125_dCDI and Rca1 could not be confirmed (M. Kies 2017). However, in this thesis it was shown that for both Dap_1-125 and Dap_1-160 interaction with Rca1 is dependent on the presence of the CDI domain (**Figure 24**). Interestingly, the interaction of full-length Dap constructs with Rca1 was not dependent on the CDI domain and stronger as for Dap_1-125 and Dap_1-160. Furthermore, the C-terminal region 126-245 in Dap interacts weakly with Rca1 and this interaction is not dependent on the presence of the PIP degron. Although the C-terminal half of Dap interacts only

weakly with Rca1 it seems to be important, since full-length Dap constructs interacted much stronger with Rca1 as the N-terminal half of Dap alone.

Since the CDI domain was essential for the interaction between Dap_1-125 and Rca1, we wondered how the stability of Dap_1-125 would be influenced, if we mutate its CDI domain. Indeed, mutation of the CDI domain (Del-38-44-RAR_Del-103-105-G) strongly stabilized Dap_1-125 during the whole cell cycle and Rca1 effects were hardly present. Accordingly, lower levels in G2, which was observed for Dap_1-125, was also not existent. The deletions in the CDI domain were designed to abolish the interaction with CycE via Del-38-44-RAR (dCyc) and with Cdk2 via Del-103-105-G (dCDK). For p27 it was shown that it preferentially binds first to CycA before it binds to Cdk2 (Lacy et al. 2004). Therefore, we asked: Would stabilizing Dap_1-125 require abolishing both interactions (Cyc and CDK), or could deletion of the dCyc motif alone be sufficient? It turned out that abrogating the interaction with CycE is sufficient to stabilize Dap_1-125, although the effect was not as strong as with the dCDI mutation (**Figure 29**). Interestingly, the dCDK mutation had the opposite effect making Dap_1-125_dCDK even more instable than Dap_1-125 in G1 and G2. Knockdown of Rca1 noticeably increased the stability of Dap_1-125_dCDK in G1 and G2, whereas coexpression of Rca1 had hardly any influence on its stability. A possible explanation for this could be the following: The degradation of Dap_1-125_dCDK via endogenous SCF-Rca1 was already quite high, why additional coexpression of Rca1 had no noticeable effect. On the other hand, knockdown of Rca1 reduced the number of endogenous SCF-Rca1 significantly so that a clear effect was present. However, knockdown of Rca1 does also not completely eliminate endogenous SCF-Rca1 complexes since the knockdown only impedes the expression of new Rca1 proteins. Preexisting Rca1 proteins are not targeted by the knockdown, since it operates at mRNA level.

We were interested, whether the dCDK mutation could also facilitate instability in case of full-length Dap constructs and/or increase Rca1 effects. To reduce CRL4-Cdt2 dependent effects as much as possible, Dap PIP degron mutants were used and a knockdown of Cdt2 was applied. However, the high stability of Dap_dCDK_dPIPa and the small extent of Rca1 effects on this construct showed that the dCDK mutation does not significantly affect full-length Dap constructs. Instead, the dCDK mutation only has effects on the fragment Dap_1-125. Subsequent experiments (see below) gave rise to a possible explanation for this discrepancy.

In summary, the results indicated that at least for Dap_1-125 binding to CycE/Cdk2 is involved in its degradation mechanism. In the human system, degradation of the Dap homologue p21 initiated by SCF-Skp2 is also facilitated by its binding to CycE/A/Cdk2 (Abbas and Dutta 2009). CIP/KIP CKIs such as Dap, p21 and p27 are intrinsically disordered proteins (IDPs) and they only adapt a defined tertiary structure

after binding to other proteins. This mechanism can be exploited by E3s to target only CKIs that are actively regulating the cell cycle (Starostina and Kipreos 2012).

5.4.2 The N-terminus of CycE is required for degradation of Dap_1-125

The finding that CycE/Cdk2 plays a crucial role for the degradation of Dap_1-125 (chapter 5.4.1) required additional experiments to elucidate the underlying mechanism. Work conducted in the Sprenger lab indicated that N-terminal truncations of CycE (deletion of the first 235 amino acids) do not only stabilize CycE itself but also go along with stabilization of Dap_1-125 (Engelhardt 2022; Bach 2021). Thus, a link between CycE degradation and degradation of Dap_1-125 might exists. CycE degradation can also be prevented by the mutation of a phosphodegron present in the C-terminal part of CycE. The mutation of T544A_S548A in an otherwise full-length CycE construct resulted in a strong stabilization of CycE. This phosphodegron is required for the recognition by the SCF-Ago complex that is responsible for CycE ubiquitination (Hao et al. 2007). CycE_236-602 and CycE_T544A_S548A can still trigger the G1/S transition (personal communication with Sebastian Sigl), thus they are associated with Cdk2 and both can be inhibited by Dap.

However, only when CycE_236-602 was coexpressed the stability of Dap_1-125 (and Dap_1-125_dCDK) was increased compared to coexpression with wildtype CycE (**Figure 37**). In contrast, coexpression of CycE_T544A_S548A even caused lower stability of Dap_1-125 (and Dap_1-125_dCDK) compared to coexpression with wildtype CycE. Both CycE constructs are stable, thus, CycE degradation as such is not required for Dap degradation.

CycE is degraded via SCF-Ago by binding of Ago to the phosphorylated phosphodegron and Ago knockdown results in stabilization of CycE (Engelhardt 2022). We considered the possibility that Ago bound to the phosphodegron of CycE could also target the associated Dap_1-125. In this case knockdown of Ago would also influence the stability of Dap_1-125 (and Dap_1-125_dCDK). Indeed, some stabilization of Dap_1-125 was observed after Ago knockdown. However, we were aware that Dap_1-125 degradation is primarily detected in G2 cells, although degradation could occur throughout the cell cycle since co-overexpression of CycE/Cdk2 in these experiments results in a cell cycle profile with most cells residing in G2. After knockdown of Ago, we saw less G2 cells and more cells residing in G1. We do not know for certain, why Ago knockdown results in more G1 cells but in the human system it has been reported that p53 accumulates after Ago (= Fbw7 in human) knockdown (Galindo-Moreno et al. 2019). High p53 levels can lead to more cells in G1 (Levine 1997). In order to include a control with a similar cell cycle distribution, we conducted a knockdown of Cdt2. Similar to knockdown of Ago, knockdown of Cdt2 resulted in a cell cycle profile with more G1 cells. As already mentioned we did not assume that CRL4-Cdt2 targets Dap_1-

125 for degradation. In both cases, Dap_1-125 (and Dap_1-125_dCDK) showed a higher stability, but there was no difference between the knockdown of Ago and Cdt2. Thus, the observed increase is likely caused by the cell cycle distribution changes. In addition, the stability increase (0.66 -> 0.71) was less than the stability increase when a stable CycE version was used (0.66 -> 0.81). Therefore, it is unlikely that knockdown of Ago is directly involved in the degradation of Dap_1-125.

Nevertheless, we conducted one additional experiment to assess whether Dap_1-125 could be ubiquitinated by SCF-Ago. We compared the crystal structure of the human CycE/Cdk2 complex with the complex of p27 bound to CycA/Cdk2 and speculated that the N-terminal region 1-17 of Dap, which contains a lysine at position 17, could be in the proximity of the ubiquitination site of CycE. If SCF-Ago would ubiquitinate Dap, this lysine would be a good ubiquitination site. However, both Dap_18-125 and Dap_18-125_dCDK showed no increase in stability and were even less stable than Dap_1-125 or Dap_1-125_dCDK, respectively (**Figure 51**). This shows that the region 1-17 is not required for Dap degradation.

Coming back to the important difference in the two stable CycE constructs. It was the presence of the N-terminal 235 amino acids that are required for the degradation of Dap_1-125. It is unlikely that the N-terminal part of CycE has a direct contact to Dap: The structure of human p27 bound to CycA/Cdk2 shows that there is no direct contact of p27 with the N-terminal region of CycA. The strong conservation of CycA and CycE also between humans and *Drosophila*, and the conservation between p27 and Dap makes it unlikely that any part of Dap_1-125 contacts the N-terminal region of CycE.

Rather, a different mechanism seems to be involved. According to recent data, a model is proposed for the degradation of CycE (Sigl & Sprenger). In this model, the N-terminal part of CycE first needs to be phosphorylated (presumably by Cdk2 *in cis*). Then, a phosphobinding kinase (e.g. polo kinase) is recruited, which subsequently phosphorylates the phosphodegron in the C-terminus. This phosphobinding kinase could also phosphorylate Dap and this could be a limiting step for the degradation of Dap_1-125. Only the phosphorylated Dap_1-125 could be the target of SCF-Rca1.

This would be in line with the recognition mechanism of already known substrates of SCF complexes, where phosphorylation is often a prerequisite to be recognized by the SCF complex (Skaar et al. 2013). Furthermore, for p21 it was shown that binding to CycE/A/Cdk2 facilitates its degradation via SCF-Skp2 (Abbas and Dutta 2009). In addition, phosphorylation of p21 (at S130) and p27 (at T187) by CycE/Cdk2 is needed to promote degradation via SCF-Skp2 (Abbas and Dutta 2009; Lu and Hunter 2010). A similar mechanism could take place for Dap and SCF-Rca1. Other work in the Sprenger lab already indicated that phosphorylation of Dap could also be involved in its degradation (M. Kies 2017). However, concrete

phosphorylation sites were not identified so far. Future experiments are needed to extensively elucidate the role of phosphorylation for the degradation of Dap.

5.4.3 Dap_1-125 is more destabilized than PIP degron stabilized full-length Dap constructs, probably due to weaker binding to Cdk2

Dap is a target of CRL4-Cdt2 and a PIP degron is required for CRL4-Cdt2 mediated degradation of Dap. In Dap_1-125 the PIP degron is completely missing, but Dap_dPIPa with a small deletion in the PIP degron is more stable than Dap_1-125. It appears that residues in the C-terminal part of Dap (aa 126-245) impedes the destabilization of Dap. Therefore, we tested several extensions of Dap in the C-terminal direction. All analyzed Dap constructs (Dap(_dCDK)_1-140, Dap(_dCDK)_1-160 and Dap(_dCDK)_1-180) did not contain the PIP degron (aa 184-195) so that we could exclude effects via CRL4-Cdt2. It turned out that already the extension to aa 140 (Dap(_dCDK)_1-140 stabilized Dap compared to Dap_1-125 (and Dap_1-125_dCDK) to a noticeable extent. Further extension to aa 160 or aa 180 did not significantly increased the stability compared to Dap(_dCDK)_1-140. The region 126-140 is not far away of the CDI domain (aa 38-105), which was defined based on sequence alignments with p21 and p27. We showed that interaction with CycE/Cdk2 is required for degradation of Dap_1-125 and we speculated that phosphorylation of the N-terminal part of CycE by Cdk2 *in cis* is a requirement for Dap_1-125 degradation (see above). The Cdk2 binding motif identified by the crystal structure of p27/CycA/Cdk2 lies in Dap between aa 103-105. Further C-terminal extensions could therefore provide additional contacts and inhibition of Cdk2 by Dap. In the crystal structure of p27/CycA/Cdk2, more C-terminal parts of p27 were not included in the p27 used for the structure determination. However, the Alpha-fold prediction of *Drosophila* Dap shows the prediction of another helical structure between aa 123-141 (**Figure 60**). We collaborated with Prof. Dr. Till Rudack, head of the structural bioinformatics group at the University of Regensburg, and asked if and where the helical structure in Dap might bind to Cdk2.

His predictions suggested that the amino acids D125, R131, S132, E133, E135 and N136, which are all part of the alpha fold predicted helix (aa 123-141) in Dap indeed contact Cdk2 via hydrogen bonds or salt bridges, respectively. Also interesting is that it was predicted that this helix (aa 123-141) in Dap binds to the same area in Cdk2 as CSK1 – a protein which can modulate the activity of CycE/Cdk2 (Kõivomägi et al. 2011) (personal communication with Till Rudack). This finding would also be in line with the observation that the mutation dCDK destabilizes Dap_1-125: It appears that strong binding to Cdk2 impedes degradation of Dap_1-125 and loosening of this interaction facilitates it. This likely relates to the Cdk2 activity, which will differ depending on whether Dap_1-125 or Dap_1-125_dCDK is bound. Dap_1-

125_dCDK can also be stabilized by the extension aa 124-140, probably because the extension can compensate for the loss of aa 103-105 (CDK). Furthermore, this extended Cdk2 binding region (aa 126-140) could explain why Dap_1-125 is more instable compared to Dap_dPIPa: In Dap_dPIPa binding to Cdk2 is strong, whereas in Dap_1-125 this interaction is weaker, which promotes degradation. In full-length constructs such as Dap_dCDK_dPIPa the included region 126-140 could mask the effect of the dCDK mutation, which was only observed for Dap_1-125. It will be necessary to determine if there are indeed differences in the CycE/Cdk2 activity when the different Dap constructs are bound. In summary, Dap degradation requires binding first to CycE, a prerequisite for the formation of a Dap/Cdk2/CycE complex. The requirments of the N-terminal region of CycE for Dap degradation is then likely indirect by a phosphorylation event *in cis* mediated by the Cdk2 bound in the complex. Dap is making contacts to Cdk2 with the region 103-105, but also with the helix in the region 123-141. Strong inhibition of Cdk2 will prevent the cis-phosphorylation and therefore will stabilize Dap.

As previously mentioned, full-length Dap constructs showed Rca1 effects, even if indirect effects via CRL4-Cdt2 were strongly reduced (chapter 5.3). Based on this we considered it as likely that SCF-Rca1 targets Dap for degradation. Rca1 effects were also observed for full-length Dap constructs with the dCDI mutation. Therefore, the Rca1 effects were present for full-length Dap constructs, although both the extended Cdk2 binding region 126-140 was included and binding to cyclin E was abolished. This contradicts the findings that were gained from the analysis of Dap_1-125 constructs at first glance. However, we have shown that interaction of full-length Dap with Rca1 is – in contrast to Dap_1-125 – not dependent on the CDI domain (**Figure 35**). This could indicate that other C-terminal regions in Dap (aa 126-245) allow binding of Rca1 and SCF-Rca1 is able to target full-length Dap_dCDI constructs to some extent. At least in case of the mutation dPIPa, which caused very strong stabilization, we observed the following: Rca1 knockdown caused higher stabilization of Dap_dPIPa (in G1 14.6 % and in G2 11.0 %) than of Dap_dCDI_dPIPa (in G1 7.7 % and in G2 1.79 %). Furthermore, coexpression of Rca1 caused higher destabilization of Dap_dPIPa (in G1 4.8 % and in G2 5.4 %) than of Dap_dCDI_dPIPa (in G1 0.0 % and in G2 3.3 %). It must be emphasized that this trend was not continuously observed for all juxtapositions of Dap PIP degron mutants with or without functional CDI domain, respectively. However, in case of these Dap versions the disturbing influence via CRL4-Cdt2 could have been too high to allow meaningful interpretations. Based on the data above we think that binding to CycE also promotes degradation of full-length Dap constructs, but might – in contrast to Dap_1-125 – not be essential, since C-terminal regions in Dap compensate for the loss and Rca1 can still recognize full-length Dap_dCDI constructs to some extent.

Based on the data above we propose the following model (**Figure 61**): Degradation of Dap and Dap_dCDI via SCF-Rca1 might take place to some small extent via binding of the C-terminal part of Dap to SCF-Rca1, independently of CycE/Cdk2. Dap, which is not bound to CycE is unstructured and cannot be recognized by SCF-Rca1. Then, Dap binds to CycE, which causes the formation of a structure in Dap. In addition, Dap binds to Cdk2. At the end of G1 phase, an unknown kinase is activated, which phosphorylates Cdk2. This phosphorylation weakens the interaction between Dap and Cdk2. Accordingly, inhibiton of Cdk2 is reduced and Cdk2 can phosphorylate the N-terminus of CycE (aa 1-235), which is bound to it, *in cis*. A kinase can recognize this phosphorylation site at the N-terminus of CycE and thereafter phosphorylates the C-terminus of CycE and the N-terminus of Dap. SCF-Rca1 can now recognize Dap in its structured (induced by CycE binding) and phosphorylated form.

In summary, both co-IPs and flow cytometry provided many indications that Dap is a substrate of SCF-Rca1 and that CycE/Cdk2 is involved in the degradation mechanism. However, we are aware that small effect sizes and at least for full-length Dap constructs disturbing indirect Rca1 effects via CRL4-Cdt2 reduces the significance of our results obtained by flow cytometry. This was the reason why we wanted to establish additional methods, which would allow to detect ubiquitination of Dap by SCF-Rca1 directly (see chapter 5.6).

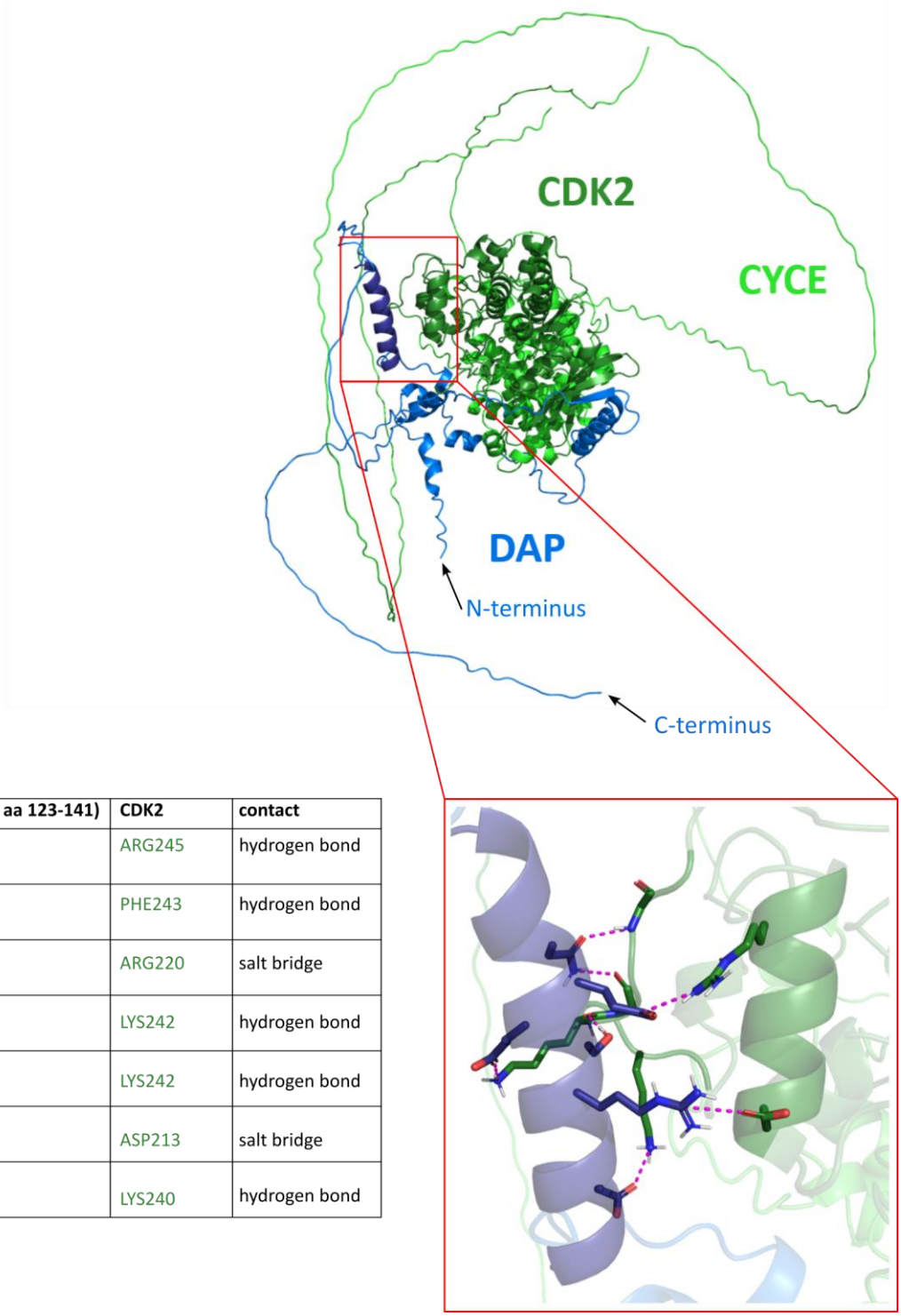

Dap (helix aa 123-141)	CDK2	contact
ASN136	ARG245	hydrogen bond
ASN136	PHE243	hydrogen bond
GLU135	ARG220	salt bridge
GLU133	LYS242	hydrogen bond
SER132	LYS242	hydrogen bond
ARG131	ASP213	salt bridge
ASP125	LYS240	hydrogen bond

Figure 60 | Alpha fold prediction of Dap bound to CycE/Cdk2 reveals that a helix in Dap makes contact to Cdk2
There is no crystal structure of *Drosophila* Dap. However, an alpha-fold prediction of Dap shows the prediction of another helical structure between the amino acids 123 – 141 (depicted in dark blue). Predictions of Prof. Dr. Till Rudack, head of the structural bioinformatics group at the University of Regensburg, suggested that this helix (aa 123-141) binds to a helix (depicted in dark green) in Cdk2. The amino acids of these helices in Dap or Cdk2 respectively are shown in the table to the left.

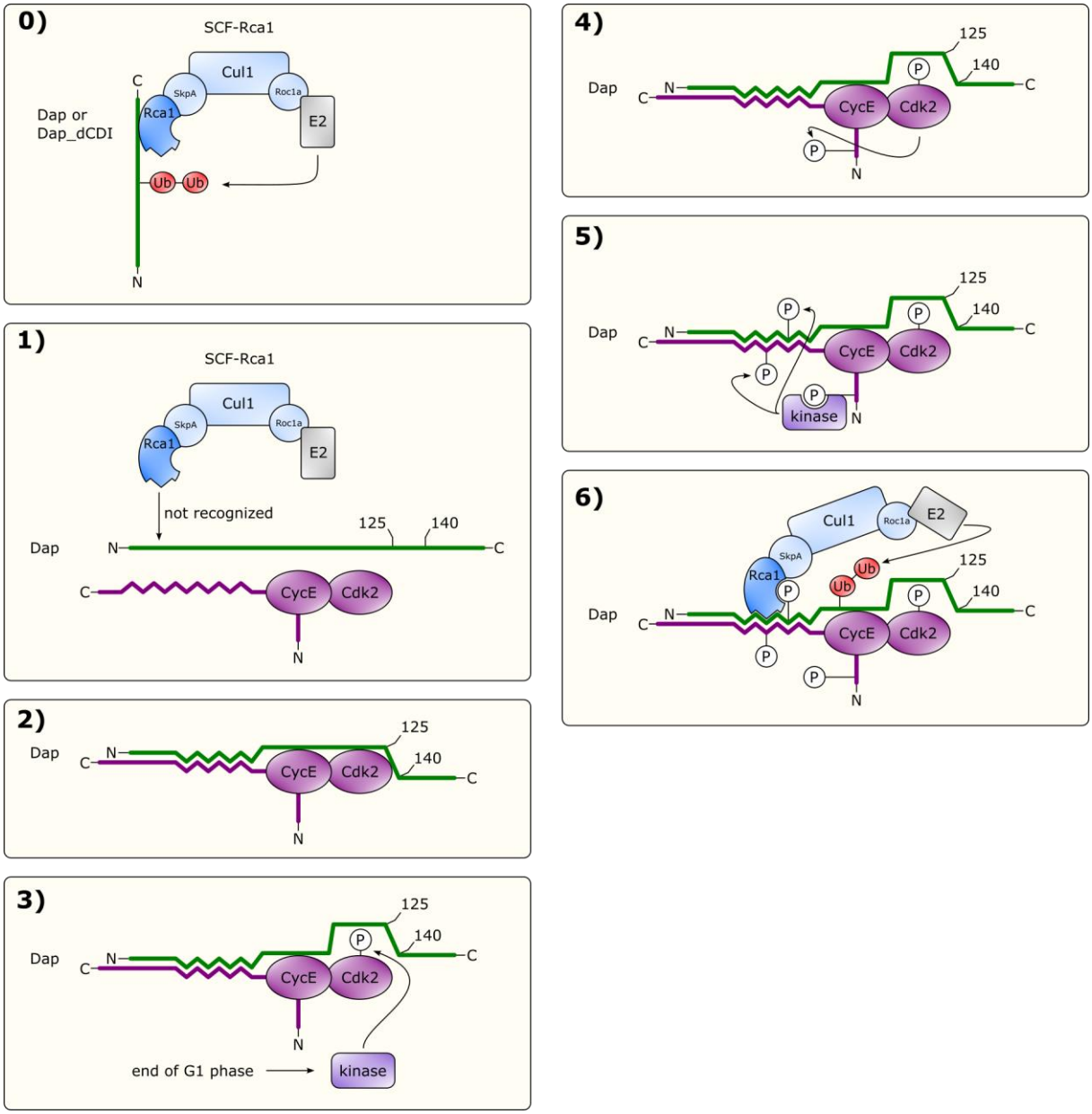

Figure 61 | Model illustrating how Dap is potentially targeted for degradation by SCF-Rca1
Model illustrating how Dap is potentially targeted for degradation by SCF-Rca1 **0)** Degradation of Dap and Dap_dCDI via SCF-Rca1 might take place to some small extent via binding of the C-terminal part of Dap to SCF-Rca1, independently of CycE/Cdk2. **1)** Dap, which is not bound to CycE is unstructured and cannot be recognized by SCF-Rca1. **2)** Dap binds to CycE, which causes the formation of a structure in Dap. In addition, Dap binds to Cdk2. In contrast to Dap_1-125, Dap additionally binds Cdk2 via the region 126-140 and therefore binds more strongly to Cdk2 than Dap_1-125. **3)** At the end of G1 phase, a kinase is activated, which phosphorylates Cdk2. This phosphorylation weakens the interaction between Dap and Cdk2. **4)** Accordingly, inhibiton of Cdk2 is reduced and Cdk2 can phosphorylate the N-terminus of CycE (aa 1-235), which is bound to it, *in cis*. **5)** A kinase can recognize this phosphorylation at the N-terminus of CycE and thereafter phosphorylates the C-terminus of CycE and the N-terminus of Dap. **6)** SCF-Rca1 can now recognize Dap in its structured (induced by CycE binding) and phosphorylated form.

5.5 The C-terminus of Dap is sufficient for degradation via CRL4-Cdt2

Degradation of Dap and p21 via CRL4-Cdt2 is mediated via their PIP degrons in the C-terminal region (aa 184-195 in case of Dap). As far as we know in the literature it is not described that regions in the N-terminal half of Dap or p21 contribute to recognition by CRL4-Cdt2. However, we showed by co-IPs that the N-terminus of Dap (aa 1-160 and aa 1-125) interact with Cdt2. In contrast, interaction of Cdt2 was weak for Dap_1_126 and even not detectable for Dap_160-245. Thus, we wondered whether Dap constructs lacking the N-terminal half can still be degraded via CRL4-Cdt2. Indeed, both Dap_126-245 and Dap_160-245 showed great instability during S phase. The fact that knockdown of Cdt2 or PIP degron mutations stabilized these constructs shows that they are degraded via CRL4-Cdt2. This indicates that interaction of Dap via its C-terminal part is sufficient to be recognized by CRL4-Cdt2.

We were also interested whether Rca1 can influence the stability of these C-terminal Dap constructs. After knockdown of Cdt2, coexpression of Rca1 still destabilized Dap_126-245 and Dap_160-245 in G1 and G2, and knockdown of Rca1 caused stabilization. In contrast, Rca1 effects on Dap_126-245 with mutations in the PIP degron were ambigious: Whereas coexpression of Rca1 caused instability of Dap_126-245_Q184A_K195A in G1 and G2, the opposite was true for Dap_126-245_dPIPa. Interaction of Rca1 with Dap_126-245(_dPIPa) was weak and interaction with Dap_160-245 was even not detectable via co-IP. However, interaction of Rca1 with both Dap_126-245 and Dap_160-245 may take place to some extent and this interaction could be sufficient for degradation via SCF-Rca1.

In summary, the results are to ambigious to allow meaningful interpretations in regard to whether the C-terminal Dap fragments can be degraded via SCF-Rca1 or whether all Rca1 effects were indirectly caused by remaining CRL4-Cdt2 activity. However, the results strongly indicate that C-terminal fragments of Dap can be degraded by CRL4-Cdt2, even if they lack the N-terminal half of Dap. This raises the question why Dap interacts via its N-terminal half with Cdt2, if this interaction is apparently not essential for degradation via CRL4-Cdt2. One possible explanation for this is that the increased binding affinity of Dap to Cdt2 fine-tunes the degradation rate of Dap or the order in which it is targeted via CRL4-Cdt2 compared to other CRL4-Cdt2 substrates. This would be plausible, since for instance for the E3 APC/C it was shown that binding affinity of substrates contributes to the order in which substrates are targeted by APC/C (Bansal and Tiwari 2019).

5.6 Establishment of methods for direct detection of ubiquitination of Dap by SCF-Rca1

As described previously, flow cytometry analysis (in combination with co-IPs) provided a lot of evidence that Dap is a target of SCF-Rca1. However, we also wanted to establish methods that would show more directly that Dap is ubiquitinated by SCF-Rca1. To this end, we wanted to establish two approaches – TUBE-ligase trapping as well as an SCF-Rca1 *in vitro* ubiquitination assay. A description of these methods can be found in the results part of this thesis (chapter 4.23). So far, detection of ubiquitinated Dap by SCF-Rca1 was not possible using these methods. However, in this thesis important findings were obtained, which could help to detect ubiquitinated Dap by SCF-Rca1 in future experiments: It was shown that for our TUBE-ligase trapping setup nanobodies are better suited for precipitation than conventional antibodies, since nanobodies did not lead to a diffuse band (may have been caused by heavy and light chains of the antibody), which complicate detection of ubiquitinated Dap constructs. Furthermore, for the *in vitro* ubiquitination assay it was started to establish a positive control. This positive control makes use of the F-box protein Slmb fused to a GFP nanobody (vhh-GFP). Proteins fused to GFP can then serve as a substrate of an SCF-4xFLAG-Slmb-vhh-GFP complex. In this thesis it was already shown that SkpA and Cul1 can be coprecipitated using 4xFLAG-Slmb-vhh-GFP for precipitation, which is a prerequisite for the *in vitro* ubiquitination assay. This paves the way for further investigation. Currently, in the Sprenger lab optimization steps are conducted for both methods – TUBE-ligase trapping and the SCF-Rca1 *in vitro* ubiquitination assay – to finally allow detection of ubiquitinated Dap by SCF-Rca1.

5.7 A fragment of Rca1 can be ubiquitinated *in vitro* by APC/C-Fzr

Beside the analysis of the degradation mechanism of Dap, in this thesis also a side project was pursued regarding Rca1 as a substrate of APC/C. In previous work, there were already strong indications that Rca1 is not only an inhibitor of APC/C-Fzr, but also switches to be a substrate of it during the cell cycle (Morgenthaler 2013; Polz 2021). This statement was mainly based on flow cytometry (similar to the analysis conducted in this thesis regarding Dap and SCF-Rca1). An *in vitro* ubiquitination assay would allow direct detection of ubiquitinated Rca1 by APC/C-Fzr and therefore could substantiate the statement of Dap being a substrate of APC/C-Fzr. For a detailed description of how the APC/C *in vitro* ubiquitination assay was conducted and how APC/C-Fzr, but not APC/C-Fzy was enriched see chapter 4.24.

Full-length Rca1 could not be obtained in sufficient amounts by expression in *E. coli*, *Drosophila* or *Sf21* (using baculoviruses). However, previous flow cytometry analysis indicated that the region 204-299 in Rca1 is sufficient to promote degradation of Rca1 via APC/C-Fzr (Morgenthaler 2013; Polz 2021). Expression of 6xHis-10xHA-CHE-Rca1_204-411 in *E. coli* and purification by means of an ÄKTA system was successful. Indeed, ubiquitinated 6xHis-10xHA-CHE-Rca1_204-411 was detected via western blot after conduction of

the APC/C *in vitro* ubiquitination assay. To exclude that the tag 6xHis-10-HA-CHE and not Rca1_204-411 was ubiquitinated, the tag alone was also expressed, purified and used for the APC/C *in vitro* ubiquitination assay. However, ubiquitinated 6xHis-10xHA-CHE was not detected indicating that specifically Rca1_204-411 was ubiquitinated by APC/C-Fzr. Therefore, the statement that Rca1 acts as a substrate of APC/C-Fzr was confirmed.

6. Material

6.1 Chemicals

Table 1 | List of Chemicals

Chemical	Distributor
Acetic acid (CH_3COOH, HAc)	Merck KGaA
Acrylamide 30%/bisacrylamide	Carl Roth GmbH
Agarose ultra	Invitrogen GmbH
Ampicillin	Carl Roth GmbH
APS (ammonium persulfate)	Merck KGaA
ATP (100 mM)	New England Biolabs
Bacto Pepton	Becton
Bacto Trypton	Becton
Bacto Yeast Extract	Becton
Beta-Mercaptoethanol	Fluka
Bortezomib	Selleckchem.com
Bromophenol blue	SERVA Electrophoresis
CH_3COOK (potassium acetate)	Merck KGaA
Chloramphenicol	Sigma-Aldrich Chemie GmbH
Coomassie Brilliant Blue	Sigma-Aldrich Chemie GmbH
CTP (100 mM)	New England Biolabs
DMSO (Dimethyl sulfoxide)	Merck KGaA, Sigma-Aldrich Chemie GmbH
dNTP mix (dATP, dCTP, dGTP, dTTP)	New England Biolabs
DTT (1,4-dithiothreitol)	AppliChem GmbH
EDTA (ethylenediaminetetraacetic acid)	Fluka
Ethanol	Carl Roth GmbH
Ethidiumbromide	SERVA Electrophoresis
Euroagar	Becton
FuGENE HD	Promega Corporation
GeneRuler DNA Ladder Mix	ThermoScientific
Gentamycine	Unknown
Glycerol	Carl Roth GmbH
Glycine	AppliChem GmbH
GTP (100mM)	New England Biolabs
HCl (hydrochloric acid)	Merck KGaA
HEPES (2-[4-(2-hydroxyethyl)piperazin-1-yl]ethanesulfonic acid)	AppliChem GmbH
Hoechst 33342	Sigma-Aldrich Chemie GmbH
Hygromycin B Gold	InvivoGen
Imidazole	AppliChem GmbH
IPTG (Isopropyl β-D-1-thiogalactopyranoside)	AppliChem GmbH
Kanamycin	AppliChem GmbH
KH_2PO_4 (potassium dihydrogen phosphate)	Sigma-Aldrich Chemie GmbH
Liquid nitrogen	AG Schneuwly (University of Regensburg)
Methanol	Carl Roth GmbH
$MgCl_2$	Merck
NaCl (Sodium chloride)	Carl Roth GmbH, Merck
NaOH (sodiumhydroxide)	Gerbu Trading GmbH
NaN_3 (sodium azide)	Sigma-Aldrich Chemie GmbH
Phusion GC buffer	Thermo Scientific
Phusion HF buffer	Thermo Scientific
Precision Plus Protein Standard	Bio-Rad Laboratories
Protease inhibitor mix	Bimake

Chemical	Distributor
Rabbit reticulocyte lysate	Promega (Rabbit Reticulocyte Lysate System)
Restriction buffers 10X	New England Biolabs
Schneider s Drosophila medium	Invitrogen, PAN Biotech
SDS (sodium dodecyl sulfate)	Carl Roth GmbH, SERVA Electrophoresis
Skim milk powder Gloria	Nestle
Spermidine	Sigma-Aldrich Chemie GmbH
T4 ligase Buffer 10X	New England Biolabs
TEMED (tetramethylethylenediamine)	Fluka
Tris (tris(hydroxymethyl)aminomethane)	Carl Roth GmbH
Triton X-100	Fluka
Tween20	Carl Roth GmbH
UTP (100 mM)	New England Biolabs
X-gal	AppliChem GmbH

6.2 Kits

Table 2 | List of Kits

Kit	Distributor
Invisorb Spin DNA Extraction Kit	STRATEC Molecular GmbH
FastGene Gel/PCR Extraction Kit	Nippon genetics
GeneJET Plasmid Midiprep Kit	Thermo Scientific
MSB Spin PCRapace Kit	MSB Spin PCRapace Kit STRATEC Molecular GmbH
PureYield Plasmid Midiprep system	Promega
Rabbit Reticulocyte Lysate System	Promega

6.3 Proteins and Enzymes

Table 3 | List of proteins and enzymes

Protein/Enzyme	Distributor
6xHis-4xFLAG-Ubiquitin	Own production
6xHis-10xHA-CHE (pFSR-1514)	Own production
6xHis-10xHA-CHE_Rca1_204-299 (pFSR-1492)	Own production
6xHis-Uba1 (pFSR-0523)	Own production
6xHis-Vihar (pFSR-1304)	Own production
BSA (bovine serum albumin)	Sigma-Aldrich Chemie GmbH
FBS (fetal bovine serum)	AG Medenbach
GFP-nanobody-6xHis (pOT-241)	Own production
T4 DNA Ligase	Sigma-Aldrich Chemie GmbH
Lysozyme	Boehringer Mannheim, Fluka, Sigma-Aldrich Chemie GmbH
Phusion DNA polymerase	STRATEC Molecular GmbH
Restriction endonucleases	New England Biolabs
RNase A	AppliChem GmbH
RNase Inhibitor	AG Medenbach
Shrimp Alkaline Phosphatase (rSAP)	New England Biolabs
T7 RNA polymerase	New England Biolabs

6.4 Oligonucleotides

Oligonucleotides used for molecular cloning can be accessed from the internal AG Sprenger database.

6.5 Plasmids

Mutations in proteins were annotated as suggested by Dunnen and Antonarakis (Dunnen and Antonarakis 2000). The plasmid maps can be accessed from the Vector NTI database of the AG Sprenger.

Table 4 | List of plasmids used for flow cytometry analysis

Number	Name **Nickname**
pFSR-1406	actPro(L)-HA-NLS-GFP-ddT2A-HA-NLS-CHE-Dap_Del-126-245 **Dap_1-125**
pFSR-1637	actPro(L)-HA-NLS-GFP-T2A-HA-NLS-CHE-Dap_Del-126-245-ddT2A-NLS-4XFLAG **Dap_1-125-T2Aa**
pFSR-1638	actPro(L)-HA-NLS-GFP-T2A-HA-NLS-CHE-Dap_dCDI_Del-126-245-T2A-NLS-4XFLAG **Dap_1-125_dCDI-T2Aa**
pFSR-1809	actPro(L)-HA-NLS-GFP-ddT2A-HA-NLS-CHE-Dap_Del-38-44-RAR_Del-126-245-ddT2A-NLS-4XFLAG **Dap_1-125_dCyc-T2Aa**
pFSR-1808	actPro(L)-HA-NLS-GFP-ddT2A-HA-NLS-CHE-Dap_Del-103-105-G_Del-126-245-ddT2A-NLS-4XFLAG **Dap_1-125_dCDK-T2Aa**
pFSR-1714	actPro(L)-HA-NLS-GFP-ddT2A-HA-NLS-CHE-Dap_Del-1-125 **Dap_126-245**
pFSR-1715	actPro(L)-HA-NLS-GFP-ddT2A-HA-NLS-CHE-Dap_Del-1-125_Del-184-188 **Dap_126-245_dPIPa**
pFSR-1716	actPro(L)-HA-NLS-GFP-ddT2A-HA-NLS-CHE-Dap_Del-1-125_Q184A_K195A **Dap_126-245_Q184A_K195A**
pFSR-2081	actPro(L)-HA-NLS-GFP-ddT2A-HA-NLS-CHE-Dap_Del-1-159 **Dap_160-245**
pFSR-2008	actPro(L)-HA-NLS-GFP-T2A-HA-NLS-CHE-Dap_Del-1-17_Del-126-245-T2A-NLS-4xFLAG **Dap_18-125-T2Aa**
pFSR-2009	actPro(L)-HA-NLS-GFP-T2A-HA-NLS-CHE-Dap_Del-1-17_Del-103-105-G_Del-126-245-T2A-NLS-4xFLAG **Dap_18-125_dCDK-T2Aa**
pFSR-2010	actPro(L)-HA-NLS-GFP-ddT2A-HA-NLS-CHE-Dap_Del-141-245 **Dap_1-140**
pFSR-2003	actPro(L)-HA-NLS-GFP-ddT2A-HA-NLS-CHE-Dap_Del-103-105-G_Del-141-245 **Dap_1-140_dCDK**
pFSR-2004	actPro(L)-HA-NLS-GFP-ddT2A-HA-NLS-CHE-Dap_Del-161-245 **Dap_1-160**
pFSR-2005	actPro(L)-HA-NLS-GFP-ddT2A-HA-NLS-CHE-Dap_Del-103-105-G_Del-161-245 **Dap_1-160_dCDK**
pFSR-2006	actPro(L)-HA-NLS-GFP-ddT2A-HA-NLS-CHE-Dap_Del-181-245 **Dap_1-180**
pFSR-2007	actPro(L)-HA-NLS-GFP-ddT2A-HA-NLS-CHE-Dap_Del-103-105-G_Del-181-245 **Dap_1-180_dCDK**
pFSR-1288	actPro(L)-HA-NLS-GFP-ddT2A-HA-NLS-CHE-Dap **Dap**
pFSR-1238	actPro(L)-HA-NLS-GFP-ddT2A-HA-NLS-CHE-Dap_Del-38-44-RAR_Del-103-105-G **Dap_dCDI**
pFSR-1935	actPro(L)-HA-NLS-GFP-ddT2A-HA-NLS-CHE-Dap_S154A **Dap_S154A**
pFSR-1804	actPro(L)-HA-NLS-GFP-ddT2A-HA-NLS-CHE-Dap_Q184A **Dap_Q184A**

Number	Name **Nickname**
pFSR-1668	actPro(L)-HA-NLS-GFP-ddT2A-HA-NLS-CHE-Dap_Del-38-44-RAR_Del-103-105-G_Q184A **Dap_dCDI_Q184A**
pFSR-1910	actPro(L)-HA-NLS-GFP-ddT2A-HA-NLS-CHE-Dap_Del-103-105_Q184A **Dap_dCDK_Q184A**
pFSR-1904	actPro(L)-HA-NLS-GFP-ddT2A-HA-NLS-CHE-Dap_K195A **Dap_K195A**
pFSR-1699	actPro(L)-HA-NLS-GFP-ddT2A-HA-NLS-CHE-Dap_Del-38-44-RAR_Del-103-105-G_K195A **Dap_dCDI_K195A**
pFSR-1959	actPro(L)-HA-NLS-GFP-ddT2A-HA-NLS-CHE-Dap_Del-103-105_K195A **Dap_dCDK_K195A**
pFSR-2067	actPro(L)-HA-NLS-GFP-ddT2A-HA-NLS-CHE-Dap_Q184A_K195A **Dap_Q184A_K195A**
pFSR-1703	actPro(L)-HA-NLS-GFP-ddT2A-HA-NLS-CHE-Dap_Del-38-44-RAR_Del-103-105-G_Q184A_K195A **Dap_dCDI_Q184A_K195A**
pFSR-1941	actPro(L)-HA-NLS-GFP-ddT2A-HA-NLS-CHE-Dap_Del-103-105_Q184A_K195A **Dap_dCDK_Q184A_K195A**
pFSR-1875	actPro(L)-HA-NLS-GFP-ddT2A-HA-NLS-CHE-Dap_K195R **Dap_K195R**
pFSR-1876	actPro(L)-HA-NLS-GFP-ddT2A-HA-NLS-CHE-Dap_Del-38-44-RAR_Del-103-105-G_K195R **Dap_dCDI_K195R**
pFSR-1877	actPro(L)-HA-NLS-GFP-ddT2A-HA-NLS-CHE-Dap_R194A_R196A **Dap_R194A_R196A**
pFSR-1878	actPro(L)-HA-NLS-GFP-ddT2A-HA-NLS-CHE-Dap_Del-38-44-RAR_Del-103-105-G_R194A_R196A **Dap_dCDI_R194A_R196A**
pFSR-1879	actPro(L)-HA-NLS-GFP-ddT2A-HA-NLS-CHE-Dap_R194A_K195A_R196A **Dap_R194A_K195A_R196A**
pFSR-1880	actPro(L)-HA-NLS-GFP-ddT2A-HA-NLS-CHE-Dap_Del-38-44-RAR_Del-103-105-G_R194A_K195A_R196A **Dap_dCDI_R194A_K195A_R196A**
pFSR-1405	actPro(L)-HA-NLS-GFP-ddT2A-HA-NLS-CHE-Dap_Del-184-188 **Dap_dPIPa**
pFSR-1363	actPro(L)-HA-NLS-GFP-ddT2A-HA-NLS-CHE-Dap_Del-38-44-RAR-_Del-103-150-G_Del-184-188 **Dap_dCDI_dPIPa**
pFSR-2078	actPro(L)-HA-NLS-GFP-ddT2A-HA-NLS-CHE-Dap_Del-103-105-G_Del-184-188 **Dap_dCDK_dPIPa**
pFSR-1639	actPro(L)-HA-NLS-GFP-ddT2A_HA-NLS-CHE-Dap_Del-38-44-RAR_Del-103-105-G_Q184A_I187A_T188A **Dap_dCDI_Q184A_I187A_T188A**
pFSR-1621	actPro(L)-HA-NLS-GFP-ddT2A_HA-NLS-CHE-Dap_Del-38-44-RAR_Del-103-105-G_R194A_L197A **Dap_dCDI_R194A_L197A**
pFSR-1625	actPro(L)-HA-NLS-GFP-ddT2A_HA-NLS-CHE-Dap_Del-38-44-RAR_Del-103-105- G_Q184A_I187A_T188A_F190A_M191A_K195A **Dap_dCDI_PIP-6A**
pFSR-1280	actPro(L)-HA-NLS-Cdt1_Del-102-743-CHE-ddT2A-HA-NLS-GFP **Cdt1_1-101**
pFSR-1212	actPro(L)-HA-NLS-GFP-BX-ddT2A-HA-NLS-CHE **HA-NLS-CHE**

Table 5 | List of plasmids used for coexpression in flow cytometry analysis

Number	Name **Nickname**
pFSR-0955	PubPro-3xHA-Rca1 **Rca1**
pFSR-0977	PubPro-3XHA-Rca1_Del-164-203-PG-(DFbox) **Rca1_dFbox**
pFSR-1339	PubPro-3XHA-Rca1_A344T **Rca1_A344T**
pFSR-1345	PubPro-3XHA-Rca1_S285R **Rca1_S285R**
pFSR-1660	PubPro-3xHA-Rca1_Del_406-411 **Rca1_dRL**
pFSR-1664	UAS-Mir1(Rca1)-Gal4-Mix (pFSR-1594 (UAS-Mir1(Rca1-5´-UTR)) + pFSR-1545 (PubPro-Gal4-Delta)) **Rca1 KD**
pFSR-1724	UAS-Mir1(Cdt2)-Gal4-Mix (pFSR-1720 (UAS-Mir1(Cdt2)) + pFSR-1545 (PubPro-Gal4-Delta)) **Cdt2 KD**
pFSR-1663	UAS-Mir1(Cul4)-Gal4-Mix (pFSR-1640 (UAS-Mir1(Cul4)) + pFSR-1545 (PubPro-Gal4-Delta)) **Cul4 KD**
pFSR-1989	UAS-Mir1(Ago)-Gal4-Mix (pFSR-1903 (UAS-Mir1(Ago)) + pFSR-1545 (PubPro-Gal4-Delta)) **Ago KD**
pFSR-1784	HA-CycE/Cdk2-HA-Mix (pFSR-1184 (PubPro-HA-CycE) + pFSR-986 (PubPro-Cdk2-HA)) **CycE/Cdk2**
pFSR-1977	NLS-4xFLAG-CycE/Cdk2-HA Mix (pFSR-1946 (PubPro-NLS-4xFLAG-CycE) + pFSR-986 (PubPro-Cdk2-HA)) **NLS-4xFLAG-CycE/Cdk2-HA**
pFSR-1925	NLS-4xFLAG-CycE_Del-1-143/Cdk2-HA-Mix (pFSR-1894 (NLS-4xFLAG-CycE_144-602) + pFSR-986 (Cdk2-HA)) **NLS-4xFLAG-CycE_144-602/Cdk2-HA**
pFSR-1978	NLS-4xFLAG-CycE_Del-1-202/Cdk2-HA Mix (pFSR-1970 (NLS-4xFLAG-CycE_203-602) + pFSR-986 (Cdk2-HA)) **NLS-4xFLAG-CycE_203-602/Cdk2-HA**
pFSR-1926	NLS-4xFLAG-CycE_Del-1-235/Cdk2-HA-Mix (pFSR-1895) (NLS-4xFLAG-CycE_236-602) + pFSR-986 (Cdk2-HA)) **NLS-4xFLAG-CycE_236-602/Cdk2-HA**
pFSR-2076	NLS-4xFLAG-CycE_T544A_S548A/Cdk2-HA Mix (pFSR-2013) (NLS-4xFLAG-CycE_T544A_S548S) + pFSR-986 (Cdk2-HA)) **NLS-4xFLAG-CycE_T544A_S548A/Cdk2-HA**

Table 6 | List of plasmids used for co-immunoprecipitations

Number	Name **Nickname**
pFSR-1263	PubPro-4xFLAG-Dap **4xFLAG-Dap**
pFSR-1230	PubPro-4XFLAG-Dap_Del-38-44-RAR_Del-103-105-G **4xFLAG-Dap_dCDI**
pFSR-1710	PubPro-4xFLAG-Dap_Del-38-44-RAR_Del-103-105-G_Q184A **4xFLAG-Dap_dCDI_Q184A**
pFSR-1711	PubPro-4xFLAG-Dap_Del-38-44-RAR_Del-103-105-G_K195A **4xFLAG-Dap_dCDI_K195A**

Number	Name **Nickname**
pFSR-1712	PubPro-4xFLAG-Dap_Del-38-44-RAR_Del-103-105-G_Q184A_K195A **4xFLAG-Dap_dCDI_Q184A_K195A**
pFSR-1116	PubPro-4XFLAG-Dap-38-44-RAR_Del-103-105-G_Del-184-188 **4xFLAG-Dap_dCDI_dPIPa**
pFSR-1838	PubPro-4xFLAG-Dap-Del-38-44-RAR_Del-103-105-G_R194A_R196A **4xFLAG-Dap_dCDI_R194A_R196A**
pFSR-1837	PubPro-4xFLAG-Dap-38-44-RAR_Del-103-105-G_R194A_K195A_R196A **4xFLAG-Dap_dCDI_R194A_K195A_R196A**
pFSR-1428	PubPro-NLS-4xFLAG-Dap_Del-126-245 **NLS-4xFLAG-Dap_1-125**
pFSR-1972	PubPro-NLS-4xFLAG-Dap_Del-38-44-RAR_Del-103-105-G_Del_126-245 **NLS-4xFLAG-Dap_1-125_dCDI**
pFSR-2028	PubPro-NLS-4xFLAG-Dap_Del-161-245 **NLS-4xFLAG-Dap_1-160**
pFSR-1975	PubPro-NLS-4xFLAG-Dap_Del-38-44-RAR_Del-103-105-G_Del-161-245 **NLS-4xFLAG-Dap_1-160_dCDI**
pFSR-1846	PubPro-4xFLAG-Dap_Del-1-125 **4xFLAG-Dap_126-245**
pFSR-1046	PubPro-4XFLAG-Dap_Del-1-125_Del-184-188 **4xFLAG-Dap_126-245_dPIPa**
pFSR-1858	PubPro-4xFLAG-Dap_Del-1-159 **4xFLAG-Dap_160-245**
pFSR-1718	PubPro-4xFLAG-PCNA **4xFLAG-PCNA**
pFSR-1733	PubPro-4xFLAG-Cdt2 **4xFLAG-Cdt2**
pFSR-1774	PubPro-4xFLAG-Cdt2_E712M **4xFLAG-Cdt2_E712M**
pFSR-1967	PubPro-4xFLAG-Slmb_1-198-GFP_enhancer_nanobody **4xFLAG-Slmb-vhh-GFP**
pFSR-1327	PubPro-4XFLAG-SkpA **4xFLAG-SkpA**
pFSR-0986	PubPro-Cdk2_T18A_Y19F_HA **Cdk2-HA**
pFSR-1184	PubPro-HA-CycE **HA-CycE**
pFSR-0955	PubPro-3xHA-Rca1-rosyUTR **3xHA-Rca1**
pFSR-1717	PubPro-3xHA-PCNA **3xHA-PCNA**
pFSR-1732	PubPro-3xHA-Cdt2 **3xHA-Cdt2**
pFSR-1773	PubPro-3xHA-Cdt2_E712M **3xHA-Cdt2_E712M**
pFSR-1966	PubPro-3xHA-SkpA **3xHA-SkpA**
pFSR-1968	PubPro-3xHA-Cul1 **3xHA-Cul1**
pFSR-1965	PubPro-3xHA-Roc1a **3xHA-Roc1a**
pFSR-1791	PubPro-GFP-Rca1-4xUBA-4xFLAG **GFP-Rca1-4xUBA-4xFLAG**

Table 7 | List of plasmids used for the APC/C in vitro ubiquitination assay and coupling of proteins to agarose beads

Number	Name **Nickname**
pFSR-0688	T7Exp-6xHis-4xFLAG-Ubiquitin **6xHis-4xFLAG-Ubiquitin**
pFSR-0523	T7Exp-6xHis-Uba1 **6xHis-Uba1**
pFSR-1304	T7Exp-6xHis-Vihar **6xHis-Vihar**
pFSR-1514	T7Exp-6xHis-10xHA-CHE **6xHis-10xHA-CHE**
pFSR-1492	T7Exp-6xHis-10xHA-CHE-Rca1_204-299 **6xHis-10xHA-CHE-Rca1_204-299**
pOT-241	T7Exp-GFP_enhancer_nanobdy-IGg1(CH3)-6xHIS **GFP-nanobody-6xHis**

6.6 Bacterial strains

Table 8 | Bacterial strains

Strain	Genotype	Distributor
DH5α (electrocompetent)	F- *endA1 glnV44 thi-1 recA1 relA1 gyrA96 deoR nupG purB20 φ80dlacZΔM15 Δ(lacZYA-argF)* U169, hsdR17($r_K^-m_K$+), λ^-	AG Sprenger
Rosetta™ (DE3) pLysS (chemically competent)	F- *ompT hsdS$_B$* ($r_B^-m_B^-$) *gal dcm* (*DE3*) *pLysSRARE* (*Cam^R*)	AG Sprenger

6.7 Eukaryotic cell lines

Table 9 | Eukaryotic cell lines

Cell line	Distributor
S2R+	AG Sprenger
SF21	AG Längst

6.8 Antibodies

6.8.1 Primary antibodies

Table 10 | Primary antibodies

Antigen	Number	Source	Dilution for Western Blot	Dilution for co-IP	Distributor
FLAG	374	Mouse	1:5000	1:333	Sigma
GFP	387	Mouse	1:5000		Roche
HA	395	Mouse	1:5000	1:333	Cavance
His	394	Mouse	1:1000	-	Santa Cruz

6.8.2 Secondary antibodies

Table 11 | Secondary antibodies

Antigen	Number	Source	Dilution for Western Blot	Fluorochrome	Distributor
Mouse	381	Goat	1:10000	IRDye 680LT	Li-Cor

6.9 Solutions and buffers

Table 12 | Solutions and buffers

Solution/buffer	Components	Concentration
Ampicillin stock solution	Ampicillin In 50 % glycerol	50 mg/ml
APS solution 10 %	APS In H_2O	10 % (w/v)
DNA/RNA Loading buffer 6X (Purple Loading Dye)	Ficoll®-400 EDTA Tris-HCl SDS Dye1 (pink/red) Dye2 (blue) pH 8.0	2.5% (w/v) 10mM 3.3mM 0.08% 0.02% 0.0008%
dNTP mix (2 mM each)	dNTP mix In H_2O	2 mM

Solution/buffer	Components	Concentration
EasyPrep buffer	Tris, pH 8.0 EDTA, pH 8.0 Sucrose Lysozym RNase A BSA In H_2O	10 mM 1 mM 150 mg/ml 2 mg/ml 0.2 mg/ml 0.1 mg/ml
IP Lysis buffer	HEPES, pH 7.7 NaCl EGTA NaF Triton X-100 Glycerol In H_2O For use Protease inhibitor mix was freshly added.	50 mM 150 mM 1 mM 10 mM 1 % (v/v) 10 % (v/v)
IP Washing buffer	HEPES, pH 7.7 NaCl Triton X-100 Glycerol In H_2O	50 mM 150 mM 1 % (v/v) 10 % (v/v)
LSB 2X	Tris, pH 6.8 SDS Glycerol Bromphenol blue Beta-Mercaptoethanol In H_2O	120 mM 4 % (w/v) 20 % (v/v) 0.04 % (w/v) 10 % (v/v)
Milk powder solution	Skim milk powder Sodium azide In PBS	5 % (m/v) 0.01 % (m/v)
PBS	NaCl Na_2HPO_4 NaH_2PO_4 pH In H_2O	130 mM 7 mM 3 mM 7.2
PBST	Tween 20 In PBS	0.1 % (v/v)
Resolving gel (SDS-PAGE)	For 10 ml resolving gel:	

Gel	H_2O (ml)	Acrylamide 30%/Bisacrylamide (ml)	1.5 M Tris/HCl pH 8.8 (ml)	10 % SDS (ml)	10 % APS (µl)	TEMED (µl)
8 %	4.7	2.7	2.5	0.1	100	10
9 %	4.4	3.0	2.5	0.1	100	10
10 %	4.1	3.3	2.5	0.1	100	10
11 %	3.7	3.7	2.5	0.1	100	10
12 %	3.4	4.0	2.5	0.1	100	10
13 %	3.1	4.3	2.5	0.1	100	10
14 %	2.7	4.7	2.5	0.1	100	10
15 %	2.4	5.0	2.5	0.1	100	10

Resolving gels were stored as 50 ml stock solutions without APS and TEMED.

<table>
<tr><th>Solution/buffer</th><th>Components</th><th>Concentration</th></tr>
<tr><td>SDS solution 10 %</td><td>SDS
In H_2O</td><td>10 % (w/v)</td></tr>
<tr><td>Stacking gel (SDS-PAGE)</td><td colspan="2">For 10 ml stacking gel:
<table><tr><th>Gel</th><th>H_2O (ml)</th><th>Acrylamide 30%/Bisacrylamide (ml)</th><th>1.5 M Tris/HCl pH 6.8 (ml)</th><th>10 % SDS (ml)</th><th>10 % APS (µl)</th><th>TEMED (µl)</th></tr><tr><td>4 %</td><td>6.1</td><td>1.3</td><td>2.5</td><td>0.1</td><td>100</td><td>10</td></tr></table>
The stacking gel was stored as 50 ml stock solution without APS and TEMED.</td></tr>
<tr><td>TAE buffer</td><td>Tris, pH 8.0
EDTA
In H_2O</td><td>40 mM
10 mM</td></tr>
<tr><td>Transfer buffer 3 (Western blot)</td><td>Methanol
Tris, pH 7.5
EDTA, pH 8.0
Sodium acetate
SDS
In H_2O</td><td>20 % (v/v)
40 mM
2 mM
20 mM
0.05 % (v/v)</td></tr>
<tr><td>Turbo Laemmli running buffer 10X</td><td>Tris
Glycin
SDS
In H_2O</td><td>250 mM
9.46 M
10 g/l</td></tr>
</table>

6.10 Media and Agar plates

Table 13 | Media and Agar plates

Medium/Agar plate	Components	Concentration
LB agar plate	Euroagar In LB medium (autoclaved) Solution is boiled for casting plates. Before adding any antibiotic, the solution is first cooled down to 50 °C	1.7 % (w/v)
LB medium (autoclaved)	BactoTrypton Bacto Yeast Extract NaCl pH In H_2O	10 g/l 5 g/l 10 g/l 7.2
Schneider's *Drosophila* complete medium	GIBCO FBS Penicillin Streptomycin In Schneider's *Drosophila* Medium	10 % (v/v) 1 % (v/v) 1 % (v/v)

6.11 Consumable material

Table 14 | Consumable material

Equipment	Distributor
12-well plate	Cellstar
6-well plate	Sarstedt
Affi-Gel	BIO-RAD
Cell culture flask, 250 ml, 75 cm²	Cellstar
Cell scraper	Sarstedt
Centrifugal concentrator Vivaspin 20 30,000 MWCO	Sartorius
Cups (0.5 ml, 1.5 ml, 2 ml)	Eppendorf, Sarstedt
Electroporation cuvettes	Peqlab
Falcons 15 ml, 50 ml	Sarstedt
GIBCO FBS (fetal bovine serum)	Invitrogen GmbH
Glass pasteur pipettes 150 mm	BRAND
Nitrocellulose membrane	Schleicher & Schuell BioScience
Parafilm “M” Laboratory Film	Pechiney
PCR-Cups 200 µl	Sarstedt
Petri dishes 92 X 16 mm	Sarstedt
Pipet tips 10 µl, 200 µl, 1000 µl	Eppendorf, Sarstedt
Protein G Plus-Agarose Beads	Santa Cruz
Trypsin/EDTA solution	PAN Biotech
Tubes 3,5 ml	Sarstedt
Whatman paper	Whatman International Ltd

6.12 Software

Table 15 | Software

Software	Developer
Canvas X	ACD Systems International Inc.
Citavi6	Swiss Academic Software GmbH
ContigExpress	Invitrogen
FCS Express 4	De Novo Software
Filemaker Pro 15	Filemaker Inc.
ImageJ 1.53c	NIH
Microsoft Office	Microsoft Corp.
Origin 2022	OriginLab
Vector NTI Advance 11	Invitrogen
ImageStudio Light	LI-COR Biosciences
Inkscape	Inkscape
RStudio	RStudio
UNICORN start 1.0	GE Healthcare

6.13 Equipment

Table 16 | Equipment

Equipment	Distributor
Acrylamide gel apparatus	Bio-Rad Laboratories
Agarose gel electrophoresis apparatus HE33	Hoefer
ÄKTAstart	GE Healthcare
Beaker 250 ml, 500 ml, 5 L	Schott, VITLAB, VWR
Cell culture incubator	Hereaus
Centrifuge 5424	Eppendorf
Centrifuge Heraeus Multifuge 1S	Thermo Scientific
Centrifuge MEGA STAR 1.6R	VWR
Centrifuge RC-5b	Sorvall
Clean bench	Ceag Schirp Reinraumtechnik
Clean bench MARS	SCANLAF
Clean bench Mars Safety Class 2	SCANLAF
Culture roller drum TC-7	New Brunswick Scientific
Electrophoresis power supply EPS 200/600	Pharmacia Biotech
Electroporation apparatus Easyject Prima	Equibio
Erlenmeyer flask	DURAN Group GmbH
FastPette V2 Pipette Controller	Labnet
Flow cytometer CyFlow space	Partec
Freezer	AEG, Bosch, Siemens
Freezer C760	New Brunswick Scientific
French Pressure Cell Press	American instrument company
Fuchs-Rosenthal Counting chamber (16 mm², 0.2 mm cell depth)	Hausser Scientific
Glass bottle 250 ml, 500 ml, 1 L	Schott
Glass pipettes 1 ml, 5 ml, 10 ml, 25 ml	Hirschmann
Glass tube	Schuett-biotec
Gyrotory Water Bath shaker G76	New Brunswick Scientific
Heating block (Digital Dry Bath, dual position)	Benchmark Scientific
HisTrap FF Crude 5 ml (affinity column)	Cytiva
Ice Bucket	-
Ice maker MF22	Scotsman
Incubator Heraeus B 5050 E	Heraeus
Incubator Sanyo MIR-153	Sanyo
Incubator WB120K (equipped with culture roller drum TC-7)	Mytron
Incubator Innova™ 42	Thermo Fisher
Inverted microscope CKX41 (equipped with Reflected Fluorescence System with Light Source X-Cite 120Q)	Olympus
LED Transilluminator	Nippon Genetics
Magnetic stirrer	Heidolph
Marienfeld superior counting chamber	Marienfeld
Measuring cylinder	VITLAB
Microliter syringe 705	Hamilton
Microwave	Vestel
Mini-PROTEAN® Tetra system	Bio-Rad
Odyssey Infrared Imaging system	LI-COR
PerfectBlue Semi-Dry Electro Blotter	Peqlab
pH meter 766 Caltimatic	Knick
Plastic boxes 11 cm x 7 cm x 4 cm (Coomassie/Antibody staining)	-
Refrigerator	AEG, Bosch
Rocking Shaker ST 5	Ingenieurbüro CAT M. Zipperer GmbH
Scale Kern EW6200-2NM	Kern & Sohn GmbH
Scale Mettler AE50	Mettler Toledo Intl. Inc.

Equipment	Distributor
Sieve (2 cm² diameter)	Own production
Spectrophotometer / Fluorometer DS-11 FX+	DeNovix
Sonifier Branson 250D	Heinemann
Superdex 75 10/300 GL	GE Healthcare
Table centrifuge ROTOFIX 32 A	Hettich
Test-Tube-Rotator 34528	Snijders Scientific
Thermocycler GTC96S	Cleaver Scientific Ltd
ThermoMixer F1.5	Eppendorf
UV Crosslinker	Stratalinker
UVP ChemStudio	Analytik Jena
Vacuum Blotting Pump, 2016 Vacugene	LKB Bromma
Vacuum gas pump VP86	VWR
Vacuum manifold	Promega
Vornado™ Vortex Mixer	Benchmark Scientific
Water purification system	ELGA
Wide-Field Fluorescence Microscope Excitation Light Source X-Cite 120Q	Excelitas Technologies

7 Methods

7.1 DNA/RNA methods

7.1.1 Molecular cloning

Recombinant DNA was first cloned *in silico* using the cloning software Vector NTI Advance 11. Then molecular cloning was conducted as follows (see table 17):

Table 17 | Protocol for molecular cloning

Day	Protocol		Result
Day 1	1)	In several cases it was necessary to obtain the insert DNA via PCR (see section 7.1.2). If this was not the case, it was directly started with step 2).	Recombinant plasmid consisting of Vector and Insert DNA fragments
	2)	Plasmids and/or PCR products were digested by restriction endonucleases (see section 7.1.4)	
	3)	Insert and Vector DNA was isolated by gel electrophoresis (see section 7.1.3) and subsequently gel extraction	
	4)	Insert and Vector DNA was quantified (see section 7.1.15)	
	5)	If necessary, Vector DNA was dephosphorylated by the phosphatase rSAP (see section 7.1.5)	
	6)	Ligation of Vector and Insert DNA (see section 7.1.6)	
Day 2	1)	Electrocompetent *E. coli* cells were transformed with ligation mix (see section 7.1.7)	LB agar plates coated with transformed cells
	2)	Cells were plated on LB agar plates containing antibiotic to allow only growth of cells that contain plasmids	
Day 3	1)	Several clones were used for inoculation of pre-cultures (see section 7.1.10)	Pre-cultures for screening
Day 4	1)	Cells containing the recombinant plasmid were lysed using the Easy Prep method (see section 7.1.11) and subsequently identified by restriction digest or colony PCR (see section 7.1.9)	*E. coli* culture containing the recombinant plasmid
	2)	Main culture was inoculated with positive clone	
Day 5	1)	Plasmid DNA was isolated from the *E. coli* culture by alkaline lysis (see section 7.1.11.2)	Isolated recombinant plasmid
	2)	Ethanol precipitation of the plasmid DNA (see section 7.1.12)	
	3)	Yield and purity of the isolated plasmid DNA was determined by absorption measurement (DeNovix) as well as gel analysis (see section 7.1.15	

7.1.2 DNA amplification by PCR

DNA was amplified by polymerase chain reaction (PCR) according to Mullis et al (Mullis et al. 1986). Phusion High-Fidelity Polymerase was used to catalyze the reaction (see table 18).

Table 18 | Reaction mix for PCR

Component	Amount
DNA (template)	100 ng
Forward primer (100 mM)	1 µl
Reverse primer (100 mM)	1 µl
dNTP mix (2 mM each dNTP)	5 µl
5X Phusion HF buffer	10 µl
H2O	Ad 50 µl
Total volume	**50 µl**

The following PCR program was used to amplify DNA (see table 19).

Table 19 | program for PCR

Steps	Temperature	Duration	Cycles
1) Initial denaturation	96 °C	30 sec	
2) Denaturation	96 °C	10 sec	
3) Primer annealing	65 °C	20 sec	30 x
4) Elongation	72 °C	30 sec/1 kb	
5) Final elongation	72 °C	5 min	
6) Hold	4 °C	∞	

PCR products were purified using the MSB Spin PCRapace KIT according to the manufacturer´s instructions.

7.1.3 Agarose gel electrophoresis

DNA fragments were separated by agarose gel electrophoresis. To this end, 0.8 % agarose gels containing ethidium bromide (10 mg/ml) were used. 6x Purple loading dye was added to the DNA samples, which were subsequently loaded onto the gel. To estimate the size of the DNA fragments, GeneRuler DNA Ladder Mix was used as a reference. Electrophoresis was carried out for 45 min with 90 V. Gels were documented using a UVP ChemStudio system.

7.1.4 Restriction digestion of DNA

DNA was digested by restriction endonucleases and buffers according to the manufacturer's instructions. For the reaction mixture 0.5 µl of restriction endonuclease each was used per 20 µl total volume (see table 20).

Table 20 | Reaction mixture for restriction digestion

Component	Amount
DNA	variable
10X restriction buffer	1/10 of total volume
Restriction endonuclease	1/40 of total volume
H2O	Ad total volume
Total volume	**variable**

7.1.5 Dephosphorylation of DNA ends

After restriction digestion, vector DNA ends were dephosphorylated by the Shrimp Alkaline Phosphatase (rSAP) to prevent re-ligation. The reaction mixture was incubated at 37 °C for one hour (see table 21).

Table 21 | Desphosphorylation of DNA ends by rSAP

Component	Amount
Digested vector DNA	variable
CutSmart Buffer (10X)	1/10 of total volume
rSAP	1/20 of total volume
H2O	Ad total volume
Total volume	**variable**

7.1.6 Ligation of DNA fragments

For ligation reactions a 3:1 molar ratio of insert to vector DNA was used. To estimate the background of undigested vector or vector re-ligation, a ligation reaction without insert was included. The reaction mixture was incubated at 24 °C for 1 hour or at 18 °C overnight (see table 22).

Table 22 | Reaction mixture for ligation

Component	Amount
Vector DNA	50 ng
Insert DNA	x ng (so that the molar ratio of insert to vector is 3:1)
10X T4 ligase buffer	1 µl
T4 DNA ligase	0.5 µl
H2O	Ad 10 µl
Total volume	**10 µl**

7.1.7 Transformation of electrocompetent cells

E. coli cells (DH5α) were transformed by electroporation according to the following protocol (see table 23).

Table 23 | Protocol for transformation of electrocompetent *E. coli* DH5α cells

Steps	Description
1)	100 µl of electrocompetent *E. coli* DH5α cells was thawed on ice and diluted with 100 µl H_2O
2)	100 µl of the mixture were transferred into precooled electroporation cuvettes
3)	2 µl of the ligation reaction mixture were added to the cuvettes
4)	Electroporation was performed with the following settings: voltage: 2.5 kV; capacitance: 25 µF; resistance: 200 ohms
5)	The transformed cells were transferred into 1 ml LB_0 medium
6)	Cells were incubated for 1 h at 37 °C, if antibiotic other than ampicillin was used
7)	100 µl of the cell suspension were plated onto LB plates (with the appropriate antibiotic)
8)	Plates were incubated overnight at 37 °C

7.1.8 Transformation of chemical competent cells

Chemically competent *E. coli* cells (Rosetta) were transformed according to the following protocol (see table 24).

Table 24 | Protocol for transformation of chemically competent *E. coli* Rosetta cells

Steps	Description
1)	100 µl of chemically competent *E. coli* DH5α cells was thawed on ice and diluted with 100 µl H_2O
2)	Up to 200 ng DNA solution was added to the cell suspension
3)	The cells were incubated on ice for 20 min
4)	The cells were heat shocked at 40 °C for 30 sec
5)	The cell suspension was incubated on ice for 2 min
6)	900 ml LB_0 was added to the cells. Thereafter, 100 µl of the cell suspension were plated onto LB plates (with the appropriate antibiotic)
7)	Plates were incubated overnight at 37 °C

7.1.9 Screening for recombinant clones

To screen *E.coli* colonies for recombinant plasmids either test digestion (7.1.9.1) or colony PCR (7.1.9.2) was conducted.

7.1.9.1 Screening via test digestion of mini prep DNA

To screen via test digestion, a *E. coli* pre-culture (2.5 ml) was inoculated and the plasmid DNA was isolated by means of the Easy Prep method (see section 7.1.11.1). Thereafter, the DNA was digested in such a way so that the recombinant clone (positive) could be distinguished from the parent plasmids based on the pattern of DNA bands on an agarose gel.

7.1.9.2 Screening via colony PCR

To screen via colony PCR, primers were selected so that the length of the PCR product allowed the discrimination between recombinant clone (positive) or parent plasmids. Several clones on the corresponding plate were used as a template for the PCR. Two controls (backbone and insert plasmid) were included to test for unspecific bands. The following master mix for these individual PCRs was used (see table 25).

Table 25 | Mastermix for Colony PCR (amount refers to one reaction)

Component	Amount
Forward primer (100 mM)	0.25 µl
Reverse primer (100 mM)	0.25 µl
dNTP mix (2 mM each dNTP)	1.5 µl
5X Phusion HF buffer	3 µl
Phusion polymerase	0.15 µl
H2O	9.85 µl
Total volume	**15 µl**

Following protocol was used for colony PCRs (see table 26).

Table 26 | Protocol for Colony PCR

Steps	Description
1)	1.5 ml reaction tubes with 200 µl LB medium with the appropriate antibiotic were prepared
2)	Colony was picked with plastic crystal tip and pipetted up and down in PCR tube to detach a few cells
3)	The tip with the remaining cells was transferred into the 1.5 ml reaction tube. For the two controls (backbone and insert plasmid) 0.5 µl of the corresponding plasmid was used as template instead.
4)	PCR was conducted (see section 7.1.2)
5)	Size of PCR product was determined by gel electrophoresis
6)	50 ml LB medium with the appropriate antibiotic was inoculated with a positive colony from the 1.5 ml reaction tube

7.1.10 Inoculation of *E.coli* cultures

LB medium with the appropriate antibiotic was inoculated with individual colonies on LB agar plates or pre-cultures. Thereafter, the glas tubes / Erlenmyer flasks were rotated/shaken overnight at 37 °C.

7.1.11 Isolation of DNA

7.1.11.1 Mini scale isolation of plasmid DNA

To screen for recombinant clones, small amounts of DNA were isolated according to a modified protocol (EasyPreps) from Berghammer and Auer (Berghammer and Auer 1993) (see table 27).

Table 27 | Protocol for Mini scale isolation of plasmid DNA

Steps	Description
1)	1.5 ml of a 2.5 ml overnight pre-culture was centrifuged at 14,000 rpm for 1 min
2)	After the supernatant was discarded, the pellet was resuspended in 50 µl EasyPrep buffer
3)	The suspended cells were incubated at 102 °C for 1 min
4)	Immediately after boiling the samples were cooled on ice for 2 min
5)	The lysed cells were centrifuged at 14,000 rpm for 15 min
6)	5 µl of the supernatant were used for restriction digestion

7.1.11.2 Midi scale isolation of plasmid DNA

To isolate larger amounts of DNA, which can be used for subsequent experiments, alkaline lysis based on the protocol by Birnboim and Doly (Birnboim and Doly 1979). To this end, the GeneJET Plasmid Midiprep Kit and the following protocol was used (see table 28).

Table 28 | Protocol for Midi scale isolation of plasmid DNA

Steps	Description
1)	A 50 ml *E. coli* culture was centrifuged at 4,500 rpm for 10 min
2)	After the supernatant was discarded, the pellet was resuspended in 3 ml Resuspension Solution
3)	3 ml Lysis Solution was added, inverted 3 times, and incubated for 3 min at room temperature
4)	3 ml Neutralization/Wash Solution was added and inverted 3 times
5)	4.5 ml technical ethanol was added and inverted 3 times
5)	The cell lysate was centrifuged for 25 min at 4,500 rpm
6)	The supernatant was transferred through a sieve into a new 50 ml reaction tube
7)	4.5 ml technical ethanol were added and the tube was inverted 3 times
8)	The solution was loaded onto a PureYield Binding Column, which was placed onto a vacuum manifold
9)	The liquid passed through the column by applying a vacuum (DNA bound to the column)
10)	1 x 5 ml Wash Solution as well as 2 x 10 ml Column Wash Solution was added and passed through the column
11)	The membrane of the column was dried by applying vacuum for at least 20 min. After removing the column, the tip of the column was dried with a paper towel to remove remaining ethanol The column was placed into a new 50 ml reaction tube, 600 µl H_2O were added, and incubated for 2 min
12)	The reaction tube with the column inside was centrifuged for 2 min at 1,500 rpm to elute the DNA

7.1.12 Ethanol precipitation of plasmid DNA

7.1.13 Preparative isolation of DNA fragments from agarose gels

First, DNA fragments were separated by electrophoresis in agarose gels. Thereafter, the gel was placed on a LED transilluminator to see DNA bands. A gel block containing the corresponding DNA was cut out with a scalpel and transferred into a 1.5 ml reaction tube. The DNA was isolated using the FastGene Gel/PCR Extraction Kit according to the manufacturer´s instructions.

7.1.14 Isolation of PCR products

PCR products were purified by the MSB Spin PCRapace Kit according to the manufacturer´s instructions.

7.1.15 Quantification of DNA

7.1.15.1 Quantification of DNA by photometric measurement

Both yield and purifity of isolated DNA was determined using the Fluorometer DS-11 FX+ from DeNovix. The purity was assessed by the 260/280 nm as well as the 260/230 nm absorbance ratio.

7.1.15.2 Quantification of DNA by gel analysis

If plasmids should be used for cell transfection, DNA quantification by photometric measurement (see section 7.1.15.1) was not precise enough. In this case, the plasmid concentration was additionally determined by gel analysis as follows. The corresponding plasmid DNA was digested by restriction endonucleases (see section 7.1.4) so that a DNA fragment of 2 – 3 kb was produced. After agarose gel electrophoresis, the corresponding DNA band was quantified based on its intensity and size. The bands of the DNA ladder for which the amount of DNA was known were used as a reference. The quantification was carried out using the software ImageJ.

7.1.16 Sequencing of plasmid DNA

Plasmids were sequenced by the company SeqLab. To this end, the following reaction mixture was used (see Table 29)

Table 29 | Reaction mixture for sequencing

Component	Amount
Plasmid DNA	600 ng
Primer	30 pmol
H_2O	Ad 12 µl
Total volume	**12 µl**

7.2 Protein Methods

7.2.1 SDS-PAGE

Proteins were separated based on their molecular weight by discontinuous sodium dodecyl sulfate polyacrylamide gel electrophoresis (SDS-PAGE) (Laemmli 1970). To this end, polyacrylamide gels were poured using an acrylamide gel system. Based on the protein size, the percentage for the gel was chosen. Protein samples were mixed with 2x Laemmli Sample Buffer (2xLSB) and subsequently boiled at 100 °C for 5 min. The samples as well as the protein ladder All Blue (BIO-RAD) were loaded onto the gel. Electrophoresis was conducted at 200 V for 60 min.

7.2.2 Western blot

After SDS-PAGE (see section 7.2.1) proteins in the polyacrylamide gel were electrophoretic transferred on a nitrocellulose membrane. To this end, a semi dry blotting system was used. Per gel two whatman paper

and a nitrocellulose membrane were soaked in transfer buffer 3. Thereafter, a blotting stack was assembled from cathode to anode in the following order: Whatman paper, polyacrylamide gel, nitrocellulose membrane. Blotting was carried out at 70 mA per gel for 90 min.

7.2.3 Immunostaining of Western blots

To detect specific proteins, which were blotted on a nitrocellulose membrane (see section 7.2.2), immunostaining was conducted. The following protocol was used for immunostaining.

Table 30 | Protocol for Immunostaining of Western blots

Steps	Description
1)	The nitrocellulose membrane was covered with Ponceau S staining solution and shaken for 20 min on a tilting shaker
2)	The membrane was washed 3 times with H2O. Thereafter, the membrane was scanned
3)	To block the membrane it was covered with milk powder solution and shaken for 30 min on a tilting shaker
4)	The membrane was washed 3 times with 5 ml PBST each
5)	The membrane was incubated with the corresponding primary antibody (5 ml PBST + antibody) for 90 min shaking at room temperature
5)	The membrane was washed 3 times with 5 ml PBST each
6)	The membrane was incubated with the corresponding secondary antibody (5 ml PBST + antibody) for 60 min shaking at room temperature. The box with the membrane was protected from light so that the fluorophore of the secondary antibody was not damaged
7)	The membrane was washed 3 times with PBS to remove unbound antibodies

After immunostaining the antibody labeled proteins were detected using an Odyseey Infrared System according to the manufacturer´s instructions. The scanned images were evaluated with the software ImageJ.

7.2.4 Detection of protein interaction partners by co-immunoprecipitation

Interaction between proteins was analyzed by co-immunoprecipitation (co-IP). To this end, either Protein G beads were used (see table 31).

Table 31 | Protocol for co-immunoprecipitations

Day	Steps	Description
Day 1	1)	*Drosophila* S2R+ cell were seeded in a 6-well plate
Day 2	1)	One well was transfected only with the plasmid, which expresses the prey protein (negative control). The remaining wells were additionally transfected with the plasmid that expresses the bait protein
Day 4	1)	The medium from the wells was carefully removed
	2)	Adherent cells were detached by adding 1 ml cold PBS and forcefully pipetting up and down. Thereafter, the cell suspension was transferred into a precooled 1.5 ml reaction tube
	3)	The cell suspension was centrifuged for 3 min at 2,500 rpm and 4 °C
	5)	The supernatant was discarded and the pellet was washed with 1 ml cold PBS
	6)	The suspension was centrifuged for 3 min at 2,500 rpm at 4 °C
	7)	The cells were resuspended in 500 µl cold lysis buffer (containing protease inhibitors) and incubated rotating for 20 min at 4 °C
	8)	Cell debris was pelleted by centrifuging for 15 min at 12,000 rpm and 4 °C
	9)	25 µl of the supernatant was transferred to a 1.5 ml reaction tube that contained 25 µl 2xLSB. The samples were incubated for 5 min at 100 °C (input samples)
	10)	The remaining supernatant was transferred into a 1.5 reaction tube and the antibody used for precipitation was added
	11)	The solution was incubated for 30 min rotating at 4 °C (antibody can bind to antigen). During this incubation time, the Protein G beads were prepared (see the following steps)
	12)	20 µl bead suspension of Protein G beads per well (+ 20 %) were transferred into a 1.5 ml reaction tube
	13)	The bead suspension was centrifuged for 1 min at 1,000 rpm
	14)	The supernatant was discarded (not complete to avoid removing the beads)
	15)	The beads were washed twice in 1 ml IP wash buffer
	16)	After removing the supernatant of the last washing step, the beads were resuspended in 100 µl IP wash buffer per well (+ 20 %)
	17)	100 µl bead suspension per well was transferred into individual eppis
	18)	The solution with the proteins and antibody (see step 11) was added to the bead suspension (see step 17) and incubated rotating overnight at 4 °C
Day 5	1)	The bead suspension was centrifuged for 1 min at 1,000 rpm and 4 °C and the supernatant was discarded
	2)	The beads were washed twice in IP wash buffer rotating for 10 min at 4 °C each
	3)	The beads were centrifuged for 1 min at 1,000 rpm and 4 °C. Thereafter, most of the liquid was removed with an Eppendorf pipette. The rest of liquid was removed with a syringe and a 24G needle (beads are bigger)
	4)	The beads were resuspended in 35 µl 2xLSB and incubated for 5 min at 100 °C (IP samples)

The input and IP samples (each 10 µl) were analyzed by SDS-PAGE and Western blot. Samples were loaded twice on two individual gels so that one membrane could be stained against the tag of the be prey protein and the other one against the tag of the bait protein.

7.2.5 Testing protein solubility

Before proteins were expressed in large-scale for purification, it was tested in small-scale at which temperature the expression and solubility of a protein of interest was best. Proteins were heterologously expressed in *E. coli* Rosetta™ pLysS strain using pET plasmids with T7 promotors. To this end, the following protocol was applied (see Table 32).

Table 32 | Protocol for testing protein solubility

Day	Steps	Description
Day 1	1)	LB medium (20 ml) containing Chloramphenicol (85 µg/ml) and a second antibiotic depending on the expression plasmid was inoculated with a transformed *E. coli* Rosetta colony.
	2)	The pre-culture was incubated overnight shaking at 37 °C and 140 rpm.
Day 2	1)	The OD_{600} value of the pre-culture was measured.
	2)	80 ml main culture (LB medium with the same antibiotics as the pre-culture) was inoculated with the pre-culture so that the OD_{600} value was 0.1.
	3)	The main culture was incubated shaking at 37 °C and 140 rpm until an OD_{600} of 0.4 – 0.6 was reached (after approx. 2 h)
	4)	The main culture was divided into four flasks with 20 ml culture each
	5)	To three of the cultures IPTG (1 mM) was added to induce protein expression (IPTG +). To the remaining culture no IPTG was added and served as a negative control (IPTG -).
	6)	The cultures were incubated overnight at the following temperatures: Culture 1 (IPTG -): 37 °C Culture 2 (IPTG+): 18 °C Culture 3 (IPTG+): 24 °C Culture 4 (IPTG+): 37 °C
Day 3	7)	The OD_{600} value of the four cultures was measured. Thereafter, 4 OD_{600} of each culture were harvested into 2 ml reaction tubes.
	8)	The cell suspensions were centrifuged at 14,000 rpm for 2 min at 4 °C. From here on, the samples were kept on ice.
	9)	The pellets were resuspended in 600 µl Buffer A of the corresponding protein purification method that was used afterwards (e.g. IMAC Buffer A in case of IMAC purification)
	10)	The cell suspensions were sonicated by a Sonopuls HD2070 for 4 min using 40 % pulse intensity and 40 % duty cycle. The samples were placed in an ice box during this process to avoid excessive heating.
	11)	20 µl of the obtained lysates were added to 20 µl 2xLSB each and incubated for 5 min at 100 °C (cell extract samples).
	12)	40 µl of the remaining cell suspensions were centrifuged for 2 min at 14,000 rpm and 4 °C.
	13)	20 µl of the supernatants were mixed with 20 µl 2xLSB each and incubated for 5 min at 100 °C (supernatant samples).
	14)	After the remaining supernatant was discarded, the pellets were resuspended in 40 µl 2xLSB each and incubated for 5 min at 100 °C (pellet samples).
	15)	To assess expression and solubility of the protein of interest, 10 µl of each sample were subjected to SDS-PAGE and subsequent Western blot analysis.

7.2.7 Large scale protein expression in *E. coli* Rosetta™ pLysS

After the temperature for best expression and solubility for a protein of interest in *E. coli* Rosetta™ pLysS was determined, the protein was expressed in larger quantities for subsequent protein purification. To this end, the following protocol was used (see Table 33).

Table 33 | Protocol for large scale protein expression in E. coli Rosetta pLysS

Day	Steps	Description
Day 1	1)	LB medium (50 ml) containing Chloramphenicol (85 µg/ml) and a second antibiotic depending on the expression plasmid was inoculated with a transformed *E. coli* Rosetta colony.
	2)	The pre-culture was incubated overnight shaking at 37 °C and 140 rpm.
	3)	The OD_{600} value of the pre-culture was measured.
	4)	1 L main culture (LB medium with the same antibiotics as the pre-culture) was inoculated with the pre-culture so that the OD_{600} value was 0.1. The main culture was incubated shaking at 37 °C and 140 rpm until an OD_{600} of 0.4 – 0.6 was reached (after approx. 2 h)
	5)	IPTG (1 mM) was added to the culture to induce protein expression
	6)	The culture was incubated overnight at 140 rpm and the temperature that turned out to be best for expression and solubility
Day 2	1)	The cell suspension was centrifuged for 10 min at 5,000 rpm at 4 °C.
	2)	The pellet was resuspended in 50 ml Buffer A of the corresponding protein purification method that was used afterwards (e.g. IMAC Buffer A in case of IMAC purification)
	3)	A protease inhibitor cocktail (1:1000) was added to the mixture
	4)	The cell suspension was sonicated for 8 min by a Sonifier Branson 250 D (40 % pulse intensity, pulse on: 2 sec, pulse off: 2 sec)
	5)	The cell lysate was centrifuged for 40 min at 14,000 rpm at 4 °C. Thereafter, the supernatant was transferred into a new centrifuge beaker and the centrifugation was repeated with the same settings.
	6)	The supernatant was filtered through a 0.2 µm filter into a 50 ml reaction tube.
	7)	50 µl of the filtered supernatant were added to 50 µl 2xLSB and incubated for 5 min at 100 °C (input sample)
	8)	The remaining filtered supernatant was applied to protein purification using the ÄKTA start

7.2.8 Protein purification using the ÄKTA start

The protein solution that was obtained in section 7.2.7, was subsequently used for protein purification (either affinity or ion exchange chromatography) using the ÄKTA start. To this end, the following protocol was used (Table 34).

Table 34 | protocol for purification of proteins using the ÄKTA start

	Steps	Description
System cleaning	1)	A flow rate of 5 ml/min was applied
	2)	Sample tubing was washed with 3 ml H_2O
	3)	System was washed with 5 ml H_2O
	4)	Fraction collection tubing was washed with 2 ml H_2O. The 2 ml H_2O were collected in a 2 ml reaction tube to check, whether all of the applied 2 ml H_2O was collected in the tube. If not, this was a sign that there was a constipation in the ÄKTA start and appropriate cleaning steps were applied.
Connecting the corresponding column	1)	Flow rate was set to 0.5 ml/min
	2)	The column was connected drop-to-drop
Connecting the sample	1)	The sample was stored in a 50 ml reaction tube. In the lid of this tube two holes were drilled.
	2)	Through one hole of the lid, the column tubing was inserted. The other hole was used to avoid negative pressure.
Equilibration of the column	1)	The Buffers A and B were connected to the ÄKTA start
	2)	A program was started that equilibrated the column with 5 column volumes (CV) of Buffer A (flow rate: 1 ml/min)
Sample application	1)	50 ml of the protein sample were loaded onto the column. In case of HisTrap and ion exchange columns a flow rate of 1 ml/min was applied. In case of GSTrap columns a flow rate of 0.5 ml/min was applied.
	2)	The flow-through was collected in 15 ml fractions
Wash out unbound	1)	To wash out unbound proteins 10 CV of Buffer A was applied (flow rate: 1 ml/min)
	2)	The flow-through was collected in one fraction
Elution and fractionation	1)	Elution started by applying a linear gradient of 0 – 60 % Buffer B (12 CV; flow rate: 1 ml/min)
	2)	Elution continued with a steeper gradient (60 % - 80 % Buffer B within 4 CV; flow rate: 1 ml/min)
	3)	The eluted protein was collected in 1 ml fractions
Column cleaning	1)	The column was cleaned applying 10 CV of Buffer B (flow rate: 1 ml/min)
Equilibration	1)	The column was equilibrated in 5 CV of Buffer A. If further proteins were purified, the protocol was repeated from the step “Connecting the sample” after the sample tubing was washed with 3 ml H_2O. Otherwise, the protocol continued with the steps shown below
Washing and storage	1)	The column was washed with 5 ml H_2O, followed with 3 ml 20 % ethanol (flow rate: 1 ml/min)
	2)	The flow rate was set to 0.5 ml/min
	3)	The column was dismounted drop-to-drop and stored at 4 °C
System cleaning	1)	The flow rate was set to 5 ml/min
	2)	Sample tubing was washed with 3 ml 20 % ethanol
	3)	System was washed with 10 ml 20 % ethanol
	4)	Fraction collection tubing was washed with 2 ml 20 % ethanol

Based on the UV sensor (280 nm) of the ÄKTA start a chromatogram was recorded. This chromatogram allowed to assess in which fractions protein was present. Each 20 µl of these 1 ml fractions were mixed with 20 µl 2xLSB and incubated for 5 min at 100 °C. The rest of the fractions was stored at 4 °C. The samples were analyzed by SDS-PAGE and subsequent Coomassie staining. Depending on the purity as well as the amount of protein, certain fractions were subjected to subsequent dialysis (see section 7.2.9).

7.2.9 Dialysis of proteins

Usually the buffer in which the protein was present after protein purification was not suited for subsequent experiments. Therefore, the buffer was exchanged using dialysis with GeBAflex Midi tubes

(molecular cutoff: 6-8 kDa). To this end, the GeBAflex tube was first filled with 1 ml H_2O and incubated for 5 min. Thereafter, the water was removed and replaced with 1 ml of a protein fraction. The tube was inserted into a floating rack and placed in a beaker with 500 ml of dialysis buffer and incubated for at least 3 h at 4 °C under stirring. Thereafter, the buffer in the beaker was replaced by fresh dialysis buffer and the tube was incubated once more for at least 3 h at 4 °C. Thereafter, the protein solution was transferred into a new 1.5 ml reaction tube and used for subsequent experiments.

7.2.10 Measuring protein concentration

To determine the protein concentration of a (dialyzed) protein fraction the Bradford assay was used. To this end, the following protocol was used (see table 35).

Table 35 | Protocol for the Bradford assay

Steps	Description
1)	Bio-Rad Protein Assay Dye Reagent Concentrate (Bradford solution) was diluted with H_2O in a 1:16 ratio (800 µl per sample)
2)	A solution with 1 mg/ml BSA was made
3)	The following volumes (µl) of the BSA solution were mixed with each 800 µl diluted Bradford solution in a plastic cuvette: 1.6, 2.8, 4, 5, 6, 8
4)	The OD_{595} value of the different BSA solutions was measured to create a reference line depicting the dependency of the OD_{595} value on the protein concentration
5)	Different volumes of the protein fraction were mixed with 800 µl diluted Bradford solution. It was tried to find volumes that resulted in staining intensities that were comparable with those of the BSA solutions. Thereafter, the OD_{595} value of these protein solutions was determined.
6)	The protein concentration of the protein fraction was calculated based on the BSA reference line.

7.2.11 *Drosophila* APC/C *in vitro* ubiquitination assay

By means of an Drosophila APC/C in vitro ubiquitination assay it was determined, whether potential substrates of APC/C-Fzr, are ubiquitinated by this E3 *in vitro*. All proteins required for the assay with the exception of APC/C-Fzr were obtained by heterologous expression in *E. coli* Rosetta. Thereafter, the proteins were purified using an ÄKTA start (see section 7.2.8). The following proteins were purified and used for the assay: 6xHis-4xFLAG-Ubiquitin, 6xHis-Uba1 (E1), 6xHis-Vihar (E2), 6xHis-10xHA-CHE (control for potential substrate 6xHis-10xHA-CHE_Rca1_204-299) and 6xHis-10xHA-CHE-Rca1_204-299. In contrast, APC/C-Fzr was obtained by co-immunoprecipitation using *Drosophila* embryos that expressed a tagged APC/C subunit: Cdc16-MYC-TEV-GFP. To enrich APC/C-Fzr, but not APC/C-Fzy, we used *Drosophila* embryos that were incubated for 17 hours at 18 °C. At these stages, most cells in the embryo are in the G1

state and the APC/C is mainly associated with Fzr, but not Fzy (Raff et al. 2002). The *Drosophila* embryos were homogenized and lysed. Thereafter, APC/C-Fzr was coprecipitated via precipitation of Cdc16-MYC-TEV-GFP using GFP nanobodies coupled to Affi-Gel beads (BIO-RAD). The proteins expressed in *E.coli* as well as the Affi-Gel beads with APC/C-Fzr were mixed and shaken for 1 hour at 30 °C. Thereafter, the reaction was stopped by adding 2xLSB. The samples were incubated for 5 min at 100 °C and subsequently used for SDS-PAGE and Western blot. To prove that precipitation of Cdc16-MYC-TEV-GFP was successful, this protein was detected via Western blot using anti-GFP antibodies.

7.3 Cell culture methods

7.3.1 Cultivation of *Drosophila* S2R+ cells

Drosophila S2R+ cells were cultivated in 75 cm^2 tissue flasks, which contained 14 ml complete Schneider´s *Drosophila* medium. The cells were incubated at 27 °C and split twice a weak (see section 7.3.1.1).

7.3.1.1 Splitting of cells

Cells were splitted twice a week into tissue flasks containing fresh complete Schneider´s *Drosophila* medium. This ensured constant cell growth and optimal supply with nutrients. The procedure for splitting was as follows (see table 36).

Table 36 | Protocol for splitting of cells

Steps	Description	Amount for 25 cm^2 tissue flask	Amount for 75 cm^2 tissue flask
1)	The old medium was removed from the cells	-	-
2)	The cells were washed carefully with PBS so that detached cells (dead cells) were removed but not the adherent cells	2.5 ml	5 ml
3)	Trypsin/EDTA solution was added and incubated for 2 min at room temperature	2 ml	5 ml
4)	The adherent cells were detached by pipetting up and down	-	-
5)	The cell suspension was transferred to a 15 ml reaction tube and centrifuged at 2,000 rpm for 2 min.		
6)	After the supernatant was discarded, the cells were resuspended in complete Schneider´s medium	4 ml	8 ml
7)	Fresh complete Schneider´s medium was added to a new flask		
8)	Cell suspension was added to the flask	1 ml	2.5 ml

7.3.1.2 Determination of cell numbers

To determine the number of *Drosophila* S2R+ cells, a Fuchs-Rosenthal counting chamber (total area: 16 mm; depth: 0.2 mm; cubic content: 3.2 µl; number of small square chambers: 256) was used. 80 µl Trypan-Blue solution (1:1 mix H_2O: Trypan-Blue) was added to 20 µl cell suspension and incubated for 2 min. This staining allowed the discrimination of living from dead cells. The mixture was transferred into the counting

chamber and the number of cells within a small square was counted using a microscope. The cells of 16 squares were counted in this manner. The mean value of cells within one square was used to calculate the cell density according to the following formula:

$$\frac{mean\ value\ of\ counted\ cells\ per\ square\ \times dilution\ factor}{area\ [mm^2] \times depth\ [mm]} = X \times 10^6 \left[\frac{cells}{ml}\right]$$

7.3.1.3 Seeding of cells

After splitting (see section 7.3.1.1) the cells were seeded in 6-well (for co-IPs) or in 12-well (for flow cytometry analysis) plates. Following cell numbers and amount of complete Schneider´s *Drosophila* medium was used for this purpose (see table 37). The volume for inoculation was calculated based on the previously determined cell number (see section 7.3.1.2).

Table 37 | Protocol for seeding of cells

Microwell plate	Cell number	Amount of medium
6-well plate	450,000	3 ml
12-well plate	125,000	1.5 ml

7.3.2 Transfection of cells

Drosophila S2R+ cells were transiently transfected 24 h after seeding. The transfection mixture was dependent on whether a 6- or 12-well plate was used (see table 38).

Table 38 | Mixture for transfection

Component	Amount for 6-well plate	Amount for 12-well plate
Plasmid DNA	600 ng	200 ng
Schneider´s *Drosophila* medium	Ad 150 µl	Ad 75 µl
Total volume	150 µl	75 µl
FuGENE HD	3 µl	1 µl

Transfection was carried out as follows (see table 38).

Table 39 | Protocol for transfection of S2R+ cells

Steps	Description
1)	FuGENE HD is vortexed for 20 sec
2)	The mixture for transfection is prepared (table 38). After adding FuGENE HD, the mix is immediately vortexed for 3 sec
3)	The mixture is incubated for 15 min at room temperature
4)	After the mixture was added into each well, the plate was gently moved to allow equal distribution of the mix in the medium

7.3.4 Cell preparation

7.3.4.1 Cell preparation for flow cytometry

The stability of proteins during the cell cycle was determined in transiently transfected *Drosophila* S2R+ cells by flow cytometry. This method was applied 3 days after transfection. The preparation of the cells for flow cytometry (see section 7.4) was conducted as follows (see table 40).

Table 40 | Protocol for cell preparation for flow cytometry

Steps	Description
1)	6.4 µl Hoechst were added to each well of a 12-well plate. To allow distribution of Hoechst in the medium the plate was gently moved and incubated for at least 20 min.
2)	The medium of the first 4 wells was removed.
3)	The first 4 wells were washed gently with 1 ml PBS to remove remaining detached (dead) cells.
4)	1 ml Trypsin/EDTA solution containing 6.4 µl Hoechst was added to the first 4 wells.
5)	The cells of the first well were detached by forcefully pipetting up and down and subsequently transferred through a filter into a 3.5 ml glas tube.
6)	400 µl PBS were passed through the filter and added to the glas tube.
7)	If the sample should also be analyzed by Western blot, 300 µl of the cell suspension were transferred into a 1.5 ml reaction tube and centrifuged at 2,500 rpm for 2 min 30 sec. The pellet was resuspended in 40 µl 2xLSB and incubated for 5 min at 100 °C.
8)	The cell suspension was used for flow cytometry analysis
9)	Steps 5) - 8) were repeated for the remaining 3 wells. After preparation of well 3, the next 4 wells of the plate were prepared as described in the steps 2) – 8). This procedure was repeated for all remaining wells

7.4 Flow cytometry of S2R+ cells

7.4.1 Procedure for measurement

Transiently transfected *Drosophila* S2R+ cells were analyzed by flow cytometry with a Sysmex/Partec CyFlow Space cytometer. An overview of the whole workflow can be found in **Figure 62**. The fluorescence of Hoechst, GFP and CHE were detected using the following light sources and optical filters (see Table 41). To identify single cells, forward and side scatter signals (FSC/SSC) were used.

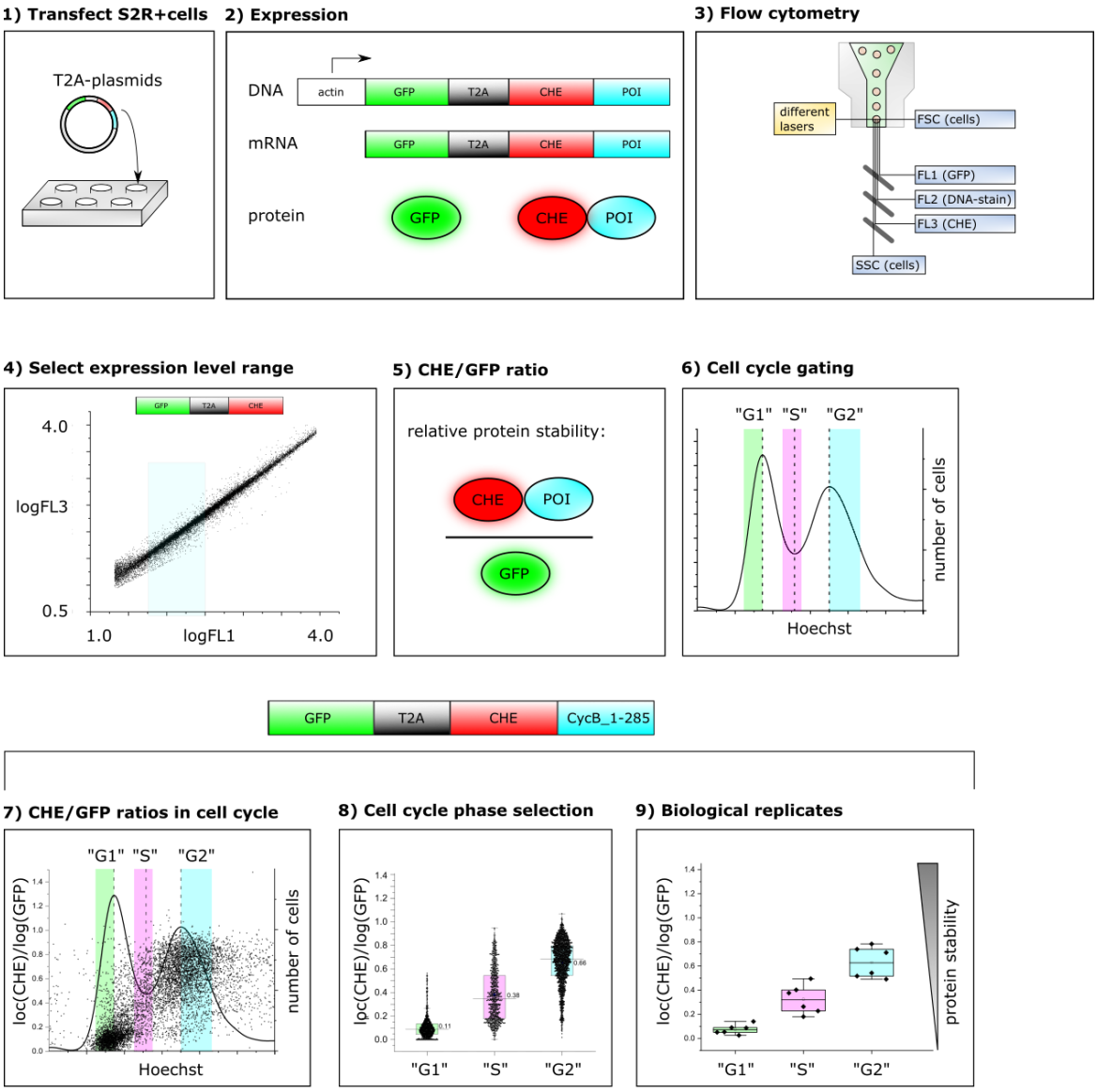

Figure 62 | Workflow for the RPS system

1) *Drosophila* S2R+ cells were transiently transfected with T2A-plasmids. **2)** These T2A-plasmids allowed the stoichiometrical expression of two proteins under the control of one promoter. We expressed GFP as a reference protein as well as a protein of interest (POI) fused to CHE. **3)** The transiently transfected cells were analyzed by flow cytometry. Different excitation lasers and detection filters (see also Table 41) were used to measure the fluorescence of GFP (FL1), DNA-stain (Hoechst; FL2) and CHE (FL3). FSC (forward scatter) and SSC (side scatter) were used to determine, whether signals derived from *Drosophila* cells. **4)** For the evaluation of our flow cytometry data we did not take all the measured signals into account. Rather, we analyzed only cells within a certain expression level range so that meaningful results could be obtained. **5)** We used the ratio of CHE to GFP signal to assess the relative protein stability of our POI. **6)** By measuring the DNA content via the Hoechst signal we were able to determine in which cell cycle phase the measured cells were. Certain areas (green, red, blue) were defined in which cells were most likely in G1, S and G2 phase. However, this classification can never be absolutely accurate. That is why G1, S and G2 are written in quotation marks. For instance, in "G1" there are also some cells, which are in early S phase. **7)** By combining step 5) and 6) the relative protein stability could be assessed for each cell cycle phase individually. The black curve represents the number of cells during the cell cycle. The black dots represent the log(CHE)/log(GFP) values for the protein CycB_1-285 fused to CHE. Most data points in "G1" are small, while the data points in "S" and "G2" are higher indicating that CycB_1-285 is primarily degraded in G1 phase. **8)** The log(CHE)/log(GFP) values (black dots) of all analyzed cells, which were part of a certain selection ("G1", "S", "G2") were represented as plots. The mean of these datapoints was used for the next step. **9)** The mean of the datapoints from 8) was considered as one replicate. To increase the meaningfulness of our analysis we conducted several replicates and used them for statistical evaluation.

Table 41 | Light sources and optical filters for CyFlow Space

Fluorophore	Excitation laser	Detection filter
Hoechst 33342	365 nm High Power UV-LED	FL2 – Bandpass filter BP 455/50
GFP	488 nm blue solid state laser	FL1 – Bandpass filter BP 527/30
CHE	561 nm yellow laser	FL3 – Bandpass filter BP 630/75
Scatter parameters	**Excitation laser**	**Detection filter**
Forward scatter	488 nm blue solid state laser	Longpass filter IBP 488
Side scatter	488 nm blue solid state laser	Longpass filter IBP 488

7.4.2 Gating of cell populations and data export

The raw data, which was collected by the CyFlow Space, was imported into the software FCS express. To identify single cells a “cell” gate based on the FSC and SSC signals was used. This was possible, since the size and granularity of particles are reflected in certain FSC and SSC values. Particles other than single cells such as not separated cells (cell aggregates), cell debris and other contaminations result in FSC and SSC values which are outside the “cell” gate. Furthermore, a “DNA” gate was used to discriminate the Hoechst signal from other signals in the FL2 channel. Doublet discrimination (e.g. two cells stuck together) was achieved based on the signal height and width of the Hoechst signal. The combination of “cell” and “DNA” gate (referred to as “cells-DNA”) was applied to identify single cells with Hoechst signal (**Figure 63**). The values for the FL1, FL2 and FL3 channel within the gate “cells-DNA” were exported in the file format comma-separated value (csv). Subsequently, the csv files were important into the software *OriginLab* and certain macros were applied for the evaluation of the data (chapter 7.4.3).

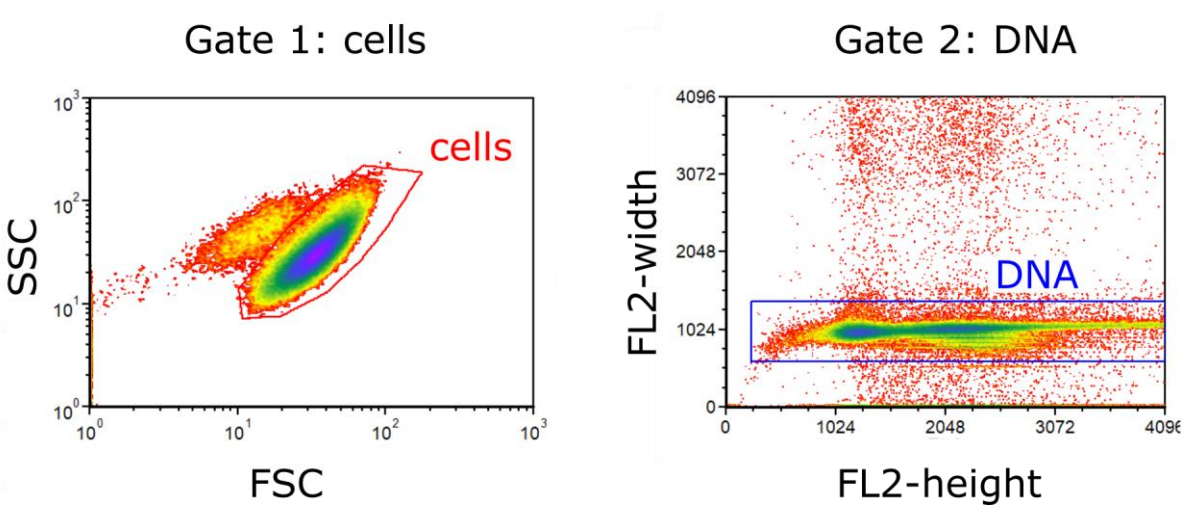

Figure 63 | Identification of individual cells by means of the gates "cells" and "DNA"
Using the FSC and the SSC values cells were selected based on their size and granularity (gate 1: cells). Using the peak height and width of the Hoechst signal (FL2) cells were selected based on their DNA content (gate 2: DNA). Gate 1 and 2 were combined resulting in the gate “cells and DNA”. Thereafter, all values for DNA (FL2), GFP (FL1), CHE (FL3) in the combination gate “cells and DNA” were exported and used for further evaluation using the software OriginLab (chapter 7.4.3).

7.4.3 Analysis of flow cytometric data using OriginLab

The csv files, which were created previously (chapter 7.4.2), were subsequently analyzed using the software *OriginLab*. The files were imported into the OriginLab file “FACS-template-58.opju”. Thereafter, the macros “Hoechst-Com” and “workflow-script-T57” were applied. These macros executed the following commands (see Table 42):

Table 42 | Commands of macros, which were used for the evaluation of flow cytometry data in OriginLab

Steps	Description
1)	Compensation for DNA (Hoechst) signal detected in GFP (FL1) channel: A script (written in Labtalk) is used. First, the function "nlfit" is applied to fit a sigmoidal curve to the data. Second, the script calls a python file that uses the fitted curve and the Hoechst signal of the data to iteratively remove background GFP signal
2)	Determine background for GFP signal (and similarly for CHE signal) using non-transfected cells, sort FL1 values, determine FL1 value of the first 99.5 % of cells
3)	Set positive GPF (FL1) value: FL1 values that are at least 5% above the background signal
4)	Split cells in "positive" and "negative" for GFP (FL1)
5)	Calculate cell cylce distribution curves for all negative cells determine first and second peak values
6)	Cell cycle gating. DNA value ranges for the different gates "G1", "S" and "G2" were defined as follows: "G1" = first peak value – 300; "S" = value of lowest point between peaks -200 to + 100; "G2" = second peak value + 500
7)	Splitting of data (cells) into "G1", "S" and "G2" and "all" population
8)	Selection of low-medium expression level range for further analysis and splitting of cells into different expression level ranges
9)	Calculation of GFP/CHE ratio for determination of relative protein stability index value. We use the log(GFP) and log(CHE) values (see also chapter 7.4.4). log(FL3 (CHE))/log(FL1 (GFP)) represents the relative protein stability index.
10)	The values of each cell can be displayed in a box-plot, e.g. a box plot in which "G2" cells that express CHE-CyclinB_1-285 are expressed and RNAi against Rca1 was performed.
11)	The mean of all datapoints is calculated and is used as one datapoint for the summary barplots shown in this thesis.

7.4.4 The meaning of relative protein stability values

To represent the relative stability of a protein of interest fused to CHE compared to the reference protein GFP, a logarithmic scale was chosen. There are a couple of reasons why a logarithmic scale instead of a linear scale is better suited for that purpose: A logarithmic scale enables the representation of a large data range on a single graph without losing to much resolution of small changes. This high resolution by a logarithmic scale is achieved, since smaller values are expanded while larger values are compressed. This allows us to detect alterations in protein stability better. On the other hand, it can also be challenging to intuitively interpret logarithmic scales correctly. Therefore, the following explains how to interpret changes of the relative protein stability values in this thesis correctly.

The relative protein stability of a protein of interest (POI) fused to CHE is represented by the log(CHE)/log(GFP) value. For our evaluation we used multivariant measurements (each one consisting of one signal for GFP, CHE, and Hoechst, respectively) in which the value for GFP was between 56 (log(56) = 1.75) and 316 (log(316) = 2.5). Within this range (1.75-2.5) for GFP values and their corresponding CHE values within individual cells, the log(CHE)/log(GFP) value was determined. For instance, if the GFP value was 316 and the CHE value was 237, the calculation was as follows: log(CHE)/log(GFP) = log(237)/log(316)

= 2.37/2.5 = 0.95. We refer to this value also as a "stability index". If this log(CHE)/log(GFP) value is below 1, this means that the value for CHE is lower than the one for GFP. If the log(CHE)/log(GFP) value would be exactly 1, the GFP and CHE values are identical (e.g. log(316)/log(316) = 1). Therefore, in the example above (log(CHE)/log(GFP) =0.95) it can be concluded that less POI fused to CHE is in the cells. This is in our experiments most likely caused by increased degradation of the POI since transcriptional and translational changes should not be induced. In most cases, we were interested in the relative change in the stability of a POI under certain experimental condition, e.g. after overexpression of another protein. In this case, we compare the stability values in the reference setup and in the experimental setup. As an example, our CHE-tagged protein of interest (POI) has a stability index of 0.95. After overexpression of another protein, the stability index drops to 0.9. This means that less POI is present in the cells and the difference is again likely caused by degradation. One can also determine from this difference in the log values the actual amount of degradation. For this, a calibration curve was calculated. To create the calibration graph, for each log(CHE)/log(GFP) difference of 0.05 the associated degradation in % was looked up (in total 19 steps from the start 1.0 till 0.1; 1, 0.95, 0.9, …) (**Figure 64**). This was done for all possible reference protein (GFP) level situations from level of 56 (log(56) = 1.75) to 316 (log(316) = 2.5). Due to the logarithmic values, each log difference resulted in a certain range of degradation. For the calculation of the calibration curve, the average of this degradation range was used. Using a polynomal fit calculation in the Origin program, the following formula was obtained: y = y0 + A*exp(R0*x), where y is the degradation rate in %, y0 the y-intercept (99.53829), A the scaling factor (-99.62054), R0 the growth rate (exponential factor; -5.087) and x is 1 minus the corresponding log(CHE)/log(GFP) value.

In case of our example with a control stability index of the POI of 0.95 and then dropping to a stability index of 0.9 in the experimental situation, one can determine the relative degradation as follows: Stability index of 0.9 relates to 40 % less protein level than GFP and stability index of 0.9 relates to 53 % less protein level compared to GFP. Thus, under the experimental condition, 13 % (53 % - 40 %) less of the POI is present and we assume, that this is caused by the induced degradation of the POI. Starting with a different starting stability index, for example 0.7 and then dropping to 0.65 means that 5 % less protein is present (0.7 represent 78 % less protein, 0.65 represents 83 % less protein (compared to GFP) and the difference is then 5 %. These two samples highlight the nonlinear logarithmic way how the data is presented. This has the advantage that effects on proteins with a high starting turnover rate (e.g. starting stability index is already low) can be displayed.

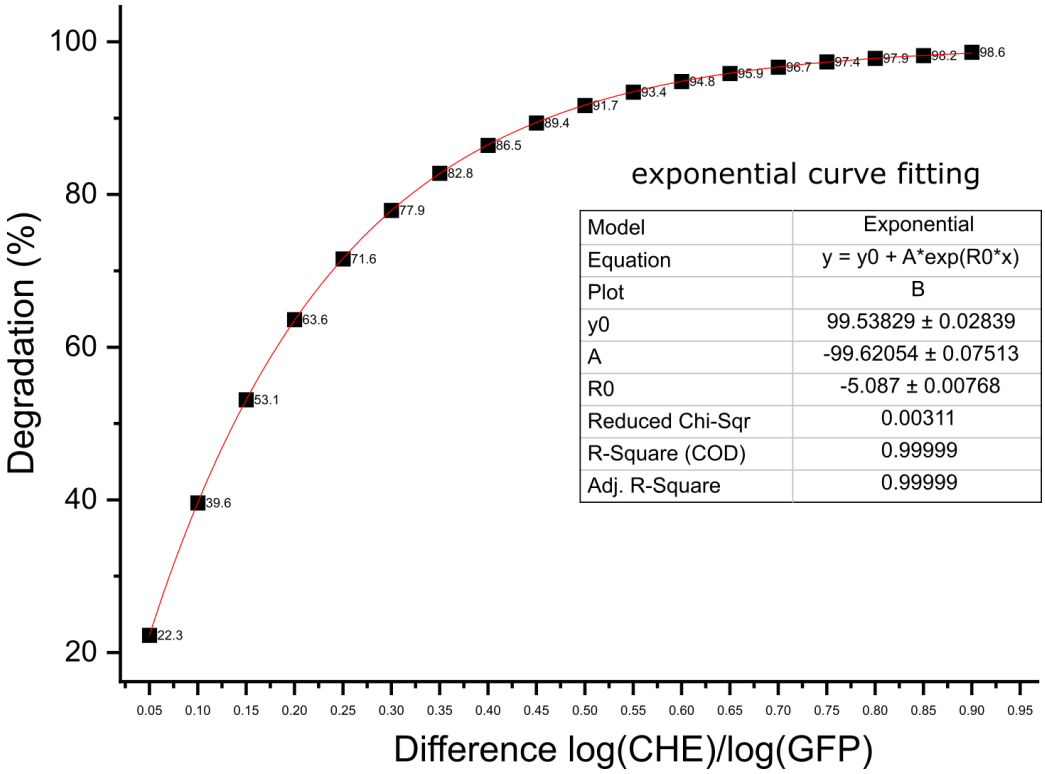

Figure 64 | Calibration curve and formula that allows calculation of degradation in % based on log(CHE)/log(GFP) values
To allow the calculation of the percentage degradation of a protein of interest under an experimental condition, the log(CHE)/log(GFP) values were backtraced to the fluorescent protein values. For each log(CHE)/log(GFP) difference of 0.05, the associated degradation (in %) was looked up for all different fluorescent reference protein values of GFP (56 - 312). In total, 19 log steps (1, 0.95, 0.9, …, 0.1) were included. For each difference in log values, a certain range in degradation is obtained, depending on the initial reference values (log 1.75 - 2.5). Each individual degradation rate is shown within a box as a dot. The difference log(CHE)/log(GFP) refers to the value log(CHE)/log(GFP) = 1. For instance, let's assume our protein of interest has a log(CHE)/log(GFP) value of 0.9 in the reference level and a log(CHE)/log(GFP value of 0.85 in an experimental level. The reference protein level is therefore 40 % less of GFP level and in the experimental situation the protein level is 53 % less compared to GFP. Thus, in the experimental situation, 13 % of the protein of interest was degraded.

7.4.5 Representation of data

The flow cytometry data (see step 11 in table 42) was depicted as barplots. The right end of the barplot represents the mean of the dataset. The error bar shows the confidence interval (probability: 95%).

7.4.6 Statistical analysis

To conduct statistical analysis the software R-studio was used. First, it was tested whether data sets were normal distributed with the Shapiro-Wilk test. In case of normal distribution Welch´s t-test was performed. If at least one dataset was not normally distributed, the Mann-Whitney-U-test was used.

8. List of Figures

9. List of Tables

10 Abbreviations

Table 43 | Abbreviations

Abbreviation	Expansion
µ	micro
AG	“Arbeitsgruppe” (workgroup)
AMP	adenosine monophosphate
APC/C	Anaphase promoting complex/Cyclosome
ATP	adenosine triphosphate
bp	base pair
Cdk	Cyclin dependent kinase
CKI	Cyclin-dependent kinase inhibitor
CRL	Cullin-RING ubiquitin ligase
C-terminal	carboxy-terminal
co-IP	co-immunoprecipitation
Cyc	Cyclin
Da	Dalton
D-box	destruction box
dFbox	deleted F-box
DNA	deoxyribonucleic acid
dNTP	deoxynucleotide triphosphate
dPIP	deleted PIP degron
DUB	deubiquitinating enzyme
E. coli	*Escherichia coli*
e.g.	exempli gratia (for example)
et al.	et alii
FBS	fetal bovine serum
FSC	forward scatter
g	gram
G1	gap1
G2	gap2
GFP	green fluorescent protein
h	hour
H_2O	water
HA	haemagglutinin
LB	Luria Broth
log	logarithm
min	minute(s)
mRNA	messenger RNA
MS	mass spectrometry
n	nano
Ni-NTA	nickel(II)-nitrilotriacetic acid
NLS	nuclear localization signal
N-terminal	amino-terminal
PAGE	polyacrylamide gel electrophoresis
PBS	phosphate buffer saline
PCR	polymerase chain reaction
PIP	PCNA interacting protein
RNA	ribonucleic acid
rpm	rounds per minute
SCF	Skp/Cullin/F-box complex
sec	seconds
Abbreviation	**Expansion**
SSC	side scatter

TAE	Tris/Acetate/EDTA
TEV	Tobacco Etch Virus
UBA	ubiquitin-associated
UTR	untranslated region
UV	ultra violette
V	voltage
WB	western blot
WT	wild type
ZBR	zinc-binding region

11 Single and three letter code for amino acids

Table 44 | Single and three letter for amino acids

One letter code	Three letter code	Amino acid
A	Ala	Alanine
C	Cys	Cysteine
D	Asp	Aspartate
E	Glu	Glutamate
F	Phe	Phenylalanine
G	Gly	Glycine
H	His	Histidine
I	Ile	Isoleucine
K	Lys	Lysine
L	Leu	Leucine
M	Met	Methionine
N	Asn	Asparagine
P	Pro	Proline
Q	Gln	Glutamine
R	Arg	Arginine
S	Ser	Serine
T	Thr	Threonine
V	Val	Valine
W	Trp	Tryptophan
Y	Tyr	Tyrosine

12 References

Abbas, Tarek; Dutta, Anindya (2009): p21 in cancer: intricate networks and multiple activities. In *Nature reviews. Cancer* 9 (6), pp. 400–414. DOI: 10.1038/nrc2657.

Abbas, Tarek; Dutta, Anindya (2011): CRL4Cdt2: master coordinator of cell cycle progression and genome stability. In *Cell cycle (Georgetown, Tex.)* 10 (2), pp. 241–249. DOI: 10.4161/cc.10.2.14530.

Abbas, Tarek; Sivaprasad, Uma; Terai, Kenta; Amador, Virginia; Pagano, Michele; Dutta, Anindya (2008): PCNA-dependent regulation of p21 ubiquitylation and degradation via the CRL4Cdt2 ubiquitin ligase complex. In *Genes & development* 22 (18), pp. 2496–2506. DOI: 10.1101/gad.1676108.

Abukhdeir, Abde M.; Park, Ben Ho (2008): P21 and p27: roles in carcinogenesis and drug resistance. In *Expert reviews in molecular medicine* 10, e19. DOI: 10.1017/S1462399408000744.

Akutsu, Masato; Dikic, Ivan; Bremm, Anja (2016): Ubiquitin chain diversity at a glance. In *Journal of cell science* 129 (5), pp. 875–880. DOI: 10.1242/jcs.183954.

Alexander, Karen E.; Rizkallah, Raed (2017): Aurora A Phosphorylation of YY1 during Mitosis Inactivates its DNA Binding Activity. In *Sci Rep* 7 (1), p. 10084. DOI: 10.1038/s41598-017-10935-5.

Alfieri, Claudio; Zhang, Suyang; Barford, David (2017): Visualizing the complex functions and mechanisms of the anaphase promoting complex/cyclosome (APC/C). In *Open biology* 7 (11). DOI: 10.1098/rsob.170204.

Amador, Virginia; Ge, Sheng; Santamaría, Patricia G.; Guardavaccaro, Daniele; Pagano, Michele (2007): APC/C(Cdc20) controls the ubiquitin-mediated degradation of p21 in prometaphase. In *Molecular cell* 27 (3), pp. 462–473. DOI: 10.1016/j.molcel.2007.06.013.

Araki, Marito; Wharton, Robin P.; Tang, Zhanyun; Yu, Hongtao; Asano, Maki (2003): Degradation of origin recognition complex large subunit by the anaphase-promoting complex in Drosophila. In *The EMBO journal* 22 (22), pp. 6115–6126. DOI: 10.1093/emboj/cdg573.

Bach, Richard (2021): Regulation of cell division in Drosophila. 6-week master module.

Badciong, James C.; Haas, Arthur L. (2002): MdmX is a RING finger ubiquitin ligase capable of synergistically enhancing Mdm2 ubiquitination. In *The Journal of biological chemistry* 277 (51), pp. 49668–49675. DOI: 10.1074/jbc.M208593200.

Ban, Kenneth H.; Torres, Jorge Z.; Miller, Julie J.; Mikhailov, Alexei; Nachury, Maxence V.; Tung, Jeffrey J. et al. (2007): The END network couples spindle pole assembly to inhibition of the anaphase-promoting complex/cyclosome in early mitosis. In *Developmental Cell* 13 (1), pp. 29–42. DOI: 10.1016/j.devcel.2007.04.017.

Bansal, Shivangee; Tiwari, Swati (2019): Mechanisms for the temporal regulation of substrate ubiquitination by the anaphase-promoting complex/cyclosome. In *Cell Div* 14 (1), p. 14. DOI: 10.1186/s13008-019-0057-5.

Bard, Jared A. M.; Goodall, Ellen A.; Greene, Eric R.; Jonsson, Erik; Dong, Ken C.; Martin, Andreas (2018): Structure and Function of the 26S Proteasome. In *Annual review of biochemistry* 87, pp. 697–724. DOI: 10.1146/annurev-biochem-062917-011931.

Bassermann, Florian; Eichner, Ruth; Pagano, Michele (2014): The ubiquitin proteasome system - implications for cell cycle control and the targeted treatment of cancer. In *Biochimica et biophysica acta* 1843 (1), pp. 150–162. DOI: 10.1016/j.bbamcr.2013.02.028.

Bennett, Eric J.; Rush, John; Gygi, Steven P.; Harper, J. Wade (2010): Dynamics of cullin-RING ubiquitin ligase network revealed by systematic quantitative proteomics. In *Cell* 143 (6), pp. 951–965. DOI: 10.1016/j.cell.2010.11.017.

Berger, Daniel (2017): Establishment of the CRISPR/Cas9 method for endogenous protein tagging to perform APC/C activity assays. master thesis.

Berghammer, H.; Auer, B. (1993): "Easypreps": fast and easy plasmid minipreparation for analysis of recombinant clones in E. coli. In *BioTechniques* 14 (4), 524, 528.

Besson, Arnaud; Dowdy, Steven F.; Roberts, James M. (2008): CDK inhibitors: cell cycle regulators and beyond. In *Developmental Cell* 14 (2), pp. 159–169. DOI: 10.1016/j.devcel.2008.01.013.

Birnboim, H. C.; Doly, J. (1979): A rapid alkaline extraction procedure for screening recombinant plasmid DNA. In *Nucleic acids research* 7 (6), pp. 1513–1523. DOI: 10.1093/nar/7.6.1513.

Bivik Stadler, Caroline; Arefin, Badrul; Ekman, Helen; Thor, Stefan (2019): PIP degron-stabilized Dacapo/p21Cip1 and mutations in ago act in an anti- versus pro-proliferative manner, yet both trigger an increase in Cyclin E levels. In *Development (Cambridge, England)* 146 (13). DOI: 10.1242/dev.175927.

Bloom, Joanna; Cross, Frederick R. (2007): Multiple levels of cyclin specificity in cell-cycle control. In *Nature reviews. Molecular cell biology* 8 (2), pp. 149–160. DOI: 10.1038/nrm2105.

Boehm, E. M.; Gildenberg, M. S.; Washington, M. T. (2016): The Many Roles of PCNA in Eukaryotic DNA Replication. In *The Enzymes* 39, pp. 231–254. DOI: 10.1016/bs.enz.2016.03.003.

Boehm, Elizabeth M.; Washington, M. Todd (2016): R.I.P. to the PIP: PCNA-binding motif no longer considered specific: PIP motifs and other related sequences are not distinct entities and can bind multiple proteins involved in genome maintenance. In *Bioessays* 38 (11), pp. 1117–1122. DOI: 10.1002/bies.201600116.

Braun, Tamara Evans; Poole, Emma; Sinclair, John (2012): Depletion of cellular pre-replication complex factors results in increased human cytomegalovirus DNA replication. In *PloS one* 7 (5), e36057. DOI: 10.1371/journal.pone.0036057.

Brown, Nicholas G.; Watson, Edmond R.; Weissmann, Florian; Jarvis, Marc A.; VanderLinden, Ryan; Grace, Christy R. R. et al. (2014): Mechanism of polyubiquitination by human anaphase-promoting complex: RING repurposing for ubiquitin chain assembly. In *Molecular cell* 56 (2), pp. 246–260. DOI: 10.1016/j.molcel.2014.09.009.

Bruning, John B.; Shamoo, Yousif (2004): Structural and thermodynamic analysis of human PCNA with peptides derived from DNA polymerase-delta p66 subunit and flap endonuclease-1. In *Structure (London, England : 1993)* 12 (12), pp. 2209–2219. DOI: 10.1016/j.str.2004.09.018.

Buetow, Lori; Huang, Danny T. (2016): Structural insights into the catalysis and regulation of E3 ubiquitin ligases. In *Nature reviews. Molecular cell biology* 17 (10), pp. 626–642. DOI: 10.1038/nrm.2016.91.

Bulatov, Emil; Ciulli, Alessio (2015): Targeting Cullin-RING E3 ubiquitin ligases for drug discovery: structure, assembly and small-molecule modulation. In *The Biochemical journal* 467 (3), pp. 365–386. DOI: 10.1042/BJ20141450.

Camelo-Prieto, Diana Lorena (2022): Analysis of Dap degradation pathways during the cell-cycle in *Drosophila melanogaster*.

Cappell, Steven D.; Mark, Kevin G.; Garbett, Damien; Pack, Lindsey R.; Rape, Michael; Meyer, Tobias (2018): EMI1 switches from being a substrate to an inhibitor of APC/CCDH1 to start the cell cycle. In *Nature* 558 (7709), pp. 313–317. DOI: 10.1038/s41586-018-0199-7.

Cavadini, Simone; Fischer, Eric S.; Bunker, Richard D.; Potenza, Alessandro; Lingaraju, Gondichatnahalli M.; Goldie, Kenneth N. et al. (2016): Cullin-RING ubiquitin E3 ligase regulation by the COP9 signalosome. In *Nature* 531 (7596), pp. 598–603. DOI: 10.1038/nature17416.

Cenciarelli, C.; Chiaur, D. S.; Guardavaccaro, D.; Parks, W.; Vidal, M.; Pagano, M. (1999): Identification of a family of human F-box proteins. In *Current Biology* 9 (20), 1177-S3. DOI: 10.1016/S0960-9822(00)80020-2.

Centore, Richard C.; Havens, Courtney G.; Manning, Amity L.; Li, Ju-Mei; Flynn, Rachel Litman; Tse, Alice et al. (2010): CRL4(Cdt2)-mediated destruction of the histone methyltransferase Set8 prevents premature chromatin compaction in S phase. In *Molecular cell* 40 (1), pp. 22–33. DOI: 10.1016/j.molcel.2010.09.015.

Chao, William C. H.; Kulkarni, Kiran; Zhang, Ziguo; Kong, Eric H.; Barford, David (2012): Structure of the mitotic checkpoint complex. In *Nature* 484 (7393), pp. 208–213. DOI: 10.1038/nature10896.

Chu, Isabel M.; Hengst, Ludger; Slingerland, Joyce M. (2008): The Cdk inhibitor p27 in human cancer: prognostic potential and relevance to anticancer therapy. In *Nature reviews. Cancer* 8 (4), pp. 253–267. DOI: 10.1038/nrc2347.

Chuang, Li-Chiou; Yew, P. Renee (2005): Proliferating cell nuclear antigen recruits cyclin-dependent kinase inhibitor Xic1 to DNA and couples its proteolysis to DNA polymerase switching. In *The Journal of biological chemistry* 280 (42), pp. 35299–35309. DOI: 10.1074/jbc.M506429200.

Chuang, Li-Chiou; Zhu, Xi-Ning; Herrera, Carlos R.; Tseng, Hui-Min; Pfleger, Cathie M.; Block, Karen; Yew, P. Renee (2005): The C-terminal domain of the Xenopus cyclin-dependent kinase inhibitor, p27Xic1, is both necessary and sufficient for phosphorylation-independent proteolysis. In *The Journal of biological chemistry* 280 (42), pp. 35290–35298. DOI: 10.1074/jbc.M506430200.

Clague, Michael J.; Barsukov, Igor; Coulson, Judy M.; Liu, Han; Rigden, Daniel J.; Urbé, Sylvie (2013): Deubiquitylases from genes to organism. In *Physiological reviews* 93 (3), pp. 1289–1315. DOI: 10.1152/physrev.00002.2013.

Cormack, B. P.; Valdivia, R. H.; Falkow, S. (1996): FACS-optimized mutants of the green fluorescent protein (GFP). In *Gene* 173 (1 Spec No), pp. 33–38. DOI: 10.1016/0378-1119(95)00685-0.

Coudreuse, Damien; Nurse, Paul (2010): Driving the cell cycle with a minimal CDK control network. In *Nature* 468 (7327), pp. 1074–1079. DOI: 10.1038/nature09543.

da Fonseca, Paula C. A.; Kong, Eric H.; Zhang, Ziguo; Schreiber, Anne; Williams, Mark A.; Morris, Edward P.; Barford, David (2011): Structures of APC/C(Cdh1) with substrates identify Cdh1 and Apc10 as the D-box co-receptor. In *Nature* 470 (7333), pp. 274–278. DOI: 10.1038/nature09625.

Deshaies, Raymond J.; Joazeiro, Claudio A. P. (2009): RING domain E3 ubiquitin ligases. In *Annual review of biochemistry* 78, pp. 399–434. DOI: 10.1146/annurev.biochem.78.101807.093809.

Di Fiore, Barbara; Davey, Norman E.; Hagting, Anja; Izawa, Daisuke; Mansfeld, Jörg; Gibson, Toby J.; Pines, Jonathon (2015): The ABBA motif binds APC/C activators and is shared by APC/C substrates and regulators. In *Developmental Cell* 32 (3), pp. 358–372. DOI: 10.1016/j.devcel.2015.01.003.

Di Fiore, Barbara; Pines, Jonathon (2007): Emi1 is needed to couple DNA replication with mitosis but does not regulate activation of the mitotic APC/C. In *The Journal of cell biology* 177 (3), pp. 425–437. DOI: 10.1083/jcb.200611166.

Dienemann, Axel; Sprenger, Frank (2004): Requirements of cyclin a for mitosis are independent of its subcellular localization. In *Current Biology* 14 (12), pp. 1117–1123. DOI: 10.1016/j.cub.2004.06.024.

Du, Juan; Zhang, Junzheng; Su, Ying; Liu, Min; Ospina, Jason K.; Yang, Shengyuan; Zhu, Alan Jian (2011): In vivo RNAi screen reveals neddylation genes as novel regulators of Hedgehog signaling. In *PloS one* 6 (9), e24168. DOI: 10.1371/journal.pone.0024168.

Duan, Shanshan; Skaar, Jeffrey R.; Kuchay, Shafi; Toschi, Alfredo; Kanarek, Naama; Ben-Neriah, Yinon; Pagano, Michele (2011): mTOR generates an auto-amplification loop by triggering the βTrCP- and CK1α-dependent degradation of DEPTOR. In *Molecular cell* 44 (2), pp. 317–324. DOI: 10.1016/j.molcel.2011.09.005.

Dui, Wen; Wei, Bin; He, Feng; Lu, Wei; Li, Changqing; Liang, Xuehong et al. (2013): The Drosophila F-box protein dSkp2 regulates cell proliferation by targeting Dacapo for degradation. In *Molecular biology of the cell* 24 (11), 1676-87, S1-7. DOI: 10.1091/mbc.E12-10-0772.

Dulić, V.; Stein, G. H.; Far, D. F.; Reed, S. I. (1998): Nuclear accumulation of p21Cip1 at the onset of mitosis: a role at the G2/M-phase transition. In *Molecular and Cellular Biology* 18 (1), pp. 546–557. DOI: 10.1128/mcb.18.1.546.

Dunnen, Johan T. den; Antonarakis, Stylianos E. (2000): Mutation nomenclature extensions and suggestions to describe complex mutations: A discussion. In *Hum. Mutat.* 15 (1), pp. 7–12. DOI: 10.1002/(SICI)1098-1004(200001)15:1<7::AID-HUMU4>3.0.CO;2-N.

Eldridge, Adam G.; Loktev, Alexander V.; Hansen, David V.; Verschuren, Emmy W.; Reimann, Julie D. R.; Jackson, Peter K. (2006): The evi5 oncogene regulates cyclin accumulation by stabilizing the anaphase-promoting complex inhibitor emi1. In *Cell* 124 (2), pp. 367–380. DOI: 10.1016/j.cell.2005.10.038.

El-Mahdy, Mohamed A.; Zhu, Qianzheng; Wang, Qi-En; Wani, Gulzar; Prætorius-Ibba, Mette; Wani, Altaf A. (2006): Cullin 4A-mediated proteolysis of DDB2 protein at DNA damage sites regulates in vivo lesion recognition by XPC. In *The Journal of biological chemistry* 281 (19), pp. 13404–13411. DOI: 10.1074/jbc.M511834200.

Emberley, Ethan D.; Mosadeghi, Ruzbeh; Deshaies, Raymond J. (2012): Deconjugation of Nedd8 from Cul1 is directly regulated by Skp1-F-box and substrate, and the COP9 signalosome inhibits deneddylated SCF by a noncatalytic mechanism. In *The Journal of biological chemistry* 287 (35), pp. 29679–29689. DOI: 10.1074/jbc.M112.352484.

Enchev, Radoslav I.; Scott, Daniel C.; da Fonseca, Paula C. A.; Schreiber, Anne; Monda, Julie K.; Schulman, Brenda A. et al. (2012): Structural basis for a reciprocal regulation between SCF and CSN. In *Cell reports* 2 (3), pp. 616–627. DOI: 10.1016/j.celrep.2012.08.019.

Engelhardt, Melissa (2022): Analysis of Cyclin E degradation in Drosophila melanogaster. bachelor thesis.

Fischer, Eric S.; Scrima, Andrea; Böhm, Kerstin; Matsumoto, Syota; Lingaraju, Gondichatnahalli M.; Faty, Mahamadou et al. (2011): The molecular basis of CRL4DDB2/CSA ubiquitin ligase architecture, targeting, and activation. In *Cell* 147 (5), pp. 1024–1039. DOI: 10.1016/j.cell.2011.10.035.

Floyd, Suzanne; Pines, Jonathon; Lindon, Catherine (2008): APC/C Cdh1 targets aurora kinase to control reorganization of the mitotic spindle at anaphase. In *Current Biology* 18 (21), pp. 1649–1658. DOI: 10.1016/j.cub.2008.09.058.

Frye, Jeremiah J.; Brown, Nicholas G.; Petzold, Georg; Watson, Edmond R.; Grace, Christy R. R.; Nourse, Amanda et al. (2013): Electron microscopy structure of human APC/C(CDH1)-EMI1 reveals multimodal mechanism of E3 ligase shutdown. In *Nature structural & molecular biology* 20 (7), pp. 827–835. DOI: 10.1038/nsmb.2593.

Galea, Charles A.; Wang, Yuefeng; Sivakolundu, Sivashankar G.; Kriwacki, Richard W. (2008): Regulation of cell division by intrinsically unstructured proteins: intrinsic flexibility, modularity, and signaling conduits. In *Biochemistry* 47 (29), pp. 7598–7609. DOI: 10.1021/bi8006803.

Galindo-Moreno, María; Giráldez, Servando; Limón-Mortés, M. Cristina; Belmonte-Fernández, Alejandro; Reed, Steven I.; Sáez, Carmen et al. (2019): SCF(FBXW7)-mediated degradation of p53 promotes cell recovery after UV-induced DNA damage. In *FASEB journal : official publication of the Federation of American Societies for Experimental Biology* 33 (10), pp. 11420–11430. DOI: 10.1096/fj.201900885R.

Ganoth, D.; Bornstein, G.; Ko, T. K.; Larsen, B.; Tyers, M.; Pagano, M.; Hershko, A. (2001): The cell-cycle regulatory protein Cks1 is required for SCF(Skp2)-mediated ubiquitinylation of p27. In *Nature cell biology* 3 (3), pp. 321–324. DOI: 10.1038/35060126.

Gao, Daming; Inuzuka, Hiroyuki; Tan, Meng-Kwang Marcus; Fukushima, Hidefumi; Locasale, Jason W.; Liu, Pengda et al. (2011): mTOR drives its own activation via SCF(βTrCP)-dependent degradation of the mTOR inhibitor DEPTOR. In *Molecular cell* 44 (2), pp. 290–303. DOI: 10.1016/j.molcel.2011.08.030.

Ghorbani, Mohammad; Vasavan, Biju; Kraja, Emona; Swan, Andrew (2011): Cks85A and Skp2 interact to maintain diploidy and promote growth in Drosophila. In *Developmental biology* 358 (1), pp. 213–223. DOI: 10.1016/j.ydbio.2011.07.031.

Goldberg, Alfred L. (2003): Protein degradation and protection against misfolded or damaged proteins. In *Nature* 426 (6968), pp. 895–899. DOI: 10.1038/nature02263.

Goldenberg, Seth J.; Cascio, Thomas C.; Shumway, Stuart D.; Garbutt, Kenneth C.; Liu, Jidong; Xiong, Yue; Zheng, Ning (2004): Structure of the Cand1-Cul1-Roc1 complex reveals regulatory mechanisms for the assembly of the multisubunit cullin-dependent ubiquitin ligases. In *Cell* 119 (4), pp. 517–528. DOI: 10.1016/j.cell.2004.10.019.

Gorr, Ingo H.; Boos, Dominik; Stemmann, Olaf (2005): Mutual inhibition of separase and Cdk1 by two-step complex formation. In *Molecular Cell* 19 (1), pp. 135–141. DOI: 10.1016/j.molcel.2005.05.022.

Grosskortenhaus, Ruth; Sprenger, Frank (2002): Rca1 Inhibits APC-Cdh1Fzr and Is Required to Prevent Cyclin Degradation in G2. In *Developmental Cell* 2 (1), pp. 29–40. DOI: 10.1016/S1534-5807(01)00104-6.

Gulbis, Jacqueline M.; Kelman, Zvi; Hurwitz, Jerard; O'Donnell, Mike; Kuriyan, John (1996): Structure of the C-Terminal Region of p21WAF1/CIP1 Complexed with Human PCNA. In *Cell* 87 (2), pp. 297–306. DOI: 10.1016/S0092-8674(00)81347-1.

Guo, Hui; Tian, Tao; Nan, Kejun; Wang, Wenjuan (2010): p57: A multifunctional protein in cancer (Review). In *International journal of oncology* 36 (6), pp. 1321–1329. DOI: 10.3892/ijo_00000617.

Hansen, David V.; Loktev, Alexander V.; Ban, Kenneth H.; Jackson, Peter K. (2004): Plk1 regulates activation of the anaphase promoting complex by phosphorylating and triggering SCFbetaTrCP-dependent destruction of the APC Inhibitor Emi1. In *Molecular biology of the cell* 15 (12), pp. 5623–5634. DOI: 10.1091/mbc.e04-07-0598.

Hao, Bing; Oehlmann, Stephanie; Sowa, Mathew E.; Harper, J. Wade; Pavletich, Nikola P. (2007): Structure of a Fbw7-Skp1-cyclin E complex: multisite-phosphorylated substrate recognition by SCF ubiquitin ligases. In *Molecular Cell* 26 (1), pp. 131–143. DOI: 10.1016/j.molcel.2007.02.022.

Harper, J. Wade; Schulman, Brenda A. (2021): Cullin-RING Ubiquitin Ligase Regulatory Circuits: A Quarter Century Beyond the F-Box Hypothesis. In *Annual review of biochemistry* 90, pp. 403–429. DOI: 10.1146/annurev-biochem-090120-013613.

Hattori, Takayuki; Isobe, Tomoyasu; Abe, Kenji; Kikuchi, Hirotoshi; Kitagawa, Kyoko; Oda, Toshiaki et al. (2007): Pirh2 promotes ubiquitin-dependent degradation of the cyclin-dependent kinase inhibitor p27Kip1. In *Cancer research* 67 (22), pp. 10789–10795. DOI: 10.1158/0008-5472.CAN-07-2033.

Havens, Courtney G.; Shobnam, Nadia; Guarino, Estrella; Centore, Richard C.; Zou, Lee; Kearsey, Stephen E.; Walter, Johannes C. (2012): Direct role for proliferating cell nuclear antigen in substrate recognition by the E3 ubiquitin ligase CRL4Cdt2. In *The Journal of biological chemistry* 287 (14), pp. 11410–11421. DOI: 10.1074/jbc.M111.337683.

Havens, Courtney G.; Walter, Johannes C. (2009): Docking of a specialized PIP Box onto chromatin-bound PCNA creates a degron for the ubiquitin ligase CRL4Cdt2. In *Molecular cell* 35 (1), pp. 93–104. DOI: 10.1016/j.molcel.2009.05.012.

Havens, Courtney G.; Walter, Johannes C. (2011): Mechanism of CRL4(Cdt2), a PCNA-dependent E3 ubiquitin ligase. In *Genes & development* 25 (15), pp. 1568–1582. DOI: 10.1101/gad.2068611.

Hayashi, Akiyo; Giakoumakis, Nickolaos Nikiforos; Heidebrecht, Tatjana; Ishii, Takashi; Panagopoulos, Andreas; Caillat, Christophe et al. (2018): Direct binding of Cdt2 to PCNA is important for targeting the CRL4Cdt2 E3 ligase activity to Cdt1. In *Life science alliance* 1 (6), e201800238. DOI: 10.26508/lsa.201800238.

He, Jun; Chao, William C. H.; Zhang, Ziguo; Yang, Jing; Cronin, Nora; Barford, David (2013): Insights into degron recognition by APC/C coactivators from the structure of an Acm1-Cdh1 complex. In *Molecular cell* 50 (5), pp. 649–660. DOI: 10.1016/j.molcel.2013.04.024.

Herrero-Mendez, Angel; Almeida, Angeles; Fernández, Emilio; Maestre, Carolina; Moncada, Salvador; Bolaños, Juan P. (2009): The bioenergetic and antioxidant status of neurons is controlled by continuous degradation of a key glycolytic enzyme by APC/C-Cdh1. In *Nat Cell Biol* 11 (6), pp. 747–752. DOI: 10.1038/ncb1881.

Herzinger, Serena (2019): SCF-dependent regulation of Dap and CycE/Cdk2. master thesis.

Herzog, Franz; Primorac, Ivana; Dube, Prakash; Lenart, Peter; Sander, Björn; Mechtler, Karl et al. (2009): Structure of the anaphase-promoting complex/cyclosome interacting with a mitotic checkpoint complex. In *Science* 323 (5920), pp. 1477–1481. DOI: 10.1126/science.1163300.

Hirata, Y.; Kiuchi, K.; Chen, H. C.; Milbrandt, J.; Guroff, G. (1993): The phosphorylation and DNA binding of the DNA-binding domain of the orphan nuclear receptor NGFI-B. In *The Journal of biological chemistry* 268 (33), pp. 24808–24812.

Hishiki, Asami; Hashimoto, Hiroshi; Hanafusa, Tomo; Kamei, Keijiro; Ohashi, Eiji; Shimizu, Toshiyuki et al. (2009): Structural basis for novel interactions between human translesion synthesis polymerases and proliferating cell nuclear antigen. In *The Journal of biological chemistry* 284 (16), pp. 10552–10560. DOI: 10.1074/jbc.M809745200.

Hochegger, Helfrid; Takeda, Shunichi; Hunt, Tim (2008): Cyclin-dependent kinases and cell-cycle transitions: does one fit all? In *Nature reviews. Molecular cell biology* 9 (11), pp. 910–916. DOI: 10.1038/nrm2510.

Holland, Andrew J.; Taylor, Stephen S. (2006): Cyclin-B1-mediated inhibition of excess separase is required for timely chromosome disjunction. In *Journal of cell science* 119 (Pt 16), pp. 3325–3336. DOI: 10.1242/jcs.03083.

Holt, Liam J.; Tuch, Brian B.; Villén, Judit; Johnson, Alexander D.; Gygi, Steven P.; Morgan, David O. (2009): Global analysis of Cdk1 substrate phosphorylation sites provides insights into evolution. In *Science* 325 (5948), pp. 1682–1686. DOI: 10.1126/science.1172867.

Hsu, Jerry Y.; Reimann, Julie D. R.; Sørensen, Claus S.; Lukas, Jiri; Jackson, Peter K. (2002): E2F-dependent accumulation of hEmi1 regulates S phase entry by inhibiting APC(Cdh1). In *Nature cell biology* 4 (5), pp. 358–366. DOI: 10.1038/ncb785.

Irniger, Stefan; Piatti, Simonetta; Michaelis, Christine; Nasmyth, Kim (1995): Genes involved in sister chromatid separation are needed for b-type cyclin proteolysis in budding yeast. In *Cell* 81 (2), pp. 269–277. DOI: 10.1016/0092-8674(95)90337-2.

Jaspersen, S. L.; Charles, J. F.; Morgan, D. O. (1999): Inhibitory phosphorylation of the APC regulator Hct1 is controlled by the kinase Cdc28 and the phosphatase Cdc14. In *Current Biology* 9 (5), pp. 227–236. DOI: 10.1016/s0960-9822(99)80111-0.

Jin, Jianping; Arias, Emily E.; Chen, Jing; Harper, J. Wade; Walter, Johannes C. (2006): A family of diverse Cul4-Ddb1-interacting proteins includes Cdt2, which is required for S phase destruction of the replication factor Cdt1. In *Molecular cell* 23 (5), pp. 709–721. DOI: 10.1016/j.molcel.2006.08.010.

Jin, Jianping; Cardozo, Timothy; Lovering, Ruth C.; Elledge, Stephen J.; Pagano, Michele; Harper, J. Wade (2004): Systematic analysis and nomenclature of mammalian F-box proteins. In *Genes & development* 18 (21), pp. 2573–2580. DOI: 10.1101/gad.1255304.

Jin, Lingyan; Williamson, Adam; Banerjee, Sudeep; Philipp, Isabelle; Rape, Michael (2008a): Mechanism of ubiquitin-chain formation by the human anaphase-promoting complex. In *Cell* 133 (4), pp. 653–665. DOI: 10.1016/j.cell.2008.04.012.

Jin, Yetao; Lee, Hunjoo; Zeng, Shelya X.; Dai, Mu-Shui; Lu, Hua (2003): MDM2 promotes p21waf1/cip1 proteasomal turnover independently of ubiquitylation. In *The EMBO journal* 22 (23), pp. 6365–6377. DOI: 10.1093/emboj/cdg600.

Jin, Yetao; Zeng, Shelya X.; Sun, Xiao-Xin; Lee, Hunjoo; Blattner, Christine; Xiao, Zhixiong; Lu, Hua (2008b): MDMX promotes proteasomal turnover of p21 at G1 and early S phases independently of, but in cooperation with, MDM2. In *Molecular and Cellular Biology* 28 (4), pp. 1218–1229. DOI: 10.1128/MCB.01198-07.

Jónsson, Z. O.; Hindges, R.; Hübscher, U. (1998): Regulation of DNA replication and repair proteins through interaction with the front side of proliferating cell nuclear antigen. In *The EMBO journal* 17 (8), pp. 2412–2425. DOI: 10.1093/emboj/17.8.2412.

Kamura, Takumi; Hara, Taichi; Matsumoto, Masaki; Ishida, Noriko; Okumura, Fumihiko; Hatakeyama, Shigetsugu et al. (2004): Cytoplasmic ubiquitin ligase KPC regulates proteolysis of p27(Kip1) at G1 phase. In *Nature cell biology* 6 (12), pp. 1229–1235. DOI: 10.1038/ncb1194.

Kim, Dong Hyun; Budhavarapu, Varija N.; Herrera, Carlos R.; Nam, Hyung Wook; Kim, Yu Sam; Yew, P. Renee (2010): The CRL4Cdt2 ubiquitin ligase mediates the proteolysis of cyclin-dependent kinase inhibitor Xic1 through a direct association with PCNA. In *Molecular and Cellular Biology* 30 (17), pp. 4120–4133. DOI: 10.1128/MCB.01135-09.

Kim, Youngjo; Starostina, Natalia G.; Kipreos, Edward T. (2008): The CRL4Cdt2 ubiquitin ligase targets the degradation of p21Cip1 to control replication licensing. In *Genes & development* 22 (18), pp. 2507–2519. DOI: 10.1101/gad.1703708.

Kimata, Yuu; Baxter, Joanne E.; Fry, Andrew M.; Yamano, Hiroyuki (2008): A role for the Fizzy/Cdc20 family of proteins in activation of the APC/C distinct from substrate recruitment. In *Molecular cell* 32 (4), pp. 576–583. DOI: 10.1016/j.molcel.2008.09.023.

King, Randall W.; Peters, Jan-Michael; Tugendreich, Stuart; Rolfe, Mark; Hieter, Philip; Kirschner, Marc W. (1995): A 20s complex containing CDC27 and CDC16 catalyzes the mitosis-specific conjugation of ubiquitin to cyclin B. In *Cell* 81 (2), pp. 279–288. DOI: 10.1016/0092-8674(95)90338-0.

Kliza, Katarzyna; Husnjak, Koraljka (2020): Resolving the Complexity of Ubiquitin Networks. In *Frontiers in molecular biosciences* 7, p. 21. DOI: 10.3389/fmolb.2020.00021.

Knoblich, J. A.; Sauer, K.; Jones, L.; Richardson, H.; Saint, R.; Lehner, C. F. (1994): Cyclin E controls S phase progression and its down-regulation during Drosophila embryogenesis is required for the arrest of cell proliferation. In *Cell* 77 (1), pp. 107–120. DOI: 10.1016/0092-8674(94)90239-9.

Kõivomägi, Mardo; Valk, Ervin; Venta, Rainis; Iofik, Anna; Lepiku, Martin; Balog, Eva Rose M. et al. (2011): Cascades of multisite phosphorylation control Sic1 destruction at the onset of S phase. In *Nature* 480 (7375), pp. 128–131. DOI: 10.1038/nature10560.

Komander, David; Rape, Michael (2012): The ubiquitin code. In *Annual review of biochemistry* 81, pp. 203–229. DOI: 10.1146/annurev-biochem-060310-170328.

Kraft, Claudine; Vodermaier, Hartmut C.; Maurer-Stroh, Sebastian; Eisenhaber, Frank; Peters, Jan-Michael (2005): The WD40 propeller domain of Cdh1 functions as a destruction box receptor for APC/C substrates. In *Molecular Cell* 18 (5), pp. 543–553. DOI: 10.1016/j.molcel.2005.04.023.

Krishna, T. S.; Kong, X. P.; Gary, S.; Burgers, P. M.; Kuriyan, J. (1994): Crystal structure of the eukaryotic DNA polymerase processivity factor PCNA. In *Cell* 79 (7), pp. 1233–1243. DOI: 10.1016/0092-8674(94)90014-0.

Kurz, Thimo; Ozlü, Nurhan; Rudolf, Fabian; O'Rourke, Sean M.; Luke, Brian; Hofmann, Kay et al. (2005): The conserved protein DCN-1/Dcn1p is required for cullin neddylation in C. elegans and S. cerevisiae. In *Nature* 435 (7046), pp. 1257–1261. DOI: 10.1038/nature03662.

Lacy, Eilyn R.; Filippov, Igor; Lewis, William S.; Otieno, Steve; Xiao, Limin; Weiss, Sonja et al. (2004): p27 binds cyclin-CDK complexes through a sequential mechanism involving binding-induced protein folding. In *Nat Struct Mol Biol* 11 (4), pp. 358–364. DOI: 10.1038/nsmb746.

Laemmli, U. K. (1970): Cleavage of structural proteins during the assembly of the head of bacteriophage T4. In *Nature* 227 (5259), pp. 680–685. DOI: 10.1038/227680a0.

Lane, Mary Ellen; Sauer, Karsten; Wallace, Kenneth; Jan, Yuh Nung; Lehner, Christian F.; Vaessin, Harald (1996): Dacapo, a Cyclin-Dependent Kinase Inhibitor, Stops Cell Proliferation during Drosophila Development. In *Cell* 87 (7), pp. 1225–1235. DOI: 10.1016/S0092-8674(00)81818-8.

Lee, Eun-Woo; Lee, Min-Sik; Camus, Suzanne; Ghim, Jaewang; Yang, Mi-Ran; Oh, Wonkyung et al. (2009): Differential regulation of p53 and p21 by MKRN1 E3 ligase controls cell cycle arrest and apoptosis. In *The EMBO journal* 28 (14), pp. 2100–2113. DOI: 10.1038/emboj.2009.164.

Lee, Ji Young; Yu, Su Jin; Park, Yun Gyu; Kim, Joon; Sohn, Jeongwon (2007): Glycogen synthase kinase 3beta phosphorylates p21WAF1/CIP1 for proteasomal degradation after UV irradiation. In *Molecular and Cellular Biology* 27 (8), pp. 3187–3198. DOI: 10.1128/MCB.01461-06.

Lee, Tom V.; Ding, Tian; Chen, Zhihong; Rajendran, Vani; Scherr, Heather; Lackey, Melinda et al. (2008): The E1 ubiquitin-activating enzyme Uba1 in Drosophila controls apoptosis autonomously and tissue growth non-autonomously. In *Development (Cambridge, England)* 135 (1), pp. 43–52. DOI: 10.1242/dev.011288.

Leng, Feng; Saxena, Lovely; Hoang, Nam; Zhang, Chunxiao; Lee, Logan; Li, Wenjing et al. (2018): Proliferating cell nuclear antigen interacts with the CRL4 ubiquitin ligase subunit CDT2 in DNA synthesis-induced degradation of CDT1. In *The Journal of biological chemistry* 293 (49), pp. 18879–18889. DOI: 10.1074/jbc.RA118.003049.

Levin, D. S.; Bai, W.; Yao, N.; O'Donnell, M.; Tomkinson, A. E. (1997): An interaction between DNA ligase I and proliferating cell nuclear antigen: implications for Okazaki fragment synthesis and joining. In *Proceedings of the National Academy of Sciences of the United States of America* 94 (24), pp. 12863–12868. DOI: 10.1073/pnas.94.24.12863.

Levine, A. J. (1997): p53, the cellular gatekeeper for growth and division. In *Cell* 88 (3), pp. 323–331. DOI: 10.1016/S0092-8674(00)81871-1.

Li, Chonghua; Jin, Jianping (2010): DNA replication licensing control and rereplication prevention. In *Protein & cell* 1 (3), pp. 227–236. DOI: 10.1007/s13238-010-0032-z.

Lindon, Catherine; Pines, Jonathon (2004): Ordered proteolysis in anaphase inactivates Plk1 to contribute to proper mitotic exit in human cells. In *The Journal of cell biology* 164 (2), pp. 233–241. DOI: 10.1083/jcb.200309035.

Listovsky, Tamar; Oren, Yifat S.; Yudkovsky, Yana; Mahbubani, Hiro M.; Weiss, Aryeh M.; Lebendiker, Mario; Brandeis, Michael (2004): Mammalian Cdh1/Fzr mediates its own degradation. In *The EMBO journal* 23 (7), pp. 1619–1626. DOI: 10.1038/sj.emboj.7600149.

Littlepage, Laurie E.; Ruderman, Joan V. (2002): Identification of a new APC/C recognition domain, the A box, which is required for the Cdh1-dependent destruction of the kinase Aurora-A during mitotic exit. In *Genes & development* 16 (17), pp. 2274–2285. DOI: 10.1101/gad.1007302.

Liu, Chunming; Li, Yiming; Semenov, Mikhail; Han, Chun; Baeg, Gyeong-Hun; Tan, Yi et al. (2002): Control of β-Catenin Phosphorylation/Degradation by a Dual-Kinase Mechanism. In *Cell* 108 (6), pp. 837–847. DOI: 10.1016/S0092-8674(02)00685-2.

Lu, Zhimin; Hunter, Tony (2010): Ubiquitylation and proteasomal degradation of the p21(Cip1), p27(Kip1) and p57(Kip2) CDK inhibitors. In *Cell Cycle* 9 (12), pp. 2342–2352. DOI: 10.4161/cc.9.12.11988.

Lydeard, John R.; Schulman, Brenda A.; Harper, J. Wade (2013): Building and remodelling Cullin-RING E3 ubiquitin ligases. In *EMBO reports* 14 (12), pp. 1050–1061. DOI: 10.1038/embor.2013.173.

M. Kies (2017): Dual regulation of APC/C activity by Rca1. pHD thesis (University of Regensburg).

Mace, Peter D.; Linke, Katrin; Feltham, Rebecca; Schumacher, Frances-Rose; Smith, Clyde A.; Vaux, David L. et al. (2008): Structures of the cIAP2 RING domain reveal conformational changes associated with ubiquitin-conjugating enzyme (E2) recruitment. In *The Journal of biological chemistry* 283 (46), pp. 31633–31640. DOI: 10.1074/jbc.M804753200.

Machida, Yuichi J.; Dutta, Anindya (2007): The APC/C inhibitor, Emi1, is essential for prevention of rereplication. In *Genes & development* 21 (2), pp. 184–194. DOI: 10.1101/gad.1495007.

Maga, Giovanni; Hubscher, Ulrich (2003): Proliferating cell nuclear antigen (PCNA): a dancer with many partners. In *Journal of cell science* 116 (Pt 15), pp. 3051–3060. DOI: 10.1242/jcs.00653.

Malumbres, Marcos (2014): Cyclin-dependent kinases. In *Genome biology* 15 (6), p. 122. DOI: 10.1186/gb4184.

Margottin-Goguet, Florence; Hsu, Jerry Y.; Loktev, Alexander; Hsieh, Harn Mei; Reimann, Julie D. R.; Jackson, Peter K. (2003): Prophase destruction of Emi1 by the SCF(betaTrCP/Slimb) ubiquitin ligase activates the anaphase promoting complex to allow progression beyond prometaphase. In *Developmental Cell* 4 (6), pp. 813–826. DOI: 10.1016/s1534-5807(03)00153-9.

Marzio, Antonio; Puccini, Joseph; Kwon, Youngho; Maverakis, Natalia K.; Arbini, Arnaldo; Sung, Patrick et al. (2019): The F-Box Domain-Dependent Activity of EMI1 Regulates PARPi Sensitivity in Triple-Negative Breast Cancers. In *Molecular cell* 73 (2), 224-237.e6. DOI: 10.1016/j.molcel.2018.11.003.

Matsumoto, Marissa L.; Wickliffe, Katherine E.; Dong, Ken C.; Yu, Christine; Bosanac, Ivan; Bustos, Daisy et al. (2010): K11-linked polyubiquitination in cell cycle control revealed by a K11 linkage-specific antibody. In *Molecular cell* 39 (3), pp. 477–484. DOI: 10.1016/j.molcel.2010.07.001.

Matsusaka, Takahiro; Enquist-Newman, Maria; Morgan, David O.; Pines, Jonathon (2014): Co-activator independent differences in how the metaphase and anaphase APC/C recognise the same substrate. In *Biology open* 3 (10), pp. 904–912. DOI: 10.1242/bio.20149415.

Matyskiela, Mary E.; Rodrigo-Brenni, Monica C.; Morgan, David O. (2009): Mechanisms of ubiquitin transfer by the anaphase-promoting complex. In *Journal of Biology* 8 (10), p. 92. DOI: 10.1186/jbiol184.

Maupin-Furlow, Julie (2011): Proteasomes and protein conjugation across domains of life. In *Nature reviews. Microbiology* 10 (2), pp. 100–111. DOI: 10.1038/nrmicro2696.

Mazian, Muadz Ahmad; Suenaga, Naohiro; Ishii, Takashi; Hayashi, Akiyo; Shiomi, Yasushi; Nishitani, Hideo (2019): A DNA-binding domain in the C-terminal region of Cdt2 enhances the DNA synthesis-coupled CRL4Cdt2 ubiquitin ligase activity for Cdt1. In *Journal of biochemistry* 165 (6), pp. 505–516. DOI: 10.1093/jb/mvz001.

Mazian, Muadz Ahmad; Yamanishi, Kumpei; Rahman, Mohd Zulhilmi Abdul; Ganasen, Menega; Nishitani, Hideo (2022): CRL4Cdt2 Ubiquitin Ligase, A Genome Caretaker Controlled by Cdt2 Binding to PCNA and DNA. In *Genes* 13 (2). DOI: 10.3390/genes13020266.

Meyer, Hermann-Josef; Rape, Michael (2014): Enhanced protein degradation by branched ubiquitin chains. In *Cell* 157 (4), pp. 910–921. DOI: 10.1016/j.cell.2014.03.037.

Michelle, Caroline; Vourc'h, Patrick; Mignon, Laurence; Andres, Christian R. (2009): What was the set of ubiquitin and ubiquitin-like conjugating enzymes in the eukaryote common ancestor? In *Journal of molecular evolution* 68 (6), pp. 616–628. DOI: 10.1007/s00239-009-9225-6.

Michishita, Masato; Morimoto, Aya; Ishii, Takashi; Komori, Hirofumi; Shiomi, Yasushi; Higuchi, Yoshiki; Nishitani, Hideo (2011): Positively charged residues located downstream of PIP box, together with TD amino acids within PIP box, are important for CRL4(Cdt2) -mediated proteolysis. In *Genes to cells : devoted to molecular & cellular mechanisms* 16 (1), pp. 12–22. DOI: 10.1111/j.1365-2443.2010.01464.x.

Mishra, Amit; Godavarthi, Swetha K.; Jana, Nihar Ranjan (2009): UBE3A/E6-AP regulates cell proliferation by promoting proteasomal degradation of p27. In *Neurobiology of disease* 36 (1), pp. 26–34. DOI: 10.1016/j.nbd.2009.06.010.

Mizushima, Tsunehiro; Yoshida, Yukiko; Kumanomidou, Taichi; Hasegawa, Yuko; Suzuki, Atsuo; Yamane, Takashi; Tanaka, Keiji (2007): Structural basis for the selection of glycosylated substrates by SCF(Fbs1) ubiquitin ligase. In *Proceedings of the National Academy of Sciences of the United States of America* 104 (14), pp. 5777–5781. DOI: 10.1073/pnas.0610312104.

Moberg, K. H.; Bell, D. W.; Wahrer, D. C.; Haber, D. A.; Hariharan, I. K. (2001): Archipelago regulates Cyclin E levels in Drosophila and is mutated in human cancer cell lines. In *Nature* 413 (6853), pp. 311–316. DOI: 10.1038/35095068.

Morgan, David Owen (2007): The cell cycle. Principles of control. London, Sunderland MA: Published by New Science Press in association with Oxford University Press; Distributed inside North America by Sinauer Associates Publishers (Primers in biology), checked on 8/6/2021.

Morgenthaler, Christoph (2013): Der Zellzyklusregulator Rca1 - Inhibitor und Substrat des Anaphase-Promoting-Komplexes in Drosophila melanogaster. pHD thesis (University of Regensburg).

Moshe, Yakir; Bar-On, Ortal; Ganoth, Dvora; Hershko, Avram (2011): Regulation of the action of early mitotic inhibitor 1 on the anaphase-promoting complex/cyclosome by cyclin-dependent kinases. In *The Journal of biological chemistry* 286 (19), pp. 16647–16657. DOI: 10.1074/jbc.M111.223339.

Mullis, K.; Faloona, F.; Scharf, S.; Saiki, R.; Horn, G.; Erlich, H. (1986): Specific enzymatic amplification of DNA in vitro: the polymerase chain reaction. In *Cold Spring Harbor symposia on quantitative biology* 51 Pt 1, pp. 263–273. DOI: 10.1101/sqb.1986.051.01.032.

Murray, Andrew W. (2004): Recycling the Cell Cycle. In *Cell* 116 (2), pp. 221–234. DOI: 10.1016/S0092-8674(03)01080-8.

Nakanishi, M.; Robetorye, R. S.; Pereira-Smith, O. M.; Smith, J. R. (1995): The C-terminal region of p21SDI1/WAF1/CIP1 is involved in proliferating cell nuclear antigen binding but does not appear to be required for growth inhibition. In *The Journal of biological chemistry* 270 (29), pp. 17060–17063. DOI: 10.1074/jbc.270.29.17060.

Nakayama, Kei-ichi; Nakayama, Keiko (1998): Cip/Kip cyclin-dependent kinase inhibitors: brakes of the cell cycle engine during development. In *Bioessays* 20 (12), pp. 1020–1029. DOI: 10.1002/(SICI)1521-1878(199812)20:12<1020::AID-BIES8>3.0.CO;2-D.

Nguyen, Hanh T.; Frasch, Manfred (2006): MicroRNAs in muscle differentiation: lessons from Drosophila and beyond. In *Current opinion in genetics & development* 16 (5), pp. 533–539. DOI: 10.1016/j.gde.2006.08.010.

Nguyen, Henry C.; Wang, Wei; Xiong, Yong (2017): Cullin-RING E3 Ubiquitin Ligases: Bridges to Destruction. In *Sub-cellular biochemistry* 83, pp. 323–347. DOI: 10.1007/978-3-319-46503-6_12.

Ni, Jian-Quan; Zhou, Rui; Czech, Benjamin; Liu, Lu-Ping; Holderbaum, Laura; Yang-Zhou, Donghui et al. (2011): A genome-scale shRNA resource for transgenic RNAi in Drosophila. In *Nature methods* 8 (5), pp. 405–407. DOI: 10.1038/nmeth.1592.

Nishitani, Hideo; Shiomi, Yasushi; Iida, Hiroka; Michishita, Masato; Takami, Toshihiro; Tsurimoto, Toshiki (2008): CDK inhibitor p21 is degraded by a proliferating cell nuclear antigen-coupled Cul4-DDB1Cdt2 pathway during S phase and after UV irradiation. In *The Journal of biological chemistry* 283 (43), pp. 29045–29052. DOI: 10.1074/jbc.M806045200.

Nishitani, Hideo; Sugimoto, Nozomi; Roukos, Vassilis; Nakanishi, Yohsuke; Saijo, Masafumi; Obuse, Chikashi et al. (2006): Two E3 ubiquitin ligases, SCF-Skp2 and DDB1-Cul4, target human Cdt1 for proteolysis. In *The EMBO journal* 25 (5), pp. 1126–1136. DOI: 10.1038/sj.emboj.7601002.

Nooij, Joriene C. de; Graber, Karolina H.; Hariharan, Iswar K. (2000): Expression of the cyclin-dependent kinase inhibitor Dacapo is regulated by Cyclin E. In *Mechanisms of Development* 97 (1-2), pp. 73–83. DOI: 10.1016/S0925-4773(00)00435-4.

Nukina, Kohei; Hayashi, Akiyo; Shiomi, Yasushi; Sugasawa, Kaoru; Ohtsubo, Motoaki; Nishitani, Hideo (2018): Mutations at multiple CDK phosphorylation consensus sites on Cdt2 increase the affinity of CRL4Cdt2 for PCNA and its ubiquitination activity in S phase. In *Genes to cells : devoted to molecular & cellular mechanisms* 23 (3), pp. 200–213. DOI: 10.1111/gtc.12563.

Örd, Mihkel; Loog, Mart (2019): How the cell cycle clock ticks. In *Molecular biology of the cell* 30 (2), pp. 169–172. DOI: 10.1091/mbc.E18-05-0272.

Pan, Zhen-Qiang; Kentsis, Alex; Dias, Dora C.; Yamoah, Kosj; Wu, Kenneth (2004): Nedd8 on cullin: building an expressway to protein destruction. In *Oncogene* 23 (11), pp. 1985–1997. DOI: 10.1038/sj.onc.1207414.

Panagopoulos, Andreas; Taraviras, Stavros; Nishitani, Hideo; Lygerou, Zoi (2020): CRL4Cdt2: Coupling Genome Stability to Ubiquitination. In *Trends in cell biology* 30 (4), pp. 290–302. DOI: 10.1016/j.tcb.2020.01.005.

Pateras, Ioannis S.; Apostolopoulou, Kalliopi; Niforou, Katerina; Kotsinas, Athanassios; Gorgoulis, Vassilis G. (2009): p57KIP2: "Kip"ing the cell under control. In *Molecular cancer research : MCR* 7 (12), pp. 1902–1919. DOI: 10.1158/1541-7786.MCR-09-0317.

Pick, Elah; Hofmann, Kay; Glickman, Michael H. (2009): PCI complexes: Beyond the proteasome, CSN, and eIF3 Troika. In *Molecular cell* 35 (3), pp. 260–264. DOI: 10.1016/j.molcel.2009.07.009.

Pierce, Brian G.; Wiehe, Kevin; Hwang, Howook; Kim, Bong-Hyun; Vreven, Thom; Weng, Zhiping (2014): ZDOCK server: interactive docking prediction of protein-protein complexes and symmetric multimers. In *Bioinformatics* 30 (12), pp. 1771–1773. DOI: 10.1093/bioinformatics/btu097.

Pierce, Nathan W.; Lee, J. Eugene; Liu, Xing; Sweredoski, Michael J.; Graham, Robert L. J.; Larimore, Elizabeth A. et al. (2013): Cand1 promotes assembly of new SCF complexes through dynamic exchange of F box proteins. In *Cell* 153 (1), pp. 206–215. DOI: 10.1016/j.cell.2013.02.024.

Pines, Jonathon (2011): Cubism and the cell cycle: the many faces of the APC/C. In *Nat Rev Mol Cell Biol* 12 (7), pp. 427–438. DOI: 10.1038/nrm3132.

Polz, Jan (2021): Functional characterization of Regulator of Cyclin A1 (Rca1) as an APC/C substrate and inhibitor.

Pospiech, Helmut; Grosse, Frank; Pisani, Francesca M. (2010): The initiation step of eukaryotic DNA replication. In *Sub-cellular biochemistry* 50, pp. 79–104. DOI: 10.1007/978-90-481-3471-7_5.

Pozo, Pedro N.; Cook, Jeanette Gowen (2016): Regulation and Function of Cdt1; A Key Factor in Cell Proliferation and Genome Stability. In *Genes* 8 (1). DOI: 10.3390/genes8010002.

Prestel, Andreas; Wichmann, Nanna; Martins, Joao M.; Marabini, Riccardo; Kassem, Noah; Broendum, Sebastian S. et al. (2019): The PCNA interaction motifs revisited: thinking outside the PIP-box. In *Cell. Mol. Life Sci.* 76 (24), pp. 4923–4943. DOI: 10.1007/s00018-019-03150-0.

Radermacher, Pablo Till (2007): Untersuchungen zur Lokalisierung und Stabilitt des Zellzyklus-Proteins Rca1 in Drosophila melanogaster. diploma thesis.

Raff, Jordan W.; Jeffers, Kim; Huang, Jun-Yong (2002): The roles of Fzy/Cdc20 and Fzr/Cdh1 in regulating the destruction of cyclin B in space and time. In *The Journal of cell biology* 157 (7), pp. 1139–1149. DOI: 10.1083/jcb.200203035.

Rape, Michael; Kirschner, Marc W. (2004): Autonomous regulation of the anaphase-promoting complex couples mitosis to S-phase entry. In *Nature* 432 (7017), pp. 588–595. DOI: 10.1038/nature03023.

Reimann, Julie D.R.; Freed, Ellen; Hsu, Jerry Y.; Kramer, Edgar R.; Peters, Jan-Michael; Jackson, Peter K. (2001): Emi1 Is a Mitotic Regulator that Interacts with Cdc20 and Inhibits the Anaphase Promoting Complex. In *Cell* 105 (5), pp. 645–655. DOI: 10.1016/S0092-8674(01)00361-0.

Richard Bach (2023): Identification of SCF-Rca1 substrates by establishment of the TUBE ligase trapping and ALFA systems. Master thesis.

Richardson, H.; O'Keefe, L. V.; Marty, T.; Saint, R. (1995): Ectopic cyclin E expression induces premature entry into S phase and disrupts pattern formation in the Drosophila eye imaginal disc. In *Development (Cambridge, England)* 121 (10), pp. 3371–3379. DOI: 10.1242/dev.121.10.3371.

Richardson, H. E.; O'Keefe, L. V.; Reed, S. I.; Saint, R. (1993): A Drosophila G1-specific cyclin E homolog exhibits different modes of expression during embryogenesis. In *Development (Cambridge, England)* 119 (3), pp. 673–690. DOI: 10.1242/dev.119.3.673.

Rizzardi, Lindsay F.; Coleman, Kate E.; Varma, Dileep; Matson, Jacob P.; Oh, Seeun; Cook, Jeanette Gowen (2015): CDK1-dependent inhibition of the E3 ubiquitin ligase CRL4CDT2 ensures robust transition

from S Phase to Mitosis. In *The Journal of biological chemistry* 290 (1), pp. 556–567. DOI: 10.1074/jbc.M114.614701.

Rodier, Geneviève; Coulombe, Philippe; Tanguay, Pierre-Luc; Boutonnet, Christel; Meloche, Sylvain (2008): Phosphorylation of Skp2 regulated by CDK2 and Cdc14B protects it from degradation by APC(Cdh1) in G1 phase. In *The EMBO journal* 27 (4), pp. 679–691. DOI: 10.1038/emboj.2008.6.

Rössler, Thomas (2019): Identification of substrates of the Drosophila F-box protein Skp2 by flow cytometric and biochemical assays. PhD thesis.

Russo, A. A.; Jeffrey, P. D.; Patten, A. K.; Massagué, J.; Pavletich, N. P. (1996): Crystal structure of the p27Kip1 cyclin-dependent-kinase inhibitor bound to the cyclin A-Cdk2 complex. In *Nature* 382 (6589), pp. 325–331. DOI: 10.1038/382325a0.

Sarikas, Antonio; Hartmann, Thomas; Pan, Zhen-Qiang (2011): The cullin protein family. In *Genome biology* 12 (4), p. 220. DOI: 10.1186/gb-2011-12-4-220.

Scherer, Paul C.; Ding, Yan; Liu, Zhiqing; Xu, Jing; Mao, Haibin; Barrow, James C. et al. (2016): Inositol hexakisphosphate (IP6) generated by IP5K mediates cullin-COP9 signalosome interactions and CRL function. In *Proceedings of the National Academy of Sciences of the United States of America* 113 (13), pp. 3503–3508. DOI: 10.1073/pnas.1525580113.

Scott, Daniel C.; Sviderskiy, Vladislav O.; Monda, Julie K.; Lydeard, John R.; Cho, Shein Ei; Harper, J. Wade; Schulman, Brenda A. (2014): Structure of a RING E3 trapped in action reveals ligation mechanism for the ubiquitin-like protein NEDD8. In *Cell* 157 (7), pp. 1671–1684. DOI: 10.1016/j.cell.2014.04.037.

Scrima, Andrea; Konícková, Renata; Czyzewski, Bryan K.; Kawasaki, Yusuke; Jeffrey, Philip D.; Groisman, Regina et al. (2008): Structural basis of UV DNA-damage recognition by the DDB1-DDB2 complex. In *Cell* 135 (7), pp. 1213–1223. DOI: 10.1016/j.cell.2008.10.045.

Senga, Takeshi; Sivaprasad, Umasundari; Zhu, Wenge; Park, Jong Hoon; Arias, Emily E.; Walter, Johannes C.; Dutta, Anindya (2006): PCNA is a cofactor for Cdt1 degradation by CUL4/DDB1-mediated N-terminal ubiquitination. In *The Journal of biological chemistry* 281 (10), pp. 6246–6252. DOI: 10.1074/jbc.M512705200.

Shafi Kuchay; Shanshan Duan; Emily Schenkein; Angelo Peschiaroli; Anita Saraf; Laurence Florens et al.: FBXL2- and PTPL1-mediated degradation of p110-free p85beta regulatory subunit controls the PI(3)K signalling cascade. Available online at https://www.nature.com/articles/ncb2731.pdf, checked on 5/8/2022.

Shaner, Nathan C.; Campbell, Robert E.; Steinbach, Paul A.; Giepmans, Ben N. G.; Palmer, Amy E.; Tsien, Roger Y. (2004): Improved monomeric red, orange and yellow fluorescent proteins derived from Discosoma sp. red fluorescent protein. In *Nature biotechnology* 22 (12), pp. 1567–1572. DOI: 10.1038/nbt1037.

Sheard, Laura B.; Tan, Xu; Mao, Haibin; Withers, John; Ben-Nissan, Gili; Hinds, Thomas R. et al. (2010): Jasmonate perception by inositol-phosphate-potentiated COI1-JAZ co-receptor. In *Nature* 468 (7322), pp. 400–405. DOI: 10.1038/nature09430.

Sherr, C. J.; Roberts, J. M. (1999): CDK inhibitors: positive and negative regulators of G1-phase progression. In *Genes & development* 13 (12), pp. 1501–1512. DOI: 10.1101/gad.13.12.1501.

Shiomi, Yasushi; Nishitani, Hideo (2017): Control of Genome Integrity by RFC Complexes; Conductors of PCNA Loading onto and Unloading from Chromatin during DNA Replication. In *Genes* 8 (2). DOI: 10.3390/genes8020052.

Sivakumar, Sushama; Gorbsky, Gary J. (2015): Spatiotemporal regulation of the anaphase-promoting complex in mitosis. In *Nature reviews. Molecular cell biology* 16 (2), pp. 82–94. DOI: 10.1038/nrm3934.

Skaar, Jeffrey R.; D'Angiolella, Vincenzo; Pagan, Julia K.; Pagano, Michele (2009): SnapShot: F Box Proteins II. In *Cell* 137 (7), 1358, 1358.e1. DOI: 10.1016/j.cell.2009.05.040.

Skaar, Jeffrey R.; Pagan, Julia K.; Pagano, Michele (2013): Mechanisms and function of substrate recruitment by F-box proteins. In *Nature reviews. Molecular cell biology* 14 (6), pp. 369–381. DOI: 10.1038/nrm3582.

Smykowski, Anja; Fischer, Stefan M.; Zentgraf, Ulrike (2015): Phosphorylation Affects DNA-Binding of the Senescence-Regulating bZIP Transcription Factor GBF1. In *Plants (Basel, Switzerland)* 4 (3), pp. 691–709. DOI: 10.3390/plants4030691.

Spruck, Charles; Strohmaier, Heimo; Watson, Mark; Smith, Adrian P.L; Ryan, Aimee; Krek, Wilhelm; Reed, Steven I. (2001): A CDK-Independent Function of Mammalian Cks1. In *Molecular cell* 7 (3), pp. 639–650. DOI: 10.1016/S1097-2765(01)00210-6.

Staeva-Vieira, Eric; Yoo, Siuk; Lehmann, Ruth (2003): An essential role of DmRad51/SpnA in DNA repair and meiotic checkpoint control. In *The EMBO journal* 22 (21), pp. 5863–5874. DOI: 10.1093/emboj/cdg564.

Starostina, Natalia G.; Kipreos, Edward T. (2012): Multiple degradation pathways regulate versatile CIP/KIP CDK inhibitors. In *Trends in cell biology* 22 (1), pp. 33–41. DOI: 10.1016/j.tcb.2011.10.004.

Starostina, Natalia G.; Simpliciano, Jennifer M.; McGuirk, Michael A.; Kipreos, Edward T. (2010): CRL2(LRR-1) targets a CDK inhibitor for cell cycle control in C. elegans and actin-based motility regulation in human cells. In *Developmental Cell* 19 (5), pp. 753–764. DOI: 10.1016/j.devcel.2010.10.013.

Stemmann, O.; Zou, H.; Gerber, S. A.; Gygi, S. P.; Kirschner, M. W. (2001): Dual inhibition of sister chromatid separation at metaphase. In *Cell* 107 (6), pp. 715–726. DOI: 10.1016/s0092-8674(01)00603-1.

Sudakin, V.; Ganoth, D.; Dahan, A.; Heller, H.; Hershko, J.; Luca, F. C. et al. (1995): The cyclosome, a large complex containing cyclin-selective ubiquitin ligase activity, targets cyclins for destruction at the end of mitosis. In *Molecular biology of the cell* 6 (2), pp. 185–197. DOI: 10.1091/mbc.6.2.185.

Swanson, Christina I.; Meserve, Joy H.; McCarter, Patrick C.; Thieme, Alexis; Mathew, Tony; Elston, Timothy C.; Duronio, Robert J. (2015): Expression of an S phase-stabilized version of the CDK inhibitor Dacapo can alter endoreplication. In *Development (Cambridge, England)* 142 (24), pp. 4288–4298. DOI: 10.1242/dev.115006.

Tan, Xu; Calderon-Villalobos, Luz Irina A.; Sharon, Michal; Zheng, Changxue; Robinson, Carol V.; Estelle, Mark; Zheng, Ning (2007): Mechanism of auxin perception by the TIR1 ubiquitin ligase. In *Nature* 446 (7136), pp. 640–645. DOI: 10.1038/nature05731.

Tron, Adriana E.; Arai, Takehiro; Duda, David M.; Kuwabara, Hiroshi; Olszewski, Jennifer L.; Fujiwara, Yuko et al. (2012): The glomuvenous malformation protein Glomulin binds Rbx1 and regulates cullin RING ligase-mediated turnover of Fbw7. In *Molecular cell* 46 (1), pp. 67–78. DOI: 10.1016/j.molcel.2012.02.005.

Tugendreich, Stuart; Tomkiel, John; Earnshaw, William; Hieter, Philip (1995): CDC27Hs colocalizes with CDC16Hs to the centrosome and mitotic spindle and is essential for the metaphase to anaphase transition. In *Cell* 81 (2), pp. 261–268. DOI: 10.1016/0092-8674(95)90336-4.

Uhlmann, F.; Wernic, D.; Poupart, M. A.; Koonin, E. V.; Nasmyth, K. (2000): Cleavage of cohesin by the CD clan protease separin triggers anaphase in yeast. In *Cell* 103 (3), pp. 375–386. DOI: 10.1016/s0092-8674(00)00130-6.

Umar, Asad; Buermeyer, Andrew B.; Simon, Jeffrey A.; Thomas, David C.; Clark, Alan B.; Liskay, R.Michael; Kunkel, Thomas A. (1996): Requirement for PCNA in DNA Mismatch Repair at a Step Preceding DNA Resynthesis. In *Cell* 87 (1), pp. 65–73. DOI: 10.1016/S0092-8674(00)81323-9.

van Voorhis, Vanessa A.; Morgan, David O. (2014): Activation of the APC/C ubiquitin ligase by enhanced E2 efficiency. In *Current biology : CB* 24 (13), pp. 1556–1562. DOI: 10.1016/j.cub.2014.05.052.

Wade Harper, J. (1993): The p21 Cdk-interacting protein Cip1 is a potent inhibitor of G1 cyclin-dependent kinases. In *Cell* 75 (4), pp. 805–816. DOI: 10.1016/0092-8674(93)90499-g.

Wang, Weiping; Kirschner, Marc W. (2013): Emi1 preferentially inhibits ubiquitin chain elongation by the anaphase-promoting complex. In *Nature cell biology* 15 (7), pp. 797–806. DOI: 10.1038/ncb2755.

Wang, Yang; Hu, Xue-Jia; Zou, Xu-Dong; Wu, Xian-Hui; Ye, Zhi-Qiang; Wu, Yun-Dong (2015): WDSPdb: a database for WD40-repeat proteins. In *Nucleic acids research* 43 (Database issue), D339-44. DOI: 10.1093/nar/gku1023.

Warbrick, E. (2000): The puzzle of PCNA's many partners. In *Bioessays* 22 (11), pp. 997–1006. DOI: 10.1002/1521-1878(200011)22:11<997::AID-BIES6>3.0.CO;2-#.

Warbrick, Emma; Lane, David P.; Glover, David M.; Cox, Lynne S. (1995): A small peptide inhibitor of DNA replication defines the site of interaction between the cyclin-dependent kinase inhibitor p21WAF1 and proliferating cell nuclear antigen. In *Current Biology* 5 (3), pp. 275–282. DOI: 10.1016/S0960-9822(95)00058-3.

Watanabe, Masashi; Saeki, Yasushi; Takahashi, Hidehisa; Ohtake, Fumiaki; Yoshida, Yukiko; Kasuga, Yusuke et al. (2020): A substrate-trapping strategy to find E3 ubiquitin ligase substrates identifies Parkin and TRIM28 targets. In *Commun Biol* 3 (1), p. 592. DOI: 10.1038/s42003-020-01328-y.

Wei, Wenyi; Jin, Jianping; Schlisio, Susanne; Harper, J. Wade; Kaelin, William G. (2005): The v-Jun point mutation allows c-Jun to escape GSK3-dependent recognition and destruction by the Fbw7 ubiquitin ligase. In *Cancer cell* 8 (1), pp. 25–33. DOI: 10.1016/j.ccr.2005.06.005.

Welcker, Markus; Singer, Jeffrey; Loeb, Keith R.; Grim, Jonathan; Bloecher, Andrew; Gurien-West, Mark et al. (2003): Multisite Phosphorylation by Cdk2 and GSK3 Controls Cyclin E Degradation. In *Molecular cell* 12 (2), pp. 381–392. DOI: 10.1016/S1097-2765(03)00287-9.

Whittaker, Allyson J.; Royzman, Irena; Orr-Weaver, Terry L. (2000): Drosophila Double parked: a conserved, essential replication protein that colocalizes with the origin recognition complex and links DNA replication with mitosis and the down-regulation of S phase transcripts. In *Genes & development* 14 (14), pp. 1765–1776. DOI: 10.1101/gad.14.14.1765.

Williamson, Adam; Banerjee, Sudeep; Zhu, Xining; Philipp, Isabelle; Iavarone, Anthony T.; Rape, Michael (2011): Regulation of ubiquitin chain initiation to control the timing of substrate degradation. In *Molecular cell* 42 (6), pp. 744–757. DOI: 10.1016/j.molcel.2011.04.022.

Winston, Jeffrey T.; Koepp, Deanna M.; Zhu, Cihui; Elledge, Stephen J.; Harper, J.Wade (1999): A family of mammalian F-box proteins. In *Current Biology* 9 (20), 1180-S3. DOI: 10.1016/S0960-9822(00)80021-4.

Wu, Tao; Merbl, Yifat; Huo, Ying; Gallop, Jennifer L.; Tzur, Amit; Kirschner, Marc W. (2010): UBE2S drives elongation of K11-linked ubiquitin chains by the anaphase-promoting complex. In *Proceedings of the National Academy of Sciences of the United States of America* 107 (4), pp. 1355–1360. DOI: 10.1073/pnas.0912802107.

Xiong, Y.; Hannon, G. J.; Zhang, H.; Casso, D.; Kobayashi, R.; Beach, D. (1993): p21 is a universal inhibitor of cyclin kinases. In *Nature* 366 (6456), pp. 701–704. DOI: 10.1038/366701a0.

Yamano, Hiroyuki (2013): EMI1, a three-in-one ubiquitylation inhibitor. In *Nature structural & molecular biology* 20 (7), pp. 773–774. DOI: 10.1038/nsmb.2626.

Yang, Qiong; Ferrell, James E. (2013): The Cdk1-APC/C cell cycle oscillator circuit functions as a time-delayed, ultrasensitive switch. In *Nat Cell Biol* 15 (5), pp. 519–525. DOI: 10.1038/ncb2737.

Ye, Xin; Nalepa, Grzegorz; Welcker, Markus; Kessler, Benedikt M.; Spooner, Eric; Qin, Jun et al. (2004): Recognition of phosphodegron motifs in human cyclin E by the SCF(Fbw7) ubiquitin ligase. In *The Journal of biological chemistry* 279 (48), pp. 50110–50119. DOI: 10.1074/jbc.M409226200.

Ye, Yihong; Tang, Wai Kwan; Zhang, Ting; Di Xia (2017): A Mighty "Protein Extractor" of the Cell: Structure and Function of the p97/CDC48 ATPase. In *Frontiers in molecular biosciences* 4, p. 39. DOI: 10.3389/fmolb.2017.00039.

Zachariae, W.; Schwab, M.; Nasmyth, K.; Seufert, W. (1998a): Control of cyclin ubiquitination by CDK-regulated binding of Hct1 to the anaphase promoting complex. In *Science (New York, N.Y.)* 282 (5394), pp. 1721–1724. DOI: 10.1126/science.282.5394.1721.

Zachariae, W.; Shevchenko, A.; Andrews, P. D.; Ciosk, R.; Galova, M.; Stark, M. J. et al. (1998b): Mass spectrometric analysis of the anaphase-promoting complex from yeast: identification of a subunit related to cullins. In *Science (New York, N.Y.)* 279 (5354), pp. 1216–1219. DOI: 10.1126/science.279.5354.1216.

Zhang, Ziguo; Chang, Leifu; Yang, Jing; Conin, Nora; Kulkarni, Kiran; Barford, David (2013): The four canonical tpr subunits of human APC/C form related homo-dimeric structures and stack in parallel to form a TPR suprahelix. In *Journal of molecular biology* 425 (22), pp. 4236–4248. DOI: 10.1016/j.jmb.2013.04.004.

Zhao, Yongchao; Xiong, Xiufang; Sun, Yi (2011): DEPTOR, an mTOR inhibitor, is a physiological substrate of SCF(βTrCP) E3 ubiquitin ligase and regulates survival and autophagy. In *Molecular cell* 44 (2), pp. 304–316. DOI: 10.1016/j.molcel.2011.08.029.

Zheng, Ning; Schulman, Brenda A.; Song, Langzhou; Miller, Julie J.; Jeffrey, Philip D.; Wang, Ping et al. (2002): Structure of the Cul1-Rbx1-Skp1-F boxSkp2 SCF ubiquitin ligase complex. In *Nature* 416 (6882), pp. 703–709. DOI: 10.1038/416703a.

Zielke, Norman; Querings, Silvia; Grosskortenhaus, Ruth; Reis, Tânia; Sprenger, Frank (2006): Molecular dissection of the APC/C inhibitor Rca1 shows a novel F-box-dependent function. In *EMBO reports* 7 (12), pp. 1266–1272. DOI: 10.1038/sj.embor.7400851.

Zou, Yongxin; Mi, Jun; Cui, Jinpeng; Lu, Defen; Zhang, Xiyu; Guo, Chenhong et al. (2009): Characterization of nuclear localization signal in the N terminus of CUL4B and its essential role in cyclin E degradation and

cell cycle progression. In *The Journal of biological chemistry* 284 (48), pp. 33320–33332. DOI: 10.1074/jbc.M109.050427.

13 Zusammenfassung

Dacapo (Dap) – das *Drosophila* Homolog von p21 und p27 – kann CycE/Cdk2 inhibieren und dadurch den Übergang von der G1-Phase zu der S-Phase des Zellzyklus verhindern. Vorherige Arbeit zeigte, dass die E3 Ubiquitin Ligase CRL4-Cdt2 Dap für den Abbau markiert. Außerdem gab es Hinweise darauf, dass die E3 Ubiquitin Ligase SCF-Rca1 in den Abbau von Dap involviert sein könnte. In dieser Arbeit werden Daten gezeigt, welche bekräftigen, dass Dap ein Substrat von SCF-Rca1 ist. Des Weiteren wurden wichtige Einblicke in die genauen Mechanismen erhalten durch welche Dap von CRL4-Cdt2 und SCF-Rca1 erkannt wird.

Dap enthält in seinem C-terminus ein sogenanntes PIP-Degron, ein kurzes 12 Aminosäuren langes Motiv, welches für die Ubiquitinierung durch CRL4-Cdt2 benötigt wird. Das PIP degron ermöglicht die Bindung an die DNA-Klammer PCNA (proliferating cell nuclear antigen) und diese Assoziation wird benötigt, um von Cdt2, dem Substraterkennungsmodul, erkannt zu werden. Hier wurde gezeigt, dass die erste Aminosäure (Q184) des PIP-Degrons in Dap wichtig für die Bindung an PCNA ist und eine Alanin Mutation von Q184 den Abbau über CRL4-Cdt2 beeinträchtigt. Außerdem wurde gezeigt, dass ein basisches Cluster im C-terminalen Bereich des PIP-Degrons in Dap essentiell für dessen Abbau ist. Das basische Cluster vermittelt möglicherweise eine Interaktion mit DNA oder Cdt2. Darüber hinaus wurde gezeigt, dass Regionen in dem N-terminalen Bereich von Dap eine Interaktion mit Cdt2 vermitteln.

Rca1 enthält eine F-box und kann in einen SCF-Komplex eingebaut werden. Das Zielprotein der SCF-Rca1 Ubiquitin Ligase könnte Dap sein. Die Überexpression oder die Runterregulierung von Rca1 kann die Stabilität von Dap beeinflussen. Jedoch sind diese Effekte auf Dap teilweise indirekt durch induzierte Änderungen in der Zellzyklus-Verteilung und nachfolgendem Abbau durch CRL4-Cdt2. Um diese indirekten Effekte zu eliminieren oder zumindest zu reduzieren, wurden verschiedene Ansätze wie z.B. die Runterregulierung von Cdt2 oder die Mutation des PIP-Degrons verfolgt. Nachdem die Aktivität von CRL4-Cdt2 mit Hilfe verschiedener Strategien stark reduziert wurde, führte die Überexpression von Rca1 zu einer Abnahme der Stabilität von Dap und die Runterregulierung von Rca1 erhöhte dessen Stabilität. Dies bekräftigt unsere Theorie, dass Dap ein Substrat von SCF-Rca1 ist.

Das PIP-Degron, welches für den CRL4-Cdt2 vermittelten Abbau verantwortlich ist, fehlte vollständig in einem N-terminalen Fragment von Dap (Dap_1-125). Dieses Fragment wurde durch die Überexpression von Rca1 destabilisiert beziehungsweise durch die Runterregulierung von Rca1 stabilisiert. Dap_1-125 enthält immer noch Bindestellen für CycE und Cdk2, und kann den CycE/Cdk2-Komplex inhibieren. Mit Hilfe von Dap_1-125 Konstrukten konnten wir zeigen, dass Dap an CycE und Cdk2 binden muss, um über SCF-Rca1 abgebaut zu werden. Zusätzlich zeigten wir, dass der N-terminale Bereich von CycE in dem

CycE/Cdk2/Dap-Komplex benötigt wird, um Dap zu destabilisieren. Basierend darauf und auf weiteren Daten in dieser Arbeit, schlagen wird das folgende Modell für den Abbau von Dap über SCF-Rca1 vor: Dap (ein IDP (intrinsically disordered protein)) bindet CycE/Cdk2 in der G1-Phase, um seine Rolle als Inhibitor von CycE/Cdk2 zu erfüllen. Um den G1/S-Übergang am Ende der G1-Phase zu induzieren, phosphoryliert eine unbekannte Kinase Cdk2. Diese Phosphorylierung könnte eine eingeschränkte Aktivität der Cdk2 Kinase erlauben was eine Phosphorylierung des assoziierten CycE in der N-terminalen Region zur Folge hat. Danach wird eine Kinase zu der phosphorylierten Stelle rekrutiert und könnte CycE in der C-terminalen Region und außerdem Dap phosphorylieren. Im Anschluss wird das phosphorylierte Dap von SCF-Rca1 erkannt. Durch diesen Mechanismus könnte sichergestellt werden, dass ausschließlich Dap, welches bereits seine Funktion im Zellzyklus erfüllt hat, für den Abbau markiert wird. Dies steht im Einklang mit der Regulation von anderen CKIs (Inhibitoren von Cyc/Cdk-Komplexen), welche ebenfalls nur dann für den Abbau markiert werden, nachdem diese aktiv den Zellzyklus reguliert haben.

14 Danksagung

Zuerst möchte ich mich bei meinem Doktorvater Prof. Dr. Frank Sprenger bedanken, der mich nicht nur während meiner Doktorarbeit, sondern auch schon während meiner Bachelor- und Masterarbeit, tatkräftig unterstützt hat. Bei Fragen und Problemen hat er sich stets sehr viel Zeit für mich genommen. Dafür ein großes Dankeschön. Auch für die selbst gemischten Cocktails auf unseren Feiern möchte ich mich bedanken.

Zudem möchte ich mich bei meinem Mentor Prof. Dr. Reinhard Sterner bedanken, welcher bei meinen „Research Reports“ stets hilfreiche Ideen und Vorschläge miteinbrachte. Außerdem für die Möglichkeit in seinem Lehrstuhl sonifizieren zu können.

Ein großer Dank geht auch an Christiane Sprenger. Zum einen möchte ich mich für die unterhaltsamen und interessanten Gespräche bedanken, welche den Laboralltag immer wieder aufgelockert haben. Außerdem für die große Hilfe unter anderem in der Zellkultur ohne die ich bei weitem nicht so viele Versuche hätte durchführen können. Außerdem habe ich von ihr einiges über Chilis lernen können.

Ein weiterer Dank geht an meinen Doktoranden-Kollegen Sebastian Sigl. Es hat mir stets viel Freude bereitet mit ihm über verschiedene Theorien bezüglich Dap und CycE zu diskutieren oder zu überlegen wie wir den Prozess der Klonierung weiter optimieren könnten. Auch für seine Hilfsbereitschaft im Labor möchte ich mich bedanken.

Auch bei meinen ehemaligen Kollegen/Betreuern Jan Polz und Matthias Kies möchte ich mich für ihre Unterstützung bedanken.

Auch an die Bachelor- und Masterstudenten in unserer Arbeitsgruppe Leonie Schulz, Catherina Bischof, Jana Heidrich, Eduard Koschemakin, Nicolas Jaenisch, Lorena Camelo-Prieto, Melissa Engelhardt, Richard Bach, Johanna Gizler sowie Johannes Heiduck geht ein großer Dank. Eure Arbeit hat einen wertvollen Beitrag für diese Doktorarbeit geleistet. Insgesamt haben alle Mitglieder der Sprenger Arbeitsgruppe dafür gesorgt, dass ich mich hier sehr wohl gefühlt habe.

Außerdem möchte ich mich bei Arlett Hirsch bedanken. Zum einen für die netten Gespräche, aber auch für die Hilfe bei administrativen Angelegenheiten.

Zudem möchte ich mich auch bei den Mitgliedern der Hefe-Gruppe Simone Fabian, Julia Simmler, Phillipp Girke und Sophia Pinz bedanken, unter anderem für ihre Hilfe sowie für die gemeinsamen Spieleabende. Des Weiteren bei Andrea Brücher, Antje Machetanz-Marokane, Adelheid Weissgerber, Kerstin Forchheim und Wolfgang Mages für ihre Unterstüztung. Außerdem an Prof. Dr. Wolfgang Seufert, welcher sich dazu bereit erklärt hat, als Drittprüfer für diese Doktorarbeit zu fungieren.

Außerdem möchte ich mich bei Prof. Dr. Till Rudack bedanken, welcher mit seinen Strukturvorhersagen einen wichtigen Beitrag für diese Doktorarbeit geleistet hat.

Zum Schluss möchte ich mich bei meinen Eltern bedanken, welche mich auf meinem Weg zur Doktorarbeit stets unterstützt haben und ohne die diese Arbeit nie zustande gekommen wäre.

15 Eidesstattliche Erklärung

Ich erkläre hiermit an Eides statt, dass ich die vorliegende Arbeit ohne unzulässige Hilfe Dritter und ohne Benutzung anderer als der angegebenen Hilfsmittel angefertigt habe. Die aus anderen Quellen direkt oder indirekt übernommenen Daten und Konzepte sind unter Angabe des Literaturzitats gekennzeichnet. Die Arbeit wurde bisher weder im In- noch im Ausland in gleicher oder ähnlicher Form einer anderen Prüfungsbehörde vorgelegt. Ich versichere an Eides statt, dass ich nach bestem Wissen die reine Wahrheit gesagt und nichts verschwiegen habe.

Regensburg, den 26.02.2024

_____

Manuel Saller